UNIVERSITY OF SOUTHAMPTON
FACULTY OF PHYSICAL SCIENCES AND ENGINEERING
SCHOOL OF ELECTRONICS AND COMPUTER SCIENCE

Energy Harvesting Aided Device-to-Device Communication Networks

by

Shruti Gupta
B.Tech.(Hons), MSc

A doctoral thesis submitted in partial fulfillment of the
requirements for the award of Doctor of Philosophy
at the University of Southampton

November 2017

SUPERVISORS:
Prof. Lajos Hanzo
and
Dr. Rong Zhang
School of Electronics and Computer Science
University of Southampton
Southampton SO17 1BJ
United Kingdom

𝔇edicated to my parents.

UNIVERSITY OF SOUTHAMPTON

ABSTRACT

FACULTY OF PHYSICAL SCIENCES AND ENGINEERING
SCHOOL OF ELECTRONICS AND COMPUTER SCIENCE

Doctor of Philosophy

Energy Harvesting Aided Device-to-Device Communication Networks

by Shruti Gupta

With the ever growing demands of power and bandwidth by users, energy and spectral efficiency emanated as key criteria for designing future wireless networks. Therefore, in this thesis energy harvesting (EH) aided device-to-device (D2D) communication is designed for improving both the key design criteria, which is an intricate journey from the realm of individual analysis of EH and D2D communication to that of amalgamating the two techniques.

Specifically, with the widespread use of energy hungry smart devices, these devices become dis-functional due to outage of batteries, which can be avoided by introduction of EH capability at these nodes. In this context, an energy efficient successive relaying based network is conceived using rechargeable source and relay nodes having limited buffers for both their energy and data storage. An optimal and sub-optimal transmission policies are designed for the maximisation of the network throughput with non-causal knowledge of energy arrivals by the deadline.

On the other hand, for exploiting the spectrum efficiently, D2D communication is invoked which brings in new interference scenarios that may be circumvented by incorporating fractional frequency reuse (FFR) or soft frequency reuse (SFR) in OFDMA cellular networks. By carefully considering the downlink resource reuse of the D2D links, beneficial frequency allocation schemes are proposed, when the macrocell has employed FFR or SFR. The coverage probability and the capacity of D2D links are analytically derived under the proposed schemes.

It is imperative to integrate the benefits of EH and D2D communication aided systems for creating unparalleled opportunities in emerging applications. Therefore, a system is designed that comprises of EH aided D2D links relying on downlink resource reuse with the goal of maximizing the sum-rate of the D2D links, without degrading the quality of service (QoS) requirement of the MUs. A pair of joint resource block and power allocation algorithms are proposed for the D2D links, when there is non-causal (off-line) and causal (on-line) knowledge of the EH profiles at the D2D transmitters.

For the sake of further accentuating design flexibility and alleviating the demands of increased spectral resources, previously designed EH aided D2D communication is investigated in conjunction with heterogeneous network (HetNet). An algorithmic solution is proposed with the aim of maximising the sum-rate of these D2D links in the downlink of two-tier HetNet without unduly degrading MU's throughput, when two tiers share spec-

trum under following regimes: (a) orthogonal, (b) co-channel and (c) the proposed co-orthogonal. Low complexity heuristic methods are also proposed, which demonstrate that the optimization of the D2D-MU matching is indeed crucial for the system considered.

Declaration of Authorship

I, **Shruti Gupta**, declare that the thesis entitled **Energy Harvesting Aided Device-to-Device Communication Networks** and the work presented in it are my own and has been generated by me as the result of my own original research. I confirm that:

- This work was done wholly or mainly while in candidature for a research degree at this University;
- Where any part of this thesis has previously been submitted for a degree or any other qualification at this University or any other institution, this has been clearly stated;
- Where I have consulted the published work of others, this is always clearly attributed;
- Where I have quoted from the work of others, the source is always given. With the exception of such quotations, this thesis is entirely my own work;
- I have acknowledged all main sources of help;
- Where the thesis is based on work done by myself jointly with others, I have made clear exactly what was done by others and what I have contributed myself;
- Parts of this work have been published as: [1, 2, 3, 4].

Signed: ..... Date: .....

Acknowledgements

I would like to take this opportunity to express my deepest gratitude to my supervisors Professor Lajos Hanzo and Dr Rong Zhang. Without their insightful guidance, patience, continuous support and inexhaustible enthusiasm, I would not have been able to accomplish this formidable task. Their inspirational motivation has helped me grow both as a researcher as well as a person. Additionally, I am grateful for the lectures offered by Professor Lie-Liang Yang, Professor Sheng Chen, Professor Rob Maunder, Dr Soon Xin Ng (Michael) and Dr Mohammed El-Hajjar during the "MSc in Wireless Communications" that provided all the necessary background for the fruition of this thesis. Special thanks are also due to Dr. Sheetal Kalyani (IIT Madras) for the valuable discussions. I also extend my gratitude to all my colleagues at Southampton for their continuous support and inspiration. I also acknowledge the use of the IRIDIS High Performance Computing Facility, and associated support services at the University of Southampton, in the completion of this work. I am also indebted to the School of Electronics and Computer Science, University of Southampton, for supporting my studies under the auspices of the ECS Studentship award. Finally, I extend my heartfelt appreciation to my family and friends for their unconditional support and encouragement.

List of Publications

1. **Shruti Gupta**, Rong Zhang, and Lajos Hanzo, "Energy Harvesting Aided Device-to-Device Communication in the Over-Sailing Heterogeneous Two-Tier Downlink," *IEEE Access*, vol. PP, no. 99, pp. 1–1, 2017. DOI:10.1109/ACCESS.2017.2762091,

2. **Shruti Gupta**, Rong Zhang, and Lajos Hanzo, "Energy Harvesting Aided Device-to-Device Communication Underlaying the Cellular Downlink," *IEEE Access*, vol. 5, pp. 7405–7413, 2017. DOI: 10.1109/ACCESS.2016.2600242.

3. **Shruti Gupta**, Suman Kumar, Rong Zhang, Sheetal Kalyani, K. Giridhar and Lajos Hanzo, "Resource Allocation for D2D Links in the FFR and SFR Aided Cellular Downlink," *IEEE Transactions on Communications*, vol. 64, pp. 4434–4448, Oct. 2016. DOI: 10.1109/TCOMM.2016.2602866.

4. **Shruti Gupta**, Rong Zhang, and Lajos Hanzo, "Throughput Maximization for a Buffer-Aided Successive Relaying Network Employing Energy Harvesting," *IEEE Transactions on Vehicular Technology*, vol. 65, pp. 6758–6765, Aug. 2016. DOI: 10.1109/TVT.2015.2477808.

Contents

List of Symbols

General Symbols

$E_{n,k}$	Energy Harvested by n^{th} node at time instant t_k
t_i	Energy Harvesting Time Instant i
τ_k	k^{th} Epoch Duration
λ_e	Rate of Energy Arrival
R	Macrocell Radius
P_c^{max}	Power Budget for MBS
P_d^{max}	Power Budget for D2D links
P_d	Transmit Power of D2D links
α	Path-loss Exponent
M	Number of MUs
D	Number of D2D links
N_0	Noise power density
P_c	Transmit power of MBS
ζ	Accuracy parameter

Symbols in Ch-2

$E_{n,max}$	Energy Buffer Capacity at node n
$B_{n,max}$	Data Buffer Capacity at node n
H_{lm}	Channel Gain between nodes l and m normalized w.r.t.noise power

$L_{j,i}$	Duration of Phase j of successive relaying protocol during epoch i
$p_{Sj,i}$	Transmit power of SN in phase j of successive relaying protocol during epoch i
$p_{R1,i}$	Transmit power of RN1 during epoch i
$p_{R2,i}$	Transmit power of RN2 during epoch i
$\alpha_{Sj,i}$	Transmission Rate of SN in phase j of successive relaying protocol during epoch i
$\alpha_{R1,i}$	Transmission Rate of RN1 during epoch i
$\alpha_{R2,i}$	Transmission Rate of RN2 during epoch i
η	Percentage duration of Phase I of successive relaying protocol in Sub-Optimal Scheme.

Symbols in Ch-3

F_i	Frequency Band i
ϵ	Power Control Factor
r	Distance between D2D Tx-Rx pair
R_1	Minimum distance of D2D Tx-Rx pair
R_2	Maximum distance of D2D Tx-Rx pair
l_i	Distance between typical D2D Rx and i^{th} MBS
d_j	Distance from j^{th} D2D Tx in other macrocells to typical D2D Rx
$d_{c,i}$	Distance between i^{th} MBS and typical MU
h	Channel gain between Tx-Rx
$\gamma_U(l,r)$	SIR at D2D Rx when it is at distance l from reference MBS and with a separation of r from D2D Tx in UFR
$\gamma_C(d_c)$	SIR at MU when it is at distance d_c from reference MBS in UFR
I	Interference imposed in the system
ϕ	Set of all macrocells present in the cellular network
ψ	Set of all the interfering D2D links in other macrocells
S_c	Threshold SIR for classification of MUs into CCR and CER users

S_d	Threshold SIR for classification of D2D links into SR and LR D2D links
P_m	Transmit Power of MBS in SFR
β	Power Control factor for MBS in SFR
T	Target SIR
$\lambda(l)$	Scale parameter of Gamma Distribution
$\theta(l)$	Shape parameter of Gamma Distribution
CP	Coverage Probability of D2D links
C	Capacity of D2D links in UFR

Symbols in Ch-4

$y_{dc,\kappa}$	Matching variable for d^{th} D2D pair reusing c^{th} MU's RB in epoch κ
$P_{dc,\kappa}$	Transmit power of d^{th} D2D Tx reusing c^{th} MU's RB in epoch κ
$t_{dc,\kappa}$	Transmit duration of d^{th} D2D Tx reusing c^{th} MU's RB in epoch κ
g	Channel gain inclusive of path-loss from Tx to Rx
g^I	Interference Channel gain inclusive of path-loss interfering Tx to Rx
$r_{d,\kappa}$	Sum-rate of d^{th} D2D Tx in epoch κ
R_c	Throughput of c^{th} MU
$\lambda_{1,dc,\kappa}$	Lagrangian multiplier associated with D2D-MU matching constraint of Eq. (4.4b) in Chapter 4
$\lambda_{2,d,\kappa}$	Lagrangian multiplier associated with D2D energy causality constraint of Eq. (4.4c) in Chapter 4
$\lambda_{3,d,\kappa}$	Lagrangian multiplier associated with D2D transmission duration constraint of Eq. (4.4d) in Chapter 4
$y^*_{dc,\kappa}$	Optimized matching variable for d^{th} D2D pair reusing c^{th} MU's RB in epoch κ
$P^*_{dc,\kappa}$	Optimized transmit power of d^{th} D2D Tx reusing c^{th} MU's RB in epoch κ
$t^*_{dc,\kappa}$	Optimized transmit duration of d^{th} D2D Tx reusing c^{th} MU's RB in epoch κ

P_c^*	Optimized transmit power of MBS

Symbols in Ch-5

P_P^{max}	Power Budget for PBS
I_{Th}	Interference threshold for D2D links for sub-band selection in co-orthogonal spectrum sharing strategy
$D_{Th,d}$	Distance threshold for D2D links for sub-band selection in co-orthogonal spectrum sharing strategy
$D_{Th,c}$	Distance threshold for MU-BS association
x_c	MU-BS association
x_{pc}	MU-PBS association
β_c	Spectrum sharing strategy selection parameter
P_p	Transmit power of PBS
P_p^*	Optimized transmit power of PBS
$\eta_{dc,i}$	Lagrangian multiplier associated with D2D-MU matching constraint Eq. (5.5b) of Chapter 5
$\psi_{dc,i}$	Lagrangian multiplier associated with additional D2D-MU matching constraint of Eq. (5.5c) for co-channel spectrum sharing of Chapter 5
$\lambda_{d,i}$	Lagrangian multiplier associated with D2D power budget constraint Eq. (5.5d) of Chapter 5
$\mu_{d,i}$	Lagrangian multiplier associated with D2D energy causality constraint Eq. (5.5e) of Chapter 5
γ_i	Lagrangian multiplier associated with maximum interference tolerance constraint at MBS Eq. (5.5g) of Chapter 5
ω_i	Lagrangian multiplier associated with maximum interference tolerance constraint at PBS Eq. (5.5f) of Chapter 5

List of Acronyms

SN	Source Node
RN	Relay Node
DN	Destination Node
EH	Energy Harvesting
FD	Full Duplex
HD	Half Duplex
IPOPT	Interior Point Optimization
DF	Decode-and-Forward
KKT	Karush-Kuhn-Tucker equations
BS	Base Station
MBS	Macro Base Station
MU	Mobile Users
D2D	Device-to-Device
DL	Downlink
QoS	Quality of Service
UFR	Unity Frequency Reuse
ICIC	Inter-Cell Interference Coordination
FFR	Fractional Frequency Reuse
SFR	Soft Frequency Reuse
CCR	Cell-Centre Region
CER	Cell-Edge Region

SR	Short Range
LR	Long Range
FFA1	Fractional Frequency Allocation 1
FFA2	Fractional Frequency Allocation 2
SFA	Soft Frequency Allocation
RB	Resource Block
Tx	Transmitter
Rx	Receiver
SIR	Signal-to-Interference Ratio
OF	Objective Function
DP	Dynamic Programming
HetNet	Heterogeneous Network
PBS	Pico-Base Station
JORPA	Joint Optimization of Resource Block and Power Allocation
EPA	Equal Power Allocation
RM	Random D2D-MU Matching
MDM	Maximum Distance D2D-MU Matching

Chapter 1

Introduction

1.1 Motivation

Mobile wireless communications have evolved from first generation voice-only systems to the second, third and fourth generation wireless networks. This steady evolution witnessed the introduction of digital modulations, efficient frequency reuse, new physical layer technologies, like WCDMA, MIMO, OFDMA etc. which have significantly contributed towards satiating the ever growing quest for increasing the capacity of the networks. Besides this, with the proliferation of smart hand-held devices, user demands for power-hungry mobile broadband services are constantly increasing. The drastic growth of bandwidth- and energy-thirsty applications such as mobile video conferencing, video streaming, multimedia file sharing, online gaming etc. are already pushing the limits of current cellular systems [5]. Hence, both energy and spectral efficiency have emerged as key criteria of designing next generation wireless networks.

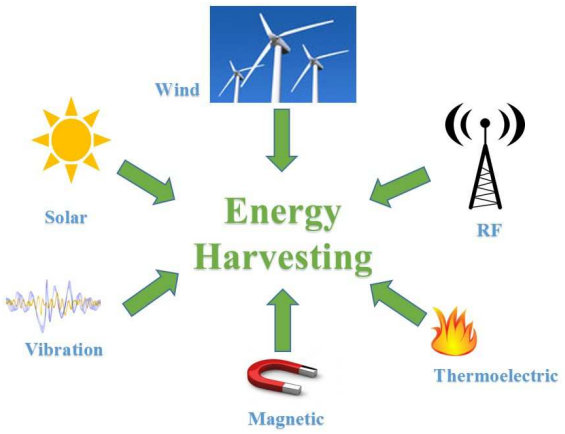

Figure 1.1: Energy Harvesting sources

Recent advances in 'green' solutions suggested a paradigm shift of power supply by decreasing the use of fossil fuels, while increasing the use of renewable sources of energy in wireless communication [6]. This has become all the more important, because the electricity

consumption of the fast expanding networks that handle mobile devices has been growing rapidly and will significantly contribute to global warming. In order to achieve this and to improve energy efficiency, energy harvesting (EH) has been proposed as a promising solution that enables the wireless devices to 'scavenge' energy from diverse natural or man-made phenomena [7, 8]. Specifically, the networks can be made self-sustainable, capable of virtually perpetual operation by harvesting energy from solar power, electromagnetic waves, thermal energy, wind energy, motion, vibration and kinetic energy, as shown in Figure 1.1. In addition to this, the expected benefits include untethered mobility, the ability to be deployed in hard-to-reach places such as remote rural areas, within concrete structures and within the human body. This allows us to develop new medical, environmental, surveillance and safety applications, which would otherwise be impossible with conventional battery-operated networks.

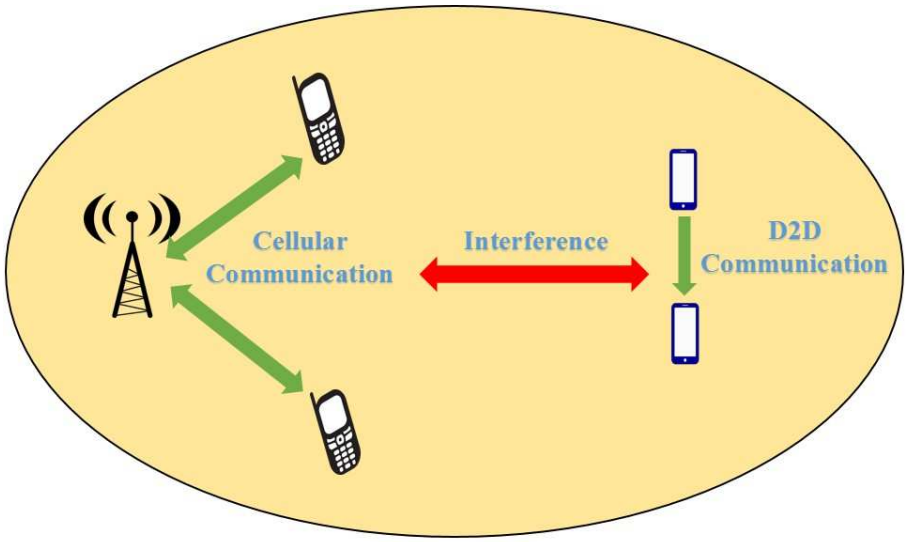

Figure 1.2: D2D Communication in cellular networks.

On the other hand, to improve the transmission capacity, the transmit power of base station (BS) can be increased in traditional cellular networks, but this imposes serious interference on other mobile users (MU) and results in a high energy consumption. Thus, traditional cellular networks are reaching their saturation point and in order to meet the ever-increasing demand for capacity, one of the most promising solution is to use the existing spectral resources efficiently. This can be accomplished in several ways such as by deploying small BSs underlying the conventional cellular networks, employing cognitive radios, spectrum sharing or direct communication between users without involving the BS, which is known as device-to-device (D2D) communication, as shown in Figure 1.2. This thesis will focus on D2D communication which enables direct communication between a pair of closely located mobile devices without any intervention of the BS and reusing the same radio resources in the cellular networks. The advantages of adopting D2D services in cellular networks include high data-rates and/or reduced power consumption (higher energy efficiency), low latency, higher spectral efficiency [9], as an explicit benefit of proximity of devices.

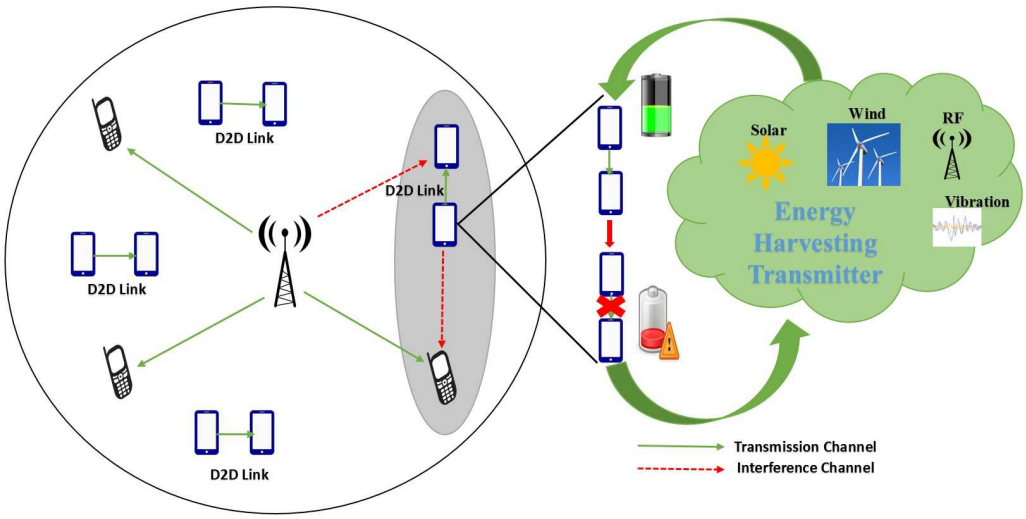

Figure 1.3: EH aided D2D Communication reusing downlink cellular resources

Furthermore, in order to improve both the energy efficiency as well as the spectral efficiency of future wireless communication networks, it is imperative to combine low-power wireless devices and energy-harvesting capabilities, as shown in Figure 1.3. This creates unprecedented opportunities in many emerging applications, such as the internet of things (IoT), that were inconceivable in the past. Therefore, against this background, in this thesis, energy harvesting as well as D2D communication are discussed in detail, before finally focusing on integrating them into energy-harvesting aided D2D communication, which are indispensable for simultaneous improvement of the energy- and spectral-efficiency of the networks. Having defined the main concept, let us now proceed by presenting a historical overview of EH aided networks, followed by that of D2D communication in cellular networks, with the gradual evolution of the amalgamation of EH and D2D communication in the cellular network.

1.2 Historical Perspective on Energy Harvesting Networks

Significant progress has been made in energy harvesting networks over the last decade, making it an interesting research area. Energy harvesting is the process of scavenging energy from the ambient environment, storing this energy in the buffer and utilising this harvested energy for communication. The nodes may harvest energy from solar cells, vibration, watermills, thermoelectric generators, etc. Thus, in contrast to the conventional energy sources used by the nodes of wireless networks, the energy availability becomes sporadic at the nodes. This means that the energy arrival process can be characterised by different stochastic arrival processes. On the other hand, this energy that arrived during the communication process can be stored in the energy buffer and consequently the size of this buffer or battery limits the amount of energy that a node can store for future use. Hence,

the challenges and constraints faced by energy harvesting devices require the redesign of the transmission algorithm, network protocols and transceiver hardware that adapts to the random energy arrival process and its storage capacity at the nodes [10].

In the literature, different network models ranging from simple single-user communication to complex cooperative networks have been investigated, which relied on energy harvesting capability at the transmitter node. Therefore, sophisticated algorithms have been conceived for diverse network models using stochastic energy arrival processes. The time-line for the evolution of network models relying on energy harvesting is seen in Figure 1.4. Although the literature of energy harvesting networks is mainly dedicated to the energy harvesting capability at the transmitter node and then utilising this energy for the network to transmit wireless information, harvesting energy at the receiver node can also be achieved using the RF signal it has just received. This can be termed as *Wireless Power Transfer* (WPT), which has been a topic of interest since Tesla's work [41]. With the maturing WPT and wireless communication fields, an important emerging research area is identified as *Simultaneous Wireless Information and Power Transfer* (SWIPT) [12]. This is expected to become a pervasive enabler to support the Internet of Things, which provides perpetual energy replenishment [42].

There is a paucity of literature on SWIPT, nonetheless the literature is also reviewed in this field along with the different models investigated in Table 1.1.

In [17, 18, 15], optimal policies conceived for minimising the transmission completion time are investigated, where a single node harvests energy stored either in an infinite [17] or in a finite buffer [18], [15]. The transmission completion time minimisation problem encountered in an AWGN broadcast channel, where the transmitter is able to harvest energy from the environment is investigated in [21] under a finite battery capacity. In [22], the optimal policy conceived for a two-user multiple access channel is investigated, where the transmitters are able to harvest energy from nature and the packets are assumed to have arrived before the transmission starts. In [24], the authors proposed an algorithm for the maximization of the sum-throughput in an interference channel constituted by two energy harvesting transmitters and two receivers.

Since wireless sensor networks (WSNs) are energy-limited, energy harvesting has been investigated in the context of sensor networks [11, 16]. Specifically, in [11], two classes of ARQ protocols were considered for ensuring reliable data collection by energy harvesting sensor nodes. The authors of [16] formulated a Markov Decision Process framework for energy harvesting aided WSNs and developed decision policies for maximizing the quality of coverage.

A system that uses energy harvesting relays was contrasted to one that uses conventional cooperative relays in [13], where it was observed that the energy usage at the relay node and its availability for relaying depends not only on the harvesting rate of the energy harvesting process, but also on the transmit power settings as well as on the total number of relay nodes in the system. On the other hand in [38], optimal power allocation was proposed both for conventional and for buffer-aided link-adaptive energy harvesting relaying systems,

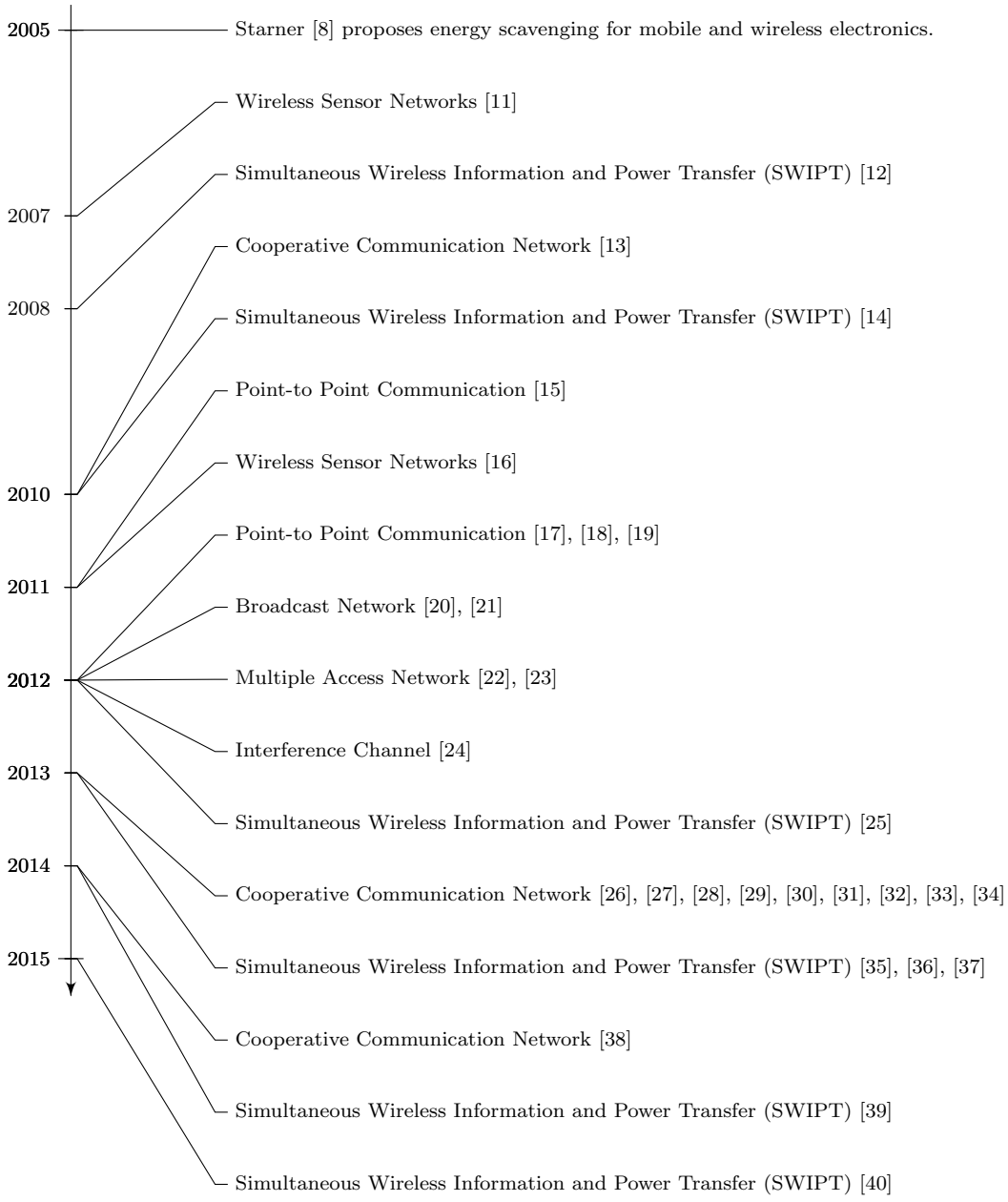

Figure 1.4: Time-line for the evolution of different energy-harvesting networks.

Year	Author(s)	Contribution
2007	Marco Tacca *et al.* [11]	Cooperative and Reliable ARQ protocols for Energy Harvesting Wireless Sensor nodes.
2010	Medapally & Mehta [13]	Voluntary Energy Harvesting Relays and Selection in Cooperative Wireless Networks.
2011	Omur Ozel *et al.* [15]	Transmission with Energy Harvesting Nodes in Fading Wireless Channel: Optimal Policies.
2011	Li & Sikdar [16]	Relay Usage Scheduling in Sensor Networks with Energy Harvesting.
2012	Yang & Ulukus [17]	Optimal Packet Scheduling in an Energy Harvesting Communication System.
2012	Tutuncuoglu & Yener [18]	Optimum Transmission Policies for Battery Limited Energy Harvesting Nodes.
2012	Ozel & Ulukus [21]	Optimal Broadcast Scheduling for an Energy Harvesting Rechargeable Transmitter with a Finite Battery Capacity.
2012	Yang & Ulukus [22]	Optimal Packet Scheduling in a Multiple Access Channel with Energy Harvesting Transmitters.
2012	Tutuncuoglu & Yener [24]	Sum-Rate Optimal Power Policies for Energy Harvesting Transmitters in an Interference Channel.
2012	Xun Zhou *et al.* [25]	Wireless Information and Power Transfer: Architecture Design and Rate-Energy Tradeoff.
2013	Orhan & Erkip [27]	Throughput Maximisation for Energy Harvesting Two Hop Networks.
2013	Liang Liu *et al.* [37]	Wireless Information and Power Transfer: A Dynamic Power Splitting Approach.
2014	Imtiaz Ahmed *et al.* [38]	Power Allocation for Conventional and Buffer Aided Link Adaptive Relaying Systems with Energy Harvesting Nodes.
2015	Rong Zhang *et al.* [40]	Energy Pattern Aided Simultaneous Wireless Information and Power Transfer.

Table 1.1: Major contributions to the development of network models for energy harvesting aided communication.

where an EH source transmits data to the destination via an EH aided decode and forward relay node. In contrast to conventional relaying, where the source and relay transmit in consecutive time slots, the transmission process of a buffer- aided link-adaptive scheme is based on a selection process (determining whether the source or the relay transmits). This depends on the state of the Source-Relay and Relay-Destination links as well as on the amount of energy available at the source and relay node. The problem of throughput maximization in energy harvesting two-hop networks relying on half-duplex relays and on successive relaying is investigated in [27] by analysing the impact of multiple relays and energy harvesting on the average throughput of the system.

The principle of SWIPT is closely related to the above-mentioned energy harvesting networks. In SWIPT, the transmitter transmits an RF signal, which is then used by the receiver to harvest energy as well as to detect the information [40]. To be more precise, in [40], Zhang *et al.* defined energy pattern aided SWIPT, where the information is implicitly transmitted both by the specific Receive Antenna (RA) pattern to which power is delivered as well as by the discretized intensity of the signal assigned to that RA pattern. In contrast to the conventional process of modulating the carrier for transmission, Zhang *et al.* proves that this energy pattern aided signal is capable of operating both in hybrid [25] as well

as in a power-split mode [37], whilst relying on low-complexity non-coherent detection. Using simulations and analytical results supported by propositions and lemmas, Zhang *et al.* confirms that this system is immune to degradation due to power conversion. Finally, the rate-power trade-off encountered in SWIPT was discussed.

Based on the above discussions, it may be concluded that having energy-harvesting capabilities at wireless devices provides a beneficial solution to energy constrained communications. Thus, the battery-powered wireless nodes, which otherwise become dis-functional once their batteries are drained, can revive themselves by harvesting energy from the surroundings and prolong the lifetime of the network.

1.3 Historical overview of Device-to-Device Communication

Device-to Device (D2D) communication enables direct communication between two devices in each other's close proximity without relaying the information through the base station. Thus, D2D communication can offload the traffic handled by the BS, which improves the latency as the end-users exchange information directly without any intervention of the BS as well as significantly enhancing the spectral efficiency by reusing the same radio resource as that assigned in the cellular network. D2D communication may not have dedicated channel resources, instead the D2D pairs tend to reuse the resources of existing mobile users (MUs). Cellular resources are limited and when D2D communication are supported under the coverage of a cellular network, the judicious allocation of cellular resources is a critical concern. Hence efficient resource reuse schemes have been studied in literature.

However, in such a co-channel sharing mode, D2D links may reuse either the uplink (UL) or downlink (DL) resources of MUs for their direct communications, thereby generating interference. When the D2D links reuse the downlink resources, they will experience interference from the BS in the same macrocell, from other co-channel D2D links in the same macrocell, from BS and co-channel D2D links in other macrocells. By contrast, in downlink reuse by the D2D link, the MU will experience interference from all the co-channel D2D links (present in the same as well as in the other macrocells) and from the co-channel MUs from other macrocells. On the other hand, when the D2D links reuse uplink resources, they will experience interference from all co-channel MUs as well as D2D links present both in the same macrocell and in other macrocells. For MUs transmitting in the uplink, the MBS is the receiver, hence the interference comes from all the co-channel D2D links (both in the same and in other macrocells) and from the co-channel MUs of other macrocells [43].

Since D2D communication underlaying cellular networks results in numerous new interference scenarios, the interference can be mitigated by using Inter-Cell Interference Coordination (ICIC), relying on Fractional Frequency Reuse (FFR) [44] and Soft Frequency Reuse (SFR) [45]. In FFR and SFR, the interference is eliminated by differentiating the frequency bands among the cells as well as by using frequency partitioning within the cell as the cell centre (CCR) and cell edge region (CER). These frequency reuse techniques have been richly investigated in the literature for different network models [46, 47, 48, 49, 50].

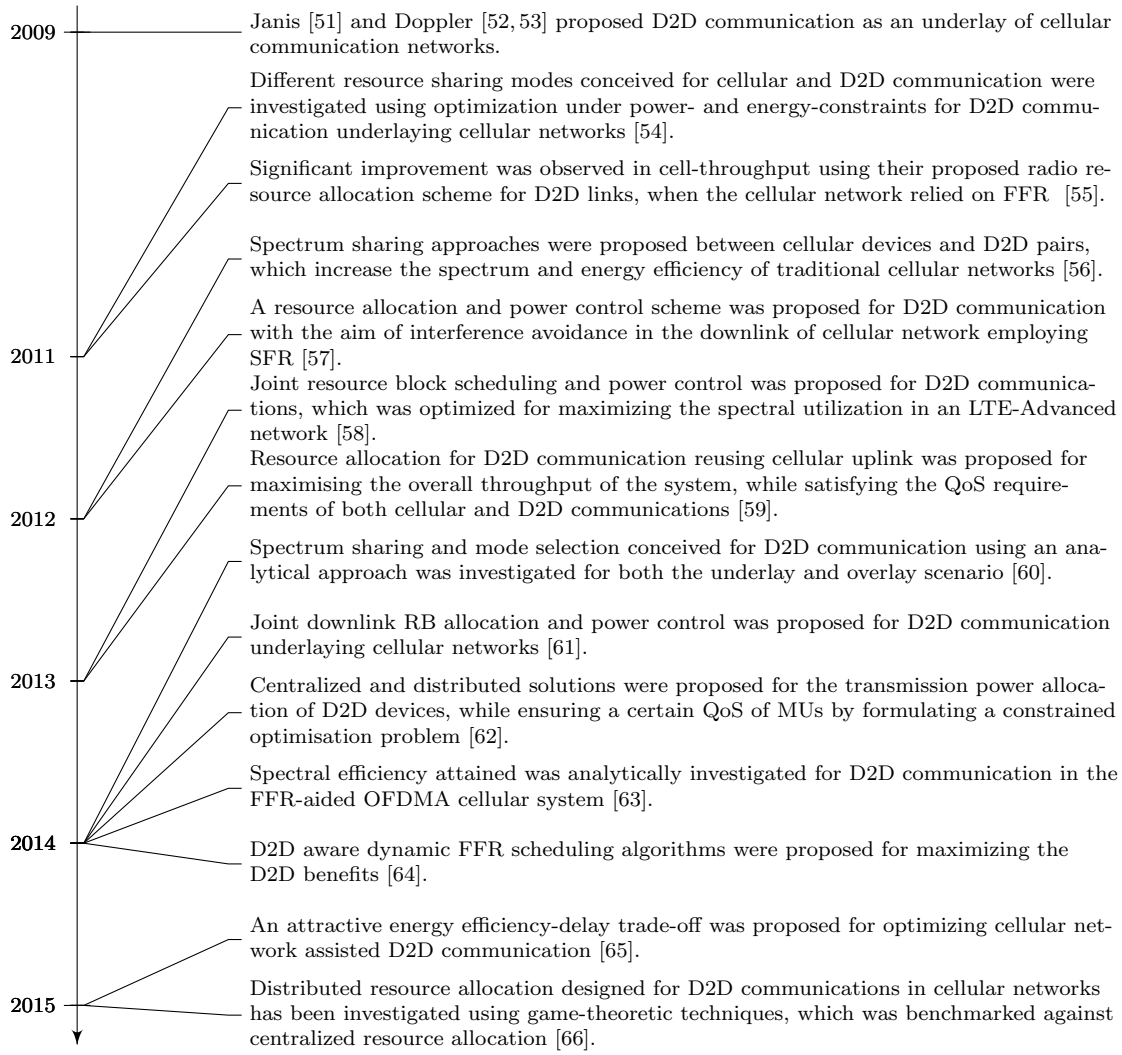

Figure 1.5: Time-line of the evolution of D2D communications.

In [46], the authors derived the throughput attained using the optimal threshold distance to partition the CER and CCR users. An algorithm was proposed in [47] for improving the network capacity and the cell-edge performance for a dynamic SFR deployment relying on realistic irregularly shaped cells. Distributed antenna system aided FFR was invoked for maximising the cell-throughput and coverage in [48]. The authors of [49] analysed the coverage probability of the frequency allocation schemes proposed for picocell users, when the macrocell employed both FFR and SFR. As a further advance, in [50], the authors proposed a so-called spectrum swapping access strategy for twin-layer networks supported by FFR.

For the sake of efficiently realizing D2D communication, it is essential to carefully manage these interference scenarios jointly with resource allocation in order to keep the interference level imposed on the MUs by D2D communication below a certain level for ensuring the quality of service (QoS) required by the MUs, whilst the requirements of D2D link should also be fulfilled with adequate quality. The literature of the resource allocation algorithms conceived for D2D communication underlaying cellular networks is summarised in Figure 1.5.

D2D communication underlaying cellular networks was conceived as a promising solution for improving the spectral efficiency of a system by Janis [51] and Doppler [52, 53]. In particular, [51] proposed a power control scheme for D2D links sharing the uplink resources of a cellular network. The authors of [52] proposed mechanisms for D2D session set-up and management involving the LTE-advanced system architecture, while Doppler *et al.* [53] investigated the feasibility of D2D as an underlay in an LTE-advanced network as well as a range of solutions invoked for controlling the interference introduced by D2D communication into the cellular network. Different cellular or D2D communication modes as well as orthogonal and non-orthogonal resource sharing modes were analysed for optimizing the sum-rate attained under specific spectral efficiency and energy constraints by Yu *et al.* in [54]. Diverse radio resource allocation schemes were proposed by Chae *et al.* for D2D communication in an FFR aided cellular network in [55]. Different design aspects of peer discovery mechanisms, physical layer procedures and radio resource management algorithms were conceived for minimizing interference both amongst the D2D pairs as well as between the D2D and cellular layers by Fodor *et al.* in [56]. In [57], resource allocation and power control was proposed for interference avoidance in D2D communication, when the cellular network relies on SFR.

In [59], Feng *et al.* proposed a three-step solution, including QoS aware admission control of D2D pairs, optimal power control designed for D2D pairs as well as their reuse partners for maximising the overall throughput of the system, when the D2D communications reuse the uplink resources. Hossain *et al.* [58] observed an improvement in spectrum utilization at the expense of a slight increase in power consumption for their proposed joint RB scheduling and power control algorithm designed for D2D communication underlaying the LTE-advanced network. D2D spectrum sharing and mode selection was investigated for both underlay and overlay scenarios in [60], where the analytical rate and coverage were derived, when the D2D links reuse the uplink resources of the cellular network. By contrast, in [61] downlink resource reuse was considered for D2D links, where a utility maximisation algorithm was proposed for joint resource allocation and power control under specific power budget and QoS constraints. Yin *et al.* [66] proposed a centralized resource allocation scheme in form of a non-convex optimization problem, which was solved using a convex approximation method along with a distributed resource allocation scheme as a Stackelberg model conceived for D2D communication in the cellular uplink. By contrast, in [65], a stochastic optimization problem was formulated for investigating the energy efficiency-delay trade-off, while ensuring network stability, average power and interference control constraints, when the D2D links reuse the uplink of a cellular network.

In a nutshell, D2D communication provides an economically favourable solution for improving the spectrum exploitation by reusing the resources of the existing cellular network, without relaying through the base station. This in turn offloads the traffic from the base station, improves the latency, and reduces the power consumption at the expense of introducing additional interference in the network.

Year	Author(s)	Contribution
2015	Sakr & Hossain [67]	Cognitive and Energy Harvesting-Based D2D Communication in Cellular Networks: Stochastic Geometry Modelling and Analysis.
2016	Howard H. Yang *et al.* [68]	Heterogeneous Cellular Network With Energy Harvesting-Based D2D Communication.
2016	Yuanwei Liu *et al.* [69]	Secure D2D Communication in Large-Scale Cognitive Cellular Networks: A Wireless Power Transfer Model.
2016	Li Jiang *et al.* [70]	Social-aware energy harvesting device-to-device communications in 5G networks.
2017	Zhenya Zhou *et al.* [71]	Energy-Efficient Stable Matching for Resource Allocation in Energy Harvesting-Based Device-to-Device Communications.
2017	Han & Huang [72]	Wirelessly Powered Backscatter Communication Networks: Modelling, Coverage, and Capacity.
2017	Joo & Kang [73]	Joint scheduling of data transmission and wireless power transfer in multi-channel device-to-device networks.
2017	Kaifeng Guo *et al.* [74]	D2D Underlaying Massive MIMO TWRN With Opportunistic Energy Harvesting.
2017	Ying Luo *et al.* [75]	Resource Allocation for Energy Harvesting-powered D2D Communication underlaying Cellular Networks.

Table 1.2: Major contributions in EH aided D2D communication.

1.4 Historical Perspective on Energy Harvesting Aided Device-to-Device Communication

Having discussed EH and D2D communication as a solution for the improvement of energy efficiency and spectral efficiency, respectively, it is necessary to integrate them for the sake of improving the design of future wireless networks. However, the research of EH aided D2D communication is still in its infancy, despite the pioneering studies mentioned in Table 1.2. Specifically, Sakr and Hossain [67] relied on the stochastic geometry approach for analysing the proposed spectrum access policies in the context of cognitive D2D communication harvesting RF energy from the ambient interference in a multi-channel uplink-downlink cellular scenario. By contrast, Liu *et al.* [69] employed stochastic geometry for characterizing the system's security level by designing wireless power transfer policies for D2D communication underlaying a cognitive cellular network, where wireless energy is harvested from power beacons and secure transmission takes place using the spectrum of the primary MBS. In [68], Yang *et al.* proposed efficient mode selection and derived the outage probability of mobile relays harvesting energy from access points for supporting D2D communication in heterogeneous networks. By contrast, in [70], Jiang *et al.* integrated energy harvesting and social networking with D2D communication for improving both the spectrum and energy efficiency of local data dissemination.

In [71], Zhou *et al.* formulated a joint power control and partner selection problem for optimizing the energy efficiency of D2D pairs reusing the cellular downlink, where D2D receivers/ cellular users harvest RF energy from their received desired transmission as well as from the interference relying on the so-called power splitting model. As a further develop-

ment, Han & Huang [72] used stochastic geometry to derive both the network capacity and the success probability of D2D transmission, which relies on the backscatter communication model powered using wireless power transmission by power beacons. Joo and Kang [73] investigated the joint scheduling problem of data transmission and wireless power transmission in multi-channel D2D communication and proposed a heuristic solution relying on greedy scheduling. In [74], Guo *et al.* characterized opportunistic energy harvesting aided D2D communication underlaying massive MIMO along with power saving by cellular users at the expense of a reduced cellular rate. Finally, in [75] Luo *et al.* derived optimal lower bound and a heuristic algorithm for a spectrum matching and power allocation problem in energy harvesting powered D2D communication.

In a nutshell, future wireless networks are facing energy and spectrum scarcity problems due to the proliferation of smart hand-held devices as well as mobile multimedia services, which are both power and bandwidth hungry. Therefore, energy harvesting aided D2D communication offers a promising solution for circumventing the impending problem of energy and spectrum scarcity in future wireless communication networks.

1.5 Novel Contributions

The novel contributions of this thesis are summarised below:

- With the aim of improving the energy efficiency by employing energy harvesting, an optimal and reduced-complexity sub-optimal transmission policies are conceived for a two-hop successive relaying network considering energy harvesting transmission nodes. The proposed system relies on finite energy and finite data storage buffers at the EH nodes as well as on the idealized non-causal knowledge of the energy arrivals at all EH nodes. An optimization problem is formulated for the throughput maximisation of the successive relaying aided network, which is solved using the Interior Point Optimization (IPOPT) method. The proposed low complexity sub-optimal transmission scheme is capable of approaching the performance of its optimal counterpart [1].

- In order to address the design criterion of spectral efficiency, we considered D2D communication relying on downlink resource reuse in a cellular network employing FFR and SFR. Inspired by the FFR scheme itself, the D2D links are classified into two categories based on a signal-to-interference-ratio (SIR) threshold, namely the short-range (SR) D2D links as well as the long-range (LR) D2D links and proposed the pair of fractional frequency allocation schemes seen in Figure 3.1(a) for D2D links, when the macrocell relies on an FFR scheme. The frequency allocation scheme of Figure 3.1(b) is proposed for the D2D links, when the macrocell has employed a SFR scheme. The coverage probability and the capacity of the D2D links corresponding to all the proposed schemes are derived analytically and were contrasted against that of the benchmark scheme, where the macrocell relies on UFR [2].

- Having explored both the energy efficiency and the spectral efficiency individually, EH capabilities are incorporated into D2D communication that relies on reusing the cellular downlink resources of multiple mobile users. The resource allocation is optimized by finding the optimal power allocation, transmission duration and D2D-MU matching formulated as a sum-rate maximization problem for the D2D links, whilst satisfying the QoS constraints of the MUs and the EH constraints of the D2D links. Efficient algorithms are also proposed for the joint optimization of D2D links for both the idealised non-causal and for the realistic causal knowledge of EH profiles, which are also often termed as off-line and on-line knowledge, respectively. The off-line algorithm invokes the classic Lagrangian Multiplier method, while the on-line algorithm employs a classic dynamic programming (DP) technique for simplifying the original high-complexity problem by partitioning it into smaller sub-problems, which rely on the Lagrangian multiplier method for each stage [3].

- In order to further exploit the available spectrum as well as the infrastructural investments of mobile network operators, the potential of EH aided D2D communication in a two-tier heterogeneous network (HetNet) is also explored for supporting multiple MUs that are associated either with macro-BS (MBS) or with pico-BSs (PBSs) under various spectrum sharing arrangements. The *co-orthogonal spectrum sharing* philosophy is proposed, which is a unification of the pair of richly investigated orthogonal and co-channel spectrum sharing strategies among the base stations. This arrangement reduces the interference imposed, when compared to the classic co-channel deployment and improves the spectrum exploitation of the orthogonal deployment [4].

- The resource allocation conceived for EH aided D2D communication underlaying a HetNet is formulated as an optimization problem maximizing the D2D sum-rate. This is achieved by invoking the joint optimization of the D2D-MU matching and the power allocation of both the D2D links as well as of the MUs, without violating the throughput constraints of the MUs and without exceeding the power budget constraints as well as the EH constraints of the D2D links. Based on the theoretical analysis of the optimization problem relying on Lagrangian method of Multipliers, an algorithmic solution is proposed which is termed as the *Joint Optimization of Resource Block and Power Allocation(JORPA)* for D2D links. The low-complexity heuristic methods are also conceived, which rely on the optimization of either the D2D transmission power or of the D2D-MU matching, while heuristically obtaining the other [4].

1.6 Outline of the Thesis

Finally, the structure of the thesis is described which is also summarized in Figure 1.6.

- **Chapter 2: Buffer-Aided Successive Relaying Network Employing Energy Harvesting**

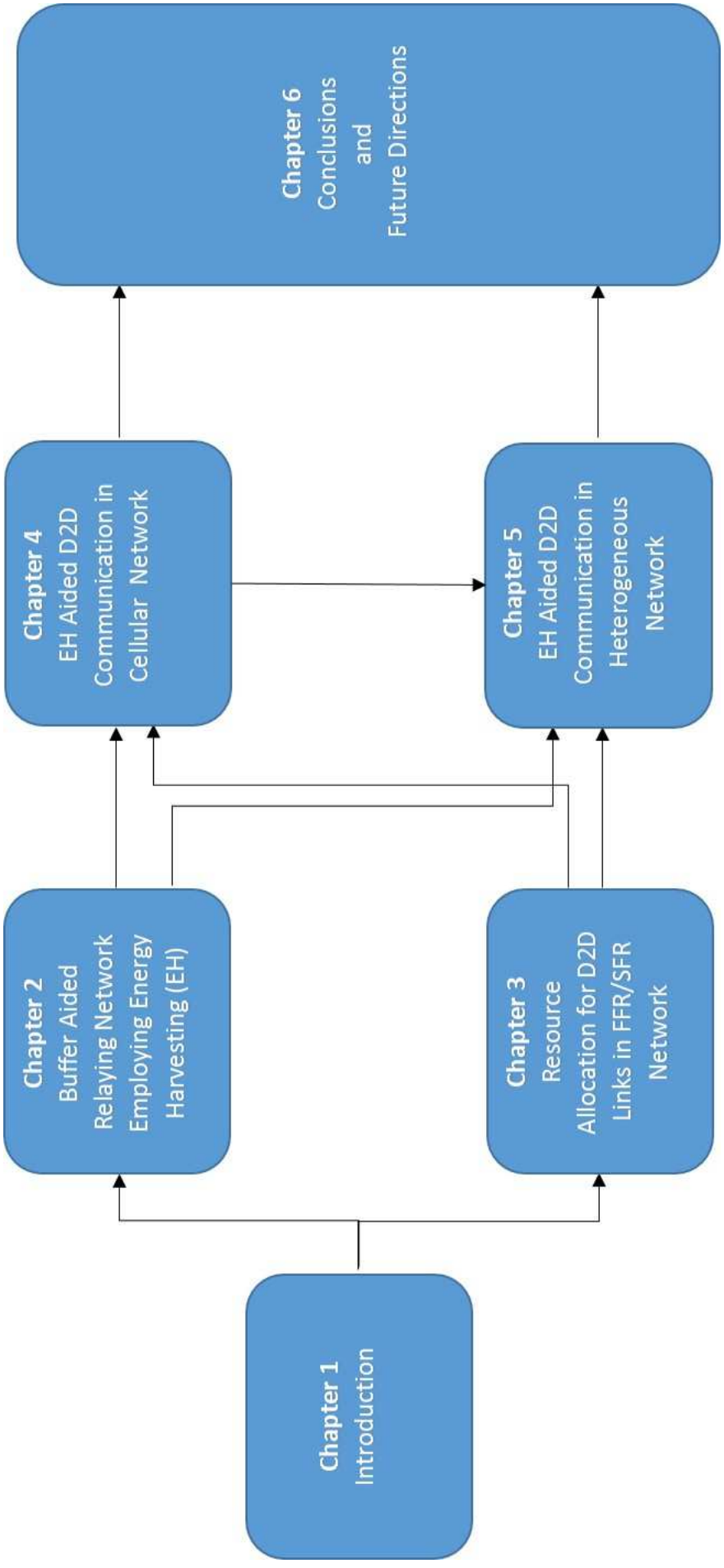

Figure 1.6: Structure of the thesis.

In Chapter 2, different aspects of energy harvesting is focussed in the context of a two-hop co-operative network relying on successive relaying with the objective of maximizing the throughput of the system. In Section 2.1, the discussions are commenced by introducing the different energy harvesting aided network models studied in the literature, which forms the basis of constructing the two-hop system model in Section 2.2. Then the properties of the optimal transmission policy are discussed before presenting the throughput maximization problem in Section 2.3. More specifically, the proposed optimal and sub-optimal transmission policies are presented in Sections 2.3.1 and 2.3.2, which are solved using the classic interior point optimization method. Finally, the quantitative analysis of the network model is facilitated for different parametric settings in Section 2.4.

- **Chapter 3: Resource Allocation for D2D Links in the FFR and SFR Aided Cellular Downlink**

  In Chapter 3, *device-to-device communication* is explored as a technique of improving the spectral efficiency in Section 1.1. More specifically, D2D communication relying on reusing the downlink resources of a cellular network in conjunction with Inter-Cell Interference Coordination (ICIC) schemes is focused. Commencing with the review of the fractional frequency reuse (FFR) and of the soft frequency reuse (SFR) ICIC schemes of Figure 3.1, the network model is described that consists of D2D pairs reusing the downlink frequency resources of multiple mobile users in Section3.2. The coverage probability and the capacity of D2D links is analytically characterized in Section 3.3. Explicitly in Section 3.3.1, the coverage probability of D2D links is derived for the pair of frequency allocation schemes proposed for D2D links, when the cellular network employs FFR. This is followed by Section 3.3.2, where the coverage probability is derived for another frequency allocation scheme, when SFR is considered. In Section 3.3.3, the analytical expressions for the capacity of D2D links under different frequency allocation schemes is obtained. Finally, the analysis of the performance of the proposed frequency allocations schemes against the unity frequency reuse scheme is presented in Section 3.4.

- **Chapter 4: Energy Harvesting Aided Device-to-Device Communication Underlaying the Cellular Downlink**

  As discussed in Section 1.1, for achieving both high energy and spectral efficiency, it is imperative to merge energy harvesting and D2D communication technologies. Hence, in Chapter 4, the integration of energy harvesting capabilities into D2D communication is explored, when D2D links employ downlink resource reuse. More specifically, Section 4.1 commences with the review of D2D communication in the context of energy harvesting followed by description of the system model in Section 4.2.1. The formulation of the D2D sum-rate maximization problem is given in Section 4.2.2. Proceeding to Section 4.3, the joint optimization algorithms are proposed relying on the classic Lagrangian method of multipliers for constrained optimization in the context of non-causal and causal knowledge of the EH profile of D2D links, termed as *off-line* and *on-line* joint optimization algorithms. Finally, the performance of the

proposed algorithms under different parametric settings is discussed in Section 4.4.

- **Chapter 5: Energy Harvesting Aided Device-to-Device Communication in the Over-Sailing Heterogeneous Two-Tier Downlink**

  In Chapter 5, energy harvesting aided D2D communication is further characterized in the context of a two-tier heterogeneous network. More specifically, considering a two-tier HetNet supporting multiple D2D pairs and mobile users associated with either a macro-base-station or a pico-base-station is presented, under different spectrum sharing strategies. Beginning with the review of EH aided D2D communications in the context of HetNets in Section 5.1. This is followed by the description of the system in Section 5.2, where the proposed *co-orthogonal spectrum sharing* and the richly documented spectrum sharing schemes of Figure 5.3 are discussed along with various mobile user association criteria as well as with the formulation of the sum-rate maximization problem. The original non-convex problem is next transformed to a more tractable convex problem, which is solved by the proposed *joint optimization of resource block and power allocation (JORPA)* algorithm invoking the Lagrangian method of multipliers for constrained optimization in Section 5.3. Some low-complexity heuristic algorithms are also presented s in Section 5.4. Finally, the performance of the JORPA algorithm as well as the heuristic algorithm is quantified for different system settings in Section 5.5.

- **Chapter 6: Conclusions and Future Directions**

  Chapter 6 summarizes the main results of this thesis and outlines a range of promising future research directions.

Chapter 2

Buffer-Aided Successive Relaying Network Employing Energy Harvesting

2.1 Introduction

Cooperative communication is capable of attaining significant throughput and reliability improvements, where the source node (SN) and cooperating relay nodes (RN) expend their energy, while processing and transmitting the signal to the destination node (DN). The nodes are typically powered through pre-charged batteries, but once these batteries are drained, the nodes become dis-functional [13], [38]. As it is mentioned in introductory chapter that an emerging solution to this design problem of energy efficiency is the use of energy harvesting (EH) [13]- [27]. The node with energy harvesting abilities has to be capable of accommodating the random arrivals of energy and its storage for utilising it later [10].

As it has been made apparent in Chapter 1, EH communication systems have been studied under different network models ranging from a single-user EH system in [17, 18, 76] to more complex EH aided broadcast channel in [20, 77] to two-way OFDM communications [78] to cooperative networks [13, 38, 27, 34, 79, 80], where the transmitting nodes have energy harvesting capability. Specifically, in [13], Medepally and Mehta investigated the benefits of relay selection relying on multiple EH amplify-and-forward RNs, whenever they have sufficient energy for transmission. By contrast, in [38] information-buffer-aided link activation was used, which was controlled both by the quality of the links as well as by the amount of energy buffered at these nodes. Two-hop networks relying either on a single or on a pair of parallel RNs using a successive relaying protocol were investigated for quantifying the benefits of both multiple relays and of EH on the average throughput of the system in [27]. In [34], the authors derived the optimal achievable rates for an EH system in the context of two-way relaying employing different relaying strategies. Furthermore,

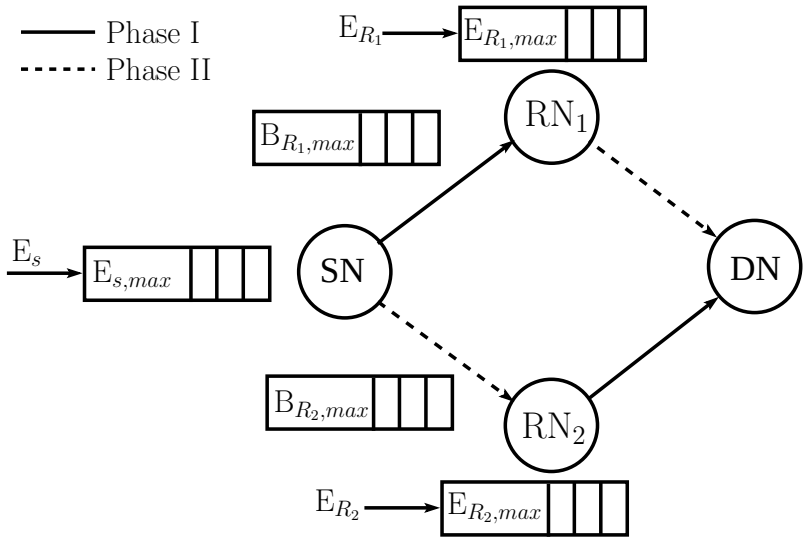

Figure 2.1: Successive Relaying Network where EH nodes are equipped with finite buffer for both energy and data storage.

a similar two-way EH relay system employing Time Division Broadcasting and Multiple Access Broadcasting , which was subjected to channel state uncertainty was considered in the context of joint energy and transmit time allocation in [79]. Utilising the structure of specific problem and generalised optimality principle, the authors of [80] formulated a new algorithm for constrained utility maximisation problems encountered in cooperative network of wireless sensor nodes.

Inspired by the performance of cooperative communication systems relying on EH nodes, this chapter considers a successive relaying model, which is capable of mimicking a full duplex (FD) RN, despite relying on a pair of half duplex (HD) RNs, which are activated alternately in their transmitter and receiver modes in order to create a virtual FD relay. This HD regime reduces the complexity of the FD system, since the FD RN would require high-complexity interference cancellation at the receiver. Whilst proof-of-concept studies are indeed valuable, the ultimate purpose of most engineering studies is to attempt a real-world implementation of the proposed techniques. The model relies on the realistic constraint that EH nodes (SN, $RN1$, $RN2$) have a finite energy storage capacity and that the RNs also have limited data buffers for storing the source data. Therefore, through this study, the valuable proposals of [27] are aimed for taking a step closer to its real-world deployment. Explicitly, the novel contributions of this chapter are as follows [1]:

- A practical successive relaying model is defined constrained both by limited energy and data storage buffers at the EH nodes, which dispenses with the idealised simplifying assumption of having infinite buffers [27].
- An optimization problem is formulated for the throughput maximisation of the successive relaying aided network of Figure 2.1 having finite buffers as well as relying on the idealized non-causal knowledge of the energy arrivals at all EH nodes, which is solved using the Interior Point Optimization (IPOPT) method.
- A sub-optimal transmission scheme is also proposed that is capable of approaching the

performance of its optimal counterpart at a significantly reduced complexity, which is achieved at the expense of a marginally degraded performance.

The rest of the chapter is laid out as mentioned in Figure 2.2. The buffer-aided two-hop cooperative communication based network model relying on energy harvesting is presented in Section 2.2, which is followed by the formulation of the optimization problem in Section 2.3. Both the optimal and sub-optimal transmission policies are invoked in this section. The performance results are discussed in Section 2.4, whilst the conclusions are offered in Section 2.5.

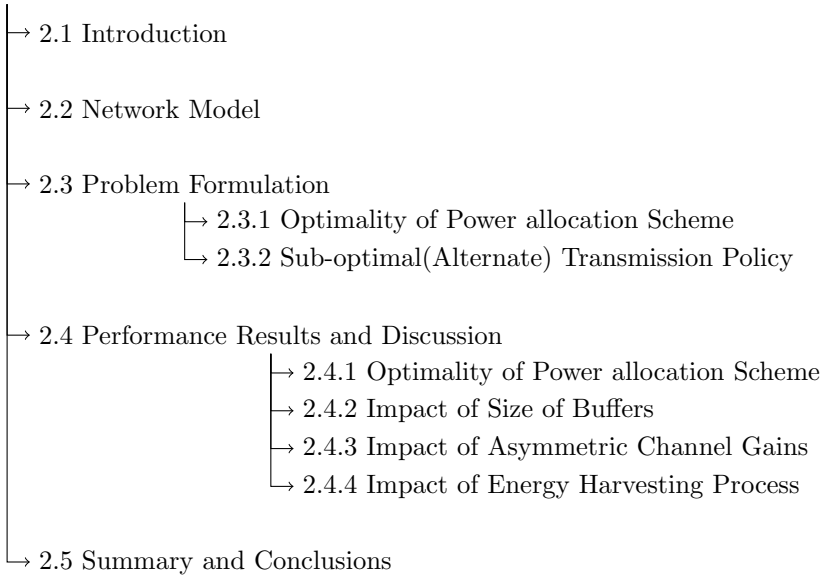

Figure 2.2: The structure of this chapter.

2.2 Network Model

Consider the successive relaying technique of [27] having two phases, where the RNs assist the SN′s transmission to the DN, as shown in Figure 2.1. In Phase I of Figure 2.1 the SN transmits to RN_1 while RN_2 simultaneously transmits to the DN. By contrast in Phase II of Figure 2.1, SN and RN_1 transmit simultaneously both to RN_2 and to DN, respectively. Thus the SN is always transmitting, while the DN is always receiving during the process.

It is assumed that there is no direct link between SN-DN and RN_1-RN_2, as well as that these are decode-and-forward (DF) HD RNs that are located sufficiently far apart from each other for avoiding any interference. Energy harvesting capability is considered at SN, RN_1 and RN_2 and finite energy buffers that can store a maximum of $E_{S,max}$, $E_{R1,max}$ and $E_{R2,max}$ units respectively, while RN_1 and RN_2 are also equipped with data buffers of $B_{R1,max}$ and $B_{R2,max}$ packets, respectively. Since the energy arrival events across the nodes follows non-uniform time series, therefore for ease of exposition, merging these arrival events into a single time series $(t_0, t_1, ..., t_K)$ by considering zero amount of energy arrivals at the nodes that do not harvest energy at some instant t_k. More explicitly, the EH processes at

the EH nodes are independent of each other. In other words, the energy arrival instances of a node may be different from those of the other nodes. For example, assume that an energy arrival occurred at node RN_1 at some instant t_k, while there was no energy arrival at the other nodes (SN and RN_2) at the time instant t_k. In the mathematical analysis, it is assumed that at time instant t_k, nodes SN and RN_2 harvested zero amount of energy. We set $t_0 = 0$ and $t_K = T$. The amount of energy harvested at SN, RN_1 and RN_2 at time instant t_k is represented as $E_{S,k}$, $E_{R1,k}$ and $E_{R2,k}$ unit, respectively, for $k = 0, 1, ...K-1$. The time interval between the two consecutive energy arrivals is termed as an *epoch*, whose length is defined as $\tau_k = t_k - t_{k-1}$. The complex-valued channel gains are considered to be constant throughout the communication process preceding the deadline. The channel gain between the nodes L and M is denoted as H_{LM}, where $L \in \{SN, R_1N, R_2N\}$ and $M \in \{RN_1, RN_2, DN\}$.

The throughput maximisation problem is considered under the idealized simplifying assumption of having prior knowledge about the energy arrivals at all the EH nodes before the commencement of the communication process. The energy expended at the nodes is assumed to be only the transmission energy and that perfect 'capacity-achieving' codes are used, which facilitate operation exactly at the Shannon capacity, thus determines the rate versus power relationship of a given link, expressed as:

$$r[p(t)] = \log_2[1 + Hp(t)] \tag{2.1}$$

where H is the channel gain of the link normalized w.r.t. the noise power and $p(t)$ is the transmission power of the node at time t. As a result of energy arrivals over the time and as a benefit of the energy storage capacity at the nodes, any feasible transmission policy should satisfy following constraints:

(a) Energy Causality Constraint: The total energy expended by a node during its transmission session should not exceed the total energy harvested by that node until that time.

(b) Energy Overflow Constraint: The energy exceeding the storage capacity of the energy buffer at the node is lost owing to overflow.

(c) Data Causality Constraint: The total data transmitted by a node during the process should not exceed the total data received by that node until that time.

(d) Data Overflow Constraint : The amount of data exceeding the storage capacity of data buffer is lost due to overflow.

2.3 Problem Formulation

In this section, some properties of the optimal transmission policy are first stipulated in the following lemmas, which will be used for formulating the throughput maximisation problem for the system of Figure 2.1.

Lemma 1. *The transmission rate/power of a node is constant between two consecutive energy arrivals, but potentially changes when new energy arrives at the node [27].*

Proof. This proof is an extension of that derived for point-to-point case in [17] to the two-hop scenario defined in this chapter. Let us assume that the transmitter nodes (SN,RN_1,RN_2) change their transmission rate between two EH instances t_i, t_{i+1}. Let us furthermore denote the rates as $r_{M,n}$, $r_{M,n+1}$ and the instant when the rate changes as t'_i, where $M \in \{SI, R2\}$ in Phase I and $M \in \{SII, R1\}$ in Phase II of the successive relaying protocol. Correspondingly, the duration of each phase can be written as $L_{I,n}$, $L_{I,n+1}$, $L_{II,n}$ and $L_{II,n+1}$. Let us now consider the duration $[t_i, t_{i+1})$. The total energy consumed in this duration at SN is $p_{SI,n}L_{I,n} + p_{SII,n}L_{II,n} + p_{SI,n+1}L_{I,n+1} + p_{SII,n+1}L_{II,n+1}$. Similarly, the total energy consumed at RN_1 is $p_{R1,n}L_{II,n} + p_{R1,n+1}L_{II,n+1}$ and that at RN_2 : $p_{R2,n}L_{I,n} + p_{R2,n+1}L_{I,n+1}$. Let us now consider SN in more detail and define:

$$
\begin{aligned}
p'_{SI} &= \frac{p_{SI,n}L_{I,n} + p_{SI,n+1}L_{I,n+1}}{t_{i+1} - t_i}, \\
p'_{SII} &= \frac{p_{SII,n}L_{II,n} + p_{SII,n+1}L_{II,n+1}}{t_{i+1} - t_i} \\
r'_{SI} &= r(p'_{SI}) = r\left(\frac{p_{SI,n}L_{I,n} + p_{SI,n+1}L_{I,n+1}}{t_{i+1} - t_i}\right) \\
r'_{SII} &= r(p'_{SII}) = r\left(\frac{p_{SII,n}L_{II,n} + p_{SII,n+1}L_{II,n+1}}{t_{i+1} - t_i}\right);
\end{aligned}
$$

Let us now use these r'_{SI}, r'_{SII} as the new transmission rates for Phase I and II at SN over $[t_i, t_{i+1})$, and keep the rest of the rates same as in original policy. It is easy to observe that the new transmission policy is feasible, since all the energy constraints are satisfied under this policy. On the other hand, the total number of packets that are departed from SN in both of the phases over this duration under this new policy can be written as:

$$
\begin{aligned}
&(r'_{SI} + r'_{SII})(t_{i+1} - t_i) = (r(p'_{SI}) + r(p'_{SII}))(t_{i+1} - t_i) && \text{(2.3a)} \\
&= \left(r\left(\frac{p_{SI,n}L_{I,n} + p_{SI,n+1}L_{I,n+1}}{t_{i+1} - t_i}\right)\right)(t_{i+1} - t_i) + && \text{(2.3b)} \\
&\qquad \left(r\left(\frac{p_{SII,n}L_{II,n} + p_{SII,n+1}L_{II,n+1}}{t_{i+1} - t_i}\right)\right)(t_{i+1} - t_i) \\
&\geq (r(p_{SI,n})L_{I,n} + r(p_{SI,n+1})L_{I,n+1}) + (r(p_{SII,n})L_{II,n} + r(p_{SII,n+1})L_{II,n+1}) && \text{(2.3c)} \\
&= r_{SI,n}L_{I,n} + r_{SI,n+1}L_{I,n+1} + r_{SII,n}L_{II,n} + r_{SII,n+1}L_{II,n+1} && \text{(2.3d)}
\end{aligned}
$$

where the inequality in Eq. (2.3c) follows from Eq. (2.1) of Section 2.2, which is a concave function of the transmission power p. Therefore, the total number of packets transmitted by SN in this duration under the new policy is higher than those that are departed under the original policy. Similarly, it can be proved that the RNs under this new policy will send more data to DN. If all the rates are kept constant, the transmissions will deliver larger

amounts of data to DN by the deadline. This contradicts to the optimality of the original transmission policy. □

Lemma 2. *Any transmission policy that yields battery overflow is strictly suboptimal policy.*

Proof. The proof for point to point link is given in [18] as Lemma 2, which can be easily extended to the case of two hops. □

Lemma 3. *The feasible transmission policy ensures that the relays are always on without decreasing the throughput of the system [27].*

Proof. The proof derived for the two-relay case extends the single-relay case of [81]. In the case of two parallel relays, consider a feasible transmission policy where one of the relays (say RN_1) is not always on, i.e. it is not transmitting or receiving data all the time. Now, if an idle time interval exists right at the beginning of Phase I, the epoch of SN in Phase II can be extended, ensuring that there is no idle time. Note that this strategy continues to satisfy all the causality and storage constraints. On the other hand, if an idle time duration occurs at the beginning of Phase II, the epoch of relay RN_1 can be delayed without violating the feasibility of the policy, because it can store more energy in the meanwhile and the previous argument can be used to extend the epoch of RN_2 during Phase I to avoid any idle time. Similarly, it can be considered in the scenario, when RN_2 is not always on. Therefore, the idle times can be removed by increasing the transmission duration of one of the nodes (SN or RNs) while keeping the total amount of transmitted data the same. Since the rate-power relation of Eq. (2.1) is concave, the new policy conveys the same amount of data to DN, while consuming less energy. Hence it is feasible. Moreover, using this proof it can be said that there exists an optimal policy, where SN and DN are always on for the twin-relay system relying on a successive relaying protocol. □

Based on Lemmas, the optimal policy can be characterized in the following way. There is a constant transmission rate for the pair of nodes between consecutive energy arrivals according to the optimal policy, as formulated in Lemma 1. Therefore, the transmission power of SN during the Phases I and II of Figure 2.1 in an epoch is constant, and given by $p_{SI,k}$ and $p_{SII,k}$, respectively. Similarly, the transmission power of RN_1 and RN_2 is denoted as $p_{R_1,k}$ and $p_{R_2,k}$, respectively. Lemma 2 invokes the introduction of the energy overflow constraints at SN, RN_1 and RN_2 in order to avoid any battery overflow. Lemma 3 implies that the attention should be restricted to the specific transmission policies, where both RN_1 and RN_2 are always on for the sake of defining a feasible transmission policy. Thus, the total transmission time between SN-RN_1 and RN_2-DN is assumed to be the same and denote this duration of Phase I between the time instants t_{k-1} and t_k as $L_{I,k}$. Similarly, assuming the same transmission time between SN-RN_2 and RN_1-DN in Phase II, is denoted as $L_{II,k}$, $k = 1, 2, ..., K$. Finally, the optimal transmission policy is identified that defines, which particular node transmits and when, along with the specific power

allocation of each node. A sub-optimal scheme is defined, where the duration of each phase of successive relaying is fixed to a particular ratio.

2.3.1 Optimal Transmission Policy

Let us now define the optimization problem of maximising the system throughput by the deadline T. Since RN_2 initially has no data in Phase I of Figure 2.1, it is assumed without loss of generality that it starts transmission by delivering $\epsilon > 0$ amount of dummy information to DN, where ϵ is sufficiently small to be ignored for the throughput optimization problem. Upon scheduling the two phases in succession, it is ensured that there is no further throughput loss for the system. In other words, at the beginning of transmission, RN_2 possesses no data from S that can be transmitted to DN, hence it commences its transmission with ϵ dummy packets. However, subsequently, the transmission phases occur in immediate succession without any interval. This ensures that there is no need to send dummy packets and thus no further loss of system throughput is imposed. Similar assumptions were also made in [27]. The optimisation problem can be formulated as follows, where the maximisation is over variables[1], $\boldsymbol{L_I}$, $\boldsymbol{L_{II}}$, $\boldsymbol{P_{SI}}$, $\boldsymbol{P_{SII}}$, $\boldsymbol{P_{R_1}}$ and $\boldsymbol{P_{R_2}}$:

$$\underset{\substack{\boldsymbol{L_I},\boldsymbol{L_{II}},\boldsymbol{P_{SI}},\\ \boldsymbol{P_{SII}},\boldsymbol{P_{R1}},\boldsymbol{P_{R2}}}}{\text{maximise}} \quad \sum_{i=1}^{K} L_{II,i}\log_2(1+H_{R_1D}p_{R_1,i}) + L_{I,i}\log_2(1+H_{R_2D}p_{R_2,i}) \tag{2.4a}$$

$$\text{subject to}: \sum_{j=1}^{i} p_{SI,j}L_{I,j} + p_{SII,j}L_{II,j} \leq \sum_{j=0}^{i-1} E_{S,j} \qquad \forall i \tag{2.4b}$$

$$\sum_{j=1}^{i} p_{R_1,j}L_{II,j} \leq \sum_{j=0}^{i-1} E_{R_1,j} \qquad \forall i \tag{2.4c}$$

$$\sum_{j=1}^{i} p_{R_2,j}L_{I,j} \leq \sum_{j=0}^{i-1} E_{R_2,j} \qquad \forall i \tag{2.4d}$$

$$\sum_{j=0}^{i} E_{S,j} - \sum_{j=1}^{i} p_{SI,j}L_{I,j} + p_{SII,j}L_{II,j} \leq E_{S,max} \qquad \forall i \tag{2.4e}$$

$$\sum_{j=0}^{i} E_{R_1,j} - \sum_{j=1}^{i} p_{R_1,j}L_{II,j} \leq E_{R_1,max} \qquad \forall i \tag{2.4f}$$

[1]Here bold letters are used for vectors, where $\boldsymbol{L_I} = [L_{I,1}, L_{I,2}, \cdots, L_{I,K}]^T$, $\boldsymbol{L_{II}} = [L_{II,1}, L_{II,2}, \cdots, L_{II,K}]^T$, $\boldsymbol{P_{SI}} = [p_{SI,1}, p_{SI,2}, \cdots, p_{SI,K}]^T$, $\boldsymbol{P_{SII}} = [p_{SII,1}, p_{SII,2}, \cdots, p_{SII,K}]^T$, $\boldsymbol{P_{R1}} = [p_{R1,1}, p_{R1,2}, \cdots, p_{R1,K}]^T$ and $\boldsymbol{P_{R2}} = [p_{R2,1}, p_{R2,2}, \cdots, p_{R2,K}]^T$

$$\sum_{j=0}^{i} E_{R_2,j} - \sum_{j=1}^{i} p_{R_2,j} L_{I,j} \leq E_{R_2,max} \quad \forall i \tag{2.4g}$$

$$\sum_{j=1}^{i} L_{II,j} \log_2(1 + H_{R_1D} p_{R_1,j}) \leq \sum_{j=1}^{i} L_{I,j} \log_2(1 + H_{SR_1} p_{SI,j}) \quad \forall i \tag{2.4h}$$

$$\sum_{j=1}^{i} L_{I,j} \log_2(1 + H_{R_2D} p_{R_2,j}) \leq \sum_{j=1}^{i} L_{II,j} \log_2(1 + H_{SR_2} p_{SII,j}) \quad \forall i \tag{2.4i}$$

$$\sum_{j=1}^{i} L_{I,j} log_2(1 + H_{SR_1} p_{SI,j}) - \sum_{j=1}^{i-1} L_{II,j} log_2(1 + H_{R_1D} p_{R_1,j}) \leq B_{R_1,max} \quad \forall i \tag{2.4j}$$

$$\sum_{j=1}^{i} L_{II,j} \log_2(1 + H_{SR_2} p_{SII,j}) - \sum_{j=1}^{i-1} L_{I,j} \log_2(1 + H_{R_2D} p_{R_2,j}) \leq B_{R_2,max} \quad \forall i \tag{2.4k}$$

$$L_{I,i} + L_{II,i} \leq \tau_i \quad \forall i \tag{2.4l}$$

$$p_{SI,i} \geq 0, p_{SII,i} \geq 0, p_{R_1,i} \geq 0, p_{R_2,i} \geq 0, L_{I,i} \geq 0, L_{II,i} \geq 0 \quad \forall i \tag{2.4m}$$

Here the constraints in Eq. (2.4b)-Eq. (2.4d) represent energy causality constraints *(constraint 1 in Section 2.2)*, while Eq. (2.4e)-Eq. (2.4g) are energy overflow constraints *(constraint 2 in Section 2.2)* at SN, RN_1 and RN_2, respectively. The data causality constraints *(constraint 3 in Section 2.2)* and data overflow constraints *(constraint 4 in Section 2.2)* at RN_1 and RN_2 are given in Eq. (2.4h)-Eq. (2.4i) and Eq. (2.4j)-Eq. (2.4k), respectively. Finally, Eq. (2.4l) is the half-duplex constraint due to the HD relays RN_1 & RN_2, while Eq. (2.4m) represents feasibility constraints at SN, RN_1 and RN_2.

The above optimization problem is non-convex owing to the constraints Eq. (2.4b)-Eq. (2.4k), which is intractable and difficult to solve in its original form. Therefore, in order for transforming Eq. (2.4) into a more tractable form the throughput of the nodes is defined in different phases based on the rate versus power relationship Eq. (2.1) mentioned in Section 2.2 as:

$$\alpha_{R1,k} = L_{II,k} \log_2(1 + H_{R1D} p_{R1,k}); \tag{2.5a}$$

$$\alpha_{R2,k} = L_{I,k} \log_2(1 + H_{R2D} p_{R2,k}); \tag{2.5b}$$

$$\alpha_{SI,k} = L_{I,k} \log_2(1 + H_{SR1} p_{SI,k}); \tag{2.5c}$$

$$\alpha_{SII,k} = L_{II,k} \log_2(1 + H_{SR2} p_{SII,k}). \tag{2.5d}$$

Now, the optimization problem can be rewritten and is defined over $\boldsymbol{L_I}$, $\boldsymbol{L_{II}}$, $\boldsymbol{\alpha_{SI}}$, $\boldsymbol{\alpha_{SII}}$,

$\boldsymbol{\alpha_{R1}}$ and $\boldsymbol{\alpha_{R2}}$ as:

$$\underset{\substack{\boldsymbol{L_I},\boldsymbol{L_{II}},\boldsymbol{\alpha_{SI}},\\ \boldsymbol{\alpha_{SII}},\boldsymbol{\alpha_{R1}},\boldsymbol{\alpha_{R2}}}}{\text{maximise}} \quad \sum_{k=1}^{K} \alpha_{R1,k} + \alpha_{R2,k} \tag{2.6a}$$

subject to :

Energy causality constraints at SN, RN_1 and RN_2 :

$$\sum_{j=1}^{k} \frac{L_{I,j}}{H_{SR1}} \left(2^{\left(\frac{\alpha_{SI,j}}{L_{I,j}}\right)} - 1\right) + \frac{L_{II,j}}{H_{SR2}} \left(2^{\left(\frac{\alpha_{SII,j}}{L_{II,j}}\right)} - 1\right) \leq \sum_{j=0}^{k-1} E_{S,j} \quad \forall k; \tag{2.6b}$$

$$\sum_{j=1}^{k} \frac{L_{II,j}}{H_{R1D}} \left(2^{\left(\frac{\alpha_{R1,j}}{L_{II,j}}\right)} - 1\right) \leq \sum_{j=0}^{k-1} E_{R1,j} \quad \forall k; \tag{2.6c}$$

$$\sum_{j=1}^{k} \frac{L_{I,j}}{H_{R2D}} \left(2^{\left(\frac{\alpha_{R2,j}}{L_{I,j}}\right)} - 1\right) \leq \sum_{j=0}^{k-1} E_{R2,j} \quad \forall k. \tag{2.6d}$$

Energy overflow constraints at SN, RN_1 and RN_2 :

$$\sum_{j=0}^{k} E_{S,j} - \sum_{j=1}^{k} \frac{L_{I,j}}{H_{SR1}} \left(2^{\left(\frac{\alpha_{SI,j}}{L_{I,j}}\right)} - 1\right) + \frac{L_{II,j}}{H_{SR2}} \left(2^{\left(\frac{\alpha_{SII,j}}{L_{II,j}}\right)} - 1\right) \leq E_{S,max} \quad \forall k; \tag{2.6e}$$

$$\sum_{j=0}^{k} E_{R1,j} - \sum_{j=1}^{k} \frac{L_{II,j}}{H_{R1D}} \left(2^{\left(\frac{\alpha_{R1,j}}{L_{II,j}}\right)} - 1\right) \leq E_{R1,max} \quad \forall k; \tag{2.6f}$$

$$\sum_{j=0}^{k} E_{R2,j} - \sum_{j=1}^{k} \frac{L_{I,j}}{H_{R2D}} \left(2^{\left(\frac{\alpha_{R2,j}}{L_{I,j}}\right)^{i}} - 1\right) \leq E_{R2,max} \quad \forall k. \tag{2.6g}$$

Data causality constraints at RN_1 and RN_2 :

$$\sum_{j=1}^{k} \alpha_{R1,j} \leq \sum_{j=1}^{k} \alpha_{SI,j} \quad \forall k; \tag{2.6h}$$

$$\sum_{j=1}^{k} \alpha_{R2,j} \leq \sum_{j=1}^{k} \alpha_{SII,j} \quad \forall k. \tag{2.6i}$$

Data overflow constraints at RN_1 and RN_2 :

$$\sum_{j=1}^{k} \alpha_{SI,j} - \sum_{j=1}^{k-1} \alpha_{R1,j} \leq B_{R1,max} \quad \forall k; \tag{2.6j}$$

$$\sum_{j=1}^{k} \alpha_{SII,j} - \sum_{j=1}^{k-1} \alpha_{R2,j} \leq B_{R2,max} \quad \forall k. \tag{2.6k}$$

Half duplex constraint due to the HD relays RN_1 & RN_2 :

$$L_{I,k} + L_{II,k} \leq \tau_k \quad \forall k. \tag{2.6l}$$

Feasibility constraints at SN, RN_1 and RN_2 :

$$\alpha_{SI,k} \geq 0, \quad \alpha_{SII,k} \geq 0, \quad \alpha_{R1,k} \geq 0; \alpha_{R2,k} \geq 0, \quad L_{I,k} \geq 0, \quad L_{II,k} \geq 0 \quad \forall k. \tag{2.6m}$$

Note that when Eq. (2.6h)-Eq. (2.6i) are evaluated at $k = K$, the total amount of data delivered to DN is equal to the amount of data transferred by RN_1 and RN_2, hence the

throughput maximisation problem corresponds to the maximisation of the amount of data transmitted by both the RNs as formulated in Eq. (2.6a). The problem in Eq. (2.6) is still a non-convex optimization problem owing to the non-convex energy storage constraints defined in Eq. (2.6e)-Eq. (2.6g), which can be efficiently solved using the IPOPT method.

The IPOPT method relies on tighter termination bounds as well as utilises comparable CPU time for evaluating a higher number of objective function values and iterations [82]. The IPOPT method involves the primal-dual interior point algorithm with the aid of a so-called filter line search method invoked for non-linear programming [82], [83], which improves its robustness. In the primal dual interior point method, both the primal and dual variables are updated, while the primal and dual iterates do not have to be feasible. The search direction in this method is obtained using Newton's method applied to the modified Karush-Kuhn-Tucker (KKT) equations. However, the basic idea behind the filter line search algorithm involves considering a trial point during the back-tracking line search, where this trial point is considered to be acceptable if it leads to sufficient progress towards achieving the optimization goal. This algorithm maintains a 'filter', which is a set of values that both the objective function and the constraint violation functions are prohibited from returning. For a trial point to be successful, the values of the objective function and the constraint violation functions evaluated at that trial point should not be a member of the filter. This filter is updated at every iteration to ensure that the algorithm does not cycle in the neighbourhood of the previous iterate [82].

2.3.2 Sub-optimal (Alternate) Transmission Policy

In this scheme, the duration of phase I in Figure 2.1 is set to be equal to $\eta\%$ of the length of an epoch, i.e. :

$$L_{I,k} = \frac{\eta}{100}\tau_k, \qquad L_{II,k} = \tau_k - \frac{\eta}{100}\tau_k \tag{2.7}$$

Using Eq. (2.7), the optimization problem is relaxed for this sub-optimal scheme and can be re-formulated by omitting Eq. (2.6l) from Eq. (2.6) as well as substituting the deterministic value of $L_{I,k}$ and $L_{II,k}$ in other constraints. This is again a non-convex optimization problem, hence it may be solved using the IPOPT method. This scheme is termed as sub-optimal, since the duration of the phases has been deliberately fixed for the sake of reducing the complexity of the optimization problem.

2.4 Performance Results and Discussion

In this section, the performance of the proposed buffer-aided successive relaying system relying on offline power allocation is evaluated in terms of the optimal throughput achieved by the deadline of T seconds. The EH process of both SN and of the RNs independently takes values from $[0, E_{max}]$ units, where the energy is distributed uniformly under an exponential inter-arrival time at a rate of λ_e units/second. The deterministic channel gains are set to the equal values $H_{SR1} = H_{SR2} = H_{R1D} = H_{R2D}$. The parametric setting for analysing the

Parameter	Value
System deadline, T	10 seconds
Amount of Energy Harvested, E_{max}	5 units
Rate of Energy Harvesting, λ_e	5 units/second
Information Buffer Size, $I_{R_1,max}/I_{R_2,max}$	2 units
Battery Size, $E_{S,max}/E_{R_1,max}/E_{R_2,max}$	5 units
Channel Gains, $[H_{SR1}, H_{SR2}, H_{R1D}, H_{R2D}]$	[4, 4, 4, 4,]

Table 2.1: Parameters used for Simulations

throughput of the system is provided in Table 2.1 except otherwise mentioned. The results quantify the throughput of the system as a function of both the data and energy buffer capacity, for both the optimal and sub-optimal schemes that are benchmarked against the infinite-storage based optimal scheme defined in [27]. The benchmark scheme of [27] is insensitive to the buffer sizes, since it considers infinite storage capacities at all the EH nodes for both the energy and data, thereby providing an upper-bound to the proposed system. The proposed schemes have been analysed under off-line EH process by dividing this section into four parts as follows:

2.4.1 Optimality of Power Allocation Scheme

The optimality of the power allocation scheme is defined using the constraints and lemmas introduced in Section 2.3 as a benefit of the EH capability at the SN and RNs. The energy-based feasibility of the transmission policy defined in this chapter is characterised using the energy-based feasibility tunnel at each of the EH node as shown in Figure 2.3.

The upper staircase-shaped curve in the figure depicts the cumulative harvested energy at the EH node during the communication process by the deadline T. The lower curve represents the upper curve shifted down by the battery-size at each node. The cumulative energy expended by the EH node obtained through the optimisation defined in this chapter forms the continuous line, that must lie inside this tunnel to conform with energy feasibility at the node. A power allocation that appears above the tunnel represents the over-expenditure of energy, which is not available at the node, thus violating the energy causality constraint. On the other hand the power allocation that slips below the tunnel yields overflow of the battery at the node, thereby certainly not an optimal policy, as defined in Lemma 2 of Section 2.3. As stated by Lemma 1, the transmission power/rate remains constant during the two energy arrivals at the nodes, therefore the power has a constant slope in an energy arrival epoch, as confirmed by Figure 2.3.

Moreover, it can be observed from Figure 2.3 that the power allocation changes at the energy arrival instant and it is positive, when the curve touches the lower 'staircase', while it is negative when it touches the upper 'staircase'. The reason behind this characteristic is that when the power curve touches the upper staircase, this means that the node has

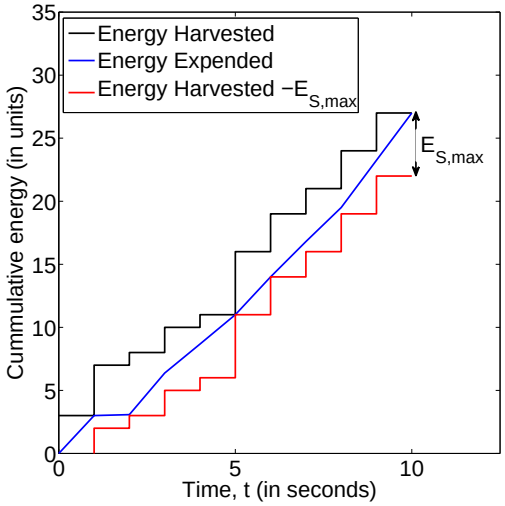

(a) Energy Feasibility Tunnel at SN

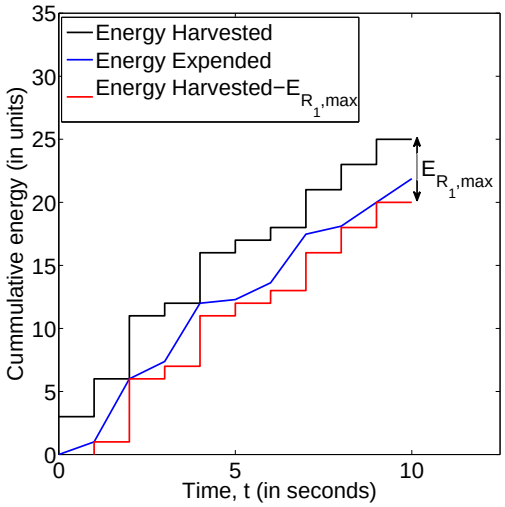

(b) Energy Feasibility Tunnel at RN_1

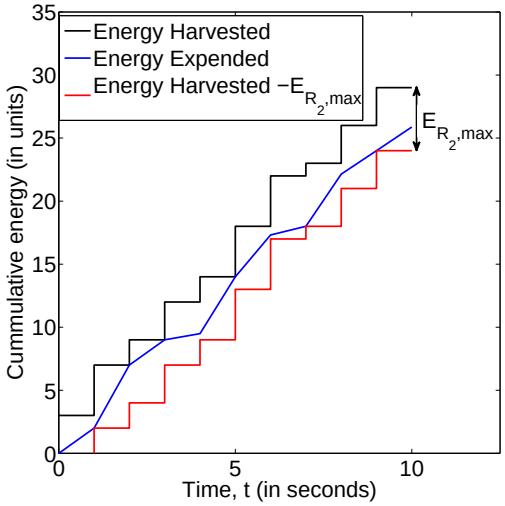

(c) Energy Feasibility Tunnel at RN_2

Figure 2.3: Energy Feasibility Tunnel at all the energy harvesting nodes in the system with battery size $E_{S,Max} = E_{R_1,Max} = E_{R_2,Max}$, and harvesting energy at rate λ_e with maximum amount of energy harvested as E_{max}. All other system parameters are summarized in Table 2.1.

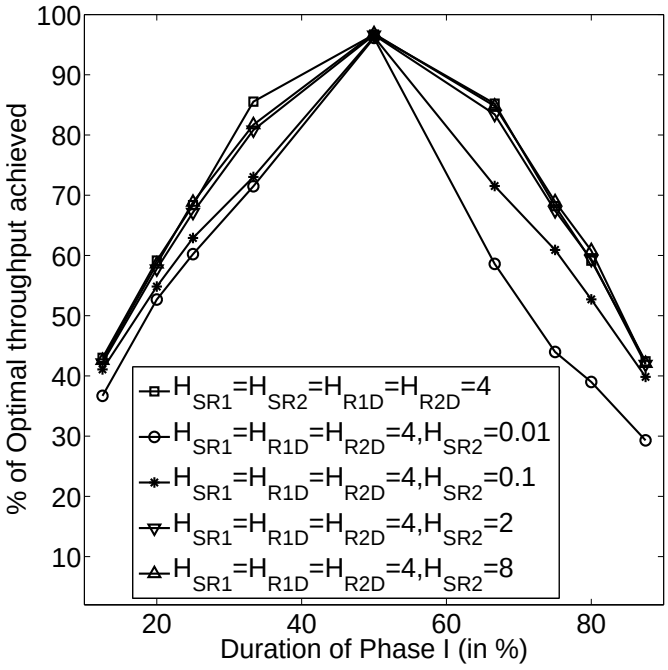

Figure 2.4: Relation between percentage of optimal throughput achieved for varying duration of Phase I occurring in an energy harvesting epoch with sufficient energy and data buffer sizes for different settings of channel gains. All other system parameters are summarized in Table 2.1.

expended all the energy it has harvested by the time instant t_i and hence for the corresponding epoch it has to use the energy harvested at t_i, resulting in a transmission power reduction for the node. On the other hand, when the power allocation curve touches the lower staircase at t_i, this means that the battery is full at that instant and thus being an optimal policy capable of avoiding any battery overflow in the corresponding epoch. The optimal power of the node increases, as also confirmed by Lemma 2 of Section 2.3. Thus, the energy feasibility curves in Figure 2.3 illustrate the optimality of the power allocation scheme defined in Section 2.3 for all the EH nodes, namely, for SN, $RN1$ and $RN2$.

The percentage duration of Phases I and II in Figure 2.1 is not fixed for the optimal scheme, while they have been fixed to a specific ratio for the sub-optimal scheme for the sake of complexity reduction. Hence, the next goal is to identify that optimality of the specific ratio of the durations of Phase I and II, which would maximise the throughput of the sub-optimal scheme. Figure 2.4 shows the specific percentage of the optimal throughput, which was actually achieved by varying the proportion of the phase I duration (L_I) in each of the EH epochs along with the symmetric ($H_{SR1} = H_{SR2} = H_{R1D} = H_{R2D} = 4$) and asymmetric settings of the channel fading gain for SN-RN_2. The performance of the sub-optimal scheme peaks, when the durations of both the phases are equal. For the other scenarios, the throughput is lower, because the amount of data transmitted between SN and DN is limited by the shorter phase. It can be seen from Figure 2.4 that as the duration of the shorter phase increases, the throughput also increases. It is interesting to note that in the scenarios of very low channel gain, i.e. for $H_{SR2} = 0.01$, $H_{SR2} = 0.1$, there exists asymmetry in the throughput achieved by system. The reason behind this trend is that when the duration of phase I is higher than that of phase II, the channel gain of path SN-

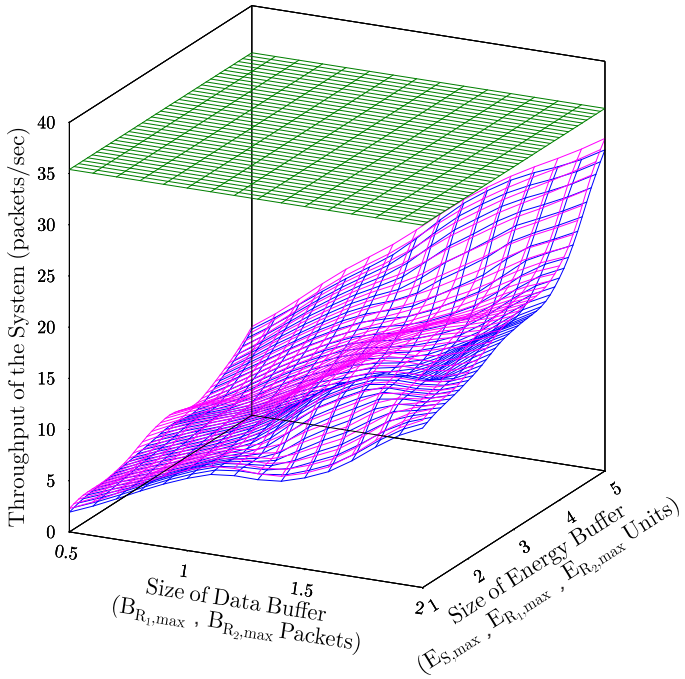

Figure 2.5: Impact of the energy and data buffer sizes at all the EH nodes on the throughput of the system by the deadline T. The constant green surface represents the throughput of the benchmark scheme [27], while the pink and blue surface depict the optimal and sub-optimal transmission policies, respectively. All the system parameters are summarized in Table 2.1.

RN_2 limits the amount of data that can be otherwise transmitted to RN_2. As depicted in Figure 2.4, when the duration of phase I is 50% of the EH epoch, the sub-optimal scheme achieves approximately 97% of the optimal scheme's throughput. Hence, in the following discussions a sub-optimal scheme is considered, where the duration of each phase is 50% of the epoch duration.

2.4.2 Impact of size of the buffers

The 3-dimensional characterization of the system of Figure 2.1 is provided in Figure 2.5. Specifically, Figure 2.5 illustrates the overall throughput of the system as a function of the size of both the energy buffer and data buffer at the EH nodes. It can be clearly observed that with the increase in the size of buffers at the EH nodes, the throughput of the proposed schemes improve owing to increased availability of energy and data storage capacity at the EH nodes supporting a larger amount of data transmission to DN. However, the throughput of the benchmark scheme [27] is constant, that is independent of the buffer sizes, as it relies on the idealised settings where EH nodes possess infinite energy and data storage capacity. Moreover, the optimal scheme performs only marginally better than the less complex sub-optimal scheme, because the duration of each phase is fixed in the sub-optimal scheme. This would in turn result in limiting the amount of data that can be transmitted to DN during successive relaying phases. In order to closely analyse the impact of the energy and data buffer capacities at the EH nodes on the overall system throughput, the 2-dimensional curves are presented corresponding to the individual analysis of the

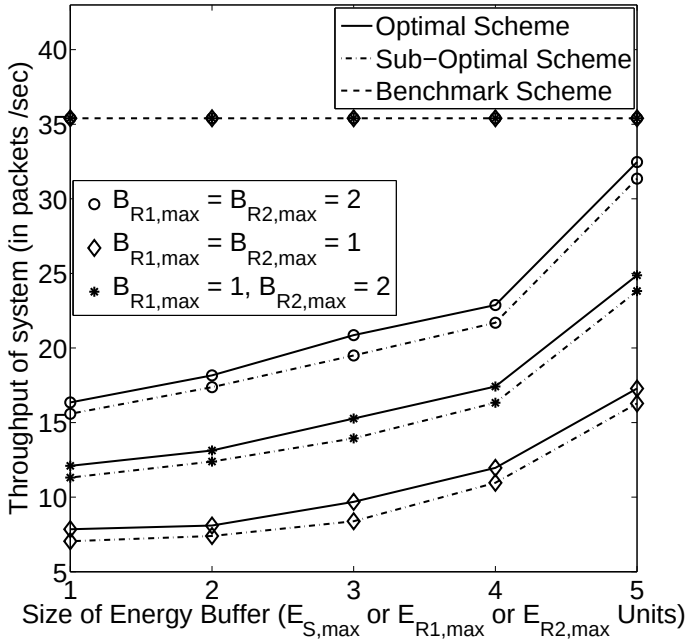

Figure 2.6: Impact of energy buffer size at all the EH nodes with sufficient (2 packets), insufficient (1 packets) and asymmetric data buffer capacity at the RNs on the throughput of the system by the deadline T. All other system parameters are summarized in Table 2.1.

energy buffer size, while keeping the data buffer size constant and vice versa.

The results of Figure 2.6 show the throughput of the system against the size of the battery in the presence of sufficient, insufficient and asymmetric data buffer sizes for both the optimal and the sub-optimal schemes. As expected, upon increasing the battery size, the throughput of the system is improved owing to the availability of increased amount of energy (due to increase in buffer size) for transmission. Moreover, it can be observed that for sufficient (or insufficient) data storage, the optimal system is capable of achieving 92% (or 50%) of the benchmark scheme's throughput performance [27], while the sub-optimal scheme performs slightly worse than the optimal scheme, reaching 88% (or 46%) of the benchmark system's throughput value in [27], when the battery capacity of the EH nodes is sufficiently high ($E_{S,max} = E_{R_1,max} = E_{R_2,max} = 5$ units). Furthermore, for asymmetric settings having unequal data buffers at RN_1 and RN_2, the throughput becomes lower than that for sufficiently large storage, since RN_1 is now acting as a bottleneck, preventing the flow of data to DN. On the other hand, for this asymmetric setting, the throughput becomes higher than that for insufficient storage, since the node RN_2 has a higher data storage capacity, thereby supporting a higher data rate to DN. The sub-optimal scheme's throughput performance was 95.2%, 90.7% and 93.7% of that of the optimal scheme for the scenarios of sufficient, insufficient and asymmetric data buffers, respectively.

Similarly, Figure 2.7 presents the throughput of the system as a function of the data buffer size at the RNs with sufficient, insufficient and asymmetric energy buffer sizes for both the optimal and sub-optimal scheme. It is clearly demonstrated that as the size of the data buffer increases, the amount of data successfully transmitted to the DN also increases for both the schemes, indicating that the optimal and sub-optimal schemes have

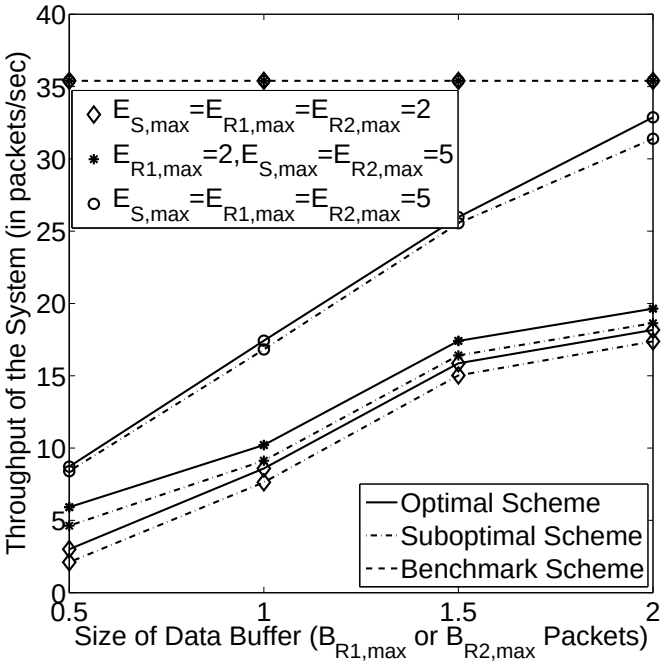

Figure 2.7: Impact of data buffer size at the RNs with both sufficient (5 units), insufficient(2 units) and asymmetric battery capacities at EH nodes over throughput of the system by the deadline T. All other system parameters are summarized in Table 2.1.

quite a similar performance. The reason behind this trend is the reduction of overflowing data buffers owing to the larger capacities of these buffers at the RNs. Furthermore, for sufficient (or insufficient) battery capacities, the optimal system having finite buffers is capable of achieving 92% (or 52%) of the throughput compared to the sub-optimal scheme that performs comparably, since it achieves 88% (or 49%) of the benchmark system's throughput [27] for the maximum data buffer size of $B_{R_1,max} = B_{R_2,max} = 2$ packets. Furthermore, for asymmetric settings having unequal energy buffers at RN_1 and RN_2, the throughput becomes lower than that for a sufficiently large storage, since RN_1 is low on energy, hence preventing the flow of data to DN. On the other hand, for this asymmetric setting, the throughput becomes higher than that for insufficient storage, since the node RN_2 has a higher energy storage capacity, consequently supporting a higher data rate to DN. Moreover, the sub-optimal scheme achieves 96.7%, 87.3% and 94.2% of the throughput of the optimal scheme for sufficient, insufficient and asymmetric energy buffers, respectively.

2.4.3 Impact of Asymmetric Channel Gains

Figure 2.8 depicts the throughput of the system as a function of the asymmetric channel gain of the SN-RN_2 path (H_{SR2}) for the scenario of having a sufficiently high data and energy buffer size at the EH nodes, where all other channel gains are set to $H_{SR1} = H_{R1D} = H_{R2D} = 4$. It can be clearly seen that as the channel gain H_{SR2} increases, the throughput of the system increases for all the schemes owing to the rate-power relationship mentioned in Eq. (2.1). This means that as the value of the channel gain increases, the amount of data transmitted from SN to RN_2 increases and so does the amount of data reaching the DN, hence also increasing the overall throughput of the system. As expected, the benchmark

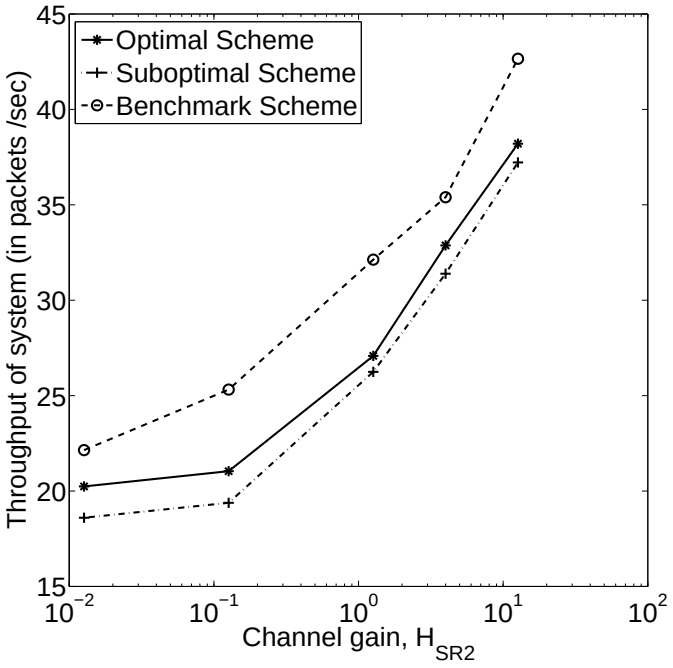

Figure 2.8: Impact of asymmetric fading from S to RN_2 for sufficient battery and data buffer capacities at EH nodes on throughput of the system by the deadline T. All the system parameters are summarized in Table 2.1.

scheme represents the upper-bound of the system's throughput for an asymmetric setting of the channel gain, as it relies on the idealized assumptions of infinite data and energy storage capacities at the EH nodes. However, the optimal scheme performs better than the sub-optimal scheme owing to the fixed duration of phases in the successive relaying protocol of the latter scheme.

In Figure 2.9, the throughput of the system is considered as a function of the data buffer capacity at the RNs for the scenario of asymmetric channel gains as well as asymmetric energy buffer capacity. Explicitly, $E_{S,max} = E_{R2,max} = 5$ units, $E_{R1,max} = 2$ units are used at the EH nodes. The benchmark scheme provides an upper bound for the proposed schemes and has a constant throughput, since it is unaffected by the data and energy buffer capacity at the EH nodes. Interestingly, the throughput of the system improves upon increasing the value of the channel gains, which becomes explicit by observing the rate-power relationship of Eq. (2.1). Moreover, the asymmetric setting of energy buffers at the EH nodes of the proposed scheme results in limiting the throughput achieved by the system, because RN_1 is acting as the bottleneck owing to the low energy buffer capacity.

2.4.4 Impact of Energy Harvesting Process

The energy harvesting processes at all the EH nodes are independent of each other and they are characterized by the amount of energy arrival and by its arrival instant. The amount of energy is modelled by a process of uniform distribution in the interval of $[0, E_{max}]$ units, while the inter-arrival process is defined by an exponential distribution associated with a rate of λ_e. In this section, the battery size of each node is set to the same storage capacity

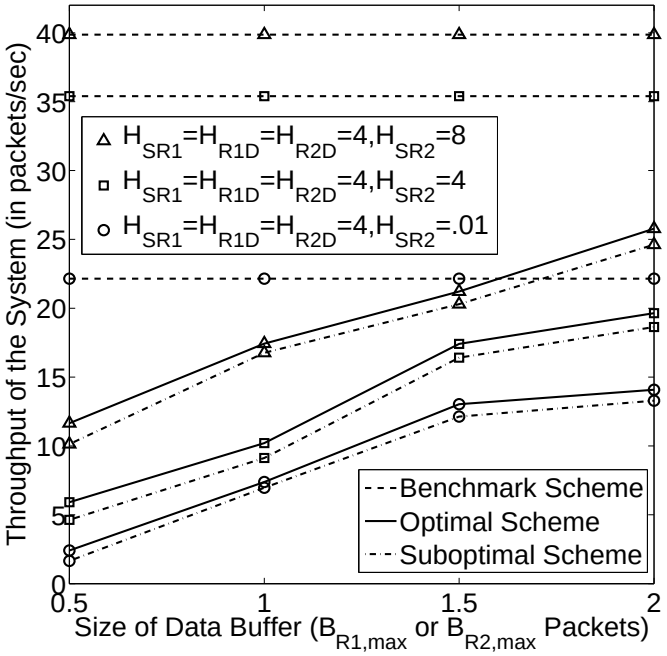

Figure 2.9: Impact of data buffer size at the RNs with asymmetric channel gains and battery capacities ($E_{S,max} = E_{R2,max} = 5$ units, $E_{R1,max} = 2$ units) at EH nodes over throughput of the system by the deadline T. All other system parameters are summarized in Table 2.1.

of $E_{S,Max} = E_{R_1,Max} = E_{R_2,Max} = 2$ Units which is insufficient for the transmission of all data in the data buffer, while the buffer size at the relay nodes is sufficient for storing the source data, $I_{R_1,Max} = I_{R_2,Max} = 2$. Let us now analyse the throughput of the system achieved by the deadline as a function of the EH parameters of E_{max} and λ_e.

The maximum amount of energy that is harvested at each node is the same and it is denoted as E_{max}, which is shown to improve the system's throughput in Figure 2.10, while the rate of harvesting is set according to Table 2.1. It is clearly observed in Figure 2.10 that as the maximum amount of energy harvested at the nodes increases, the throughput of the system also increases owing to the rate-power relationship defined in Eq. (2.1). This means that as the energy stored at the node increases, it can transmit more information and hence the overall throughput of the system achieved by the deadline T increases. Moreover, due to the associated buffer limitations, the nodes cannot store more energy than their battery size. On the other hand, in case of infinite buffer sizes, this excess energy is not wasted, because it is utilised for transmitting more data and hence the infinite buffer aided optimal policy provides an upper bound for the optimal and sub-optimal schemes defined in this chapter. Finally, the optimal scheme performs better than the sub-optimal one because due to pre-defined length of the successive relaying protocol phases, the relay nodes are limited to the transmission of a certain amount of data, which in turn leads to comparatively slower transfer of data to the destination.

The rate of energy harvested at each node is identical, which was varied for generating Figure 2.11. It is clearly observed from Figure 2.11 that as the rate of harvesting increases, the throughput of all the three schemes considered increases. This is due to the fact that as

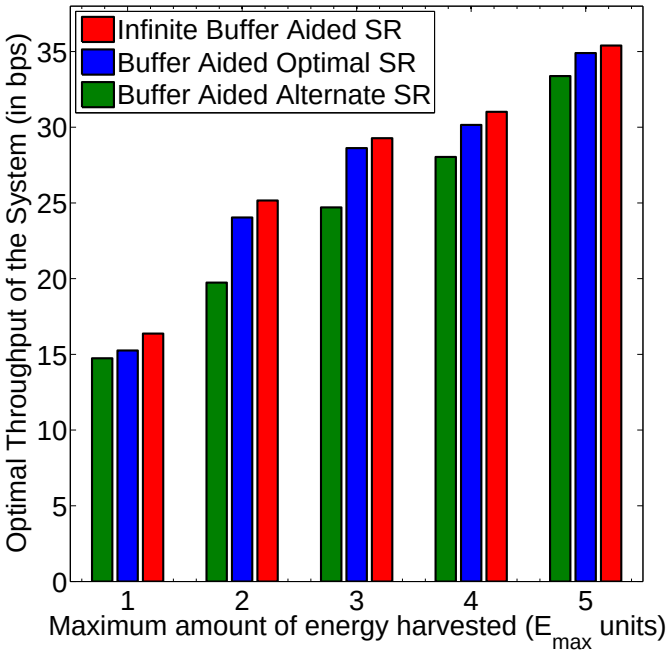

Figure 2.10: Impact of maximum amount of energy (E_{max} Units) harvested at all the EH nodes with sufficient data buffer and insufficient energy buffer capacity (2 packets and 2 units, respectively) on the overall throughput of the system by the deadline T. All other system parameters are summarized in Table 2.1.

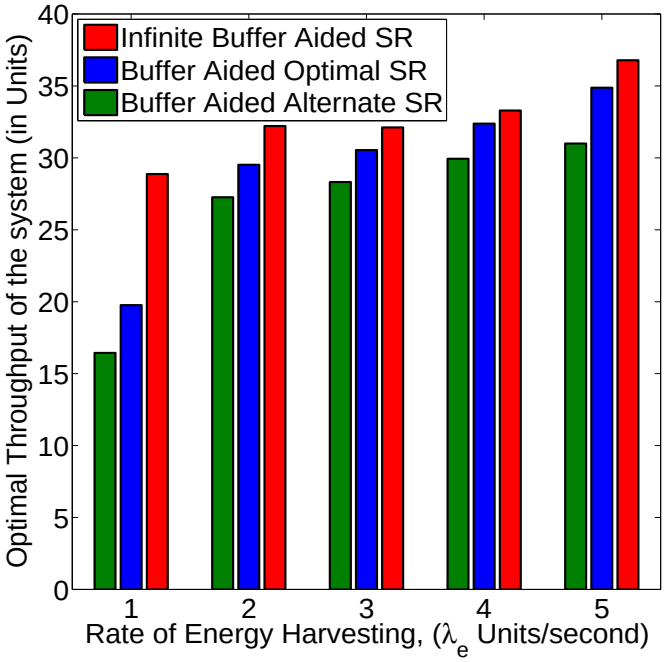

Figure 2.11: Impact of the energy harvesting rate (λ_e units/second) at all the EH nodes with sufficient data buffer and energy buffer capacity (2 packets and 5 units, respectively) on the overall throughput of the system by the deadline T. All other system parameters are summarized in Table 2.1.

the rate of harvesting increases, the number of energy arrivals by the deadline T increases, which in turn increases the cumulative amount of energy harvested at the node. Therefore, with the increase in energy available at the node owing to its increased harvesting rate λ_e, the amount of data that can be transferred from the source to destination with the

aid of relay nodes also increases, as indicated by the rate-power relationship of Eq. (2.1). Moreover, as expected, again the infinite-buffer-aided scheme provides the upper bound for the proposed schemes, while the optimal scheme outperforms the sub-optimal scheme.

2.5 Summary and Conclusions

In this chapter, one of the key design factors of reliable communication systems is considered : *energy efficiency*, as mentioned in Chapter 1, in the light of energy harvesting assisted two-hop networks using a buffer-aided successive relaying protocol. This chapter commenced by providing the details of the network model for the two-hop network in Section 2.2, where the successive relaying protocol is adopted for the transmission of source data to the destination. More particularly, the two phases of the successive relaying protocol is characterised, in which a pair of HD relay nodes, $RN1$ and $RN2$ are alternating between their transmitter and receiver modes for the sake of mimicking a FD relay node. The successive relaying protocol consists of the following two phases:

- Phase I: In this phase, SN and $RN2$ are transmitting to the nodes $RN1$ and DN, respectively. Therefore, $RN1$ is in its receiver mode, while $RN2$ is in its transmitter mode for Phase I of the protocol.
- Phase II: Following Phase I, the relay nodes alternate their operational mode. Specifically, $RN1$ switches from receiving mode to transmitting mode by forwarding the source data to DN, while SN commences its transmission to $RN2$. Therefore, SN is always in its transmitter mode, while DN is always receiving the data.

Furthermore, the specification of the transmitting nodes, namely SN, $RN1$ and $RN2$, is detailed where each node is capable of harvesting energy from the environment for transmitting the source data, while these nodes are also equipped with buffers to store both energy and data. Under the assumption of known energy arrivals, the related non-convex optimization problem is defined and proposed both the optimal and a sub-optimal scheme for maximising the data delivered to the DN by the deadline in Section 2.3. Then, using the *Interior Point Optimization* method, an efficient solution was found for both the schemes. The major constraints considered in the formulation of the optimization problem are: energy causality constraint, energy overflow constraint, data causality constraint and data overflow constraint, which are detailed in Section 2.2.

Finally, the results in Section 2.4 justify that both the optimal and sub-optimal schemes are capable of performing close to the benchmark system [27]. Explicitly, the optimality of the power allocation schemes is first evaluated in Section 2.4.1. Beginning with the presentation of the energy feasibility tunnels for all the EH nodes in Figure 2.3, which conform with the lemmas of Section 2.3 as well as the constraints of Section 2.2. The sub-optimal scheme relies on the setting of a known duration for each of the phases of the successive relaying protocol in an EH epoch. Hence, Figure 2.4 was created for identifying the optimal ratio of the Phase I and II duration that would maximise the throughput of

the sub-optimal scheme. After finding the optimal ratio to be 50%, the impact of the buffer size is presented in Section 2.4.2, specifically the impact of both the energy and data buffers in a 3-dimensional analysis of Figure 2.5, which was further characterized for close analysis of each of the buffer capacities using 2-dimensional curves in Figure 2.6 and Figure 2.7. The impact of asymmetric channel gains was discussed both in Figure 2.8 and in Figure 2.9 presented in Section 2.4.3. Finally, the effect of the energy harvesting process is evaluated in Figure 2.10 and Figure 2.11 of Section 2.4.4, where the throughput of the system is presented as a function of the amount and rate of energy harvested, respectively. Furthermore, in the light of the above study, the findings based on realistic simulation parameters may be summarised as follows:

- The performance of the sub-optimal scheme as a percentage of the throughput achieved by the optimal scheme reaches its maximum, when the two phases of the successive relaying protocol have an equal duration.
- The optimal and sub-optimal schemes are capable of achieving upto 92% and 88% of the benchmark scheme's throughput [27] for a sufficiently high energy and data buffer capacity.
- The sub-optimal scheme's throughput is consistently about 90% of that of the optimal scheme.
- For asymmetric data (or energy) buffer sizes, the attainable throughput depends on the total (i.e. collective) data (or energy) buffer capacity available in the network, not only on the smallest data buffer.
- As the channel gain increases the throughput of the proposed scheme improves for sufficient energy and data buffer capacity with optimal (or sub-optimal) scheme consistently achieving 90% (or 80%) of benchmark scheme's throughput.
- As the amount of EH increases the throughput of the proposed scheme improves even for insufficient energy buffer capacity with optimal (or sub-optimal) scheme consistently achieving 90% (or 80%) of benchmark scheme's throughput.

To conclude, this chapter considered buffer-aided energy harvesting nodes relying on a successive relaying paradigm for maximising the throughput of the system by formulating a constrained optimisation problem. Consequently, an optimal and a sub-optimal power allocation scheme were proposed, both of which were quantitatively compared against the benchmark scheme of [27]. The quantitative analysis revealed that the less complex sub-optimal scheme is capable of approaching the performance of the optimal scheme at the expense of a slight performance degradation, provided that the EH nodes are equipped with sufficiently large buffers for both energy and data storage. This chapter dealt with one of the possible *energy harvesting* solutions for improving the energy efficiency of communication systems, while in the next chapter, the issue of improving the spectral efficiency will be addressed, which is another key design criterion.

Chapter 3

Resource Allocation for D2D Links in the FFR and SFR Aided Cellular Downlink

3.1 Introduction

In Chapter 2, an energy harvesting aided cooperative communication network relying on a buffer aided successive relaying protocol was invoked for maximising the throughput. The energy harvesting system model relying on a realistic energy and data buffer size, which enhances the lifetime of the network, is only suitable when the network has sufficient bandwidth for its communication. However, with the spread of mobile devices, tablets and mobile multimedia services, the amount of traffic conveyed by the cellular networks has been escalating. Hence the macrocell base stations (MBS) have to handle more traffic in order to meet the demand of high data rate services. Clearly, there is a need for enhancing the capacity of the cellular network in order to accommodate the deluge of multimedia traffic, which requires increasing the tele-traffic capacity, employing more MBSs etc. However, the radio resources available for cellular communications are limited and the employment of more MBSs is uneconomical. Therefore, further research is required for improving the capacity of cellular systems, whilst relying on the existing infrastructure. In the prevailing cellular networks, the data of all the mobile users (MUs) is relayed through the MBSs, even though the MUs may be closely located, which in turn increases both the delay as well as the traffic load imposed on the MBSs due to the high density of users. The solution to this problem is a promising new local ad-hoc networking technology, known as Device-to-Device (D2D) communication, which allows closely located devices to communicate directly by reusing the frequency band of the operational cellular network [51, 52].

However, the D2D links impose additional interference on the communication system. Explicitly, if a D2D link relies on utilising downlink (DL) resources, then the signals transmitted by the MBS to MUs may cause interference at the D2D receivers, while the D2D

transmissions would degrade the DL channel quality of MBSs transmitting to the MUs. Furthermore, there exist interferences amongst the D2D links themselves, which reuse the same frequency bands. In order to maintain the Quality of Service (QoS) target both for the MUs and the D2D links, beneficial resource reuse schemes have been proposed for D2D communication, where the macrocell employed Unity Frequency Reuse (UFR) [62,84,85,61,58,86]. However, the interference imposed on the MUs can be significantly reduced by using Inter-Cell Interference Coordination (ICIC) schemes, such as, Fractional Frequency Reuse (FFR) and Soft Frequency Reuse (SFR). In FFR and SFR, the interference is eliminated by carefully coordinating the frequency bands used among the cells as well as by partitioning the total frequency band of each cell into a cell-centre region (CCR) and cell-edge region (CER) frequency-set. These frequency reuse techniques have been investigated in the literature in the context of different network models [46, 47, 87, 49, 50].

Furthermore, several resource allocation algorithms have been conceived for D2D communication in cellular networks using FFR [64,88,55,89,63,90] and SFR [57]. In particular, a novel D2D-aware dynamic FFR algorithm was proposed in [64]. In [88], resource allocation was designed by Wu and Zhang for D2D communication in an FFR scenario by formulating it as binary integer optimization problem. Chae *et al.* [55] observed a significant improvement in the attainable cell throughput with the aid of their radio resource allocation scheme proposed for D2D links based on their specific location in the cell, when the cellular network was relying on FFR. Kim *et al.* [89] proposed a resource allocation algorithm for eliminating the interferences imposed by the D2D links, while the spectral efficiency of D2D communication achieved in FFR-aided OFDMA cellular systems was analytically investigated by Zhu and Wang [63]. In [90], authors proposed frequency reuse scheme in FFR scenario for interference mitigation in D2D underlaying uplink of cellular networks while resource allocation and power control scheme in SFR scenario was proposed for D2D communication reusing cellular downlink in [57].

This chapter focuses attention on the cellular network employing FFR or SFR in conjunction with D2D communication relying on downlink resource reuse. The D2D links of devices are battery-operated, hence it is essential to save energy at these devices using power control in order to prevent the battery depletion as well as for reducing the interference imposed on the MUs. However, at the same time it is necessary to ensure that the power control of the D2D links does not significantly degrade the performance of these links. The main contributions of this chapter are as follows [2]:

- A pair of fractional frequency allocation schemes (FFA1 and FFA2) have been proposed for D2D links, when the macrocell relies on an FFR scheme, where the D2D links are classified into two categories based on a signal-to-interference-ratio (SIR) threshold S_d, namely the short-range (SR) D2D links and the long-range (LR) D2D links. The frequency allocation schemes are formulated as[1]:

  (a) Fractional Frequency Allocation 1 (FFA1): Consider the macrocell 0 of Fig-

[1]Note that in Figure 3.1, the different frequency reuse zones are shown only for illustration. However, the specific frequency resources used by the MUs/D2D links depend on their received SIR, rather than on the geographic location of the MUs/D2D links.

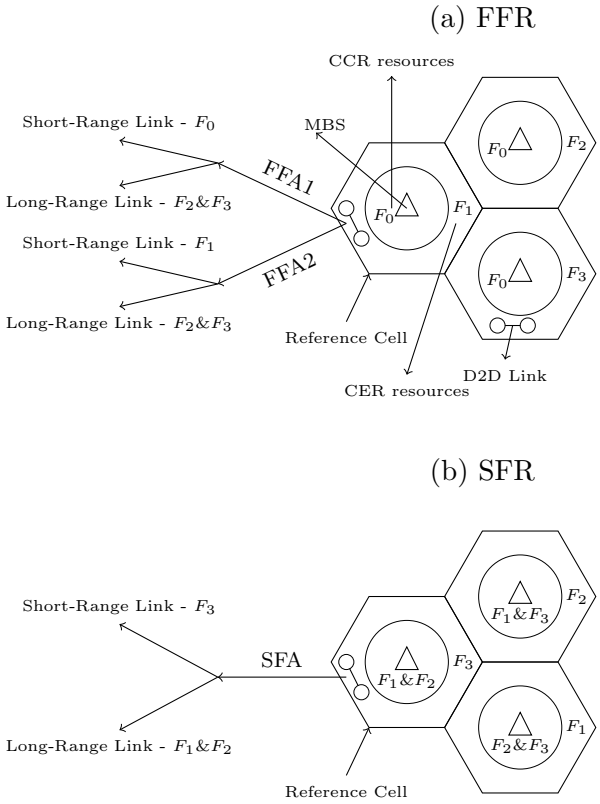

Figure 3.1: Frequency resource allocation in macrocell and D2D links in FFR and SFR

ure 3.3 as the reference cell, where F_0 is CCR frequency and F_1 is CER frequency of this macrocell while CER frequency of the neighbouring cells is F_2 and F_3. In this scheme, the CCR frequency (F_0) of the reference macrocell is allocated to the short-range D2D links and the CER frequency (F_2 and F_3) of the other macrocells to the long-range D2D links, as shown in Figure 3.1(a).

(b) Fractional Frequency Allocation 2 (FFA2): Similar to FFA1, considering the reference macrocell as macrocell 0 of Figure 3.3, in this scheme, the CER frequency (F_1) of the reference macrocell is allocated to the SR D2D links and the CER frequency (F_2 and F_3) of the other macrocells to the LR D2D links, as shown in Figure 3.1(a).

- A frequency allocation scheme have also been proposed for the D2D links, when the macrocell has employed a SFR scheme. The scheme is specified as follows:

  (a) Soft Frequency Allocation (SFA): Again considering the reference macrocell as macrocell 0 of Figure 3.3, F_3 is the CER frequency, while F_1 and F_2 represent the CCR frequency. In this scheme, the CER frequency (F_3) is allocated to the SR D2D links and the CCR frequency (F_1 and F_2) to the LR D2D links, as shown in Figure 3.1(b).

All the proposed schemes defined above are motivated by the FFR scheme itself, where the CCR users (or SR D2D links in the proposed schemes) experience more interference than the CER users (or LR D2D links). Both the coverage probability and the capacity for the

D2D links corresponding to all the proposed schemes are analytically derived. Simulation results are provided for validating the analytical results. Then the proposed schemes are compared to the benchmark scheme, where the MBS relies on UFR. The results reveal that the proposed schemes significantly outperform the benchmark scheme. The impact of the D2D links on the MUs is also quantified. Moreover, an intuition is provided concerning the selection process of the power control factor in order to strike a compelling trade-off between the energy consumption and the performance of the D2D links.

The rest of the chapter is organized, as shown in Figure 3.2. In Section 3.2, the specifications of the multi-cellular network of Figure 3.3 is provided, which forms the basis of the proposed frequency allocation schemes. This is followed by the analytical derivation of both the coverage probability and the capacity of the D2D links for the proposed frequency allocation schemes in Section 3.3. The performance results are discussed in Section 3.4, whilst the conclusions are offered in Section 3.5.

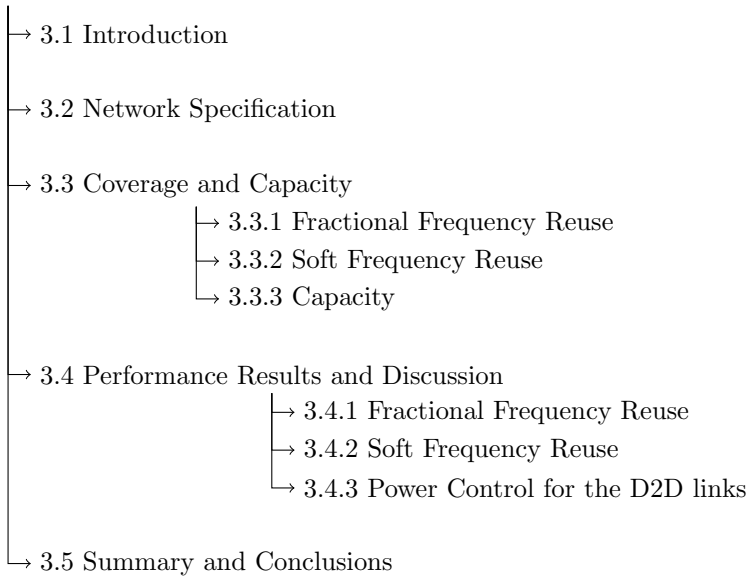

Figure 3.2: The structure of this chapter.

3.2 Network Specification

The cellular network shown in Figure 3.3 is studied, supporting both orthogonal downlink cellular users (MUs) and D2D links where each macrocell is approximated by a circle of radius R_c. Considering the downlink of a cellular system, multiple D2D links are introduced that reuse the downlink resources of multiple MUs, where each MU occupies a dedicated resource block (RB). It is assumed that each MU's RB can be reused by at most one D2D link. This means that a single D2D link can reuse the resource blocks of several MUs, but one of the MU's resource blocks can be reused by only one D2D link at a time. In essence, this may be interpreted as a mapping of one D2D link to multiple resource blocks of different MUs. A similar D2D related constraint was imposed on the cellular user's RB in [59] and [91].

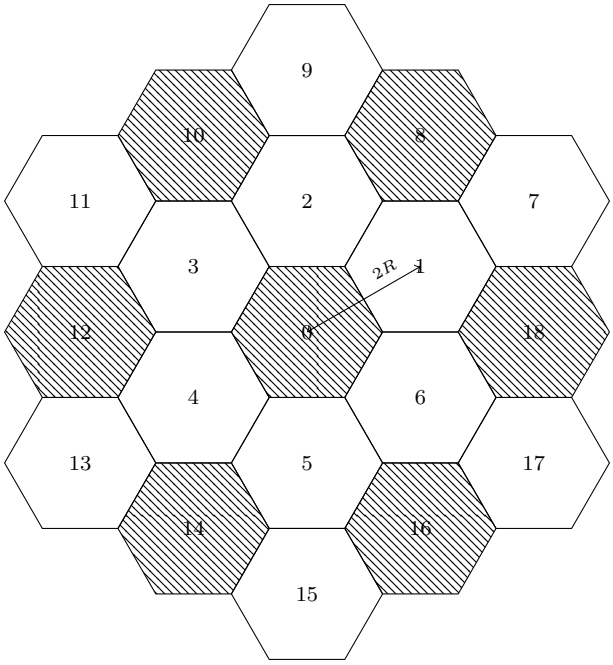

Figure 3.3: Hexagonal macrocell structure. The interference imposed by a UFR system on cell 0 is contributed by all the 18 neighbouring cells, while in a frequency reuse $\frac{1}{3}$ system it is contributed only by the shaded cells.

Figure 3.4 illustrates the resource reuse situation and also the associated interference pattern for a particular MU c and D2D link d. All possible transmission channels in the network are considered to be independent and identically Rayleigh distributed throughout this treatise. The D2D communication is incorporated as a complement to the underlying cellular communication and thus the MUs generally have a higher priority than the D2D links in a cell. The BS maintains reliable connection with the MUs under the power budget of P_c, while the D2D link reuses the randomly matched RB of the MU under the power budget P_d^{max} along with a power control factor of ϵ. All the D2D links are assumed to use a distance-dependent proportion of the total power [92]. In other words, the transmit power P_d of the D2D link is formulated as follows:

$$P_d(r) = P_d^{max} \left(\frac{r}{R_2} \right)^{\alpha\epsilon}, \quad \forall r \in [R_1, R_2] \tag{3.1}$$

where r is the distance and α is the path-loss exponent between the D2D transmitter (Tx) and receiver (Rx). The minimum and maximum distance of the D2D link are denoted by R_1 and R_2, respectively. The power control factor of $\epsilon \in [0, 1]$ controls the power transmitted by the D2D Tx. A lower power control factor allows the D2D Tx to transmit at higher power, which might result in higher coverage quality and higher capacity for the D2D link. On the other hand, a higher power control factor reduces the amount of transmit power used by the D2D link. It is apparent from Eq. (3.1) that at $\epsilon = 0$ the transmit power of all the D2D links present in the macrocell is P_d^{max}, while at $\epsilon = 1$ the transmit power would be at its minimum. Furthermore, when the D2D Tx and Rx have the maximum distance of $r = R_2$, the transmit power for that D2D link would be P_d^{max}, regardless of the value of ϵ.

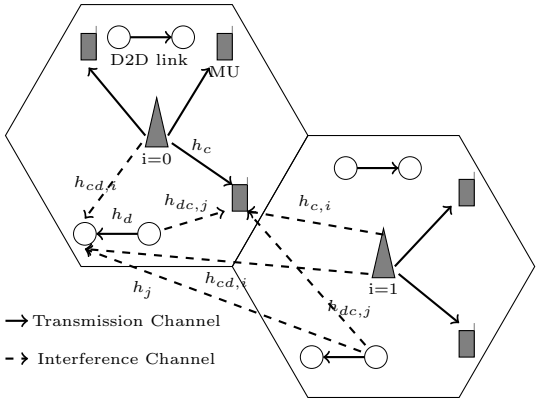

Figure 3.4: Illustration of the interfering links for two adjacent macrocells, when a D2D link is superimposed on a MU's RB.

When the MBS relies on UFR, the SIR at the D2D Rx, which is at a distance of l from the reference MBS and with a separation of r from the D2D Tx, is given by:

$$\begin{aligned} \gamma_U(l,r) &= \frac{P_d(r) h_d r^{-\alpha}}{I_{cd} + I_d}, \\ I_{cd} &= \sum_{i \in \phi} P_c^{max} h_{cd,i} l_i^{-\alpha}, \\ I_d &= \sum_{j \in \psi \setminus \{0\}} P_d(r_j) h_j d_j^{-\alpha}. \end{aligned} \tag{3.2}$$

Here $P_d(r)$ and P_c^{max} denote the transmit power of the D2D Tx and of the MBS, respectively. Furthermore, I_{cd} is the interference experienced by the D2D Rx due to the downlink cellular communication, i.e. the interference caused by the MBSs transmitting on the same frequency band in the network, while I_d is the interference imposed by D2D links in other macrocells that reuse the same frequency band. The fading-induced attenuation experienced by the channel between the D2D transmitter and receiver is h_d, while that of the channel spanning from the i^{th} MBS to the D2D Rx is $h_{cd,i}$ and that of the j^{th} D2D Tx in other macrocells to the D2D Rx is h_j. For the sake of better understanding, these channel fading gains for two adjacent macrocells are shown in Figure 3.4, which can be easily extended to the network model of Figure 3.3. Furthermore, ϕ is the set of all macrocells present in the cellular network of Figure 3.3, while ψ is the set of all the D2D links in other macrocells, operating on the same frequency set. Similarly, the SIR of MUs at a distance d_c from the MBS of the macrocell which is using UFR, can thus be written as:

$$\begin{aligned} \gamma_c(d_c) &= \frac{P_c^{max} h_c d_c^{-\alpha}}{I_c + I_{dc}}, \\ I_c &= \sum_{i \in \phi \setminus \{0\}} P_c^{max} h_{c,i} d_{c,i}^{-\alpha}, \\ I_{dc} &= \sum_{j \in \psi} P_d(r_j) h_{dc,j} l_{dc,j}^{-\alpha}, \end{aligned} \tag{3.3}$$

where h_c denotes the fading gain of the MBS to MU link, $h_{c,i}$ is fading gain experienced from the i^{th} MBS using the same frequency band to the MU and $h_{dc,j}$ is the fading gain

of the j^{th} D2D Tx to the MU link operating in the same frequency band, as shown in Figure 3.4. Here I_c represents the interference imposed by the MBSs on the MU using the same frequency band, while I_{dc} is the interference experienced by the MU due to the superimposed D2D links.

Consider two different frequency reuse schemes, namely the FFR and SFR regimes. In the FFR scenario, the total available bandwidth is divided into four orthogonal frequency bands, obeying $F = F_0 + F_1 + F_2 + F_3$. More particularly, the frequency band F_0 is common to all the macrocells for the CCR region of the network, while $F_i, i \in 1, 2, 3$ is assigned to the users in the CER of the three adjacent macrocells, as shown in Figure 3.1(a). The classification of MUs roaming in the CCR and CER of the macrocell is determined on the basis of their SIR and the predefined threshold SIR S_c. Now, in order to allocate an adequate frequency band to MU, it is required categorise them into CCR and CER users. The users that have an SIR higher than the predefined threshold SIR ($\gamma_c > S_c$) constitute the CCR users, while the ones with an SIR lower than the threshold ($\gamma_c \leq S_c$) are the CER users.

On the other hand, when considering SFR, the total available bandwidth is partitioned into three equal orthogonal frequency bands according to $F = F_1 + F_2 + F_3$, where one of the frequency bands $F_i, i \in 1, 2, 3$ is used in the CER of the macrocell ensuring that it is orthogonal to the neighbouring CER of the adjacent macrocells, while the remaining two-thirds of the frequency band is reserved for the CCR of the macrocell, as depicted in Figure 3.1(b). Moreover, the MBS would transmit at power P_m in the CCR and at the power of βP_m in the CER of the macrocell[2].

3.3 Coverage and Capacity

The coverage probability is defined as a probability of successful communication between the source and destination. In other words, the coverage probability of the D2D link is obtained as the probability of the D2D links possessing an SIR higher than the target SIR [3] (T) . It is affected by the distance r between the D2D Tx and the D2D Rx, by the transmit power $P_d(r)$ of the D2D link as well as the interference I_{cd} experienced at the D2D Rx due to the cellular communication and the interference I_d owing to the D2D communication operating in the same frequency band. Firstly, the coverage probability of the D2D links is derived, when the MBSs use UFR.

Theorem 1. *The coverage probability of the D2D links, when the MBSs use UFR is given*

[2] $P_m = \frac{P_c^{max}}{\beta}, \beta \geq 1$

[3] The target SIR for all the D2D links is considered to be the same for the analytical derivation of their coverage probability.

by Eq. (3.4).

$$CP = \int_0^{R_c} \frac{R_2}{R_2 - R_1}{}_2F_1\left[\frac{1}{\alpha - \alpha\epsilon}, \theta(l), 1 + \frac{1}{\alpha - \alpha\epsilon}, \frac{-\lambda(l) R_2^{\alpha} T}{P_d^{max}}\right] - \frac{R_1}{R_2 - R_1}{}_2F_1\left[\frac{1}{\alpha - \alpha\epsilon}, \theta(l), 1 + \frac{1}{\alpha - \alpha\epsilon}, \frac{-\lambda(l) R_1^{\alpha - \alpha\epsilon} R_2^{\alpha\epsilon} T}{P_d^{max}}\right] \frac{2l}{R_c^2} dl. \tag{3.4}$$

where R_1 and R_2 are minimum and maximum distance between D2D pair, while R_c is radius of macrocell, α is path-loss exponent and ϵ is power control factor for D2D links. The target SIR is defined by T while the power budget of D2D links is P_d^{max}. Here $\lambda(l)$ and $\theta(l)$ are shape and scale parameter of the Gamma distribution of the total interference at D2D links, while ${}_2F_1[a, b; c; z]$ is hypergeometric function.

Proof. See Appendix A.1 for the proof. □

3.3.1 Fractional Frequency Reuse

In UFR, the users roaming close to the MBS experience a lower co-channel interference than those, who are far from the MBS. However, the FFR relies on a combination of the frequency reuse factor of 1 and that of $\frac{1}{3}$, where the cell-centre users occupy a band having a reuse factor of 1 and the cell-edge users associated with a reuse factor of $\frac{1}{3}$. This implies that there is a reduction in the interference afflicted upon the cell-edge users due to the neighbouring cells. Let us first propose a pair of different frequency allocation schemes for the D2D links, when the MBSs use FFR and then derive the coverage probability of each of the proposed scheme. In order to define these two schemes, recall that the D2D link have been classified as SR D2D links and LR D2D links, based on the predefined threshold SIR (S_d). The SR D2D link is defined as the link that has an SIR higher than the threshold SIR ($\gamma_U > S_d$), while the LR D2D link has an SIR lower than the threshold SIR threshold ($\gamma_U \leq S_d$). It is important to note that the SIR of the D2D link is calculated by assuming that the D2D link experiences interference from all the macrocells as well as from all the other D2D links that are present in the other macrocells and using the same frequency. Let us now describe the two frequency allocation schemes defined for the D2D links as follows:

(a) Fractional Frequency Allocation 1 (FFA1): In this scheme, the CCR frequency of the reference macrocell is allocated to the SR D2D link and the CER frequency of the other macrocells to the LR D2D link. Upon considering the macrocell 0 of Figure 3.3 as the reference cell, F_0 is the CCR frequency, while the CER frequency of the neighbouring cells is F_2 and F_3. Therefore, in FFA1, the SR D2D links would reuse F_0, while the LR D2D links would reuse F_2 and F_3.

(b) Fractional Frequency Allocation 2 (FFA2): In this scheme, the CER frequency of the reference macrocell is allocated to the SR D2D link and the CER frequency of the other macrocells to the LR D2D link. Similar to FFA1, the reference macrocell is cell 0 of Figure 3.3, where the SR D2D links would reuse F_1, which is the CER frequency of the reference cell and the LR D2D links would reuse F_2 and F_3.

The motivation behind this definition for the pair of schemes is the FFR scheme itself. In FFR, the cell-edge users (that have a low SIR) are assigned the frequency of $F_i, i \in 1, 2, 3$, which results in a reduced co-channel interference. Correspondingly, the D2D links that have a high SIR are assigned F_0 (or F_1), while the D2D links having a low SIR are assigned F_2 or F_3 in FFA1 (or FFA2) for the sake of reducing the co-channel interference. In other words, initially try to serve the D2D link at F_0 (or F_1), i.e. find the SIR based on F_0 (or F_1). However, the D2D link that experiences a high level of interference, i.e. whose SIR is low, is allocated a new frequency from the set of frequencies F_2 or F_3, which are not contaminated by the strong interference from reference MBS as shown in Figure 3.1. The coverage probability of the D2D links when the MBSs use UFR was given by Eq. (A.9) of Appendix A.1 and now the same result is extended to the proposed schemes.

Theorem 2. *The coverage probability of a typical D2D link in the network of Figure 3.3 using FFA*1 *is given by*

$$CP_{FFA1} = \int_0^{R_c} CP(l, \max\{T, S_d\}) + \hat{CP}(l, T)[1 - CP(l, S_d)] f_L(l)\, dl, \tag{3.5}$$

where $CP(l, \max\{T, S_d\})$ *and* $CP(l, S_d)$ *are obtained using Eq. (A.8) from Appendix A.1, which is also the integrand of Eq. (3.4) by replacing* T *with* $\max\{T, S_d\}$ *and* S_d*, respectively. Similar to* $CP(l, T)$ *which is defined for the frequency* F_0*,* $\hat{CP}(l, T)$ *can be derived for frequency* F_2 *and* F_3*.*

Proof. See Appendix A.2 for the proof. □

Similarly, the coverage probability of a D2D link using FFA2 in the network of Figure 3.3 is given as follows:

$$CP_{FFA2}(l, r) = P[\tilde{\gamma}_U(l, r) > \max\{T, S_d\}] + P[\hat{\gamma}_U(l, r) > T] P[\tilde{\gamma}_U(l, r) < S_d]. \tag{3.6}$$

It is important to note that in FFA2, the SR D2D link reuses the CER frequency band for its communication process and since the transmission channels are independent of each other, the D2D links experience different fading gains as well as interference, which is characterised by the SIR denoted by $\tilde{\gamma}_U(l, r)$. However, for the LR D2D links in FFA2, the frequency band reused is the same as that reused by the LR D2D links in FFA1 and hence the SIR is denoted by $\hat{\gamma}_U(l, r)$ in the above expression. Using the expression of coverage probability of the UFR defined in Eq. (A.9), the final coverage probability expression of

typical D2D links in the FFA2 scenario can be written as:

$$CP_{FFA2} = \int_0^{R_c} \tilde{CP}(l, \max\{T, S_d\}) + \hat{CP}(l, T)[1 - \tilde{CP}(l, S_d)] f_L(l) \mathrm{d}l, \tag{3.7}$$

where similar to $CP(l, T)$, $\tilde{CP}(l, T)$ can be derived for the frequency F_1.

3.3.2 Soft Frequency Reuse

The macrocells relying on SFR techniques use one-third of the band allocated for the cell-edge users, which is set to be different from the neighbouring cells in order to avoid any interference, while the remaining two-thirds of the band is used for the cell-centre users. The MBS imposes power control for transmitting at the power of P_m for the CCR users, while at βP_m for the CER users. In this subsection, using the previous definitions of SR and LR D2D links, a frequency allocation scheme is proposed for the D2D links, which is defined as follows:

(a) Soft Frequency Allocation (SFA): In this scheme, the CER frequency is allocated to the SR D2D link and CCR frequency to the LR D2D link. Considering cell 0 of Figure 3.3 as the reference macrocell, where the CCR and CER frequency bands are F_3 and F_1, F_2 respectively. According to the definition of this scheme, the SR D2D links are allocated F_3, while the LR D2D links reuse F_1 and F_2.

Similar to the previous derivation of the coverage probability for the FFR technique, the coverage probability for the proposed scheme is derived, when network relies on SFR. Thus, the coverage probability of SFA is derived.

Theorem 3. *The coverage probability of the D2D link in SFA can be expressed as*

$$CP_{SFA} = \int_0^{R_c} CP_S(l, \max\{T, S_d\}) + \hat{CP}_S(l, T)[1 - CP_S(l, S_d)] f_L(l)\, dl, \tag{3.8}$$

where similar to $CP(l, T)$ given in Eq. (A.8) from appendix A.1, $CP_S(l, \max\{T, S_d\})$ and $\hat{CP}_S(l, T)$ can be derived for the CCR frequency and CER frequency.

Proof. See Appendix A.3 for the proof. □

3.3.3 Capacity

In this subsection, the capacity of all the proposed schemes as well as of the benchmark scheme is derived. Commencing with the benchmark scheme, the capacity is given by

[49, 93],

$$\begin{aligned} C &= E[\ln(1+SIR)] \\ &= \int_{t>0} P[\ln(1+SIR) > t]\mathrm{d}t \\ &= \int_{t>0} P[SIR > e^t - 1]\mathrm{d}t. \end{aligned} \tag{3.9}$$

Thus, the capacity is equivalent to the coverage probability evaluated at $T = e^t - 1$ and then integrated over t. The capacity of a D2D link, which is at a distance of l from the MBS is given by,

$$\begin{aligned} C(l,r) &= \int_{t=0}^{\infty} \left(\frac{P_d^{max}}{\lambda(l) r^{\alpha(1-\epsilon)} R_2^{\alpha\epsilon} + P_d^{max}} \right)^{\theta(l)} \mathrm{d}t \\ &= {}_2F_1\left(1, 1; \theta(l)+1; 1 - \frac{P_d^{max}}{\lambda(l)(e^t-1) r^{\alpha(1-\epsilon)} R_2^{\alpha\epsilon}}\right) \frac{P_d^{max}}{\theta(l)\lambda(l) r^{\alpha(1-\epsilon)} R_2^{\alpha\epsilon}}. \end{aligned} \tag{3.10}$$

By averaging Eq. (3.10) over the distance from the MBS and the distance between the D2D link, the capacity of a typical D2D link is given by

$$C = \int_0^{R_c} \int_{R_1}^{R_2} {}_2F_1\left(1, 1; \theta(l)+1; 1 - \frac{P_d^{max}}{\lambda(l) r^{\alpha(1-\epsilon)} R_2^{\alpha\epsilon}}\right) \frac{P_d^{max}}{\theta(l)\lambda(l) r^{\alpha(1-\epsilon)} R_2^{\alpha\epsilon}} \frac{1}{R_2 - R_1} \mathrm{d}r \frac{2l}{R_c^2} \mathrm{d}l \tag{3.11}$$

Now, the capacity of the D2D link is derived for the proposed FFA1 scheme. The capacity of an SR D2D link is given by

$$\begin{aligned} C_S(l,r) &= \int_{t=0}^{\infty} \frac{P[\gamma_U(l,r) > \max\{e^t - 1, S_d\}]}{P[\gamma_U(l,r) > S_d]} \mathrm{d}t \\ &= \int_{\ln(1+S_d)}^{\infty} \frac{P[\gamma_U(l,r) > e^t - 1]}{P[\gamma_U(l,r) > S_d]} \mathrm{d}t \quad + \int_{t=0}^{\ln(1+S_d)} \frac{P[\gamma_U(l,r) > S_d]}{P[\gamma_U(l,r) > S_d]} \mathrm{d}t \\ &= \frac{1}{P[\gamma_U(l,r) > S_d]} \int_{t=\ln(1+S_d)}^{\infty} \left(\frac{P_d^{max}}{\lambda(l)(e^t-1) r^{\alpha(1-\epsilon)} R_2^{\alpha\epsilon} + P_d^{max}} \right)^{\theta(l)} \mathrm{d}t + \ln(1+S_d) \end{aligned} \tag{3.12}$$

After simplification, following expression is achieved,

$$C_S(l,r) = \ln(1+S_d) + \frac{{}_2F_1\left[\theta(l), \theta(l); \theta(l)+1; (1+S_d)^{-1}\left(1 - \frac{P_d^{max}}{\lambda(l) r^{\alpha(1-\epsilon)} R_2^{\alpha\epsilon}}\right)\right] (P_d^{max})^{\theta(l)}}{P[\gamma_U(l,r) > S_d]((1+S_d)\lambda(l) r^{\alpha(1-\epsilon)} R_2^{\alpha\epsilon})^{\theta(l)}} \tag{3.13}$$

Similarly, the capacity of a LR link is given by

$$C_L(l,r) = {}_2F_1\left(1, 1; \hat{\theta}(l)+1; 1 - \frac{P_d^{max}}{\hat{\lambda}(l) r^{\alpha(1-\epsilon)} R_2^{\alpha\epsilon}}\right) \frac{P_d^{max}}{\hat{\theta}(l)\hat{\lambda}(l) r^{\alpha(1-\epsilon)} R_2^{\alpha\epsilon}} \tag{3.14}$$

Similar to $\theta(l)$ and $\lambda(l)$ which are given in Eq. (A.4) and are defined for a frequency reuse 1, $\hat{\theta}(l)$ and $\hat{\lambda}(l)$ can be derived for a frequency reuse of $\frac{1}{3}$. Then the capacity of a typical D2D link is given by

$$C_{FFA1} = \int_0^{R_c} \int_{R_1}^{R_2} C_S(l,r) P[\gamma_U(l,r) > S_d] + \frac{2}{3} C_L(l,r) P[\gamma_U(l,r) < S_d] \frac{1}{R_2 - R_1} \mathrm{d}r \frac{2l}{R_c^2} \mathrm{d}l. \tag{3.15}$$

The first term in Eq. (3.15) corresponds to the capacity of an SR D2D link that reuses F_0, whereas the second term denotes the capacity of the LR D2D link that reuses F_2 and F_3. Here the factor $\frac{2}{3}$ weights the second term due to the fact that among all the cell-edge sub-bands (F_1, F_2, F_3), only F_2 and F_3 are used by the LR link in FFA1. The capacity of the other proposed schemes such as FFA2 and SFA can be derived using the process followed for FFA1. The capacity of the D2D link employing FFA2 is :

$$C_{FFA2} = \int_0^{R_c} \int_{R_1}^{R_2} \frac{1}{3} C_S(l,r) P[\gamma_U(l,r) > S_d] + \frac{2}{3} C_L(l,r) P[\gamma_U(l,r) < S_d] \frac{1}{R_2 - R_1} \mathrm{d}r \frac{2l}{R_c^2} \mathrm{d}l. \tag{3.16}$$

and that of the D2D link employing SFA is :

$$C_{SFA} = \int_0^{R_c} \int_{R_1}^{R_2} C_S(l,r) P[\gamma_S(l,r) > S_d] + C_L(l,r) P[\gamma_S(l,r) < S_d] \frac{1}{R_2 - R_1} \mathrm{d}r \frac{2l}{R_c^2} \mathrm{d}l. \tag{3.17}$$

3.4 Performance Results and Discussion

In this section, the performance of the proposed schemes benchmarked against the scheme, when the MBS relies on UFR is studied. In the scenario when the MBSs employ UFR, the frequency is reused according to a reuse factor of 1 and hence there is no need for any further classification into CCR and CER users, since all MUs will be using the same frequency band. Furthermore, a random frequency allocation scheme is assumed for the D2D links, which means that a random D2D-MU association is considered for the resource reuse in the benchmark scenario. Furthermore, the impact of the proposed schemes is analysed on the MU coverage probability along with that of the benchmark scheme. Consider the network of 19 hexagonal cells seen in Figure 3.3, where for ease of exposition, each macrocell is approximated by a circle of radius R as mentioned in Table 3.1 except for Figure 3.6. Each macrocell is a hybrid cell consisting of C MUs and D D2D links, where the MBS is located at the centre of the macrocell, while the MUs and the D2D links relying on downlink resources are distributed uniformly in the cell. Furthermore, all resource blocks are uniformly shared among the users and D2D links. In other words, if there are K users or D2D links and R resource blocks, then each user or each D2D link is assigned $\frac{R}{K}$ resource blocks. Furthermore, for each user the SIR is computed, which is used for classifying the users into the CCR and CER. Note that the SIR is evaluated based on the CCR region. In

Parameter	Value
Radius of Cell, R	1000 m
Number of MUs, M	100
Number of D2D links, D	100
Minimum Distance of D2D Pair, R_1	30 m
Maximum Distance of D2D Pair, R_2	50 m
Power budget of MBS, P_c^{max}	46 dBm
Power budget of D2D links, P_d^{max}	20 dBm
Power control factor of D2D links, ϵ	0
Path-loss exponent, α	3

Table 3.1: Parameters used for Simulations

other words, it is first assumed that all the users are in the CCR region and then compute the SIR. Furthermore, the SIR is compared to S_c and if the MU's SIR is higher than S_c, then the user will continue to rely on the same sub-band and will assumed to be a CCR user. By contrast, if the MU's SIR is lower than S_c, the user is assumed to be a CER user and hence will camp on new sub-band. Similarly, in a D2D link scenario, first the SIR of the D2D user is evaluated assuming that the D2D link is an SR D2D link and then compare the SIR to S_d. Now, if the D2D link's SIR is higher than S_d, the D2D link is assumed to be an SR link and will continue to use the same sub-band. By contrast, if the SIR is lower than S_d, the D2D link is considered to be a LR link and hence will use a new sub-band, which is defined for the LR D2D link according to the proposed frequency allocation schemes. The distance r between the D2D Tx and Rx is also uniformly distributed in $[R_1, R_2]$, where the minimum distance R_1 and the maximum distance R_2 is set according to Table 3.1 i.e. $r \in [R_1, R_2]$, except for Figure 3.6. Similar setting for distance between D2D pair has been adopted in [94, 95, 96]. The power budget of the MBS and D2D links is set to P_c^{max} and p_d^{max}as given in Table 3.1, respectively. The random mapping of the D2D links to the MU's resource blocks is assumed and the transmit power of the D2D links is a function of the distance r, as defined in Eq. (3.1) of Section 3.2. The power control factor ϵ is set according to Table 3.1 for all the results, unless otherwise stated. This means that the D2D links transmit at the maximum power. The transmission channels experience independent Rayleigh fading and a path loss factor of α defined in Table 3.1. The simulation results are obtained using Monte Carlo simulations with 1000 runs and the proposed schemes as well as the benefits of power control in the D2D links is analysed by dividing this section into three parts as follows:

3.4.1 Fractional Frequency Reuse

In this section, the performance of the proposed frequency allocation schemes for the D2D links is analysed, when the MBS employs FFR. Explicitly, the coverage probability and

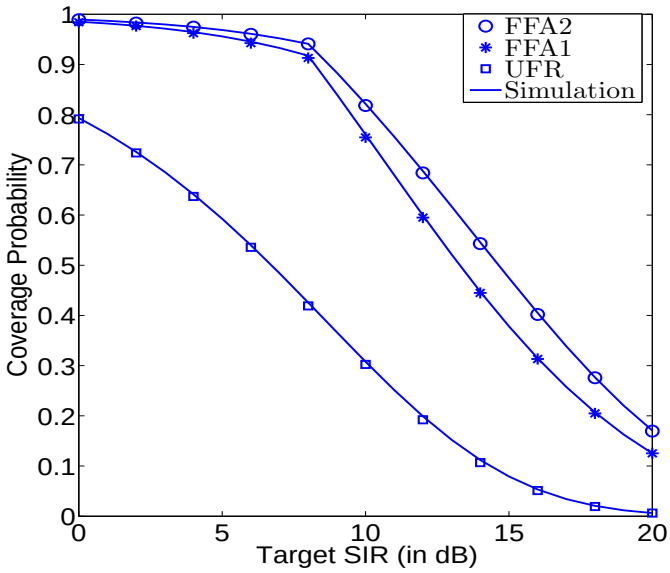

Figure 3.5: Coverage probability of the D2D link for the proposed schemes relying on FFR. Here $S_d = 8$dB, while all other system parameters are summarized in Table 3.1.

capacity of the D2D links as well as their impact on the MU's coverage probability is evaluated. Commencing with a discussion of the performance of both FFA1 and FFA2 on the coverage probability of the D2D link, where it is considered that $\alpha = 3$ and $S_d = 8$ dB. Figure 3.5 depicts the coverage probability of the D2D link for both FFA1 and FFA2, when the MBS uses FFR against the benchmark scheme of UFR. First of all, it can be clearly seen that the analytical results closely match the simulations. Secondly, UFR results in the lowest coverage probability amongst all the schemes, since the D2D link experiences interference from all the MBSs including the reference MBS[4]. Interestingly, both the proposed FFA1 and FFA2 schemes provide a significantly better performance than the UFR scheme. The reason for this trend is as follows: the LR D2D links which otherwise have a significantly lower SIR in the UFR scheme, experience no interference from the reference MBS and they experience the same amount of interference as the frequency reuse $\frac{1}{3}$ pattern. Moreover, FFA2 provides a better coverage probability than FFA1, since FFA2 utilizes the cell-edge frequency of the reference cell, whereas FFA1 utilizes the cell-centre frequency of the reference cell. This means that in FFA2 the interference experienced by the SR D2D links is reduced, since it has a frequency reuse of $\frac{1}{3}$, while in FFA1 it obey a frequency reuse 1 pattern, hence increasing the total interference, thereby decreasing the coverage probability for the latter scheme. This can be shown using the analytical expressions as well, when $S_d \geq T$. The coverage probability of a typical D2D link, when $S_d \geq T$ using FFA1 is given by Eq. (3.5),

$$CP_{FFA1} = \int_0^{R_c} [CP(l, S_d) + \hat{CP}(l, T)(1 - CP(l, S_d))] f_L(l) \mathrm{d}l,$$

[4]Here reference MBS is the one where D2D link is present.

where the term $CP(l, S_d)$ denotes the coverage probability of the D2D link, when it relies on the CCR frequency of the reference cell. Similarly, the term $[1 - CP(l, S_d)]$ denotes the coverage probability of the D2D link, when it utilises the CER frequency of the neighbouring cells. Furthermore, the coverage probability of a typical D2D link associated with $S_d \geq T$ using FFA2 is given in Eq. (3.7),

$$CP_{FFA2} = \int_0^{R_c} [\tilde{CP}(l, S_d) + \hat{CP}(l, T)(1 - \tilde{CP}(l, S_d))] f_L(l) \mathrm{d}l.$$

Here the term $\tilde{CP}(l, S_d)$ denotes the coverage probability of the D2D link when it utilises the cell-edge frequency of the reference cell. Note that $CP(l, S_d) < \tilde{CP}(l, S_d)$, where $CP(l, S_d)$ and $\tilde{CP}(l, S_d)$ are the coverage probability of the D2D links, when they utilise the CCR frequency and the CER frequency of the reference cell, respectively. In other words, while calculating $\tilde{CP}(l, S_d)$, the interference experienced by the D2D links is reduced, since it has a frequency reuse of $\frac{1}{3}$, while for calculating $CP(l, S_d)$ it obeys unity frequency reuse pattern. In order to compare the coverage probability of both the schemes, the expressions have been rearranged and given in Eq. (3.5) and Eq. (3.7) as

$$CP_{FFA1} = \int_0^{R_c} [\hat{CP}(l, T) + CP(l, S_d)(1 - \hat{CP}(l, T))] f_L(l) \mathrm{d}l, \tag{3.18}$$

and

$$CP_{FFA2} = \int_0^{R_c} [\hat{CP}(l, T) + \tilde{CP}(l, S_d)(1 - \hat{CP}(l, T))] f_L(l) \mathrm{d}l, \tag{3.19}$$

Recall that $CP(l, S_d) < \tilde{CP}(l, S_d)$ and hence it is apparent from Eq. (3.18) and Eq. (3.19) that $CP_{FFA1} < CP_{FFA2}$, which conforms with the results presented in Figure 3.5.

In Figure 3.6, the coverage probability of D2D links relying on the parameter setting of $R_c = 500m$ and $r \in [20, 40]$ is presented, which indicates that the analysis is indeed valid for any parametric setting. Moreover, a change in the value of R_c as well as r will not affect the performance trends of the proposed schemes. In other words, both the proposed FFA1 and FFA2 schemes provide a significantly better performance than the UFR scheme. Furthermore, FFA2 provides a better coverage probability than FFA1.

Figure 3.7 provides simulation results, where each D2D link has a different target SIR. In particular, the coverage probability versus the SIR threshold have been plotted, where each D2D link has been randomly assigned different target SIRs ranging between $[2, 8]$dB. Interestingly, the behaviour of the proposed schemes investigated in the scenarios, when the D2D links have different target SIRs, remain similar to that of the D2D links having the same target SIR. In other words, both the proposed FFA1 and FFA2 schemes provide a significantly better performance than the UFR scheme. Moreover, FFA2 provides a better coverage probability than FFA1. However, the coverage probability and rate expressions are not derived, when the D2D links can have different target SIR. It would be interesting

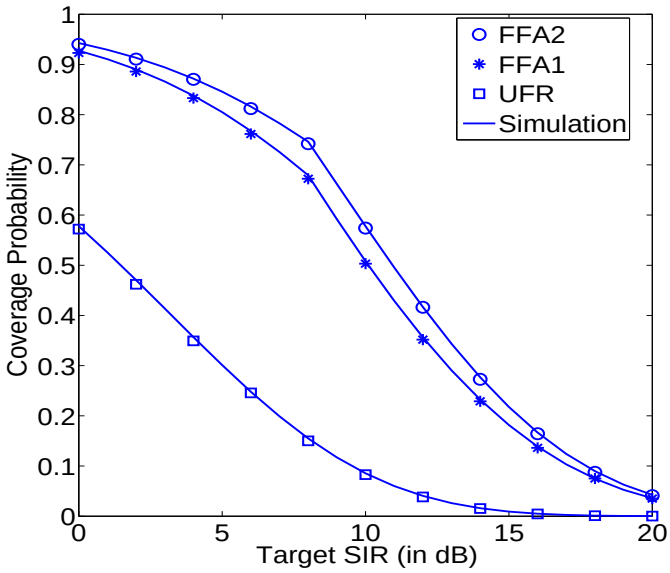

Figure 3.6: Coverage probability of the D2D link for the proposed schemes relying on FFR. Here $R_c = 500$m, $r \in [20, 40]$m, and $S_d = 8$dB. All other system parameters are summarized in Table 3.1.

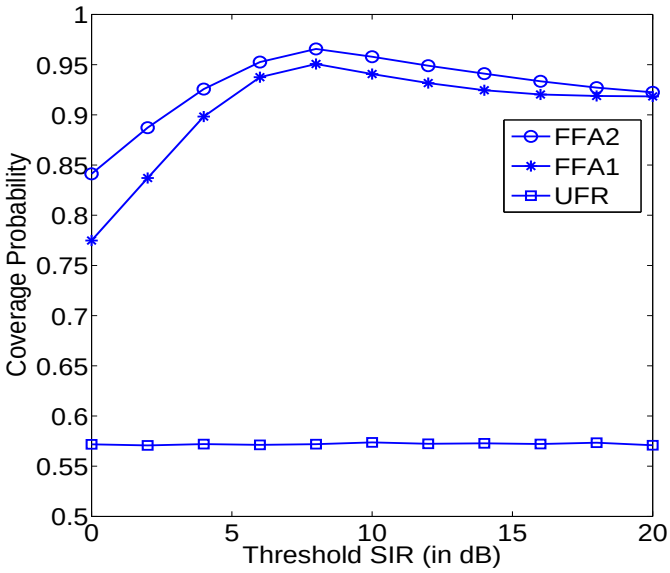

Figure 3.7: Coverage probability of the D2D link for the proposed schemes relying on FFR. Here $T \in [2, 8]$dB, while all other system parameters are summarized in Table 3.1.

to analytically study the performance of D2D links in the future work, when they have different target SIRs.

The capacity of the D2D link for the proposed schemes is shown as a function of the threshold SIR in Figure 3.8. It can be observed that as the threshold SIR increases, the capacity of FFA1 first increases and then decreases, but it has a significantly higher capacity than the benchmark scheme. A lower value of the threshold SIR may assign too many D2D links from the LR link resources to the SR link resources, while a higher value increases the number of LR D2D links. In either case, the capacity will be reduced. The reason behind this trend is the fact that the capacity of D2D links is influenced both by the SIR of the link as well as by the bandwidth allocated for the frequency resources of the CER and CCR

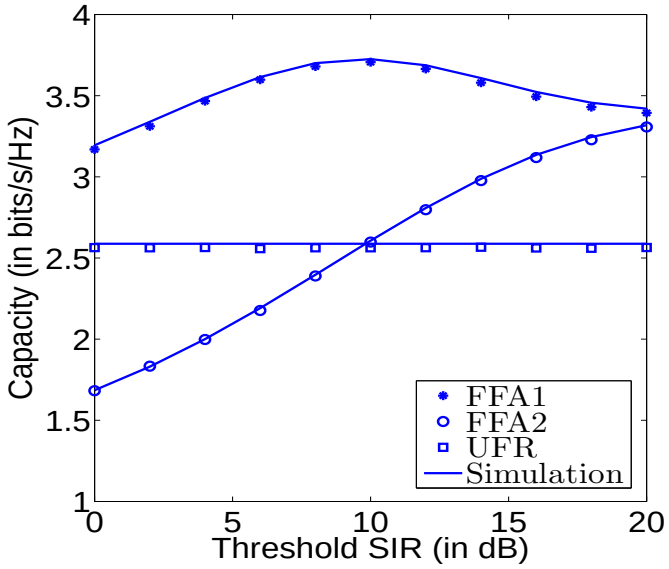

Figure 3.8: Capacity of the D2D link for the proposed schemes relying on FFR. All the system parameters are summarized in Table 3.1.

regions in the macrocell. In other words, at a lower threshold SIR, there would be more SR D2D links, which would have a higher bandwidth, but would have a lower SIR, since the interference experienced is increased owing to the employment of the CCR frequency. Hence the overall impact of both these factors would reduce the capacity of D2D links at a low threshold SIR. Similarly, at higher threshold SIRs, there may be more D2D links that are now considered as LR links, that would have provided a higher rate due to a higher SIR, but at the same time it has a lower bandwidth owing to the utilisation of the CER frequency, thereby reducing the overall rate. On the other hand, the capacity of FFA2 increases as the threshold SIR increases. This is due to the fact that in FFA2 D2D links only reuse the CER frequency resources of the MBS. This means that when the threshold SIR increases, the CER frequency resources are increased and hence the capacity of FFA2 increases. Moreover, at a higher threshold SIR, the capacity of FFA2 approaches that of FFA1 due to the fact that both the proposed schemes only use the CER frequency resources at a higher threshold SIR. Note that S_d in FFA1 and FFA2 can be chosen according to

$$CP_{FFA1,SR} = \int_0^{R_c} CP_{FFA1,SR}(l, S_d) \frac{2l}{R_c^2} \mathrm{d}l = \frac{F_0}{F}$$

and

$$CP_{FFA2,SR} = \int_0^{R_c} CP_{FFA1,SR}(l, S_d) \frac{2l}{R_c^2} \mathrm{d}l = \frac{F_1}{F},$$

respectively. Here $CP_{FFA1,SR}$ and $CP_{FFA2,SR}$ denote the specific fraction of D2D links who are categorized into SR links under FFA1 and under FFA2, respectively. Therefore, operators need to carefully choose the value of F_i for D2D links aided cellular networks since S_d and hence the performance of D2D links depends on F_i.

Now the impact of the proposed schemes on the coverage probability of the MUs is

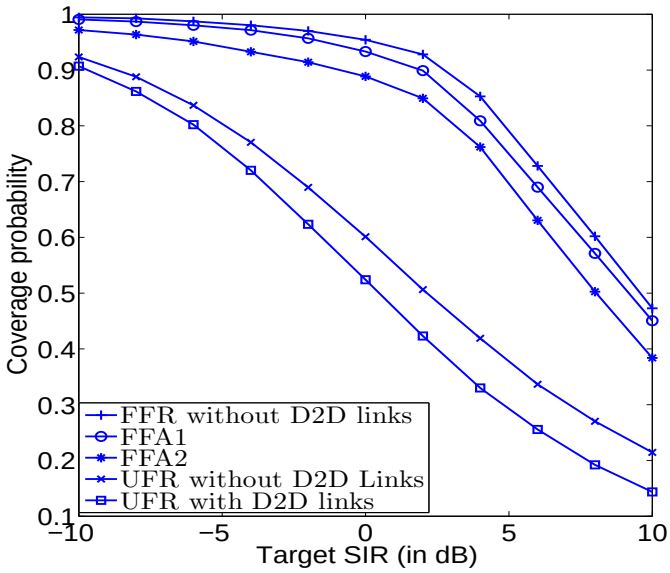

Figure 3.9: Impact of the proposed FFA1 and FFA2 schemes on the MU's coverage probability. Here $S_C = 3$dB, while all other system parameters are summarized in Table 3.1.

analysed in Figure 3.9 for five different cases: (i) when there are no D2D links and the MU uses UFR, (ii) when there are D2D links and the MU uses UFR, (iii) when the D2D links use FFA1. (iv) when the D2D links use FFA2 (v) when there are no D2D links and the MU uses FFR. All the results are plotted using simulations. It can be observed that the coverage probability of the MU is the lowest when FFA2 is used in the D2D link, since FFA2 only utilizes the CER frequency resources of the MBS. This means that the specific CER users experiencing a low SIR would now experience an even higher interference owing to the presence of D2D links that are reusing the CER user's RB, hence reducing the coverage probability of CER users. As expected, the coverage probability of MU operating in the absence of D2D links is the highest followed by the MUs when FFA1 is used in the D2D links. It is interesting to note that the coverage probability degradation of MU is lower, when the D2D links use FFA1 than in the case, when the D2D links use UFR.

3.4.2 Soft Frequency Reuse

In this section, the performance analysis of the proposed frequency allocation scheme for D2D links, when the macrocell employs SFR is presented, which is also benchmarked against the traditional UFR scheme. It is assumed that each MBS transmits at a power of $P_m (= \frac{P_c^{max}}{\beta})$ in the CCR and at a power of βP_m in the CER, for ensuring that the maximum power transmitted by any MBS does not exceed its power budget. First, the coverage probability of D2D links in the case of the SFA scheme for different values of the power control factor β is discussed. It would be fair to compare the UFR scheme to the SFA scheme, when $\beta = 1$, since the transmit power of the MBS would be the same for both schemes. It can be clearly seen from Figure 3.10 that the proposed scheme has a higher coverage probability than the benchmark scheme. Interestingly, the proposed SFA scheme associated with $\beta = 1$ provides a better coverage probability than the benchmark scheme.

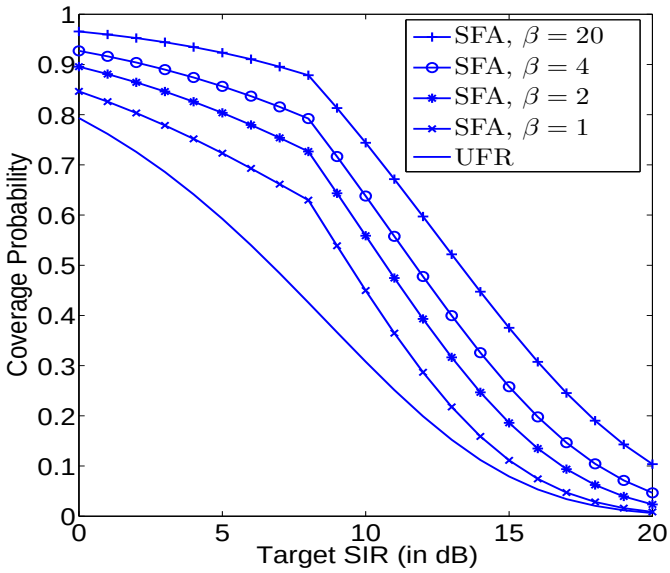

Figure 3.10: Coverage probability of the D2D link for the proposed SFA scheme . Here $S_D = 8$dB, while all other system parameters are summarized in Table 3.1.

This improvement in the coverage probability of the SFA scheme over that of the UFR scheme is due to the resultant sub-band diversity gain[5] achieved by the system, when the D2D link is classified as either an SR or LR D2D link. Moreover, it can be observed that upon increasing the value of the power control factor β, the coverage probability of D2D links is improved. The reason behind this phenomenon is that as the value of β increases, the transmit power P_m in the CCR region decreases and hence the interference imposed by the reference MBS on the LR D2D links employing SFA decreases, which results in an increased SIR, hence supporting a higher coverage probability for the D2D links.

The capacity of the D2D links is also analysed using the proposed scheme, when the MBS employs SFR, as shown in Figure 3.11. It is interesting to note that the capacity of the proposed scheme increases upon increasing the value of the power control factor β of the MBSs. As β increases, the D2D links experience a reduced interference, thereby increasing their SIR and hence improving the capacity of the D2D links. Moreover, it can be clearly seen that the proposed scheme performs significantly better than that of the UFR benchmark scheme due to the reduced interference at the D2D receivers and as a benefit of the sub-band diversity gain achieved by the proposed scheme at the D2D links. However, for the case of $\beta = 1$, there is only one reason that is the sub-band diversity gain achieved by the proposed scheme as the transmit power of MBS is same for all the schemes in the curve and hence induce same interference.

[5]A D2D link using the CCR frequency will now be assigned a new sub-band that corresponds to the CER frequency of other cell if its SIR is lower than the threshold SIR ($\gamma_U > S_d$), implying that this D2D link will now experience a new fading power, since the fading is assumed to be independent across the sub-bands. Therefore, there is gain achieved by the system due to allocation of a new sub-band and it is called sub band diversity gain.

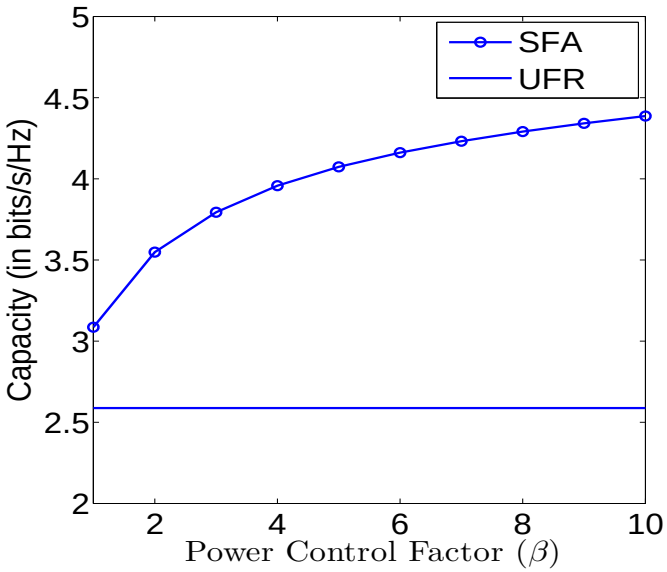

Figure 3.11: Capacity of the D2D link for the proposed schemes relying on SFR. All the system parameters are summarized in Table 3.1.

3.4.3 Power Control for the D2D links

In this section, the effects of distance-based power control on the D2D links defined in Eq. (3.1) of Section 3.2 will be analysed using simulations. First, the impact of the distance (r) is analysed on the normalised transmit power of a typical D2D link shown in Figure 3.12, parametrized by the power control factor ϵ. It can be clearly seen that as the distance between the D2D transmitter and receiver increases, the transmit power required by the link increases, as expected. It can also be observed that at $\epsilon = 0$, all the D2D Txs would transmit at an equal power of P_d^{max} and hence the normalised transmit power would be 1. However, at $\epsilon = 1$, the power received at the D2D Rx would be equal and hence the normalised transmit power is the lowest. Moreover, an interesting observation that can be made from Figure 3.12 is that as the power control factor ϵ increases, the rate at which the transmit power of the D2D Tx decreases is reducing. For example, at a distance of $r = 30m$ for the D2D link, as ϵ varies from 0 to 0.2, the normalised transmit power is reduced from 1 to 0.66. However, when ϵ changes from 0.8 to 1, the normalized power reduces from 0.195 to 0.13.

ϵ	UFR	FFA1	FFA2	SFA
0	25.7	34.9	29.0	35.6
0.5	30.3	43.3	36.8	43.8
1	34.3	50.5	44.1	50.8

Table 3.2: Energy efficiency of the four frequency reuse schemes upon varying the power control factor ϵ of the D2D links. All the system parameters are summarized in Table 3.1.

Table 3.2 shows the energy efficiency of the different schemes for different power control factors. Energy efficiency is defined as a ratio of the total average rate of D2D links to the total average power of D2D links corresponding to a particular value of the power

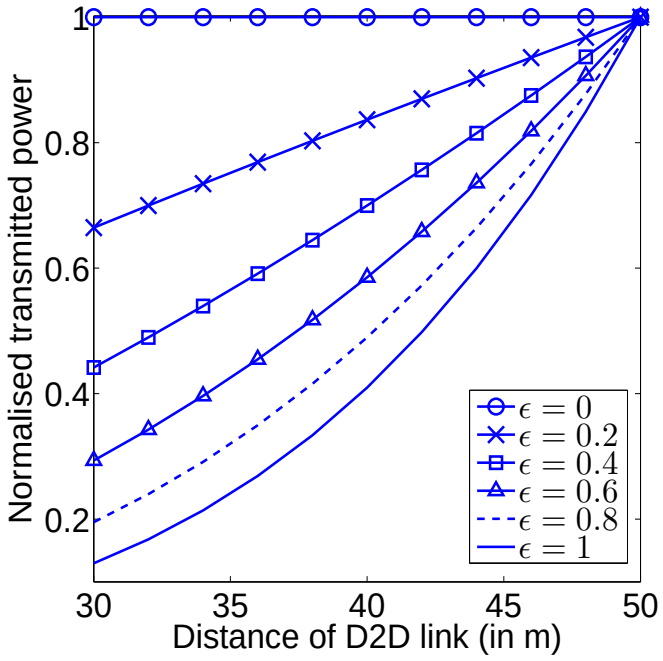

Figure 3.12: Normalised transmit power versus the D2D link length for different values of the power control factor. Here $\alpha = 4$, while all other system parameters are summarized in Table 3.1.

control factor ϵ for the different frequency allocation schemes. Therefore, the unit of energy efficiency is bits/s/Watts. Observe that all the proposed schemes provide a better energy efficiency than UFR, whilst FFA1 attains a higher energy efficiency than FFA2, since FFA1 uses a higher bandwidth compared to FFA2. Moreover, SFA achieves a higher energy efficiency than both FFA1 and FFA2, since it can use all the available bandwidth for D2D communication. Let us now analyse the impact of the power control factor on the energy efficiency. It can be observed that as the power control factor increases, the energy efficiency increases. Interestingly, the increase in energy efficiency is higher, when ϵ changes from 0 to 0.5 than when it changes from 0.5 to 1. For example, the energy efficiency improvement is 24.3% when ϵ changes from 0 to 0.5, whereas it is only 17.3%, when it changes from 0.5 to 1 for FFA1.

Finally, the impact of the power control factor ϵ is characterised on the coverage probability of the proposed schemes and of the benchmarker in Figure 3.13. It can be clearly seen that as the value of ϵ increases, i.e. the transmit power of the D2D links decreases, the coverage probability of the D2D links decreases for all the schemes, owing to the reduced SIR of the D2D links. However, the coverage probability reduction of UFR is higher than that for FFA1 and FFA2 in the lower target SIR region. This is due to the fact that the D2D link that has a low SIR due to its high power control factor can be treated as a LR D2D link and thus it will experience a low interference, which in turn would enhance the coverage probability of D2D links in the proposed schemes.

As mentioned previously, the primary motivation of proportional power control of the D2D links is to utilize its energy efficiently. It can be concluded from Figure 3.12 and Figure 3.13 that when the power control factor is around 0.5, a significant amount of power

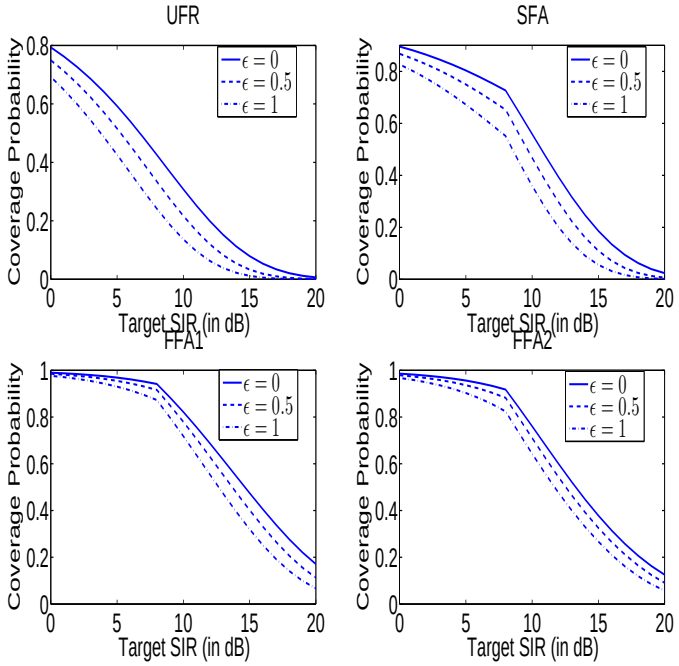

Figure 3.13: D2D coverage probability versus the target SIR for the proposed schemes parametrized by the power control factor. Here S_D = 8dB, while all other system parameters are summarized in Table 3.1.

can be saved at a marginal coverage probability degradation, especially for a low target SIR in case of FFA1 and FFA2. Moreover, Table 3.2 suggested that 0.5 is a good choice for striking a compromise in terms of energy efficiency at the D2D links for all proposed schemes. Therefore, $\epsilon = 0.5$ can be preferred over other values of ϵ.

3.5 Summary and Conclusions

In this chapter, device-to-device communication is considered, which is capable of eliminating the reliance on MBS for its communication and thus serves as a promising solution for *spectral efficiency* improvement, which is another key design factor for future communication systems, as mentioned in Chapter 1. The system model of D2D communication relying on the reuse of RBs allocated to the underlying MUs in the downlink of a cellular network was first presented in Section 3.2, where the transmission power of these D2D links is defined as the distance-proportional power, when the MBS can employ either FFR or SFR for frequency allocation at MUs. The MUs were divided into CCR and CER users depending on their SIR, while the D2D links were classed as SR and LR links. Then, three frequency allocation schemes were proposed, namely FFA1 and FFA2, when the MBS uses FFR in Section 3.3.1, while SFA when the MBS employs SFR in Section 3.3.2 for the D2D links, which are defined as:

- *FFA*1 allocates the CCR frequency (F_0) of the reference macrocell to SR D2D links, while the CER frequency (F_2 and F_3) of other macrocells to LR D2D links, as also depicted in Figure 3.1(a).

- *FFA*2 allocates the CER frequency (F_1) of the reference macrocell to the SR D2D links, while the CER frequency (F_2 and F_3) of other macrocells to LR D2D links, as shown in Figure 3.1(a).
- *SFA* allocates the CER frequency (F_3) to the SR D2D links, while the CCR frequency (F_1 and F_2) to LR D2D links, as represented in Figure 3.1(b).

Following the definitions of the proposed schemes, both the coverage probability as well as capacity of D2D links were analytically derived in Section 3.3, when the MBS employs either UFR, FFR or SFR, where the UFR scheme is treated as a benchmark scheme for the proposed frequency allocation schemes. These schemes impose less interference on the D2D links, while at the same time satisfying the QoS requirement of the MUs in the macrocell. The detailed derivation is given in Appendix A.

Finally, the performance results associated with different parametric settings were presented in Section 3.4, where it is confirmed that the simulation results conform with the analysis. Explicitly, the results section was divided into three parts, each dealing in detail with the performance results of the proposed schemes in FFR and SFR, along with the benefits of power control in D2D links. It was revealed by the performance results that the proposed frequency allocation schemes significantly outperform the UFR benchmark scheme. The coverage probability and capacity of D2D links when the MBS employs FFR was presented in Figure 3.5 - Figure 3.8, where it is clearly observed that the proposed FFA2 performs best, followed by FFA1, while the UFR scheme performs worst. The impact of D2D links on the coverage probability of MUs was also considered in Figure 3.9, where only simulation results were presented. The coverage probability and capacity of D2D links, when the MBS employs SFR was then depicted in Figure 3.10 and Figure 3.11 respectively for different values of the power control factor for MBS. The power control of the D2D links was analysed in Figure 3.12, Figure 3.13 and Table 3.2, where it was shown that the power control factor should be about 0.5 in order to strike an appealing trade-off between the energy consumption and the performance of D2D links.

To summarise, this chapter considered D2D communication underlaying the downlink of cellular networks and relying on distance-proportional power control, when the MBS employs different frequency reuse schemes, namely UFR, FFR and SFR. Specifically, three frequency allocation schemes for D2D links were proposed, when the MBS employs either FFR or SFR: FFA1 & FFA2 and SFA, respectively, in order to intelligently manage the interference in the network, which has been increased due to the introduction of D2D links. The coverage probability and capacity of D2D links were analytically obtained under the proposed frequency allocation schemes and their quantitative analysis reveals that the proposed schemes outperform the benchmark scheme. Chapter 2 dealt with the key design criterion of energy efficiency in the light of energy harvesting, while in this chapter D2D communication that complements the cellular network was invoked for improving the overall spectral efficiency of the communication system. Hence it is imperative that Chapter 4 considers the improvement of both the energy and spectral efficiency.

Chapter 4

Energy Harvesting Aided Device-to-Device Communication Underlaying the Cellular Downlink

4.1 Introduction

With the growing tele-traffic demand, the major concern of cellular service providers has become spectral efficiency and energy efficiency of the networks. The plausible solutions addressing both the design objectives are addressed individually in Chapters 2 and 3. As presented in Chapter 3, device-to-device (D2D) communication proves to be a promising local ad-hoc networking technology by virtue of its advantages, which include improving the area-spectral efficiency, offloading the tele-traffic of cellular base stations (BS), reducing the latency and expanding the BS's coverage, etc. D2D communication underlaying cellular networks allows a pair of closely located devices to communicate directly with each other by reusing the frequency band allocated in the existing cellular networks [51, 52, 2]. However, D2D communication brings about new challenge, since it imposes mutual interference between the cellular mobile users (MUs) and D2D links due to the shared cellular resources.

Therefore, conceiving efficient resource sharing schemes is essential for D2D communication, which have been studied in [59,97,98,61,58,99]. In [59], a maximum weight bipartite matching based scheme is designed for resource allocation for D2D to maximize the overall network throughput. In [97], the authors provided hybrid centralised-distributed solutions for channel allocation and power control of D2D devices by formulating a graph theoretical approach and multi-agent learning game respectively. A distributed resource allocation for D2D links is proposed whilst guaranteeing the QoS of MUs by controlling interference from D2D pairs and their power in [98] . In [61], the authors proposed an efficient algorithm for jointly optimizing the D2D-MU matching and power control for multiple D2D links by judiciously re-utilising the downlink resources of multiple MUs. The resource allocation

scheme of D2D communications based on the objective function (OF) of maximising the spectral efficiency in an LTE-Advanced network was proposed and analysed in [58], while that based on group sparse structure was proposed in [99].

These devices dissipate most of their energy, while transmitting and processing the information signal and they are typically powered by pre-charged batteries. An emerging solution discussed in Chapter 2 for improving energy efficiency of the network is the exploitation of energy harvesting (EH) [13,38,27] at the devices. This helps in prolonging the lifetime of the network, where the devices become capable of accommodating the random arrivals of energy and its storage for using it later [10]. Hence, different network models ranging from simple single-user communication to complex cooperative networks have been investigated with the aid of an energy harvesting capability at the transmitter node. In [17,18,76], beneficial power allocation strategies were designed under the corresponding EH constraints for a single-user EH system. These concepts were then further extended to the design of an efficient broadcast channel in [20, 77], of a two-user multiple access channel in [22], of two-way OFDM communications in [78] and of cooperative networks in [13,38,27,100,101,80,1], all in the context of EH.

However the research of EH aided D2D links is in its infancy, despite having a few pioneering studies [67,69,68]. Specifically, Sakr and Hossain [67] proposed beneficial spectrum access policies for RF energy harvesting aided cognitive D2D communication underlaying the uplink and downlink channels. By contrast, Liu *et al.* [69] designed wireless power transfer policies for D2D communication underlaying a cognitive cellular network, where wireless energy is harvested from power beacons and secure transmission takes place using the spectrum of the primary MBS. In [68], Yang *et al.* proposed and analysed an EH assisted heterogeneous network relying on mobile relays harvesting energy from access points for supporting D2D communication.

The EH aided network and the D2D communication underlaying the cellular downlink presented in Chapters 2 and 3, respectively, provide the guidelines for energy harvesting aided D2D communication underlaying the cellular downlink, as discussed in this chapter. Specifically, a cellular network simultaneously supporting multiple EH aided D2D links that rely on reusing the downlink cellular resources of multiple MUs is focussed. The resource allocation design was formulated as a sum-rate maximization problem for the D2D links. This objective is achieved by jointly optimizing the D2D-MU matching and the power allocation of D2D links, whilst satisfying the minimum throughput constraints of the MUs and the EH constraints of the D2D links. To the best of our knowledge, the optimization and analysis of EH aided D2D communication underlaying the downlink of cellular networks for radio resource and power allocation at the D2D links is a relatively unexplored research area, which is the motivation behind this work.

The sum-rate maximization problem subjected to both throughput and EH constraints is shown to be a non-convex mixed integer problem, which is then transformed to a more tractable convex mixed integer problem used for characterising the optimal D2D-MU matching and power allocation. Additionally, efficient algorithms are also proposed for the joint optimization of D2D links for both the idealised non-causal and for the realistic

causal knowledge of EH profiles, which are also often termed as off-line and on-line knowledge, respectively. These algorithms are characterised using extensive simulation results. In a nutshell, the major contributions of this chapter are as follows [3]:

(a) **Off-line Joint optimization Algorithm:** It is assumed that there exists prior knowledge about the energy arrivals at all the D2D links before the commencement of the communication session. In this algorithm, the classic Lagrangian Multiplier method is employed for finding the optimal D2D-MU matching, the power allocation and the transmission duration of the D2D links under the throughput constraints of the MUs and the EH constraints of the D2D links.

(b) **On-line Joint optimization Algorithm:** In this algorithm, a realistic causal energy arrival process is considered, where there is no prior knowledge about the EH profile. The classic dynamic programming (DP) technique is adopted for simplifying the complex problem by partitioning it into smaller sub-problems which then invokes the Lagrangian multiplier method for each stage in order to find the optimal power allocation, transmission time and D2D-MU matching, whilst still satisfying the constraints.

This chapter is structured according to Figure 4.1. In Section 4.2, the system model invoked for maximising the sum-rate of D2D links is discussed for both the online and offline cases. This is followed by the efficient design of the joint optimization algorithms in Section 4.3. The performance results are discussed in Section 4.4, whilst the summary and conclusions are offered in Section 4.5.

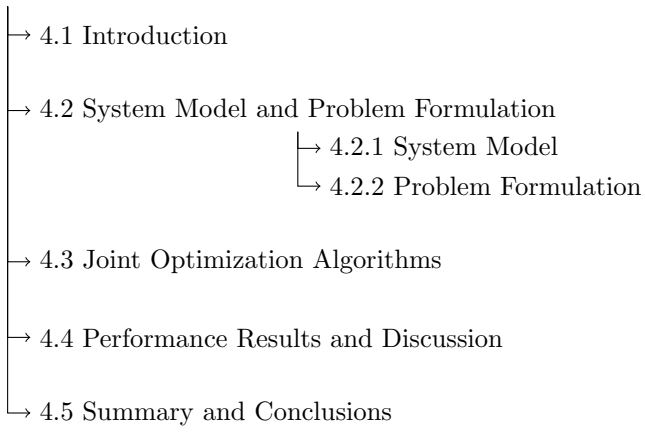

Figure 4.1: The structure of this chapter.

4.2 System Model and Problem Formulation

In this section, the system model considered is described first, which is then followed by the formulation of the sum-rate maximization problem conceived for D2D communication.

4.2.1 System Model

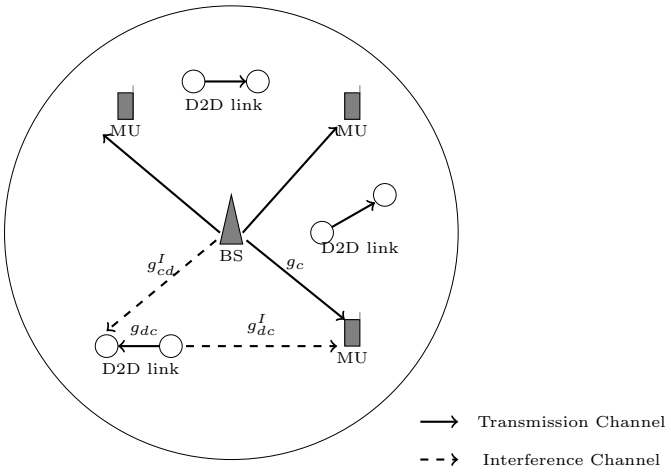

Figure 4.2: D2D Communication reusing downlink cellular resources with an illustration of interference pattern when one D2D link reuses on MU's RB

Consider resource sharing between two types of communication, namely the traditional cellular communication between the macro base station (MBS) and MU as well as the direct D2D communication between two devices, where the D2D transmitters are capable of harvesting energy from the environment. In particular, a hybrid single-cell environment of Figure 4.2 is considered, comprising $M = 3$ orthogonal downlink MUs and $D = 4$ energy harvesting D2D links. Each MU occupies a dedicated *resource block (RB*[1]*)* and it is assumed that each RB can only be used by a single D2D link [61, 59, 91]. Let $y_{dc} \in \{0, 1\}$ indicate whether the D2D link d is reusing the RB of MU c. To facilitate the assumption, $\sum_{d=1}^{D} y_{dc} = 1 \ \forall \ c$ can be stipulated. It is also assume that the D2D transmitter (Tx) harvests energy from the environment as shown in Figure 4.2, where the transmit power of the D2D link is subject to the realistic energy causality constraint. Explicitly, energy causality implies that the total energy expended by a device during its transmission session should not exceed the total energy harvested by that specific device until that particular instant in time. The amount of energy harvested is represented as $E_{d,\kappa}$ unit at time instant t_κ for $\kappa = 0, 1, ...K - 1$, where $t_0 = 0$ and $t_K = T$ is set. The time-interval between the two consecutive energy arrival events is termed as an *epoch*, whose length is defined as $\tau_\kappa = t_\kappa - t_{\kappa-1} \ \forall \kappa \in K$. The transmission channels as well as interference channels are considered to be independent and identically Rayleigh distributed channels. The transmission channel gains between the MBS and MU c is defined as g_c, while g_{dc} as the transmission channel gains between the D2D transmitter and the receiver (RX) of the D2D link d on the RB of MU c, respectively. Furthermore, g^I_{cd} and g^I_{dc} are defined as the interference channel gains between the MBS and the D2D link d on the RB of MU c as well as the interference channel spanning from the D2D link d to the MU c, respectively. These channels are clearly depicted in Figure 4.2. Hence, the data rate of the D2D link d

[1]Resource block (RB) refers to the smallest unit of system bandwidth resource that is allocated to a MU for its communication session.

at an energy arrival instant κ can be expressed as,

$$r_{d,\kappa} = \sum_{c=1}^{M} y_{dc,\kappa} \log_2 \left(1 + \frac{P_{dc,\kappa} g_{dc}}{N_0 + g_{cd}^I P_c}\right) \qquad \forall \kappa \in K, d \in D \tag{4.1}$$

where $P_{dc,\kappa} \geq 0$ and $P_c \geq 0$ are the transmit power of the D2D link subject to the energy causality constraint and the transmit power of MU c, respectively on the associated RB, while N_0 is the noise power. Since D2D communication is included as a complement to the underlying cellular communication, the MUs typically have higher priority than the D2D links. Thus, in order to protect the legacy cellular communication, a throughput target for each MU is imposed as R_c,

$$\sum_{d=1}^{D} y_{dc,\kappa} \log_2 \left(1 + \frac{P_c g_c}{N_0 + g_{dc}^I P_{dc,\kappa}}\right) \geq R_c \qquad \forall \kappa \in K, c \in M. \tag{4.2}$$

4.2.2 Problem Formulation

The goal is to maximize the sum-rate of the D2D links by the deadline T, while satisfying the energy harvesting constraints by optimally allocating the transmit power of both the D2D link as well as of the MUs and beneficially matching each D2D link with a MU, subject to the minimum throughput constraint to be met. Explicitly, the problem can be formulated as an optimization over $\boldsymbol{Y_{dc}}$, $\boldsymbol{P_{dc}}$, $\boldsymbol{T_{dc}}$ and $\boldsymbol{P_c}$, yielding[2]

$$\underset{\boldsymbol{Y_{dc}}, \boldsymbol{P_{dc}}, \boldsymbol{T_{dc}}, \boldsymbol{P_c}}{\text{maximize}} \qquad \sum_{k=1}^{K} \sum_{d=1}^{D} r_{d,k} \tag{4.3a}$$

subject to :

$$\sum_{d=1}^{D} y_{dc,\kappa} \leq 1 \quad \forall \kappa \in K, c \in M; \tag{4.3b}$$

$$\sum_{k=1}^{\kappa} \sum_{c=1}^{M} y_{dc,k} P_{dc,k} t_{dc,k} \leq \sum_{k=0}^{\kappa-1} E_{d,k} \qquad \forall \kappa \in K, d \in D \tag{4.3c}$$

$$\sum_{c=1}^{M} y_{dc,\kappa} t_{dc,\kappa} \leq \tau_\kappa \qquad \forall \kappa \in K, d \in D \tag{4.3d}$$

$$\sum_{d=1}^{D} y_{dc,\kappa} \log_2 \left(1 + \frac{P_c g_c}{N_0 + g_{dc}^I P_{dc,\kappa}}\right) \geq R_c \qquad \forall \kappa \in K, c \in M \tag{4.3e}$$

$$y_{dc,\kappa} \in \{0, 1\}; P_{dc,\kappa} \geq 0; \tag{4.3f}$$

$$0 \leq t_{dc,\kappa} \leq \tau_\kappa; P_c \geq 0 \qquad \forall \kappa \in K, c \in M, d \in D,$$

[2]Bold and upper-case letters represent matrices, while bold letters represent vectors. Here $[y_{1c,i}, y_{2c,i}, \cdots, y_{Dc,i}]^T$ is c^{th} column of $\boldsymbol{Y_{dc}}$, $[p_{1c,i}, p_{2c,i}, \cdots, p_{Dc,i}]^T$ is c^{th} column of $\boldsymbol{P_{dc}}$ and $[t_{1c,i}, t_{2c,i}, \cdots, t_{Dc,i}]^T$ is c^{th} column of $\boldsymbol{T_{dc}}$ for EH epoch corresponding to $i \in \{1, 2, \cdots, K\}$ and $c \in \{1, 2, \cdots, M\}$. Also, $\boldsymbol{P_c} = [P_1, P_2, \cdots, P_C]^T$.

where the OF in Eq. (4.3a) is a non-convex function. Furthermore, Eq. (4.3b) is the D2D-MU matching constraint, which states that only a single D2D link can reuse each RB of a MU, while Eq. (4.3c) defines the energy causality constraint imposed on the amount of transmit energy of each D2D link. A constraint is imposed on the transmission duration of each D2D link in Eq. (4.3d), which states that the D2D transmission takes place within each EH epoch and the throughput constraint of the MUs is given in Eq. (4.3e). Finally, the feasibility constraint is given in Eq. (4.3f).

The problem defined in Eq. (4.3) is a mixed integer non-linear programming problem since the matching variable $y_{dc,\kappa}$ is binary, while the other variables are continuous which is combined with a non-convex OF and throughput constraint. Hence this is a complex problem that is difficult to solve in its original form. Similar to [61], the original problem of Eq. (4.3) is thus transformed to an equivalent, but more tractable form as demonstrated below:

$$\underset{\boldsymbol{Y_{dc}},\boldsymbol{P_{dc}},\boldsymbol{T_{dc}}}{\text{maximize}} \quad \sum_{\kappa=1}^{K}\sum_{d=1}^{D}\tilde{r}_{d,\kappa} \tag{4.4a}$$

subject to :

$$\sum_{d=1}^{D} y_{dc,\kappa} \leq 1 \quad \forall \kappa \in K, c \in M; \tag{4.4b}$$

$$\sum_{k=1}^{\kappa}\sum_{c=1}^{M} y_{dc,k}P_{dc,k}t_{dc,k} \leq \sum_{k=0}^{\kappa-1} E_{d,k} \qquad \forall \kappa \in K, d \in D \tag{4.4c}$$

$$\sum_{c=1}^{M} y_{dc,\kappa}t_{dc,\kappa} \leq \tau_{\kappa} \qquad \forall \kappa \in K, d \in D \tag{4.4d}$$

$$y_{dc,\kappa} \in \{0,1\}; P_{dc,\kappa} \geq 0; \tag{4.4e}$$

$$0 \leq t_{dc,\kappa} \leq \tau_{\kappa} \qquad \forall \kappa \in K, c \in M, d \in D,$$

where $\tilde{r}_{d,\kappa}$ is obtained using the following manipulations. Assuming that the D2D link d reuses the RB of the MU c, i.e. $y_{dc,\kappa} = 1$, from Eq. (4.3e) following expression is obtained:

$$P_c \geq \frac{\alpha_c(N_0 + g^I_{dc}P_{dc,\kappa})}{g_c}, \tag{4.5}$$

where $\alpha_c = 2^{R_c} - 1$. Since the OF of Eq. (4.3a) is monotonically decreasing in P_c for a fixed $P_{dc,\kappa}$, in order to maximize the sum-rate of the D2D links, the optimal P_c must be achieved, when satisfying the equality of Eq. (4.5), i.e. for

$$P^*_c = \frac{\alpha_c(N_0 + g^I_{dc}P_{dc,k})}{g_c}. \tag{4.6}$$

This modification helps us in eliminating the explicit throughput constraint by integrating it into the transformed objective function that is obtained by substituting P^*_c in the objective

function of Eq. (4.3a) as:

$$\tilde{r}_{d,\kappa} = \sum_{c=1}^{M} y_{dc,\kappa} \log_2 \left(1 + \frac{h_{dc} P_{dc,\kappa}}{e_{dc} N_0 + f_{dc} P_{dc,\kappa}}\right), \tag{4.7}$$

where:

$$\begin{aligned} h_{dc} &= g_{dc} g_c, \\ e_{dc} &= g_c + \alpha_c g_{cd}^I, \\ f_{dc} &= \alpha_c g_{dc}^I g_{cd}^I. \end{aligned}$$

Note that in the equivalent problem of Eq. (4.4), the variables to be optimized have been reduced to $\{\boldsymbol{Y_{dc}}, \boldsymbol{P_{dc}}, \boldsymbol{T_{dc}}\}$. Now, in order to investigate the convexity of the problem, first the equivalent rate available for the D2D link will be re-written in Eq. (4.7) as follows:

$$\tilde{r}_{d,\kappa} = \sum_{c=1}^{M} y_{dc,\kappa} \log_2 \left[1 + w(P_{dc,\kappa})\right],$$

where $w(P_{dc,\kappa}) = \frac{h_{dc} P_{dc,\kappa}}{e_{dc} N_0 + f_{dc} P_{dc,\kappa}}$. Evaluation of the second-derivative of $\tilde{r}_{d,\kappa}$ w.r.t. $P_{dc,\kappa}$ is given by,

$$\tilde{r}_{d,\kappa}^{''} = \frac{w^{''}(P_{dc,\kappa})\left[1 + w(P_{dc,\kappa})\right] - \left[w^{'}(P_{dc,\kappa})\right]^2}{\ln(2)[1 + w(P_{dc,\kappa})]^2}, \tag{4.9}$$

where $w^{''}(P_{dc,\kappa}) = -\frac{2 e_{dc} f_{dc} h_{dc} N_0}{\left(e_{dc} N_0 + f_{dc} P_{dc,\kappa}\right)^3}$.

Upon substituting $w^{''}(P_{dc,\kappa})$ in Eq. (4.9), it is found that $\tilde{r}_{d,\kappa}(P_{dc,\kappa})$ is concave in $P_{dc,\kappa}$ because the second-derivative of $\tilde{r}_{d,\kappa}$ is negative. Furthermore, the OF is the sum of the increasing and concave function of $\tilde{r}_{d,\kappa}$, hence Eq. (4.4a) is concave in $P_{dc,\kappa}$ following the composition rule of [83]. Since $\tilde{r}_{d,\kappa}$ is also a function of another variable $y_{dc,\kappa}$, $y_{dc,\kappa}$ is temporarily relaxed to be within the interval $[0, 1]$ and replace $P_{dc,\kappa}$ with a new variable $x_{dc,\kappa} = y_{dc,\kappa} P_{dc,\kappa}$. Hence, it is now observed that the constraints in Eq. (4.4) are convex in $\{y_{dc,\kappa}, x_{dc,\kappa}\}$ and $\tilde{r}_{d,\kappa}(x_{dc,\kappa})$ is concave, since $\tilde{r}_{d,\kappa}(y_{dc,\kappa}, x_{dc,\kappa})$ is the perspective function of $\tilde{r}_{d,\kappa}(x_{dc,\kappa})$ [83]. Therefore, $\tilde{r}_{d,\kappa}$ is jointly concave in $y_{dc,\kappa}$ and $P_{dc,\kappa}$, which implies that Eq. (4.4) preserves the convexity of the problem.

Based on the above arguments, the optimal power allocation $\boldsymbol{P_{dc}}$, the transmission duration $\boldsymbol{T_{dc}}$ and the D2D-MU matching $\boldsymbol{Y_{dc}}$ can be analytically characterized using the classic Lagrangian method of multipliers. The Lagrangian function is defined as:

$$\begin{aligned} \mathcal{L} = &- \sum_{\kappa=1}^{K} \sum_{d=1}^{D} \sum_{c=1}^{M} y_{dc,\kappa} \log_2 \left(1 + \frac{h_{dc} P_{dc,\kappa}}{e_{dc} N_0 + f_{dc} P_{dc,\kappa}}\right) + \sum_{\kappa=1}^{K} \sum_{c=1}^{M} \lambda_{1,dc,\kappa} \left(\sum_{d=1}^{D} y_{dc,\kappa} - 1\right) \\ &+ \sum_{\kappa=1}^{K} \sum_{d=1}^{D} \lambda_{2,d,\kappa} \left(\sum_{k=1}^{\kappa} \sum_{c=1}^{M} y_{dc,k} P_{dc,k} t_{dc,k} - \sum_{k=0}^{\kappa-1} E_{d,k}\right) + \sum_{\kappa=1}^{K} \sum_{d=1}^{D} \lambda_{3,d,\kappa} \left(\sum_{c=1}^{M} y_{dc,\kappa} t_{dc,\kappa} - \tau_\kappa\right), \end{aligned} \tag{4.10}$$

where $\lambda_{1,dc,\kappa}, \lambda_{2,d,\kappa}$ and $\lambda_{3,d,\kappa}$ are the Lagrangian multipliers associated with the constraints of Eq. (4.4b), Eq. (4.4c) and Eq. (4.4d), respectively. Now, evaluating the differentiation of the Lagrangian function of Eq. (4.10) with respect to $y_{dc,\kappa}$ and equating it to zero can be written as:

$$\frac{\partial \mathcal{L}}{\partial y_{dc,\kappa}} = 0 \tag{4.11a}$$

$$-\log_2\left(1+\frac{h_{dc}P_{dc,\kappa}}{e_{dc}N_0+f_{dc}P_{dc,\kappa}}\right)+\lambda_{1,dc,\kappa}+\lambda_{2,d,\kappa}P_{dc,\kappa}t_{dc,\kappa}+\lambda_{3,d,\kappa}t_{dc,\kappa}=0 \tag{4.11b}$$

$$\lambda_{1,dc,\kappa}=\log_2\left(1+\frac{h_{dc}P_{dc,\kappa}}{e_{dc}N_0+f_{dc}P_{dc,\kappa}}\right)-\lambda_{2,d,\kappa}P_{dc,\kappa}t_{dc,\kappa}-\lambda_{3,d,\kappa}t_{dc,\kappa}. \tag{4.11c}$$

Similarly, following equations are achieved on differentiating the Lagrangian function of Eq. (4.10) with respect to $p_{dc,\kappa}$ and equating it to zero:

$$\frac{\partial \mathcal{L}}{\partial P_{dc,\kappa}} = 0$$

$$-\frac{y_{dc,\kappa}e_{dc}h_{dc}N_0}{\ln(2)\left((f_{dc}+h_{dc})P_{dc,\kappa}+e_{dc}N_0\right)\left(e_{dc}N_0+f_{dc}P_{dc,\kappa}\right)}+\lambda_{2,d,\kappa}y_{dc,\kappa}t_{dc,\kappa}=0. \tag{4.12a}$$

Finally, differentiating the Lagrangian function Eq. (4.10) w.r.t. $t_{dc,\kappa}$ and equating it to zero is given by :

$$\frac{\partial \mathcal{L}}{\partial t_{dc,\kappa}} = 0 \tag{4.13a}$$

$$\lambda_{2,d,\kappa}y_{dc,\kappa}P_{dc,\kappa}+\lambda_{3,d,\kappa}y_{dc,\kappa}=0. \tag{4.13b}$$

Now, assuming that the D2D link d reuses the RB of MU c, the optimal power allocation $P^*_{dc,\kappa}$ and transmission time $t^*_{dc,\kappa}$ derived for the D2D link from Eq. (4.12a) and Eq. (4.13b), respectively, are given as follows:

$$P^*_{dc,\kappa}=\left[\frac{\lambda_{3,d,\kappa}}{\lambda_{2,d,\kappa}}\right]^+ \tag{4.14a}$$

$$t^*_{dc,\kappa}=\frac{h_{dc}e_{dc}N_0}{\lambda_{2,d,\kappa}\ln 2(e_{dc}N_0+(f_{dc}+h_{dc})P_{dc,\kappa})(e_{dc}N_0+f_{dc}P_{dc,\kappa})}, \tag{4.14b}$$

where $[a]^+$ denotes $\max\{0,a\}$. The optimal D2D-MU matching $y^*_{dc,\kappa}$ derived for a given power and transmission time allocation by substituting Eq. (4.14a) and Eq. (4.14b) into Eq. (4.11c) and is formulated as:

$$y^*_{dc,\kappa}=1, d=\underset{1\le\hat{d}\le D}{\operatorname{argmax}}\lambda_{1,\hat{d}c,\kappa};\quad y^*_{dc,\kappa}=0, \forall \hat{d}\neq d, \tag{4.15}$$

where,

$$\lambda_{1,\hat{d}c,\kappa}=\log_2\left(1+\frac{h_{\hat{d}c}P_{\hat{d}c,\kappa}}{e_{\hat{d}c}N_0+f_{\hat{d}c}P_{\hat{d}c,\kappa}}\right). \tag{4.16}$$

All the above-mentioned results have been obtained by investigating the KKT condi-

tions of the optimization problem defined in Eq. (4.4). Specifically, investigating the KKT condition for Eq. (4.4b), it is found that for the existence of optimal matching $\lambda_{1,dc,\kappa}$ has to be higher than zero, which means that the constraint is met with equality. Since according to this constraint a single RB can be reused by at most one D2D link, the MU-D2D matching yields integer indications. Therefore, it can be observed from Eq. (4.15) that the RB of MU c can be reused by the D2D link d that has the highest $\lambda_{1,dc,\kappa}$ value and according to Eq. (4.16), $\lambda_{1,dc,\kappa}$ depends on the different channel gains, which are independent and identically distributed random variables. As a consequence, practically the probability of $\lambda_{1,dc,\kappa} = \lambda_{1,\tilde{d}c,\kappa}$ where $\tilde{d} \neq d$ is zero. Hence, the temporary relaxation of $y_{dc,\kappa}$ to be within $[0, 1]$ still results in an integer solution.

Now, since the expressions derived for $P^*_{dc,\kappa}$ and $t^*_{dc,\kappa}$ depend on the Lagrangian multipliers given in Eq. (4.14a) and Eq. (4.14b), the bounds of these multipliers is obtained, which will be used for the sake of faster convergence. Using the KKT conditions and letting $\lambda_{3,d,\kappa} = 0$ or $\lambda_{2,d,\kappa} = 0$ respectively, $\lambda^{min}_{2,d,\kappa}$ and $\lambda^{max}_{3,d,\kappa}$ are obtained as:

$$\lambda^{min}_{2,d,\kappa} = \min_{1\leq c\leq M} \left(\frac{h_{dc}}{\tau_\kappa e_{dc} N_0 \ln 2} \right)$$
$$\lambda^{max}_{3,d,\kappa} = \max_{1\leq c\leq M} \left(\frac{h_{dc} e_{dc} N_0}{\sum_{k=0}^{\kappa-1} E_{d,k} f_{dc}(f_{dc} + h_{dc}) \ln 2} \right).$$

4.3 Joint optimization Algorithms

Exploiting the results derived in Section 4.2 and different EH processes, a pair of different joint optimization algorithms are proposed for optimising the power and transmission time of the D2D links as well as the D2D-MU matching, as described below.

(a) **Off-line joint optimization algorithm:** Based on the analysis of the sum-rate maximization provided in Section 4.2.2, an iterative algorithm has been proposed for jointly optimising the power allocation, transmission duration and D2D-MU matching under the idealised simplifying assumption of an off-line EH process, where the D2D links have perfect non-causal knowledge of both the amount of energy and of the arrival instants. This is formally defined in Algorithm 4.1, which is divided into two parts. In the sub-algorithm Algorithm 4.1, for a given value of the Lagrange multipliers $\lambda_{2,d,\kappa}$ and $\lambda_{3,d,\kappa}$ associated with the energy causality and transmission duration constraint, the power allocation as well as transmission duration of the D2D links are calculated using Eq. (4.14a) and Eq. (4.14b), as mentioned in line 16 of Algorithm 4.1. It then assigns the available RBs to D2D links according to Eq. (4.15) using these power and transmission duration values in lines 17 - 18 of Algorithm 4.1. This algorithm employs the classic bisection search method for obtaining the optimal values of $\boldsymbol{\lambda_2}$, $\boldsymbol{\lambda_3}$ that minimise the dual problem of Eq. (4.4). The Lagrangian multipliers $\boldsymbol{\lambda_2}$ and $\boldsymbol{\lambda_3}$ are updated in two nested loops according to the energy causality and transmission time constraints of Eq. (4.4c) and Eq. (4.4d), as mentioned in lines

6 - 12 and lines 19 - 26 of Algorithm 4.1, respectively. This algorithm is terminated, when the allocation of transmission power, time and D2D-MU matching to the D2D links meet the accuracy threshold ζ set at line 3 of Algorithm 4.1.

Algorithm 4.1 Joint optimization for off-line EH D2D links

1: Input: R_c, g_c $\forall c$; g_{dc}, g^I_{dc}, g^I_{cd} $\forall c, d$; $E_{d,\kappa}$ $\forall d, \kappa$, t_κ $\forall \kappa$, T_{max}, K, N_0.
2: Output: $P^*_{dc,\kappa}$, $t^*_{dc,\kappa}$, $y^*_{dc,\kappa}$, P^*_c $\forall c, d, \kappa$.
3: Initialize: Set accuracy ζ, $l^a_1 = \lambda^{min}_{2,d,\kappa}$, $l^b_1 = 100$; $n = 1$, $\lambda_{2,d,\kappa}(n) = \frac{(l^a_1 + l^b_1)}{2}$, $\kappa = 1$.
4: **while** $(\kappa \leq K)$ **do**
5: **while** $|l^a_1 - l^b_1| > \zeta$ **do**
6: Find $\lambda^*_{3,d,\kappa}$, $P^*_{dc,\kappa}$, $t^*_{dc,\kappa}$, $y^*_{dc,\kappa}$ $\forall d, c$ for a given $\lambda_{2,d,\kappa}(n)$ using Sub-Algorithm below.
7: **if** $(\sum_{k=1}^{\kappa} \sum_{c=1}^{M} y_{dc,k} P_{dc,k} t_{dc,k} \leq \sum_{k=0}^{\kappa-1} E_{d,k})$ **then**
8: $l^b_1 = \lambda_{2,d,\kappa}(n)$;
9: **else**
10: $l^a_1 = \lambda_{2,d,\kappa}(n)$;
11: **end if**
12: Update $n = n + 1$, $\lambda_{2,d,\kappa}(n) = \frac{(l^a_1 + l^b_1)}{2}$.
13: **end while**
Sub Algorithm:
14: Initialize: $m = 1$, $l^a_2 = 0$, $l^b_2 = \lambda^{max}_{3,d,\kappa}$, $\lambda_{3,d,\kappa}(m) = \frac{(l^a_2 + l^b_2)}{2}$, $\tau_\kappa = t_\kappa - t_{\kappa-1}$ $\forall \kappa$.
15: **while** $|l^a_2 - l^b_2| > \zeta$ **do**
16: Calculate $P^*_{dc,\kappa}$, $t^*_{dc,\kappa}$ $\forall d, c$ with the given $\lambda_{2,d,\kappa}(n)$, $\lambda_{3,d,\kappa}(m)$ via Eq. (4.14a) and Eq. (4.14b).
17: Compute $\lambda_{1,dc,\kappa}$ for any d, c via Eq. (4.16).
18: Match D2D link d with MU c according to Eq. (4.15)
19: **if** $(\sum_{c=1}^{C} y_{dc,\kappa} t_{dc,\kappa} < \tau_\kappa)$ **then**
20: $l^b_2 = \lambda_{3,d,\kappa}(m)$;
21: **else**
22: $l^a_2 = \lambda_{3,d,\kappa}(m)$;
23: **end if**
24: Update $m = m + 1$, $\lambda_{3,d,\kappa}(m) = \frac{(l^a_2 + l^b_2)}{2}$.
25: **end while**
26: Finally obtain P^*_c $\forall$ $y_{dc,\kappa} = 1$ using Eq. (4.6).
27: $\kappa = \kappa + 1$.
28: **end while**

(b) **On-line Joint optimization Algorithm:** In practice, only realistic causal knowledge of the harvested energy is available and thus the off-line algorithm is not realistic, since the future harvested energy is unknown. However, the off-line EH process provides the upper-bound of the realistic scenario of having causal knowledge of the EH profile. In order to implement the on-line process, the classic dynamic programming (DP) approach is invoked in conjunction with the results of Section 4.2. Dynamic programming is the method of solving complex problems by partitioning them into simpler problems and then recursively solving these sub-problems in multiple stages. Hence, in order to invoke dynamic programming, the sub-problems have to be identified, and then their recursive relationship and finally identify the base case[3]. Let us

[3]base case is the trivial sub-problem, which occurs for stage 1 in the optimization problem.

first give an illustration of DP.

Illustration: Knapsack Problem - There are 4 different items that are required to be fitted into a knapsack, where the weight of the knapsack is 15 units, while the weight of each item is specified in the constraint equation of the problem considered. Determine the number of each item that should be added to the bag so that the weight restriction is not violated. Each item has a specific utility associated with being added to the knapsack, as determined by the objective function. The following knapsack problem will now be solved for maximizing the utility under the weight constraint using dynamic programming[4]:

$$\underset{\boldsymbol{X}}{\text{maximize}} \quad Z = 7X_1 + 8X_2 + 9X_3 + 4X_4 \tag{4.18a}$$

$$\text{subject to :}$$

$$3X_1 + 2X_2 + 2X_3 + X_4 \leq 15 \tag{4.18b}$$

$$X_j \geq 0; \quad \text{and} \quad \text{integer.} \tag{4.18c}$$

In this problem, different attributes of DP are defined as follows:

- **Stage:** In this problem, each stage of DP is defined by a single variable, since the problem will be solved for one variable at a time.
- **State:** It is defined as the total weight or total amount of resources available for allocation to different items in this problem.
- **Decision Variable:** It is the actual value of the variables X_1, X_2, X_3 and X_4
- **Optimization Criterion:** Maximize the OF, Z, in Eq. (4.18a).

Now, let us start solving this problem stage by stage:

- $n = 1$ implies having one more stage to go, where it is aimed for solving the following sub-problem for X_4:

$$\begin{aligned} f_1(s_1, X_4) &= 4X_4 \\ f_1^*(s_1) &= \text{maximize} \quad 4X_4 \\ &\qquad \text{subject to} \quad X_4 \leq s_1, \quad \text{with } X_4 \text{ being an integer,} \end{aligned}$$

  where s_1 is the resource available for item X_4, while $f_1^*(s_1)$ is the best value of X_4 that maximizes $f_1(s_1, X_4)$. Now assuming that s_1 is a non-negative integer, the solution for X_4 is given below:

$$X_4^* = s_1 \quad \text{and} \quad f_1^*(s_1) = 4s_1;$$

- $n = 2$ implies having two more stages to go, where it is aimed for solving the

[4]Here $\boldsymbol{X} = [X_1, X_2, X_3, X_4]^T$.

following sub-problem for X_3 and X_4:

$$\begin{aligned} f_2(s_2, X_3) &= 9X_3 + f_1^*(s_1) \\ f_2^*(s_2) &= \text{maximize} \quad 9X_3 + f_1^*(s_2 - 2X_3) \\ &\text{subject to} \quad 2X_3 \leq s_2, \quad \text{with } X_3 \text{ being an integer.} \end{aligned}$$

Here in the expression of $f_2(s_2, X_3)$, $9X_3$ comes from the OF of Eq. (4.18a), while $f_1^*(s_1)$ is included as the best value of $4X_4$. Now, since s_1 is the remaining resource available after some of it is allocated to X_3 and bearing in mind the constraint of Eq. (4.18b), if there is s_2 amount of resources available and for each X_3 the amount of resources used is $2X_3$, then $s_1 = s_2 - 2X_3$ is obtained. The above set of equations can be simplified using the solution of stage 1 as follows:

$$\begin{aligned} f_2^*(s_2) &= \text{maximize} \quad 9X_3 + 4(s_2 - 2X_3) \\ &= \text{maximize} \quad 4s_2 + X_3 \\ &\text{subject to} \quad 2X_3 \leq s_2 \quad \text{with } X_3 \text{ being an integer.} \end{aligned}$$

Once again, assuming s_2 to be a non-negative integer, the following solution is obtained:

$$X_3^* = \left\lceil \frac{s_2}{2} \right\rceil \quad \text{and} \quad f_2^*(s_2) = 4s_2 + \left\lceil \frac{s_2}{2} \right\rceil.$$

- $n = 3$ implies having three more stages to go, where the following sub-problem is solved for X_2, X_3 and X_4:

$$\begin{aligned} f_3(s_3, X_2) &= 8X_2 + f_2^*(s_2) \\ f_3^*(s_3) &= \text{maximize} \quad 8X_2 + f_2^*(s_3 - 2X_2) \\ &\text{subject to} \quad 2X_2 \leq s_3, \quad \text{with } X_2 \text{ being an integer.} \end{aligned}$$

Since the variable X_2 is considered, $8X_2$ from the OF of Eq. (4.18a) is obtained, while $f_2^*(s_2)$ is included as the best value of $9X_3 + 4X_4$. Here again, defining s_3 as the total resources available for the variables X_2, X_3 and X_4, then according to the constraint of Eq. (4.18b), i.e. $2X_2 + 2X_3 + X_4 \leq s_3$ and $2X_2$ is the resource consumption assigned to the variable X_2. Hence, $s_2 = s_3 - 2X_2$ resources are available for allocation to the variables X_3 and X_4. Similar to the previous stage, the above equation can be re-written using the expression of $f_2^*(s_2)$ as:

$$\begin{aligned} f_3^*(s_3) &= \text{maximize} \quad 8X_2 + 4(s_3 - 2X_2) + \left\lceil \frac{s_3 - 2X_2}{2} \right\rceil \\ &= \text{maximize} \quad 4s_3 + \left\lceil \frac{s_3 - 2X_2}{2} \right\rceil \\ &\text{subject to} \quad 2X_2 \leq s_3, \quad \text{with } X_2 \text{ being an integer.} \end{aligned}$$

Again, assuming s_3 to be a non-negative integer and that the coefficient of X_2

is negative in the above expression of $f_3^*(s_3)$, a maximum would occur at:

$$X_2^* = 0 \quad \text{and} \quad f_3^*(s_3) = 4s_3 + \left\lceil \frac{s_3}{2} \right\rceil.$$

- $n = 4$ implies having four more stages to go, where the following sub-problem is solved for X_1, X_2, X_3 and X_4:

$$\begin{aligned} f_4(15, X_1) &= 7X_1 + f_3^*(s_3) \\ f_4^*(15) &= \text{maximize} \quad 7X_1 + f_2^*(15 - 3X_1) \\ &\text{subject to} \quad 3X_1 \leq 15, \quad \text{with } X_1 \text{ being an integer.} \end{aligned}$$

Since the beginning of the problem have been reached $s_4 = 15$, where $7X_1$ is the utility associated with item X_1 according to Eq. (4.18a) and $f_3^*(s_3)$ is the best utility for the other variables. According to the constraint of Eq. (4.18b) the resource consumption for X_1 is $3X_1$, hence $s_3 = 15 - 3X_1$. The above equations can now be re-written as:

$$\begin{aligned} f_4^*(15) &= \text{maximize} \quad 7X_1 + 4(15 - 3X_1) + \left\lceil \frac{15 - 3X_1}{2} \right\rceil \\ &\text{subject to} \quad X_1 \leq 5, \quad \text{with } X_1 \text{ being an integer.} \end{aligned}$$

Now, evaluating for all integer values of X_1 satisfying the constraint of $X_1 \leq 5$ the values of $f_4^*(15)$ are given as:

$$\begin{aligned} X_1 = 0, &\quad f_4^*(15) = 67; \\ X_1 = 1, &\quad f_4^*(15) = 61; \\ X_1 = 2, &\quad f_4^*(15) = 54; \\ X_1 = 3, &\quad f_4^*(15) = 48; \\ X_1 = 4, &\quad f_4^*(15) = 41; \\ X_1 = 5, &\quad f_4^*(15) = 35. \end{aligned}$$

It becomes clear that the utility is maximized, when $Z = 67$. Hence the following solution is obtained:

$$\begin{aligned} &X_1^* = 0, \quad s_3 = 15 - 3X_1^* = 15; \\ &X_2^* = 0, \quad s_2 = s_3 - 2X_2^* = 15; \\ &X_3^* = \left\lceil \frac{s_2}{2} \right\rceil = \left\lceil \frac{15}{2} \right\rceil = 7, \\ &s_1 = s_2 - 2X_3^* = 1; \quad X_3^* = s_1 = 1. \end{aligned}$$

Following the above illustration, the attributes of DP are defined, when it is applied in the sum-rate optimization problem as follows:

Algorithm 4.2 Joint optimization for on-line EH D2D links

Input: R_c, $g_c \ \forall\, c$; g_{dc}, g^I_{dc}, $g^I_{cd} \ \forall\, c, d$; K, T_{max}, N_0.
Output: $P^*_{dc,k}$, $t^*_{dc,k}$, $y^*_{dc,k}$, $P^*_c \ \forall\, c, d, k$.
Initialize: Set stage $\kappa = 1$, state $S_{d,0} = 0 \ \forall\, d$, initial time instant $t_0 = 0$, final time instant $t_K = T_{max}$, termination condition for recursion using $flag = 1$.
repeat
  Compute the most probable energy arrival instant, $\tilde{t}_\kappa$ following poisson distribution.
  Generate the energy harvested amount $\tilde{E}_{d,\kappa-1} \ \forall\, d$ following uniform distribution.
  Compute the energy harvested as $E_{d,\kappa-1} = \tilde{E}_{d,\kappa-1} + S_{d,\kappa-1} \ \forall\, d$.
  Find $P^*_{dc,\kappa}$, $t^*_{dc,\kappa}$, $y^*_{dc,\kappa}$, $P^*_c \ \forall\, d, c$ using Algorithm 4.1 with $\tau_\kappa = \tilde{t}_\kappa - t_{\kappa-1}$, $E_{d,\kappa-1}$ & $K = \kappa$.
  if $(\sum_{c=1}^{C} y_{dc,\kappa} P_{dc,\kappa} t_{dc,\kappa} < E_{d,\kappa-1})$ **then**
    $S_{d,\kappa} = E_{d,\kappa-1} - \sum_{c=1}^{C} y_{dc,\kappa} P_{dc,\kappa} t_{dc,\kappa}$;
  end if
  if $(\sum_\kappa \tau_\kappa < T)$ **then**
    Generate the next actual energy arrival instant t_κ following poisson distribution.
    $\kappa = \kappa + 1$
  else
    $flag = 0$.
  end if
until $(flag = 1)$

- **Stage:** In the considered problem, different stages or sub-problems are defined as individual optimization sub-problems of the different EH epochs.
- **State:** The recursive relationship among the stages of the system are represented by the amount of unused energy available for the D2D link or by the amount of left energy after transmission across the D2D link.
- **Decision Variable:** It is the actual value of the optimization variables of $\boldsymbol{Y_{dc}}$, $\boldsymbol{P_{dc}}$, $\boldsymbol{T_{dc}}$ and $\boldsymbol{P_c}$.
- **Optimization Criterion :** Maximization of the OF of Eq. (4.4a).

Since the energy arrival time instances typically obey a Poisson process, at stage one, the next energy arrival instant is predicted to be the one, for which the probability of occurrence is maximum. Hence the serves as the base case for the problem. This is set in order to meet the constraint of Eq. (4.4d) imposed on the optimization problem of Eq. (4.4). At each stage, a simpler optimization problem is solved using Algorithm 4.1, while the amount of unused energy is input to the next stage of the optimization. This recursive algorithm conceived for the on-line EH process is formally described in Algorithm 4.2.

4.4 Performance Results and Discussion

In this section, the performance of the proposed algorithms is analysed in terms of the achievable sum-rate of the D2D links by the deadline of T seconds, where the D2D links

Parameter	Value
System Deadline, T	10 s
Maximum Energy Harvested, E_{max}	100 mJoule
Energy Arrival Rate, λ_e	3 mJ/s
Radius of Cell, R	1000 m
Number of MUs, M	10
Number of D2D links, D	10
Distance of D2D Pair, r	20 m
Throughput threshold of MUs, R_c	12 bps/Hz
Path-Loss exponent, α_d	3
Path-Loss exponent, α_c	3.5
Noise Level, N_0	-110 dBm/Hz

Table 4.1: Parameters used for Simulations

harvest energy from the environment. The EH process of the D2D links is considered to be independent of each other with uniform distribution of the amount of energy between $[0, E_{max}]$ mJoule arriving at Poisson distributed arrival instants t_k at a rate of λ_e mJoule/s. The macrocell having a radius of R m consists of C MUs and D D2D links, which are distributed uniformly and the channel spanning from the MBS and D2D TXs to the MUs or D2D RXs are considered to be i.i.d. Rayleigh fading channels following a negative-exponential path-loss model. The path-loss exponent of the channels between the D2D TXs and D2D RXs or the MUs is set to α_d while that between the MBS and MUs or the D2D RXs is set to α_c according to Table 4.1 owing to the different propagation environments in the two scenarios. Finally, the thermal noise level is set to N_0 according to Table 4.1. The parametric settings are specified in Table 4.1, except otherwise mentioned. The results quantified by invoking Monte-Carlo simulations of $10,000$ runs for obtaining the sum-rate of the D2D links as a function of the throughput threshold for the MUs, of the number of MUs and of the D2D links as well as of the distance between the D2D pair for both the off-line and on-line EH processes at the D2D links.

The distance between the D2D devices is not fixed for the first set of results given in Figure 4.3. Therefore, the goal is to find the optimal distance of the D2D pair that can maximize the D2D sum-rate. As expected, it can be observed from the results that as the distance of the D2D pair increases, the achievable sum-rate of the D2D links is reduced. The reason behind this trend is that upon increasing the distance, the D2D transmission experiences an increased path-loss and hence requires a higher transmission power for improving the sum-rate. It can be seen from the figure that as the distance increases from 20 m to 25 m, there is an approximately 68% D2D sum-rate reduction for both the algorithms, hence assuming a D2D pair distance of 20 m is a reasonable choice for the further analysis. Moreover, from Figure 4.3, it can also be observed that on average

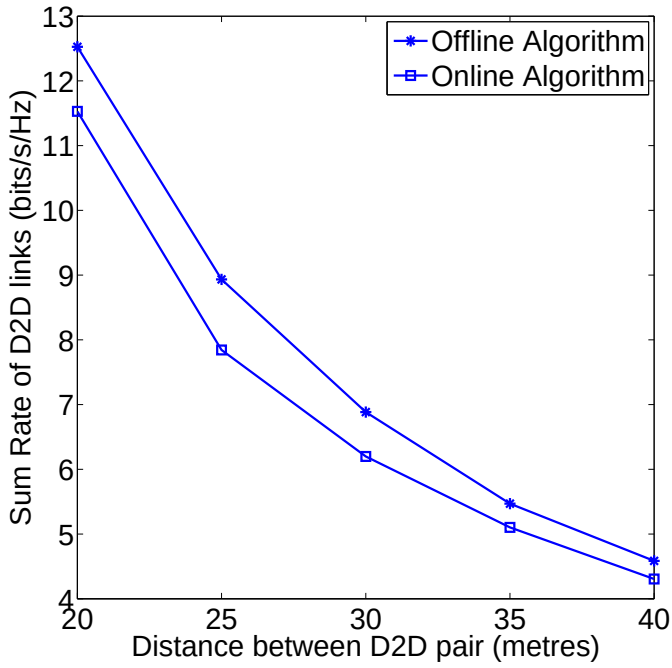

Figure 4.3: Sum-rate of the D2D links versus the distance between D2D pair. All the system parameters are summarized in Table 4.1.

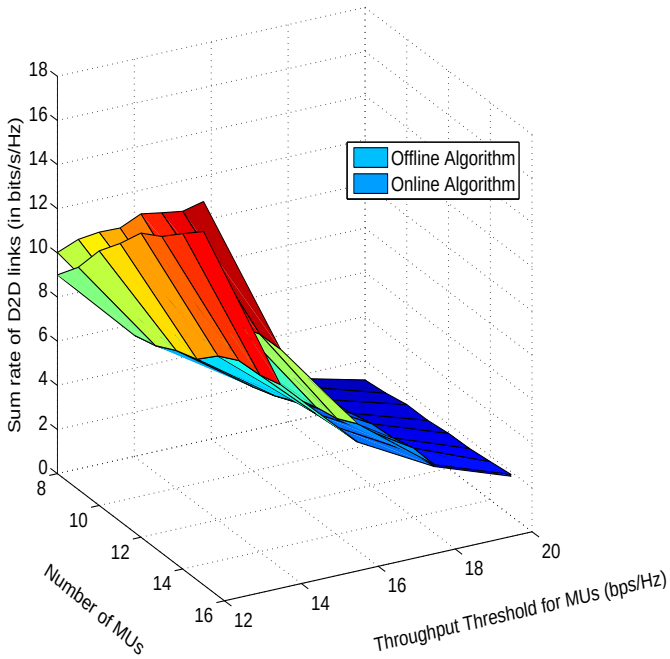

Figure 4.4: Sum-rate of the D2D links for varying number of MUs and throughput thresholds of MUs. All the system parameters are summarized in Table 4.1.

the on-line algorithm achieves 91% of the sum-rate attained by the off-line algorithm. This is due to the fact that the off-line algorithm provides an upper-bound for the system, since it relies on the unrealistic assumption of non-causal knowledge of the EH process of the D2D links.

In Figure 4.4, the sum-rate of the D2D links is represented as a function of both the number of MUs and of the throughput requirement of the MUs with a fixed number of

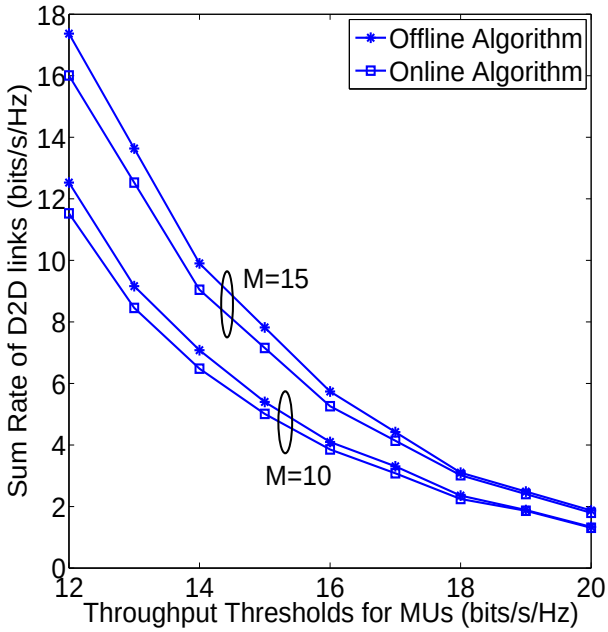

Figure 4.5: Sum-rate of the D2D links for different throughput thresholds of MUs for two set of values of number of MUs (10 and 15). All other system parameters are summarized in Table 4.1.

D2D links. It can be clearly observed that as the number of MUs increases, there is an increase in the sum-rate of D2D links owing to the availability of a larger number of resources (RBs) for the same number of D2D links owing to supporting a higher transmission rate for certain D2D links. However, upon increasing the throughput requirement of the MUs, a diminishing trend is observed, because increasing the throughput implies that the interference experienced by the MUs should be lower, which in turn results in a lower transmit power for the D2D TXs and hence a lower sum-rate for the D2D links. Moreover, the realistic on-line algorithm relying on causal knowledge of the EH profile performs closely to the upper-bound provided by the off-line algorithm that relies on the idealistic assumption of having non-causal knowledge of the EH profiles of D2D links. For the sake of closely analysing the impact of the number of MUs and of the throughput thresholds on the sum-rate of the D2D links, the 2-dimensional curves are presented corresponding to the individual analysis of the number of MUs, while keeping the throughput requirement constant and vice versa.

The results of Figure 4.5 characterize the sum-rate of D2D links as a function of the throughput requirement of the MUs for two different numbers of MUs. As the throughput threshold increases, the performance of both algorithms deteriorates. This implies that as the throughput requirement increases, the interference introduced by the D2D links should be low for meeting the throughput constraint of the MU, which in turn means that the transmission power and hence the rate of the D2D link will be lower. Moreover, it can be seen that similar trends can be observed, if there are higher number of MUs, except that there is an overall increase in the achieved sum-rate owing to availability of a larger number of RBs to be reused by the D2D links. It is clear from Figure 4.5 that the on-line algorithm

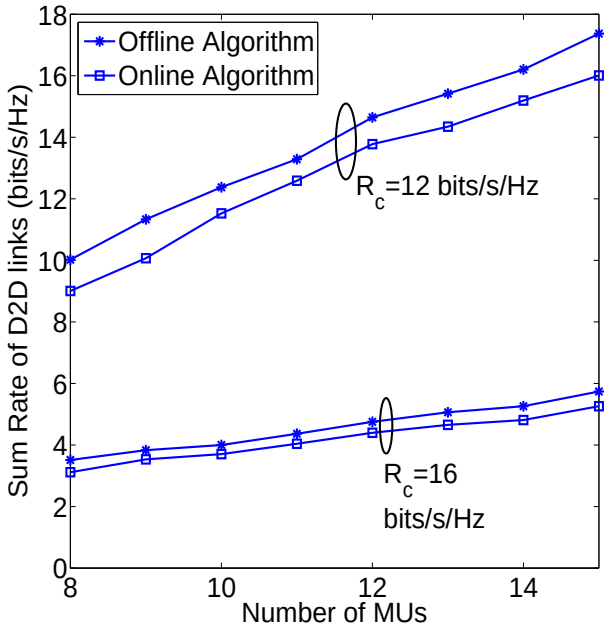

Figure 4.6: Sum-rate of the D2D links versus the number of MUs for two different values of throughput threshold of 12 and 16 bits/s/Hz. All other system parameters are summarized in Table 4.1.

achieves approximately 94% of the off-line algorithm's sum-rate on an average. The reason behind this phenomenon is the realistic assumption of only having causal knowledge of the EH process of the D2D links in the former algorithm.

In Figure 4.6, the D2D sum-rate is presented as the function of number of MUs for a fixed set of throughput requirement, $R_c \in \{12, 16\}$ bits/s/Hz. Upon increasing the number of MUs, the D2D links have more cellular resources available for them and this leads to an increase in the D2D sum-rate. As in the above-mentioned results, the on-line algorithm conforms with the previous results, achieving a sum-rate of 92% of the upper-bound given by the off-line algorithm. Moreover, for a throughput threshold of 16 bits/s/Hz, similar trends are observed but the sum-rate attained is consistently lower than that, when the throughput of 12 bits/s/Hz is considered due to the reduction in the transmission power of the D2D TXs for ensuring a higher throughput requirement at the MUs.

Finally, the sum-rate of the D2D links is depicted in Figure 4.7 as a function of the number of D2D links, when there are only 10 MUs in the network requiring a throughput threshold of 12 bits/s/Hz . As expected, there is an increase in the sum-rate of the D2D links upon increasing in their number. It is interesting to note that the rate at which the sum-rate of the D2D links is increasing is reduced owing to the fact that upon increasing the number of the D2D links, it becomes harder to satisfy the throughput constraint for the MUs. Hence, the performance of the D2D links tends to saturate. Again, the on-line algorithm achieves 94% of the sum-rate of the upper-bound given by the off-line algorithm.

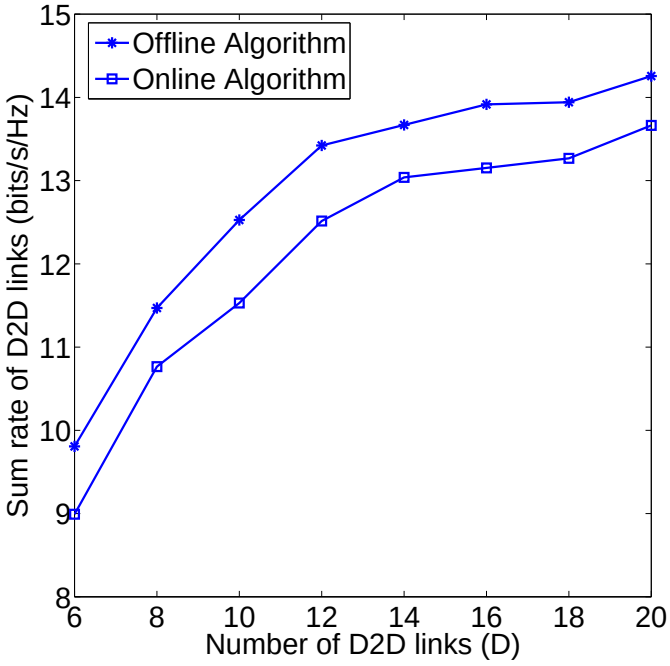

Figure 4.7: Sum-rate of the D2D links for varying number of D2D links. All other system parameters are summarized in Table 4.1.

4.5 Summary and Conclusions

In this chapter, a downlink resource reuse system is studied in the presence of multiple MUs and multiple underlay D2D links that are capable of harvesting energy from the surroundings. Therefore, these underlaying energy harvesting aided D2D links are capable of improving both the spectral- and the energy-efficiency of the system, which are key design criteria for future communication systems, as illustrated in Chapter 1. Commencing with the discussion of the system model for energy harvesting aided D2D links reusing the RBs allocated to MUs in the downlink of the cellular network in Section 4.2.1, two different energy harvesting scenarios were considered:

- *Off-line*: This is an idealistic scenario, where each D2D transmitter has a non-causal knowledge of both the arrival instant and of the amount of energy, before the commencement of transmission.
- *On-line*: This is a realistic scenario, where there is no prior knowledge about the energy harvesting profile at the D2D transmitters.

In Section 4.2.2, a sum-rate maximization problem was then formulated for D2D communication, whilst protecting the cellular transmission. This optimization problem was found to be a non-convex mixed integer programming problem, which first had to be transformed into a more tractable convex optimization form by obtaining the optimal MU power, whilst meeting the throughput constraints. Upon incorporating relaxed D2D-MU matching variables into the problem, the optimal resource reuse, power allocation as well as the transmission duration were analytically characterised for the D2D links using the classic Lagrangian method of multipliers for the off-line EH process. On the other hand, for

on-line EH at the D2D links, a Dynamic Programming algorithm was invoked, where each stage incorporates a smaller problem solved by using the Lagrangian method. Based on the analytical results, in Section 4.3 two algorithms were proposed for the joint optimization of the D2D-MU matching, of the power allocation and of the transmission duration for both causal and non-causal EH processes at the D2D links.

Finally, the proposed methods were characterized using the performance results of Section 4.4, where both the algorithms relied on different parametric settings. More specifically, first a reasonable optimal distance between each D2D pair was obtained in Figure 4.3, which suggested that this distance should be fixed to 20 m for further analysis in this chapter. Then in Figure 4.4 the 3-dimensional quantization of the sum-rate of D2D links was presented with respect to both the number of MUs as well as to the throughput requirement of the MUs, which was then bifurcated into two separate figures for closely analysing the impact of the throughput requirements, whilst keeping the number of MUs constant and vice versa in Figure 4.5 and Figure 4.6, respectively. In Figure 4.7, Section 4.4 was concluded with the performance analysis of the sum-rate of D2D links as a function of the number of D2D links.

In a nutshell, a system comprised of D2D links and MUs was considered, where the D2D links are capable of harvesting energy from the environment and reuse the RBs in the downlink of cellular networks. A pair of algorithms were proposed for maximising the sum-rate of D2D links under the EH and the throughput constraints considered, where the algorithms differ in terms of having either non-causal and causal knowledge of the EH profile at the D2D links. Hence they were termed as off-line and on-line algorithms, respectively. Finally, the performance results revealed that the proposed on-line algorithm is capable of achieving 92% of the performance attained by the off-line algorithm, which also provides an upper-bound for the problem. In this chapter, energy harvesting D2D links were incorporated in a cellular network as a solution for improving both the energy and spectral efficiency of the system. Hence in the next chapter a heterogeneous cellular network relying on energy harvesting aided D2D links will be considered, which further justifies the system model conceived for addressing the key design criteria of communication systems.

Chapter 5

Energy Harvesting Aided Device-to-Device Communication in the Over-Sailing Heterogeneous Two-Tier Downlink

5.1 Introduction

In Chapter 2, for optimising the device's operation and prolonging the lifetime of devices and networks, an energy harvesting aided cooperative communication system was conceived for improving the energy efficiency of the network, especially that of battery-powered wireless devices. These EH aided devices are capable of scavenging energy from the ambient energy resources (e.g. solar, wind, thermal, RF energy etc.), which results in the random arrival of energy, and hence the devices have to store this energy to be used later [10]. However, with the spread of mobile devices and multimedia services, the existing spectral resources are unable to meet the demands of tele-traffic. In this spirit, in Chapter 3, a promising D2D ad-hoc communication scheme was presented which enables a pair of mobile users in each other's proximity to establish a direct link for bypassing the base stations, while reusing the spectrum allocated for traditional cellular communication, thereby offloading the backhaul traffic and enhancing the spectral efficiency [51, 59]. After individually exploring the two major design criteria of energy and spectral efficiency in Chapters 2 and 3, the integration of energy harvesting with D2D communication underlaying the cellular downlink was inevitable and hence it was discussed in Chapter 4.

Moreover, the evolution of mobile communication networks has always been motivated by the quest for increasing the capacity in order to meet the continuing tele-traffic increase spurred by the proliferation of wireless services. However, there is a limit to the capacity that can be achieved by the current cellular infrastructure. Hence, future cellular wireless

networks are expected to accommodate infrastructural changes for supporting the escalating tele-traffic demands. In order to efficiently exploit both the spectrum as well as the infrastructural investments of mobile network operators, heterogeneous networks (HetNets) have been considered as promising techniques for future wireless systems [102]. In HetNets, various low-power micro-, pico- and femto-BSs are distributed across the traditional macro cell network for improving both the coverage and capacity of conventional systems [103]. Hence, in this chapter the benefits of both the HetNets and the techniques developed in Chapter 4 are amalgamated in order to achieve an increased design flexibility.

However, D2D communication underlaying HetNets will bring about many new challenges, including sophisticated interference management due to the co-existence of different traffic patterns, different spectral bands and diverse user densities in the network etc. Hence, recent research activities have been devoted to investigating the potential of D2D-based heterogeneous networks [104, 105, 106, 107]. Furthermore, the research of HetNets incorporating EH aided underlay D2D links, is still in its infancy, despite the promising early studies [68]. Yang *et. al.* [68] considered a HetNet environment, where the energy is harvested from the access points by the mobile users, which can also act as relays once they have stored sufficient harvested energy. These mobile relays then utilise their harvested energy in the D2D transmission mode for relaying the downlink transmissions from the access points. Specifically, Yang *et. al.* [68], investigated the effects of various energy harvesting related parameters, as well as those of the access point density and of the user density on the outage probability.

This chapter considers a two-tier HetNet supporting multiple MUs that are associated either with macro-BS (MBS) or with pico-BSs (PBSs) under various spectrum sharing arrangements as well as multiple underlaying D2D links relying on energy harvesting and reusing the downlink cellular resources for their communication. At the current state-of-the-art, most existing contributions advocate uplink resource reuse for the D2D links [51, 59, 105, 106]. However, when the D2D links are close to the BS, the near-far effects may impose strong interference on the MU's transmission. Despite this limitation, there is a paucity of contributions on downlink resource reuse at the D2D links, even though this is also important, especially, because it also reflects the worst case interference scenario. Hence this problem is considered in this chapter[1]. The resource allocation is formulated as an optimization problem maximizing the D2D sum-rate, which is achieved by invoking the joint optimization of the D2D-MU matching, and the power allocation of both the D2D links as well as of the MUs, without violating the throughput constraints of the MUs and without exceeding the power budget constraints as well as the EH constraints of the D2D links. There are typically two types of spectrum sharing strategies among the BSs of different tiers in HetNets, namely orthogonal spectrum sharing and co-channel spectrum sharing. In this chapter, a spectrum sharing strategy is also proposed, termed as *Co-orthogonal spectrum sharing*, which subsumes both of the above arrangements. The major contributions of this chapter are as follows [4]:

[1]The methodologies developed in this work can be readily extended to uplink resource reuse scenarios by simply considering the throughput guarantee at the BS.

- Co-orthogonal spectrum sharing: In the proposed arrangement, N sub-channels are shared amongst the MBS and PBSs, while the remaining $(M - N)$ channels are orthogonally shared among the MBS and PBSs. This means that for N sub-channels, the system operates in co-channel deployment, while for the remaining $(M-N)$ channels, the system operates in orthogonal deployment. This arrangement reduces the interference imposed, when compared to the classic co-channel deployment associated with $N = M$ and improves the spectrum exploitation of orthogonal deployment having $N = 0$.

- The sum-rate maximization problem of energy harvesting D2D links reusing the downlink resources of a two-tier HetNet is formulated as a mixed integer non-linear program, which is transformed into a more tractable form and its solution is obtained using the classic Lagrangian method of multipliers.

- Based on the theoretical analysis of the optimization problem, an algorithmic solution termed as the *Joint Optimization of Resource Block and Power Allocation(JORPA)* is proposed for D2D links.

- The following heuristic methods are also proposed:

  (a) *Equal Power Allocation (EPA):* In this method, the power consumption of the D2D links relies on the harvesting and dissipation strategy associated with equally sharing the power over all the reused RBs, while using optimal D2D-MU matching.

  (b) *Random D2D-MU Matching (RM):* In this method, the D2D-MU matching is random, while the power consumption is optimized based on the EH and the maximum power budget constraints.

  (c) *Maximum Distance D2D-MU Matching (MDM):* In this method, D2D-MU matching is based on the maximum distance between the D2D link and MU, while the power consumption is optimized under the EH and on the maximum power budget constraints.

- The proposed JORPA algorithm and the heuristic methods were analysed in the context of different parametric settings. The performance results reveal that the proposed heuristic EPA method is capable of achieving approximately 96% of the sum-rate attained by the JORPA algorithm at a much lower complexity, while the other two heuristic methods perform less well compared to the JORPA solution, indicating that the D2D-MU matching parameters constitute a more crucial set of variables in the problem formulation. Hence, it is required to achieve optimized D2D-MU matching, while the power can be heuristically assigned.

- The impact of the presence of D2D communication in two-tier HetNet was evaluated in terms the MU's throughput associated with either the MBS or the PBSs. The proposed co-orthogonal scheme is capable of achieving 50% higher than the required throughput of MUs associated with the MBS while 24% higher than that required by the MUs served by the PBSs.

To the best of our knowledge, the optimization and analysis of EH aided D2D communication in the downlink of HetNets is a relatively unexplored research area in the context of both the radio resource and power allocation of the D2D links as well as of the MUs. Hence exploring this interesting area is the motivation behind this work.

The rest of the chapter is organized as shown in Figure 5.1. In Section 5.2, the system model is presented, followed by the formulation of the optimization problem. The optimization problem is then analysed and an algorithmic solution relying on the Lagrangian method of multipliers is proposed in Section 5.3, followed by the heuristic methods in Section 5.4. The proposed algorithms are then quantitatively analysed and discussed in Section 5.5. Finally conclusions are provided in Section 5.6.

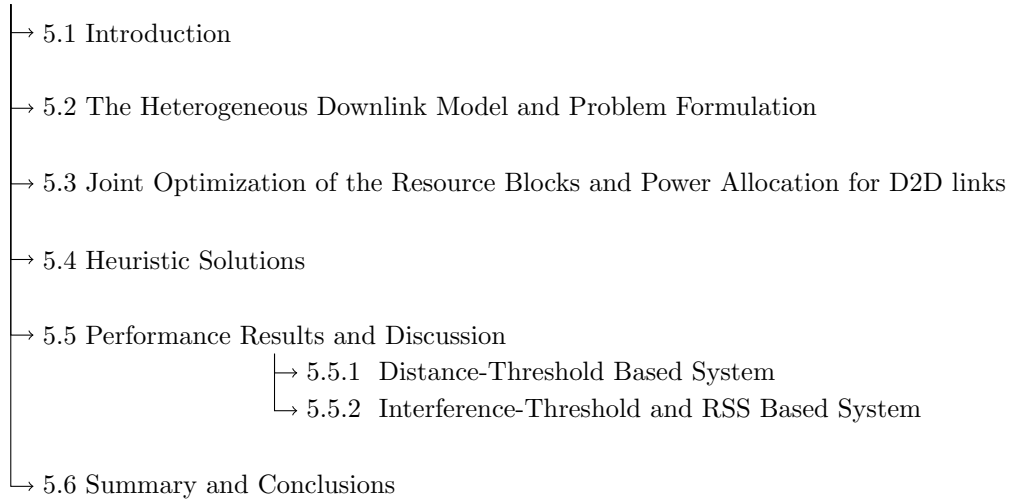

Figure 5.1: The structure of this chapter.

5.2 The Heterogeneous Downlink Model and Problem Formulation

Consider a hybrid single cell environment comprising a macro-BS (MBS) covering a cell of radius R overlaid by P randomly located pico-BSs (PBSs). In this HetNet setting, there are D energy harvesting D2D links reusing the downlink (DL) resources of M MUs, as shown in Figure 5.2. The power budget of the MBS is denoted by P_C^{max}, while that of each PBS is P_P^{max}, where the DL transmit power allocated for each MU associated with either the MBS or one of the PBSs is obtained through optimization, as described later in this section. It is assumed that the DL transmission of each BS activates all of its allocated sub-channels all the time. The two well-known spectrum sharing schemes that have been richly documented in the literature [108] are described below along with the proposed strategy :

(a) *Co-Channel Spectrum Sharing:* Each tier transmits on all the sub-channels of Figure 5.3(a). In this figure, the MBS and PBSs share a pool of S DL channels, where each of the P PBSs has $\frac{S}{P}$ orthogonal sub-channels. Hence, the MUs DL reception

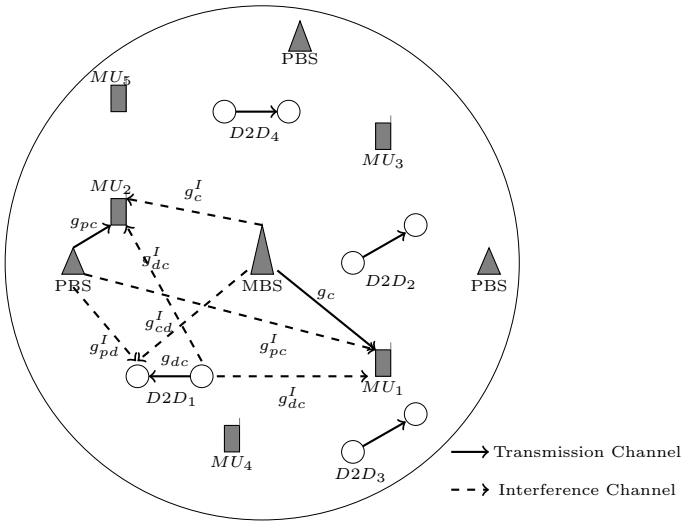

Figure 5.2: An illustration of the relevant transmission and interference patterns in the heterogeneous cellular network, when HetNet supports co-channel spectrum sharing. The D2D links share the MU's downlink resources for their transmission. Here the $D2D_1$ link reuses the RB of MU_1 associated with the MBS, hence this D2D link imposes interference on the MUs communicating within the same RB (MU_2) operating under co-channel deployment, as depicted in the figure.

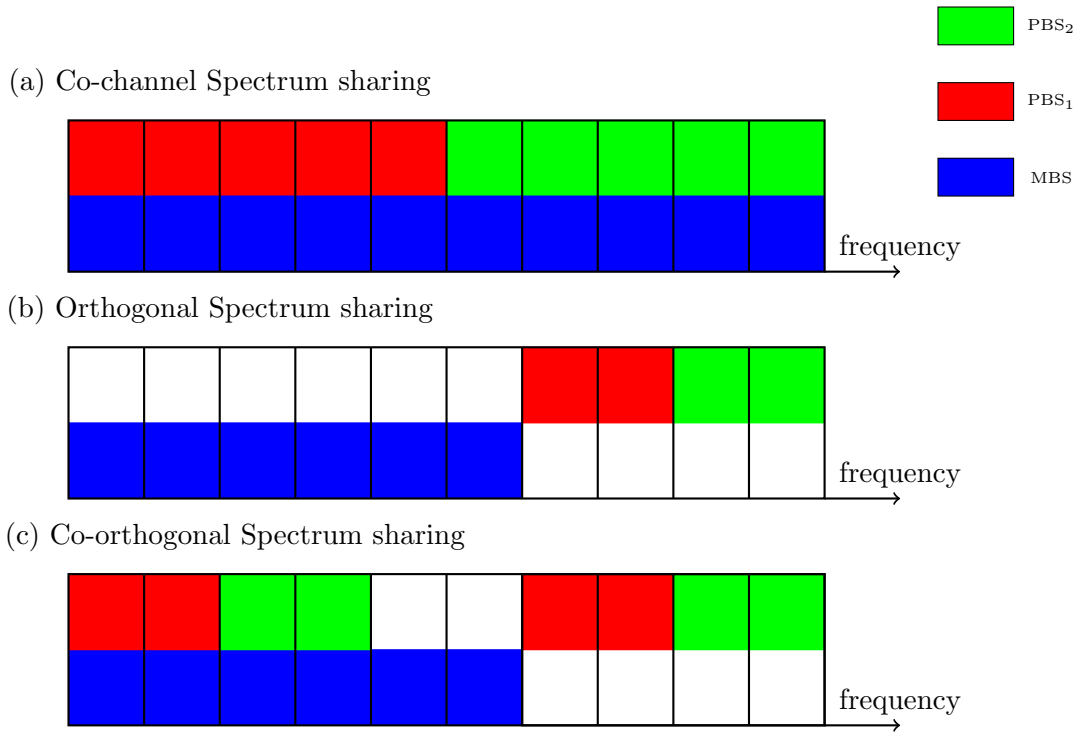

Figure 5.3: An illustration of the different spectrum sharing regimes when there are S sub-channels for distribution among the single MBS and P PBSs with $S = 10$, $N = 4$ and $P = 2$.

associated with the MBS is contaminated by one of the PBSs transmitting in the DL to the MUs associated with it, while all the PBSs DL transmissions suffer from the interference inflicted by the MBS's DL transmission on all the channels. Moreover, the D2D communications reusing the DL RBs of the MUs experience interference both from the MBS and PBSs present in the system. For example, if there are $P = 2$ PBSs and $S = 10$ sub-channels, then these 10 sub-channels are used for the co-channel sub-band. Thus, the MBS will use all 10 sub-channels and each of the $P = 2$ PBSs will use 5 sub-channels orthogonally in this co-channel sub-band, as shown in Figure 5.3(a).

(b) *Orthogonal Spectrum Sharing:* Both the MBS and the PBSs are allocated a dedicated set of sub-channels, which are orthogonal to each other. If there are S channels, then the set of PBSs is exclusively supported by N sub-channels, while the remaining $(S - N)$ sub-channels are allocated to the MBS. Then each PBS is allocated a dedicated set of orthogonal sub-channels by partitioning the N sub-channels among P PBSs, as shown in Figure 5.3(b). This arrangement reduces the co-channel interference imposed by the MBS and PBSs on the D2D links, which is achieved at the expense of granting only a reduced bandwidth for each MBS and PBSs. For example, if there are $P = 2$ PBSs, $S = 10$ and $N = 4$ sub-channels, then these 4 sub-channels are earmarked for pool of PBSs for orthogonal deployment. Thus, the MBS will use remaining 6 sub-channels and each of the $P = 2$ PBSs will use 2 sub-channels orthogonally.

(c) *Co-orthogonal spectrum sharing:* The proposed strategy is a unification of the pair of richly investigated channel allocation strategies mentioned above. In the hybrid deployment, S sub-channels are allocated for ensuring that N sub-channels are used by the MBS and by all the PBSs in a co-channel interfering fashion, while the remaining $(S - N)$ sub-channels are orthogonally distributed among the MBS and PBSs in the system. This is shown in Figure 5.3(c). Thus, this channel allocation deployment caters for a reduced interference at the D2D links, when it reuses the RBs of MUs served in orthogonal spectrum sharing, while it efficiently exploits the bandwidth at each BS by relying on co-channel deployment as well. For example, if there are $P = 2$ PBSs, $S = 10$ and $N = 4$ sub-channels, then these 4 sub-channels are used for the co-channel sub-band, while the remaining 6 are earmarked for orthogonal reuse. Thus, the MBS will use all 4 sub-channels and each of the $P = 2$ PBSs will use 2 sub-channels orthogonally in this co-channel sub-band. Furthermore, from the orthogonal set of sub-bands, each of the BSs will use 2 additional sub-channels, which are orthogonally distributed between the two tiers.

In case of the co-orthogonal sharing, the D2D links can reuse any of the sub-bands and for the sake of intelligently reducing the interference experienced by the D2D links, two different threshold based sub-band selection criteria are invoked for employment by the D2D links. The threshold is used in order to decide, whether the D2D link should reuse the RB of the MUs served by an orthogonal sub-band or whether it should opt for using a

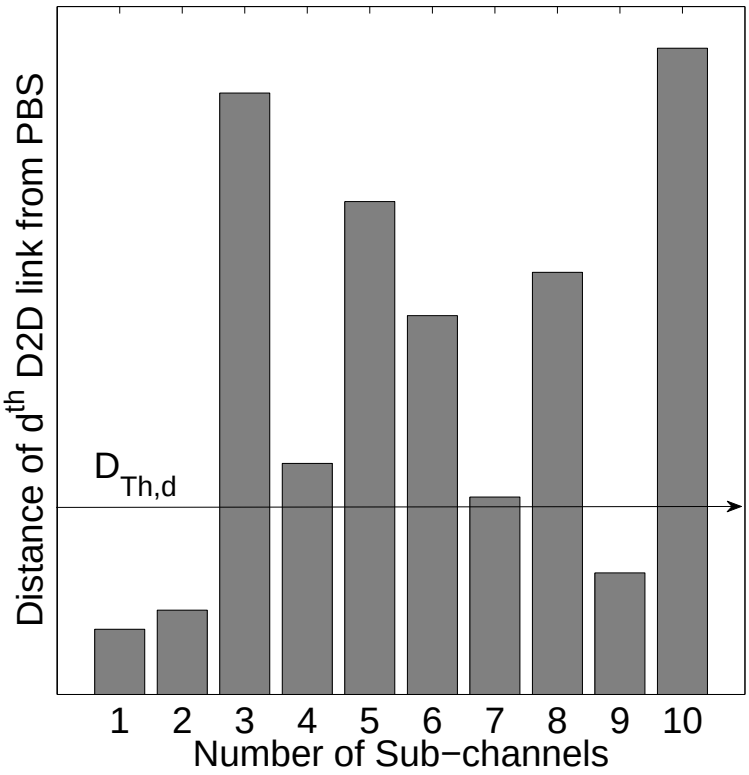

(a) Distance based sub-band selection

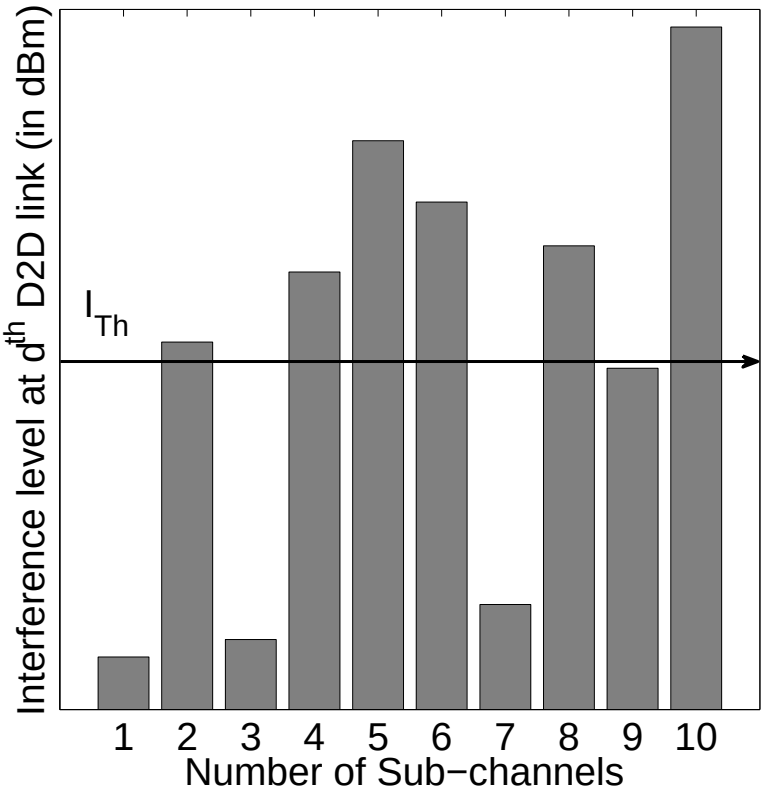

(b) Interference based sub-band selection

Figure 5.4: Different sub-band Selection schemes adopted at D2D links when S=10 sub-channels, N=4 sub-channels, P=1 PBSs

co-channel sub-band. The two sub-band selection criteria are given below:

(a) **Distance-Threshold $D_{Th,d}$:** The distance between the d^{th} D2D link and the PBSs is defined as $d_{pd}, \forall p \in P$. If the distance of the d^{th} D2D link from all the PBSs in the network is higher than the threshold, i.e. $d_{pd} \geq D_{Th,d}, \forall p \in P$ then the d^{th} D2D reuses the RBs of MUs that are served by the orthogonal spectral sub-band allocated to their serving BSs. Otherwise it reuses that by the co-channel sub-band allocated for their serving BSs. It can be seen in Figure 5.4(a) that on the sub-channels 1, 2 and 9 the distance of d^{th} D2D link from the PBS is lower than the threshold $D_{Th,d}$ and hence when these sub-channels are reused at the d^{th} D2D link, it opts for using a co-channel sub-band, while on all other sub-channels it reuses an orthogonal sub-band. Hence, if $D_{Th,d} = 2R$, then all the D2D links will aim for reusing the co-channel sub-band, thereby reducing the system's design to that of a co-channel spectrum sharing scenario. By contrast, at $D_{Th,d} = 0$ the system relies on orthogonal spectrum sharing and for $D_{Th,d} \in (0, 2R)$ it defines the proposed co-orthogonal spectrum sharing scenario.

(b) **Interference-threshold I_{Th}:** When implementing this flexible spectrum sharing scheme, the total interference imposed on the d^{th} D2D link by all the BSs is denoted as $I_d, \forall d \in D$. If the total interference at the d^{th} D2D link is higher than the threshold I_{Th} ($I_d \geq I_{Th}$), then the d^{th} D2D link reuses the RBs of those specific MUs that are served by the orthogonal spectral sub-band allocated to their serving BSs. Otherwise it reuses the RBs of the MUs served by the co-channel sub-band allocated by their serving BSs. This is clearly depicted in Figure 5.4(b), where the interference experienced by the d^{th} D2D links is shown for all the M sub-channels available for the DL transmission of MUs. It can be seen in Figure 5.4(b) that on the sub-channels 1, 3, 7 and 9 the d^{th} D2D link experiences interference below the threshold I_{Th} and hence when these sub-channels are reused at the d^{th} D2D link, it opts for using a co-channel sub-band, while on all other sub-channels it reuses an orthogonal sub-band. Therefore, if $I_{Th} = 0$dBm, then all the D2D links will aim for reusing the co-channel sub-band, which results in a co-channel spectrum sharing scenario. By contrast, for $I_{Th} >= (P_C^{max} + P_p^{max})$ the system relies on orthogonal spectrum sharing and for $I_{Th} \in (0, \{P_C^{max} + P_p^{max}\})$ it defines the proposed co-orthogonal spectrum sharing scenario.

These threshold-based switching schemes are introduced for the reduction of the overall interference on the D2D links, which is comprised of that emanating from the MBS and/or PBS depending on the choice of spectrum sharing scheme adopted. The distance-based switching relies on the unrealistic assumption that the interference is reduced purely on the basis of the distance from the interferers. Hence, this assumption is eliminated and a more practical system is considered that relies on the interference-based switching scheme at the D2D links. On the other hand, the MUs are randomly associated with the orthogonal or co-channel sub-bands available at their associated BSs. The downlink is studied and it is assumed that each MU can be served by only a single BS. A binary MU-BS association

flag is defined, $x_c \in \{0, 1\}$, which indicates that when $x_c = 1$, the MU is associated with the MBS, while $x_c = 0$ denotes the MU-PBS association. This MU-BS association is also defined on the basis of two different methods:

(a) **DL Transmission Distance:** This MU-BS association is defined on the basis of a distance-threshold $D_{Th,c}$ from the PBS. If the distance between the MU and any of the P PBSs is less than or equal to the threshold, the MU is assumed to be served by the closest PBS. Otherwise it is served by the MBS.

(b) **Received Signal Strength (RSS):** In this method, the MU-BS association is defined on the basis of the signal strength experienced by the MU from all the BSs. Each MU is associated with the specific BS that provides the maximum received signal power to the MU. If the signal strength received at the MU from the MBS is higher than that received from the PBSs, this MU is served by the MBS, otherwise it is served by the PBSs. Moreover, since the power budget of the MBS is higher than that of the PBS, biasing is introduced at the PBSs in order to support traffic off-loading from the MBS to the PBSs. This in turn means that for calculating the signal strength from the PBSs, the biasing factor B_p will be taken into account for the MU's association.

For the sake of convenient exposition, another binary parameter $x_{pc} \in \{0, 1\}$ is defined, which denotes the association of the MUs with their respective PBSs, implying that $x_{pc} = 1$ if MU c is associated with the p^{th} PBS and 0 otherwise. Each MU is served by a single dedicated downlink RB obtained from the pool of sub-channels allocated to its associated BS and it is assumed that each MU's downlink RB can be reused by only a single D2D link. This constitutes a one-to-many mapping, where a single D2D link can be mapped to multiple RBs of different MUs [61, 2]. Let $y_{dc} \in \{0, 1\}$ represent the D2D-MU matching. Then, if the RB of the c^{th} MU is reused by the D2D link d, then $y_{dc} = 1$, otherwise y_{dc} is set to zero. Hence, for the sake of satisfying this assumption, $\sum_{d=1}^{D} y_{dc} = 1 \ \forall \ c$ is stipulated. Moreover, for the co-channel spectrum sharing scenario there exists an additional constraint that prevents the D2D links from reusing the same RB of different MUs that are served by BSs of different tiers and are in a co-channel scenario with each other, as facilitated by $\sum_{c \in M_{co}} \sum_{d=1}^{D} y_{dc} = 1$. [2]

An energy harvesting capability is considered at the D2D transmitter (Tx), and as a consequence, the energy causality constraint is imposed on the transmit power of the D2D link, which implies that during the communication process, the device's total energy expenditure should not exceed its total energy harvested upto that time instant. The amount of energy harvested at the time instant t_i is denoted as $E_{d,i}$ units for $i \in [0, K-1]$, where the harvesting process starts at $t_0 = 0$ and its deadline is $t_K = T$. An *epoch* is defined as the time interval between two consecutive energy arrival events, whose length is defined as $\tau_i = (t_i - t_{i-1})$. The idealised simplifying assumption is considered that the transmitter knows both the arrival instant and the amount of energy non-causally, i.e. in advance. Throughout this treatise, all the channels in the network obey independent and

[2] M_{co} refers to the set of MUs served on the downlink RB in co-channel by their respective BSs.

identical Rayleigh distribution. The transmission channel gain between the MBS (or p^{th} PBS) and c^{th} MU are defined as g_c (or g_{pc}). Similarly, g_{dc} represents the gain of the channel traversing from the D2D TX to the receiver (RX) of the d^{th} D2D link reusing the RB of MU c. Furthermore, the interference channel's gain spanning from the MBS (or p^{th} PBS) to the d^{th} D2D link on the c^{th} MU's RB is denoted by g^I_{cd} (or g^I_{pd}). Similarly, g^I_{dc} represents the gain of the interference channel spanning from the D2D link d to the c^{th} MU. Based on the channel allocations at the BS as well as MU-BS association, g^I_c and g^I_{pc} are defined as another set of interference channel gains of the links spanning from the MBS to the MUs associated with the PBSs and that from the p^{th} PBS to the MUs associated with the MBS, respectively. Figure 4.2 clearly illustrates all the above-mentioned channels gains.

For an energy arrival instant t_i, the d^{th} D2D link's data rate can be expressed in Eq. (4.1)[3],

$$r_{d,i} = \sum_{c=1}^{M} y_{dc,i} \log_2 \left(1 + \frac{P_{dc,i} g_{dc}}{(\beta_c x_c + (1-\beta_c)) P_c g^I_{cd} + \sum_{p=1}^{P} (1-\beta_c x_c) x_{pc} P_p g^I_{pd}) + N_0 B} \right) \forall i, d \tag{5.1}$$

where $P_{dc,i} \geq 0$ denotes the transmit power of the d^{th} D2D link on the c^{th} MU's RB at time instant t_i, which is constrained by the energy causality as well as power budget, while $P_c \geq 0$ and $P_p \geq 0$ are the allocated transmit power of the MBS and that of the p^{th} PBS to the associated MU c under their power budgets, respectively, while N_0 is the noise density and B is system bandwidth. Furthermore, β_c denotes the spectrum sharing strategy employed by the BS in the downlink for the c^{th} MU, where $\beta_c = 1$ represents perfect orthogonality while $\beta_c = 0$ corresponds to co-channel spectrum sharing.

Since the existing cellular communication is complemented by D2D communication for the sake of improving both the bandwidth efficiency and network capacity, the MUs have a higher priority than the D2D links. Thus, a QoS target is introduced for each MU associated with the MBS or PBSs in terms of their minimum required throughput of R_c or R_p, respectively, for preventing the undue degradation of the cellular communication,

$$\sum_{d=1}^{D} y_{dc,i} x_c \log_2 \left(1 + \frac{P_c g_c}{N_0 B + g^I_{dc} P_{dc,i} + (1-\beta_c x_c) I_P} \right) \geq R_c \qquad \forall i, c \tag{5.2}$$

and

$$\sum_{d=1}^{D} y_{dc,i} (1-x_c) \log_2 \left(1 + \frac{\sum_{p=1}^{P} x_{pc} P_p g_{pc}}{N_0 B + g^I_{dc} P_{dc,i} + (\beta_c x_c + (1-\beta_c)) I_M} \right) \geq R_p \qquad \forall i, c \tag{5.3}$$

where $I_P = \sum_{p=1}^{P} x_{pc} p^I_p g^I_{pc}$ is the interference arriving from the active PBSs, while $I_M = p^I_c g^I_c$ is the interference emanating from the MBS that is active, when the system operates either in co-channel or co-orthogonal spectrum sharing environments. Note that the transmit power of the serving PBSs is formulated as a summation for ensuring that the expression accounts for the power of the p^{th} transmitting PBS for the c^{th} MU, since x_p

[3]Here $y_{dc,i}$ refers to D2D-MU matching for the i^{th} epoch of EH.

would be 1 only for the transmitting PBS and 0 for others.

This chapter aims to maximize the sum-rate of EH aided D2D links achieved by the deadline of T, while satisfying the energy causality constraints at the D2D links as well as meeting the throughput constraints of the cellular communication by appropriately matching each D2D link with the MU for resource reuse and assigning the optimal power for both the D2D transmission and for the downlink transmission of MUs associated with the BSs under their respective power budgets. Explicitly, this resource allocation problem can be formally stated as an optimization over variables[4], $\boldsymbol{Y_{dc}}$, $\boldsymbol{P_{dc}}$, $\boldsymbol{P_c}$ and $\boldsymbol{P_p}$:

$$\underset{Y_{dc},P_{dc},P_c,P_p}{\text{maximize}} : \quad \sum_{i=1}^{K}\sum_{d=1}^{D} r_{d,i} \tag{5.4a}$$

subject to :

$$\sum_{d=1}^{D} y_{dc,i} \leq 1 \quad \forall i \in K, c \in M; \tag{5.4b}$$

$$\sum_{c\in M_{co}}\sum_{d=1}^{D}(1-\beta_c)y_{dc,i} \leq 1 \quad \forall i \in K; \tag{5.4c}$$

$$\sum_{c=1}^{M} y_{dc,i}P_{dc,i} \leq P_D^{max} \quad \forall i \in K, d \in D; \tag{5.4d}$$

$$\sum_{\kappa=1}^{i}\sum_{c=1}^{C} y_{dc,\kappa}P_{dc,\kappa}\tau_\kappa \leq \sum_{\kappa=0}^{i-1} E_{d,\kappa} \quad \forall i \in K, d \in D; \tag{5.4e}$$

$$\sum_{c=1}^{M}(1-x_c)x_pP_p \leq P_P^{max} \quad \forall i \in K, \forall p \in P; \tag{5.4f}$$

$$\sum_{c=1}^{M} x_cP_c \leq P_C^{max} \quad \forall i \in K; \tag{5.4g}$$

$$\sum_{d=1}^{D} y_{dc,i}x_c\log_2\left(1+\frac{P_cg_c}{N_0B+g_{dc}^IP_{dc,i}+(1-\beta_cx_c)I_P}\right) \geq R_c \quad \forall i \in K, c \in M; \tag{5.4h}$$

$$\sum_{d=1}^{D} y_{dc,i}(1-x_c)\log_2\left(1+\frac{\sum_{p=1}^{P} x_{pc}P_pg_{pc}}{N_0B+g_{dc}^IP_{dc,i}+(\beta_cx_c+(1-\beta_c))I_M}\right) \geq R_p \quad \forall i \in K, c \in M; \tag{5.4i}$$

$$y_{dc,i} \in \{0,1\}; P_{dc,i} \geq 0; P_c \geq 0; P_p \geq 0 \quad \forall i \in K, c \in M, d \in D. \tag{5.4j}$$

where the objective function (OF) of Eq. (5.4a) is a non-convex function. Eq. (5.4b) represents the constraint imposed on the D2D-MU matching, which implies that each RB of MU can only be reused by at most one D2D link. By contrast, in case of co-channel spectrum sharing there exists an additional constraint in terms of D2D-MU matching given by Eq. (5.4c) that avoids the multiple reuse of the same RB by D2D links. The power

[4]Bold and capital letters represent matrices, while bold letters represent vectors. Here $[y_{1c,i}, y_{2c,i}, \cdots, y_{Dc,i}]^T$ is c^{th} column of $\boldsymbol{Y_{dc}}$, while $[p_{1c,i}, p_{2c,i}, \cdots, p_{Dc,i}]^T$ is c^{th} column of $\boldsymbol{P_{dc}}$ for EH epoch corresponding to $i \in \{1,2,\cdots,K\}$ and $c \in \{1,2,\cdots,M\}$. Also, $\boldsymbol{P_c} = [P_1, P_2, \cdots, P_C]^T$ and $[P_{1c}, P_{2c}, \cdots, P_{Pc}]^T$ is c^{th} column of $\boldsymbol{P_p}$ where $c \in \{1,2,3,\cdots,M\}$.

budget constraint of each D2D link d reusing the cellular RBs is stated by Eq. (5.4d), while the amount of energy consumed by each D2D link's transmission is constrained by the amount of energy harvested, as demonstrated in Eq. (5.4e). Furthermore, the MBS and PBSs maintain reliable connections with their associated MUs under the power budget P_C^{max} and P_P^{max} given in Eq. (5.4g) and Eq. (5.4f) respectively. This is followed by the throughput constraints of the MUs associated with either the MBS or with one of the P PBSs, as formulated in Eq. (5.4h) and Eq. (5.4i), respectively. Finally, Eq. (5.4j) represent the feasibility constraints.

5.3 Joint Optimization of Resource Block and Power Allocation for D2D links

Since the OF and the throughput constraints in Eq. (5.4) are non-convex and the variables are either binary or continuous, a non-convex mixed integer non-linear programming problem is identified, which is a challenging one in its original form. In this section, the problem of Eq. (5.4) will be first transformed to a more tractable form according to Proposition 1, followed by the analysis of this problem.

Proposition 1. *The problem of Eq. (5.4) is equivalent to the following optimization problem:*

$$\underset{Y_{dc},P_{dc}}{maximize} \quad \sum_{i=1}^{K}\sum_{d=1}^{D}\tilde{r}_{d,i} \tag{5.5a}$$

subject to :

$$\sum_{d=1}^{D} y_{dc,i} \leq 1 \quad \forall i \in K, c \in M; \tag{5.5b}$$

$$\sum_{c\in M_{co}}\sum_{d=1}^{D}(1-\beta_c)y_{dc,i} \leq 1 \quad \forall i \in K; \tag{5.5c}$$

$$\sum_{c=1}^{M} y_{dc,i}P_{dc,i} \leq P_D^{max} \quad \forall i \in K, d \in D; \tag{5.5d}$$

$$\sum_{\kappa=1}^{i}\sum_{c=1}^{M} y_{dc,\kappa}P_{dc,\kappa}\tau_\kappa \leq \sum_{\kappa=0}^{i-1} E_{d,\kappa} \quad \forall i \in K, d \in D; \tag{5.5e}$$

$$\sum_{d=1}^{D}\sum_{c=1}^{M}(1-x_c)x_{pc}\frac{\alpha_p}{g_{pc}}y_{dc,i}P_{dc,i}g_{dc}^I \leq P_P^{max} - \sum_{c=1}^{M}(1-x_c)x_{pc}\frac{\alpha_p}{g_{pc}}\left[(\beta_c x_c + (1-\beta_c))I_M + N_0B\right] \quad \forall i \in K, p \in P; \tag{5.5f}$$

$$\sum_{d=1}^{D}\sum_{c=1}^{M} x_c\frac{\alpha_c}{g_c}y_{dc,i}P_{dc,i}g_{dc}^I \leq P_C^{max} - \sum_{c=1}^{M} x_c\frac{\alpha_c}{g_c}\left[(1-\beta_c x_c)I_P + N_0B\right] \quad \forall i \in K; \tag{5.5g}$$

$$y_{dc,i} \in \{0,1\}; P_{dc,i} \geq 0; \quad \forall i \in K, c \in M, d \in D. \tag{5.5h}$$

where $\alpha_c = 2^{R_c} - 1$, $\alpha_p = 2^{R_p} - 1$ *and,*

$$\tilde{r}_{d,i} = \sum_{c=1}^{M} y_{dc,i} \log_2 \left(1 + \frac{g_{dc} P_{dc,i}}{e_{dc} N_0 B + f_{dc} P_{dc,i} + I_{dc}}\right), \tag{5.6}$$

$$e_{dc} = 1 + (\beta_c x_c + (1 - \beta_c)) \frac{\alpha_c}{g_c} g^I_{cd} + (1 - \beta_c x_c) \sum_{p=1}^{P} \frac{x_{pc} \alpha_p g^I_{pd}}{g_{pc}} \quad \forall d \in D, c \in M;$$

$$f_{dc} = (\beta_c x_c + (1 - \beta_c)) \frac{\alpha_c}{g_c} g^I_{cd} g^I_{dc} + (1 - \beta_c x_c) \sum_{p=1}^{P} \frac{x_{pc} \alpha_p g^I_{pd}}{g_{pc}} g^I_{dc} \quad \forall d \in D, c \in M;$$

$$I_{dc} = (1 - \beta_c) \left[\frac{\alpha_c}{g_c} g^I_{cd} I_P + \sum_{p=1}^{P} \frac{x_{pc} \alpha_p g^I_{pd}}{g_{pc}} I_M \right] \forall d \in D, c \in M.$$

Proof. Since, the transmit powers of the MBS and PBSs are optimized using the problem given in Eq. (5.4) are unknown, it is necessary to consider a reasonable value for the interferences I_M and I_P for the sake of transforming the problem into a more tractable form. Therefore, an equal power distribution[5] is considered at all the BSs. Hence the interfering powers of the PBSs and MBS can be written in the form of, $P^I_p = \frac{P^{max}_P}{\sum_{c=1}^{C} x_{pc}}$ and $P^I_c = \frac{P^{max}_C}{\sum_{c=1}^{C} x_c}$, respectively. Assuming that the RB of the MU c associated with the MBS is reused by the d^{th} D2D link, i.e. $x_c = 1$, $y_{dc,i} = 1$, from Eq. (5.2), following is achieved,

$$P_c \geq \frac{\alpha_c}{g_c} \left(N_0 B + g^I_{dc} P_{dc,i} + (1 - \beta_c x_c) I_P\right), \tag{5.8}$$

where $\alpha_c = 2^{R_c} - 1$. Similarly, assuming $x_c = 0$, $x_{pc} = 1$, $y_{dc,i} = 1$, which means that the d^{th} D2D link reuses the c^{th} MU's RB that is served by the p^{th} PBS, from Eq. (5.3), following is obtained

$$P_p \geq \frac{\alpha_p}{g_{pc}} \left(N_0 B + g^I_{dc} P_{dc,i} + [\beta_c x_c + (1 - \beta_c)] I_M\right), \tag{5.9}$$

where $\alpha_p = 2^{R_p} - 1$. Since increasing P_c and P_p monotonically decreases the OF value of Eq. (2.4a) for a fixed $P_{dc,i}$, the optimal value of P_c and P_p maximising the D2D sum-rate must be attained by satisfying the equality in Eq. (5.8) and Eq. (5.9), i.e. ,

$$P^*_c = \frac{\alpha_c}{g_c} \left(N_0 B + g^I_{dc} P_{dc,i} + (1 - \beta_c x_c) I_P\right) \tag{5.10}$$

and,

$$P^*_p = \frac{\alpha_p}{g_{pc}} \left(N_0 B + g^I_{dc} P_{dc,i} + [\beta_c x_c + (1 - \beta_c)] I_M\right). \tag{5.11}$$

Thus, the explicit throughput constraints are eliminated using the above modifications

[5]Dynamic power allocation is a reasonable method to allocate power in downlink at BSs, however, in this work, we consider equal power allocation for the sake of not over complicating the problem at hand.

and substituting P_c^* and P_p^* into the OF of Eq. (5.4a) yields the transformed OF given in Eq. (5.6). Similarly, P_c^* and P_p^* can be substituted into the constraint of Eq. (5.4g) and Eq. (5.4f) to arrive at the modified constraint of Eq. (5.5g) and Eq. (5.5f). Thus the transformed and more tractable form of the original problem Eq. (5.4) can be written as Eq. (5.5). □

Note that the optimization variables have been reduced to $\{\mathbf{Y_{dc}}, \mathbf{P_{dc}}\}\forall d \in D, c \in M$ in the equivalent problem of Eq. (5.5). Consequently, the feasibility of Eq. (5.4) is now explicitly revealed by Eq. (5.5f) and Eq. (5.5g), which implies that the interference power generated by the D2D links should not exceed the remaining power of the BSs. Although the problem is still a mixed integer non-linear problem, it is more readily solvable in this form, which will be seen by first investigating the convexity of the transformed problem of Eq. (5.5) in Lemma 4.

Lemma 4. *The equivalent maximization problem in Eq. (5.5) preserves convexity with respect to the variables* $\{\mathbf{Y_{dc}}, \mathbf{P_{dc}}\}\forall d \in D, c \in M$.

Proof. Let us re-write the equivalent rate for the D2D link of Eq. (5.6), $\tilde{r}_{d,i}$ as:

$$\tilde{r}_{d,i} = \sum_{c=1}^{M} y_{dc,i} \log_2[1 + w(P_{dc,i})],$$

where $w(P_{dc,i}) = \frac{g_{dc}P_{dc,i}}{e_{dc}N_0B + f_{dc}P_{dc,i} + I_{dc}}$. Evaluation of the second order derivative of $\tilde{r}_{d,i}$ is given by,

$$\tilde{r}''_{d,i} = \frac{w''(P_{dc,i})[1 + w(P_{dc,i}))] - [(w'(P_{dc,i}))^2]}{\ln(2)[1 + w(P_{dc,i})]^2}, \tag{5.12}$$

where $w''(P_{dc,i}) = -\frac{2g_{dc}f_{dc}(e_{dc}N_0B + I_{dc})}{(e_{dc}N_0 + f_{dc}P_{dc,i} + I_{dc})^3} \leq 0$.

Upon substituting $w(P_{dc,i})$ into Eq. (5.12), it is found that the second derivative of $\tilde{r}_{d,i}$ is negative and hence $\tilde{r}_{d,i}$ is a concave function of $P_{dc,i}$. Following the composition rule of [83], which states that the sum of monotonically increasing and concave functions is also a concave function, it can now be deduced that the OF of Eq. (5.5a) is concave in $P_{dc,i}$. Note that since $\tilde{r}_{d,i}$ relies on another variable $y_{dc,i}$, which is binary, it is temporarily considered that $y_{dc,i}$ to be a continuous variable lying within the interval $[0, 1]$ and replace $P_{dc,i}$ by a new variable $z_{dc,i} = y_{dc,i}P_{dc,i}$. Using this temporary relaxation on $y_{dc,i}$ and newly defined variable $z_{dc,i}$, it is not difficult to see that the constraints in Eq. (5.5) are jointly convex in $\{y_{dc,i}, z_{dc,i}\}$. Moreover, it is important to note that $\tilde{r}_{d,i}(y_{dc,i}, z_{dc,i})$ is the perspective function of $\tilde{r}_{d,i}(z_{dc,i})$ [83] and relying on the above property $\tilde{r}_{d,i}(z_{dc,i})$ is also concave since $\tilde{r}_{d,i}(p_{dc,i})$ is concave. According to [83], the perspective operation preserves convexity, which means that if a function is convex (or concave), then the perspective function of that function is also convex (or concave), thus it can be deduced that $\tilde{r}_{d,i}$ is jointly concave with respect to both $y_{dc,i}$ and $z_{dc,i}$. Therefore, Eq. (5.5) preserves the

convexity of the problem. □

Based on this analysis, the classic Lagrangian constrained optimization method is invoked and then both the transmit power $\mathbf{P_{dc}}$ as well as the D2D-MU matching $\mathbf{y_{dc}}$ are analytically characterized in the following Proposition 2.

Proposition 2. *Assuming that the d^{th} D2D link reuses the RB of the c^{th} MU, the power allocation $P^*_{dc,i}$ for the D2D link is formulated as Eq. (4.14a),*

$$P^*_{dc,i} = \left[\sqrt{\left(\frac{s^{(1)}_{dc}}{2s^{(0)}_{dc}}\right)^2 - \frac{s^{(2)}_{dc}(\lambda_{dc,i}, \mu_{dc,i}, \omega_i, \gamma_i)}{s^0_{dc}}} - \left(\frac{s^{(1)}_{dc}}{2s^{(0)}_{dc}}\right) \right]^+, \tag{5.13}$$

where $[a]^+$ denotes $\max\{0, a\}$, $\boldsymbol{\lambda}$, $\boldsymbol{\mu}$, $\boldsymbol{\omega}$, $\boldsymbol{\gamma}$ are Lagrangian multipliers[6] associated with Eq. (5.5d)-Eq. (5.5g), respectively, and

$$\begin{aligned} s^{(0)}_{dc} &= (f_{dc} + g_{dc}) f_{dc}; \\ s^{(1)}_{dc} &= (2f_{dc} + g_{dc})(I_{dc} + e_{dc} N_0 B); \\ s^{(2)}_{dc}(\lambda_{d,i}, \mu_{d,i}, \omega_i, \gamma_i) &= (I_{dc} + e_{dc} N_0 B)^2 - \\ &\qquad \frac{g_{dc}(I_{dc} + e_{dc} N_0 B) g_c}{\ln(2)\left[\lambda_{d,i} + \mu_{d,i}\tau_i + \gamma_i x_c \frac{\alpha_c}{g_c} g^I_{dc} + \omega_i (1 - x_c) \sum_{p=1}^{P} \frac{x_p \alpha_p}{g_{pc}} g^I_{dc}\right]}. \end{aligned}$$

The D2D-MU matching $y^*_{dc,i}$ for a given power allocation of $P_{dc,i}$ is given by:

$$y^*_{dc,i} = 1, d = \underset{\substack{1 \le \hat{d} \le D \\ 1 \le c \le M_{co}}}{argmax} \; H_{\hat{d}c,i}; \qquad y^*_{dc,i} = 0, \forall \hat{d} \neq d, \tag{5.15}$$

where $H_{dc,i}$ is given in Eq. (5.16).

$$\begin{aligned} H_{dc,i} &= \eta_{dc,i} + (1 - \beta_c)\psi_{dc,i} \qquad (5.16) \\ &= \log_2\left(1 + \frac{g_{dc} P_{dc,i}}{e_{dc} N_0 B + f_{dc} P_{dc,i} + I_{dc}}\right) - \\ &\qquad \left(\lambda_{d,i} + \mu_{d,i}\tau_i + \gamma_i x_c \frac{\alpha_c}{g_c} g^I_{dc} + \omega_i (1 - x_c) \sum_{p=1}^{P} \frac{\alpha_p x_p}{g_{pc}} g^I_{dc}\right) P_{dc,i}. \end{aligned}$$

Moreover, for orthogonal spectrum sharing ($\beta_c = 1$), M_{co} is an empty set and the constraint of Eq. (5.5c) is inactive, i.e. $\psi_{dc,i} = 0$. Hence, the above equation reduces to

$$y^*_{dc,i} = 1, d = \underset{1 \le \hat{d} \le D}{argmax} \; H_{\hat{d}c,i}; \qquad y^*_{dc,i} = 0, \forall \hat{d} \neq d. \tag{5.17}$$

Proof. See Appendix B for proof. □

[6]Here $[\lambda_{1,i}, \lambda_{2,i}, \cdots, \lambda_{D,i}]^T$ is the i^{th} column of $\boldsymbol{\lambda}$, $[\mu_{1,i}, \mu_{2,i}, \cdots, \mu_{D,i}]^T$ is the i^{th} column of $\boldsymbol{\mu}$, where $i \in [1, 2, \cdots, K]$, while $\boldsymbol{\omega} = [\omega_1, \omega_2, \cdots, \omega_K]^T$ and $\boldsymbol{\gamma} = [\gamma_1, \gamma_2, \cdots, \gamma_K]^T$.

Remark 1: It can be observed both from Eq. (5.15) as well as from Eq. (5.17) that the c^{th} MU's RB corresponding to the highest value of $H_{dc,i}$ will be reused by the d^{th} D2D link. According to Eq. (5.16), $H_{dc,i}$ depends on the different independent and identically distributed random channel gains. Therefore, practically speaking, the probability of having $H_{\hat{dc},i} = H_{\tilde{dc},i}$ where $\tilde{d} \neq d$ is infinitesimally low. Hence, the temporary relaxation imposed on $y_{dc,i}$ to be continuous variables lying in $[0, 1]$ still produces a binary solution.

Based on the above analysis, an iterative algorithm is proposed, which is termed as the *joint optimization of the RB and of the power allocation (JORPA)*. This algorithm simultaneously derives the optimized transmit power of both the D2D links and that of the MUs along with D2D-MU matching relying on the idealistic setting of an off-line EH process, where the D2D links are perfectly aware of the energy arrival instants. This is formally stated in Algorithm 5.1. For a given power allocation of the D2D links obtained from Eq. (4.14a) defined in line 31 of Algorithm 5.1, it allocates the adequate-quality cellular RBs to the D2D links according to Eq. (5.17) and/or Eq. (5.15), depending upon the specific spectrum sharing scenario considered, as given in lines 33-37. This algorithm minimises the dual problem of Eq. (5.5) by finding the optimal values of $\lambda_{d,i}$, $\mu_{d,i}$, γ_i and ω_i using the popular bisection based search method employed for updating these multipliers in each of the four nested loops.

The Lagrangian multipliers γ_i and ω_i are updated according to the maximum tolerable interference inflicted by the D2D links upon the MUs associated with the MBS (lines 19-25) or PBSs (Lines 11-17), respectively, which are then fed into the sub-algorithm. This sub-algorithm is constituted by a pair of nested loops, each updating the Lagrangian multipliers $\lambda_{d,i}$ and $\mu_{d,i}$ according to both the power budget and to the energy causality constraints of Eq. (5.5d) and Eq. (5.5e) at the D2D links, in lines 38-43 and 45-50 of Algorithm 5.1 respectively. Finally, the power allocation of the MUs associated with the MBS or PBSs is obtained using Eq. (5.10) and Eq. (5.11), respectively. The termination condition of this algorithm ensures that the assignment of the RBs to the D2D links and the power allocated both to the D2D links and to the MUs become sufficiently accurate by initializing the accuracy threshold ζ to a small value at line 3 of Algorithm 5.1.

Now, according to Eq. (5.13) and Eq. (5.16), $P^*_{dc,i}$ and $H^*_{dc,i}$ are functions of the Lagrangian multipliers as well as the proposed JORPA algorithm requires upper bounds for Lagrangian multipliers (lines $6, 8, 27, 29$) for initiating the optimization for the resource allocation problem. Hence, for the sake of achieving a faster convergence, the bounds of these multipliers are defined in Lemma 5.

Lemma 5. *The optimal Lagrangian Multipliers $\lambda^*_{d,i}$, $\mu^*_{d,i}$, γ^*_i and ω^*_i lie in the interval $[0, \lambda^{max}_{d,i}]$,$[0, \mu^{max}_{d,i}]$,$[0, \gamma^{max}_i]$ and $[0, \omega^{max}_i]$, respectively, where upper bounds are given by,*

$$\lambda^{max}_{d,i} = \underset{1\leq c\leq M}{argmax}\left(\frac{g_{dc}}{\ln(2)(I_{dc} + e_{dc}N_0B)}\right), \tag{5.18a}$$

$$\mu^{max}_{d,i} = \underset{1\leq c\leq M}{argmax}\left(\frac{g_{dc}}{\ln(2)\tau_i(I_{dc} + e_{dc}N_0B)}\right), \tag{5.18b}$$

$$\gamma_i^{max} = \underset{\substack{1\le c\le M\\ 1\le d\le D}}{argmax}\left(\frac{g_{dc}g_c}{\ln(2)(I_{dc}+e_{dc}N_0B)x_c\alpha_c g_{dc}^I}\right), \tag{5.18c}$$

$$\omega_i^{max} = \underset{\substack{1\le c\le M\\ 1\le d\le D}}{argmax}\left(\frac{g_{dc}}{\ln(2)(I_{dc}+e_{dc}N_0B)(1-x_c)\sum_{p=1}^{P}\frac{xp\alpha_p}{g_{pc}}g_{dc}^I}\right). \tag{5.18d}$$

Proof. Using Eq. (4.14a) and the constraints of Eq. (5.5g) and Eq. (5.5f), it is surmised that there exists at least one $P_{dc,i}^* \ge 0$ in the c^{th} RB for any d and c, which satisfies:

$$p_{dc,i}^* \ge 0$$

$$\left[\sqrt{\left(\frac{s_{dc}^{(1)}}{2s_{dc}^{(0)}}\right)^2 - \frac{s_{dc}^{(2)}(\lambda_{dc,i},\mu_{dc,i},\gamma_{dc,i})}{s_{dc}^0}} - \left(\frac{s_{dc}^{(1)}}{2s_{dc}^{(0)}}\right)\right]^+ \ge 0$$

Algorithm 5.1 Algorithm for Joint optimization of RB and Power Allocation (JORPA).

Input: P_C^{max}, P_P^{max}, P_D^{max} $\forall d$, R_c, g_c, g_c^I, x_c, β_c $\forall c$; x_{pc} $\forall$ MUs associated with PBS; g_{dc}, g_{dc}^I, g_{cd}^I, g_{pc}, g_{pc}^I, g_{pd}^I $\forall\, c,d,p$; $E_{d,i}$ $\forall\, d,i$, t_i $\forall i$ T_{max}, K, N_0, B, M_{co}.
Output: $P_{dc,i}^*$, $y_{dc,i}^*$ $\forall\, c,d,i$, P_c^*, P_p^* $\forall\, c$ $\forall p$.
Initialize: Set accuracy ζ, $i=1$, $P_c^I = \frac{P_C^{max}}{\sum_{c=1}^{M}x_c}$ and $P_p^I = \frac{P_p^{max}}{\sum_{c=1}^{M}x_{pc}}$ for calculating I_M and I_P.
Let $P_{sur} = P_C^{max} - \sum_{c=1}^{M} x_c\frac{\alpha_c}{g_c}\left[\sum_{p=1}^{P}((1-\beta_c x_c)I_P) + N_0B\right]$ and $P_{sur,P} = P_P^{max} - \sum_{c=1}^{M}(1-x_c)\frac{x_{pc}\alpha_p}{g_{pc}}[(\beta_c x_c + (1-\beta_c))I_M + N_0B]$.
for $(i = 1 : K)$ **do**
    Set $\gamma_a = 0$, $\gamma_b = \gamma_i^{max}$; $n=1$, $\gamma_i(n) = \frac{(\gamma_a+\gamma_b)}{2}$.
    while $|\gamma_a - \gamma_b| > \zeta$ **do**
        Set $\omega_a = 0$, $\omega_b = \omega_i^{max}$; $o=1$, $\omega_i(o) = \frac{(\omega_a+\omega_b)}{2}$.
        while $|\omega_a - \omega_b| > \zeta$ **do**
            Find $\mu_{d,i}^*$, $\lambda_{d,i}^*$, $P_{dc,i}^*$, $y_{dc,i}^*$ $\forall\, d,c$ for a given $\gamma_i(n)$ and $\omega_i(o)$ using Sub-Algorithm below.
            Let $P_{sur,P}^{'} = \sum_{d=1}^{D}\sum_{c=1}^{M}(1-x_c)\frac{x_p\alpha_p}{g_{pc}}y_{dc,i}P_{dc,i}g_{dc}^I$
            if $P_{sur,P}^{'} \le P_{sur,P}$ **then**
                $\omega_b = \omega_i(o)$;
            else
                $\omega_a = \omega_i(o)$;
            end if
            Update $o = o+1$, $\omega_i(o) = \frac{(\omega_a+\omega_b)}{2}$.
        end while
        Let $P_{sur}^{'} = \sum_{d=1}^{D}\sum_{c=1}^{M} x_c\frac{\alpha_c}{g_c}y_{dc,i}P_{dc,i}g_{dc}^I$
        if $P_{sur}^{'} \le P_{sur}$ **then**
            $\gamma_b = \gamma_i(n)$;
        else
            $\gamma_a = \gamma_i(n)$;
        end if
        Update $n = n+1$, $\gamma_i(n) = \frac{(\gamma_a+\gamma_b)}{2}$.
    end while

Algorithm 5.1 Algorithm for Joint optimization of RB and Power Allocation (JORPA).

Sub Algorithm:

Initialize: $m = 1$, $\mu_a = 0$, $\mu_b = \mu_{d,i}^{max}$, $\mu_{d,i}(m) = \frac{(\mu_a+\mu_b)}{2}$.
while $|\mu_a - \mu_b| > \zeta$ **do**
Initialize: $l = 1$, $\lambda_a = 0$, $\lambda_b = \lambda_{d,i}^{max}$, $\lambda_{d,i}(l) = \frac{(\lambda_a+\lambda_b)}{2}$, $\tau_i = t_i - t_{i-1}$ $\forall i$.
repeat
Calculate $P_{dc,i}^{*}$ $\forall$ d, c, i with the given $\gamma_i(n)$, $\omega_i(o)$, $\mu_{d,i}(m)$ and $\lambda_{d,i}(l)$ via Eq. (5.13).
Compute $H_{dc,i}$ for any d, c via Eq. (5.16).
if $\beta_c = 0$ **then**
Match d^{th} D2D link with c^{th} MU using to Eq. (5.15)
else
Match d^{th} D2D link with c^{th} MU using to Eq. (5.17)
end if
if $(\sum_{c=1}^{M} y_{dc,i} P_{dc,i} \leq P_D^{max})$ **then**
$\lambda_b = \lambda_{d,i}(l)$;
else
$\lambda_a = \lambda_{d,i}(l)$;
end if
Update $l = l + 1$, $\lambda_{d,i}(l) = \frac{(\lambda_a+\lambda_b)}{2}$.
until $|\lambda_a - \lambda_b| < \zeta$ $\forall d, i$
if $\sum_{\kappa=1}^{i} \sum_{c=1}^{M} y_{dc,\kappa} P_{dc,\kappa} \tau_\kappa > \sum_{\kappa=0}^{i-1} E_{d,\kappa}$ **then**
$\mu_b = \mu_{d,i}(m)$;
else
$\mu_a = \mu_{d,i}(m)$;
end if
Update $m = m + 1$, $\mu_{d,i}(m) = \frac{(\mu_a+\mu_b)}{2}$.
end while
end for
Finally obtain P_c^{*} $\forall$ $y_{dc,i} = 1$ and $x_c = 1$ using Eq. (5.10) and P_p^{*} $\forall$ $y_{dc,i} = 1$ and $x_c = 0$ using Eq. (5.11) .

$$(I_{dc} + e_{dc} N_0 B)^2 - \frac{g_{dc}(I_{dc} + e_{dc} N_0) g_c}{\ln(2) \left[\lambda_{dc,i} + \mu_{dc,i} \tau_i + \gamma_i x_c \frac{\alpha_c}{g_c} g_{dc}^I + \omega_i (1 - x_c) \sum_{p=1}^{P} \frac{x_p \alpha_p}{g_{pc}} g_{dc}^I \right]} \leq 0.$$

For the different combination of $\lambda_{d,i} = 0$ and/or $\mu_{d,i} = 0$ and/or $\gamma_i = 0$ and/or $\omega_i = 0$, $\lambda_{d,i}^{max}$, $\mu_{d,i}^{max}$, γ_i^{max} and ω_i^{max} are obtained. □

The mathematical proof of convergence for Algorithm 5.1 has been omitted, because the algorithm invokes the bisection search method for obtaining the optimal values of Lagrangian multipliers, whose convergence was shown in [109, 110]. However, in Figure 5.5, the convergence of the proposed JORPA algorithm is characterized for each energy harvesting epoch under all three of the spectrum sharing strategies considered. This algorithmic convergence is achieved for each Monte-Carlo run before obtaining the final results by averaging over the 10,000 Monte-Carlo simulation runs. It can be observed that as the number of iterations in the algorithm increases, the sum-rate of the D2D links becomes constant for all the three spectrum sharing schemes.

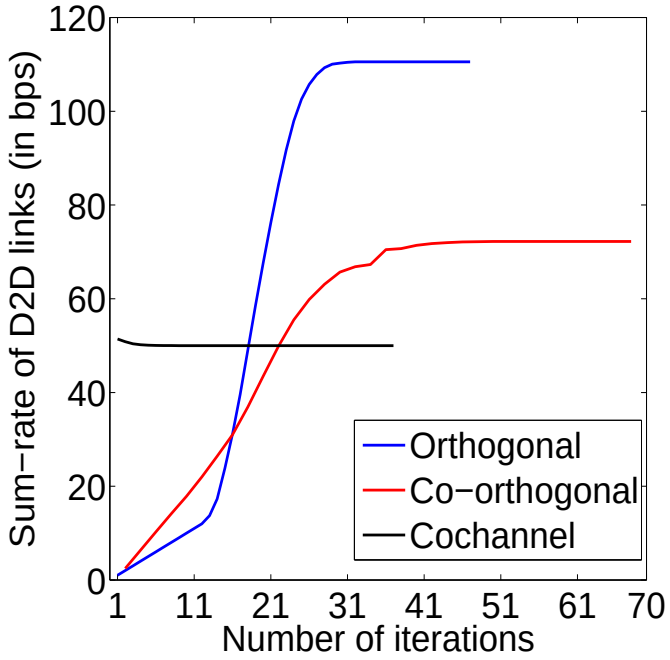

Figure 5.5: Convergence of the algorithm as a sum-rate of D2D links with respect to the number of iterations. These results were extracted for the parameters of Table 5.2 with $P = 1$, $D = 8$ and $C = 10$.

5.4 Heuristic Solutions

Since the complexity[7] of the optimized solution is potentially excessive owing to the presence of four nested loops in the proposed JORPA Algorithm 5.1, the following heuristic methods are conceived, where the optimization variables of $\mathbf{P_{dc}}$ and $\mathbf{y_{dc}}$ are reduced to a single one, while heuristically obtaining the other variables. The details of the methods are as follows:

- *Equal Power Allocation (EPA)*: In this method, a simple plausible *harvesting and dissipation* strategy is invoked for allocating power to the D2D link. In this harvesting and dissipation strategy, the transmit power of the D2D links is obtained by equally distributing the energy harvested to the reused RBs without violating the maximum power budget of D2D transmission, which results in satisfying the constraints given in Eq. (5.5d) and Eq. (5.5e) heuristically. Based on this heuristic power allocation, the D2D-MU matching is then optimized using the reduced complexity optimization problem by satisfying the constraints Eq. (5.5b) and Eq. (5.5c). Moreover, the maximum tolerable interference level of each of the BSs is never exceeded, which is ensured by disabling the D2D transmissions on the RBs of specific BSs, when the constraints of Eq. (5.5f)-Eq. (5.5g) would become violated.

- *Random D2D-MU Matching (RM)*: According to this method, the power allocation is optimized by the random mapping of the D2D links to the MU's resource blocks, while ensuring that the constraints of Eq. (5.5b) and Eq. (5.5c) are still satisfied. The transmit power is then optimized under the constraints of Eq. (5.5d) and Eq. (5.5e),

[7]The complexity analysis of the JORPA and heuristic algorithms is beyond the scope of this work.

where again, the maximum tolerable interference constraints of the BSs are never exceeded, which is guaranteed by setting the D2D-MU matching to zero for the specific DL RBs of the BSs when they are about to be violated.

- *Maximum Distance D2D-MU Matching (MDM)*: According to this method, the D2D links are matched to that specific MU's RB, which is at the largest distance from the D2D link in order to reduce the interference it inflicts upon the MUs, while satisfying the constraints of Eq. (5.5b) and Eq. (5.5c). The transmit power is then optimized under the constraints of Eq. (5.5d) and Eq. (5.5e), where again, the maximum tolerable interference constraints of the BSs are never exceeded, which is guaranteed by setting the D2D-MU matching to zero for the specific DL RBs of the BSs, when the constraints would become violated.

5.5 Performance Results and Discussion

In this section, the performance of both JORPA algorithm as well as of the heuristic methods is analysed for the achievable D2D sum-rate with the deadline of $T = 10$ seconds, where the D2D links have an energy harvesting capability and reuse the radio resources of the MUs associated with the MBS or PBSs in different spectrum sharing scenarios. The EH processes of each D2D link are independent and they are composed of two random processes: the energy arrival obeys a uniform distribution between $[0, E_{max}]$ mJoule and the arrival instants are defined as Poisson-distributed at a rate of λ mJoule/s. The MBS is located at the origin, while the PBSs are distributed randomly in the cell of radius R, where the BSs are assumed to utilise all the radio resources allocated to them all the time. the simulation results are bifurcated into two parts where the performance of the system in distance-threshold based settings is first analysed followed by the interference-threshold and RSS based system setting, where latter system provides with more realistic and practical system eliminating the idealistic assumptions of former. The parametric settings for the quantitative analysis of this chapter are given in Table 5.1 and Table 5.2 for distance-threshold based system and interference-threshold based system, respectively, [108,111,112]. Based on the difference in the power budgets of the BSs, the throughput requirements are different for the MUs associated with the MBS and for those associated with the PBSs. The system is comprised of uniformly distributed MUs and D2D links, where the distance threshold $D_{Th,d}$ as well as interference-threshold I_{Th} for D2D links while the distance-threshold $D_{Th,c}$ as well as the bias B for the MU association, are also set to those in Table 5.1 and Table 5.2, respectively, unless otherwise mentioned. The channels obey i.i.d. Rayleigh distribution and a path-loss model having different path-loss exponents due to the different propagation environments encountered in the different scenarios. The distance d_l between the D2D pair is set to vary in the interval of $[20, 40]$m. These performance results are obtained under Monte-Carlo simulations of $10,000$ runs for both the parametric settings.

Parameter	Value
Maximum amount of energy Harvested, E_{max}	100 mJ
Rate of energy harvesting, λ	3 mJ/second
Radius of cell, R	500m
Power Budget for MBS, P_C^{max}	46dBm
Power Budget for PBS, P_P^{max}	30dBm
Power Budget for D2D links, P_d^{max}	20dBm
Target throughput for MUs associated with MBS R_c	8bps/Hz
Target throughput for MUs when associated with PBS R_p	4bps/Hz
Distance-threshold for D2D links from PBS $D_{Th,d}$	250m
Distance-threshold for MU association $D_{Th,c}$	200m
Path-loss exponent for D2D TX -D2D RX/MU, α_d	4
Path-loss exponent for PBS - MU/D2D RX, α_p	3.5
Path-loss exponent for MBS - MU/D2D RX, α_c	3
Thermal noise density, N_0	-174dBm/Hz
System Bandwidth	10MHz

Table 5.1: Parametric Settings for the Simulations

5.5.1 Distance-Threshold Based System

In this section, the sub-band selection criteria adopted by the D2D links for the co-orthogonal scheme relies on the distance-threshold $D_{Th,d}$, while the MU-BS association is defined on the basis of the distance threshold $D_{Th,c}$ of the MUs from all the PBSs. the simulation results quantify the D2D sum-rate for different parameter settings, such as those of the D2D distance-threshold from the PBS, of the throughput threshold of the MUs associated with either the MBS or PBSs, of the number of MUs and D2D links as well as of the number of PBSs in conjunction with different channel deployment schemes at the BSs.

the first aim is to find the optimal threshold $D_{Th,d}$ of the D2D links w.r.t. the PBSs for the sum-rate maximisation of the D2D links in the proposed co-orthogonal spectrum sharing scenario. This distance-threshold is used for triggering the distance-dependent switching of D2D links from the ideal scenario of only reusing RBs orthogonally to the aggressive co-channel reuse. Therefore, in Figure 5.6, the D2D sum-rate for different values of the threshold $D_{Th,d}$ is analysed. It can be observed from Figure 5.6 that as the distance-threshold of D2D link increases from the PBS, the D2D sum-rate decreases. This is because the system is evolving from being completely orthogonal towards gradual co-channel deployment, where the interference experienced by the D2D links in the former scenario is lower than in the latter one owing to the interfering downlink transmissions arriving only from a single BS at a time. Therefore, in the orthogonal channel deployment scenario the

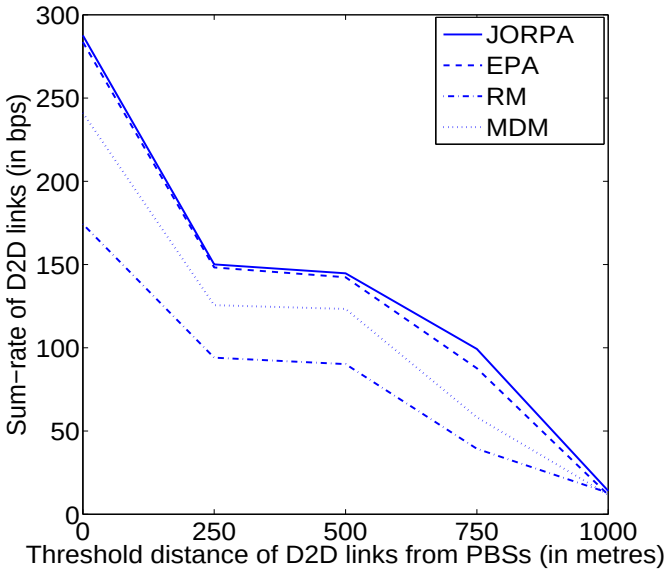

Figure 5.6: Effect of the distance-threshold for D2D links from the PBS on the D2D sum-rate. All the system parameters are summarized in Table 5.1.

sum-rate of the D2D links is at its maximum, when $D_{Th,d} = 0m$, while in the co-channel scenario it is at its minimum, when $D_{Th,d} = 1000m$. Moreover, when $D_{Th,d} \in (0, 1000)$, upon increasing the threshold, the number of D2D links reusing the RBs of the co-channel sub-band is increasing. Hence an increased interference is imposed, thereby reducing the sum-rate of D2D links. The heuristic methods are also analysed upon varying the distance-threshold. It is observed that the 'EPA Heuristic' performs close to the JORPA method of Algorithm 5.1, achieving approximately 98% of the optimal performance at a substantially lower complexity. On the other hand, the 'RM algorithm' performs worse than the 'MDM algorithm', since in the MDM Algorithm, the D2D-MU matching is based on the maximum distance, which tends to reduce the interference it imposes on the MUs, thereby supporting a higher D2D transmission power. Hence a better sum-rate is observed for the latter scheme. Furthermore, both the heuristic 'RM and MDM algorithms' perform worse than the JORPA scheme as well as than the heuristic 'EPA algorithm', which demonstrates the importance of the optimisation discussed in this chapter along with an indication that the choice of D2D-MU matching variable is more crucial for this sum-rate maximisation. Based on the performance results of Figure 5.6 , it is reasonable to set $D_{Th,d} = 250m$ for co-orthogonal deployment, since it supports a higher sum-rate for the D2D links than distance-threshold values.

The D2D sum-rate recorded for different values of the throughput requirements of the MUs associated with the MBS, when the throughput threshold of the MUs served by PBSs is fixed is represented in Figure 5.7. As expected, a diminishing trend is observed upon increasing the throughput threshold of the MUs associated with the MBS, because the power of the MBS transmitted to the MUs should be higher for the sake of increasing the throughput, while a lower interference should be inflicted upon the MUs, which in turn implies that the interference imposed on the D2D links by the MBS increases, while its transmit power has to be reduced in order to meet the throughput requirements. Moreover,

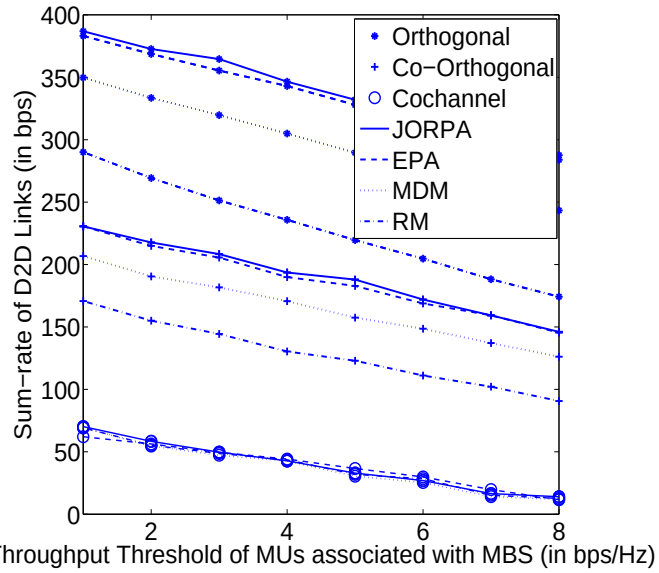

Figure 5.7: Impact of the throughput threshold of MU associated with MBS on the D2D sum-rate. All the system parameters are summarized in Table 5.1.

the orthogonal deployment performs better than the other two deployments, since the D2D links are interfered only by one BS at any particular instant, depending on their D2D-MU matching invoked for resource reuse. On the other hand, the co-orthogonal regime performs better than the co-channel deployment, because in the former case the MUs associated with the MBS can either be deployed in an orthogonal or co-channel sub-band reuse pattern and hence in order to maximise the D2D sum-rate for meeting a higher QoS constraint, depending on their threshold $D_{Th,d}$, some D2D links tend to reuse the resources of the MUs supported by the orthogonal sub-band, which in turn improves the over-all sum-rate in the former case. Again, the heuristic methods were analysed and it was observed that the EPA Algorithm achieves 98% of the optimal sum-rate, while the other two heuristic algorithms perform worse than JORPA scheme and the EPA Algorithm, which in turn shows that it is necessary to optimise the D2D-MU matching for the sake of sum-rate maximisation problem, as considered in this chapter.

The achievable D2D sum-rate is analysed in Figure 5.8 for different values of the throughput target of the MUs associated with the PBS, when that of the MUs associated with the MBS is fixed. Interestingly, it can be observed that upon increasing the QoS requirement of the MUs associated with the PBS, it is observed that the D2D sum-rate remains almost constant. The reason behind this trend is the lower power budget of the PBSs in the system setting. This suggests that for increasing the throughput threshold of the MUs associated with the PBS, the transmit power of the PBS should increase, while the interference experienced at these MUs should be lower. However, the transmit power of the PBS is limited by its power budget. Hence, the PBS does not increase the interference it imposes on the D2D links beyond a certain limit, which in turn results in negligible change in the sum-rate of D2D links, despite increasing the QoS of the MUs associated with the PBS. Moreover, the orthogonal deployment performs better than the other two deployments owing to transmission only by a single BS on each RB, while the co-orthogonal

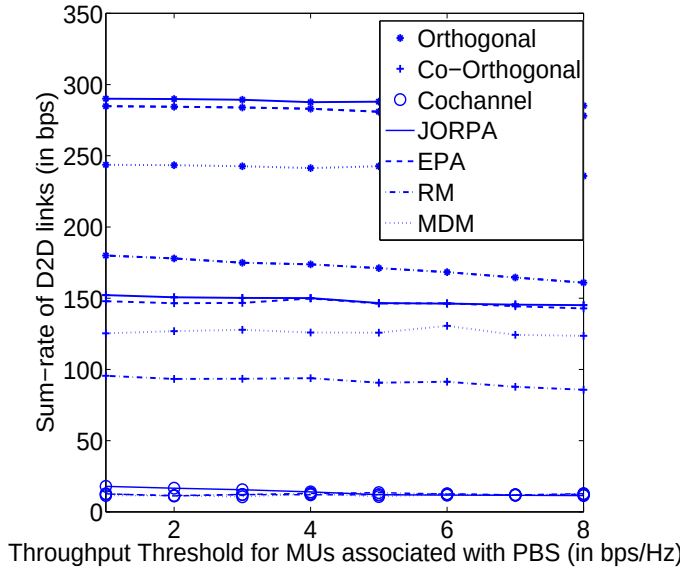

Figure 5.8: Impact of the throughput threshold of MU associated with PBS on the D2D sum-rate. All the system parameters are summarized in Table 5.1.

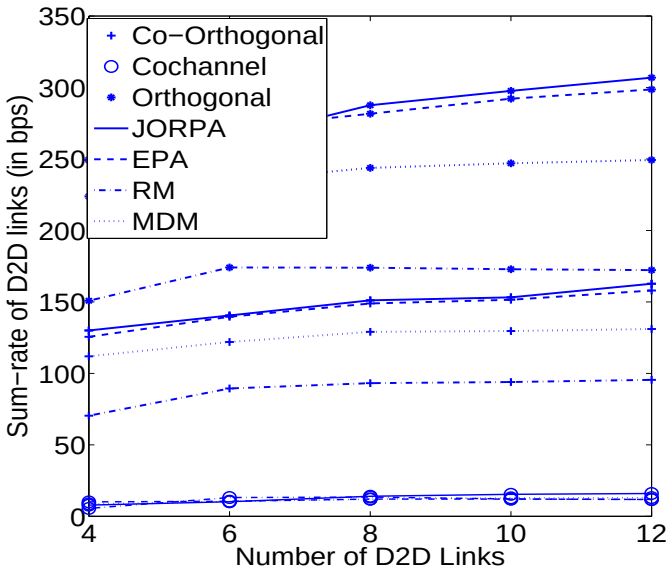

Figure 5.9: Impact of varying number of D2D links on the D2D sum-rate. All the system parameters are summarized in Table 5.1.

deployment performs better than the co-channel deployment, since it subsumes both the orthogonal and co-channel regimes. Again, the heuristic methods follow similar trends, further supporting the fact that D2D-MU matching is important for the maximisation of the D2D sum-rate.

The impact of varying the number of D2D links on the D2D sum-rate is then analysed in Figure 5.9. As expected, upon increasing the number of D2D links, the D2D sum-rate increases for all the three spectrum sharing strategies. However, the orthogonal sharing performs best owing to the reduced interference inflicted upon the D2D links, when compared to the other two strategies. Moreover, upon comparing the co-channel and co-orthogonal spectrum sharing, it can be seen from Figure 5.9 that the co-orthogonal regime performs

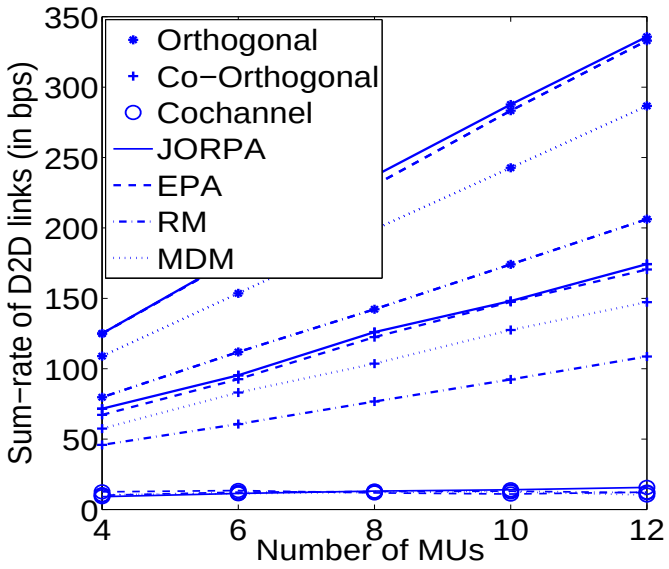

Figure 5.10: Impact of varying number of MUs on the D2D sum-rate. All the system parameters are summarized in Table 5.1.

better than the co-channel solution owing to the availability of RBs suffering from lower interference for reuse by the D2D links due to the resource partitioning into two sub-bands supporting orthogonal and co-channel RBs for downlink transmission to the MUs in the former case. Interestingly, the sum-rate increase of the D2D links slows down owing to the reduced number of RBs becoming available for reuse by each D2D link. Again, similar to the previous results, the heuristic methods follow their expected trend.

Figure 5.10 characterizes the effect of varying the number of MUs on the D2D sum-rate. As expected, upon increasing the number of MUs, the sum-rate of D2D links is increased for all the three channel sharing scenarios. This trend is observed due to the fact that upon increasing the number of MUs, the number of RBs available for D2D reuse also increases and hence the D2D links receive more resources to reuse for transmitting their information, thereby enhancing their overall sum-rate. The orthogonal channel deployment performs best, followed by the co-orthogonal and co-channel deployment owing to the different levels of interference experienced by the D2D links under the different spectrum sharing strategies. Bearing in mind the previous results, the heuristic methods are also expected to follow similar trends.

Finally, Figure 5.11 represents the D2D sum-rate versus the number of PBSs. As the number of PBSs increases, there is a reduction in the traffic to be conveyed by the MBS, which implies that the MUs association with the PBSs increases, hence the transmission power of the PBSs decreases, which in turn reduces the amount of interference received by the D2D links from the PBSs. However, the transmit power of the MBS increases owing to the equal power distribution, as discussed in Section 5.3. Therefore, the orthogonal channel deployment performs best, since the D2D links suffer from the interference arriving either from the MBS or PBSs and given the increased number of the PBSs, more MUs are associated with PBSs. Hence, when the D2D links reuse the RBs of MUs associated with PBSs, the interference is further reduced, thereby increasing their sum-rate. However, in

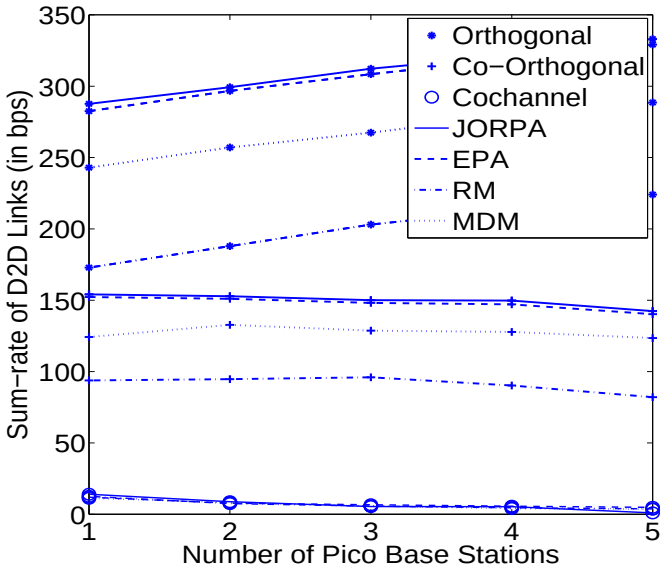

Figure 5.11: Impact of varying number of Pico Base stations on the D2D sum-rate. All the system parameters are summarized in Table 5.1.

case of co-channel deployment the sum-rate decreases, since even though in the presence of more PBSs the MUs tend to become associated with PBSs, which results in the reduction of their transmit power, but at the same time the MBS also shares the spectral resources with the PBSs, which results in an increased MBS transmit power owing to its reduced traffic load. Hence, the overall interference experienced by the D2D links is increased due to the co-channel sharing, thereby reducing their sum-rate in the presence of more PBSs. It can also be seen from Figure 5.11 that the co-orthogonal deployment follows similar trends to the co-channel deployment owing to the increased interference inflicted upon the D2D links due to reusing RBs in the co-channel sub-band. Nonetheless, it has a better performance than the co-channel deployment as a benefit of partitioning the resources into orthogonal and co-channel sub-bands as well as due to the improved chances of the D2D links being matched with MUs supported in orthogonal sub-band, which reduces the interference. Here again, as expected, the heuristic methods exhibit similar trends, emphasizing the need for optimisation, especially that of the D2D-MU matching parameter.

5.5.2 Interference-Threshold and RSS Based System

In this section, D2D link rely on interference-threshold based switching criteria for the selection of sub-band in the co-orthogonal scheme while MU-BS association is defined on the basis of the signal strength received by each MU. The simulation results quantify the D2D sum-rate for different parameter settings, such as those of the D2D interference-threshold as well as bias for received signal strength from PBS, of the throughput threshold of the MUs associated with either the MBS or PBSs, of the number of MUs as well as of the number of PBSs for different channel deployment schemes at the BSs.

The first aim is to find the optimal threshold of the D2D links w.r.t. the interferers for the sum-rate maximization of the D2D links in the proposed co-orthogonal spectrum

Parameter	Value
Maximum amount of energy Harvested, E_{max}	100 mJ
Rate of energy harvesting, λ	3 mJ/second
Radius of cell, R	500m
Power Budget for MBS, P_C^{max}	46dBm
Power Budget for PBS, P_P^{max}	30dBm
Power Budget for D2D links, P_d^{max}	20dBm
Target throughput for MUs associated with MBS R_c	8bps/Hz
Target throughput for MUs when associated with PBS R_p	4bps/Hz
Interference-threshold for D2D links I_{Th}	**40dBm**
Biasing Factor for PBS B_p	**20dB**
Path-loss exponent for D2D TX -D2D RX/MU, α_d	4
Path-loss exponent for PBS - MU/D2D RX, α_p	3.5
Path-loss exponent for MBS - MU/D2D RX, α_c	3
Thermal noise density, N_0	-174dBm/Hz
System Bandwidth	10MHz

Table 5.2: Parametric Settings for the Simulations

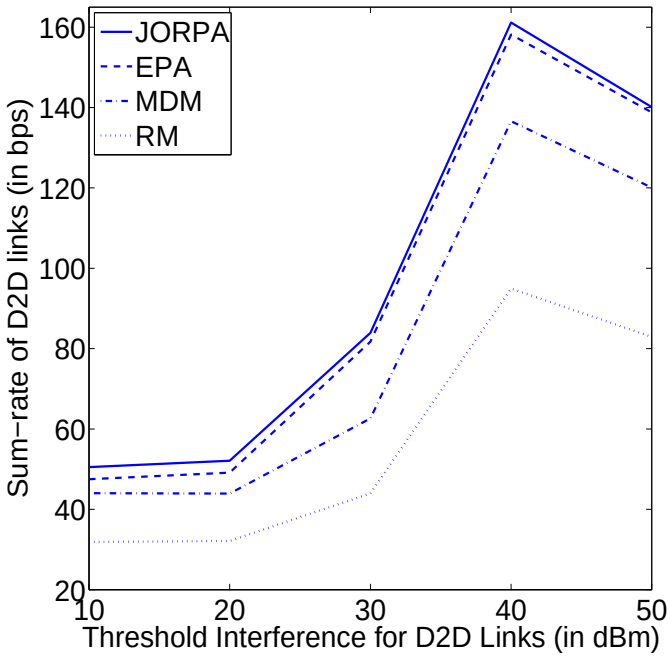

Figure 5.12: Effect of the interference-threshold for D2D links from the PBS on the D2D sum-rate. All the system parameters are summarized in Table 5.2.

sharing scenario, where the interference-threshold, I_{Th}, is used for defining the interference-dependent switching of D2D links from the ideal scenario of only reusing RBs orthogonally

to the aggressive co-channel reuse mode. Therefore, in Figure 5.12, the D2D sum-rate for different values of the threshold $I_{Th}$is analysed. It can be observed from Figure 5.12 that as the interference-threshold of the D2D links increases, the D2D sum-rate increases. This is because the system evolves from operating in completely co-channel fashion towards gradual orthogonal deployment, where the interference experienced by the D2D links in the former scenario is higher than in the latter one owing to the interfering DL transmission from all the active BSs at a time instant. Hence, for co-channel deployment the sum-rate of the D2D links is achieved, when $I_{Th} = 0$ dBm, while in the orthogonal scenario it is achieved, when $I_{Th} \geq (P_C^{max} + P_P^{max})$ dBm. Moreover, when $I_{Th} \in (0, P_C^{max} + P_P^{max})$ dBm, upon increasing the threshold, the number of D2D links reusing the RBs of the orthogonal sub-band is increased. Hence reduced interference is imposed, thereby increasing the sum-rate of D2D links. However, increasing the threshold further, $I_{Th} > 40$dBm results in a sum-rate reduction for the D2D links, which might be due to the fact that the number of D2D links reusing the orthogonal sub-bands has been increased, but the number of MUs using RBs within this sub-band still remained the same. This in turn means that there is a reduction in the number of orthogonal RBs available for reuse upon increasing the number of D2D links relying on orthogonal reuse. This results in a sum-rate reduction for the D2D links. The heuristic methods upon varying the interference-threshold are also analysed. It is observed in Figure 5.12 that the EPA performs similarly to the proposed JORPA algorithm of Algorithm 5.1, achieving approximately 96% of the sum-rate achieved by JORPA at a substantially lower complexity. On the other hand, the RM algorithm performs worse than the MDM algorithm, since in MDM, the D2D-MU matching is based on the maximum distance, which tends to reduce the interference imposed on the MUs, thereby supporting a higher D2D transmission power. Hence a better sum-rate is observed in Figure 5.12 for the latter scheme. Furthermore, both the MDM and RM algorithm perform worse than the JORPA algorithm as well as than the EPA algorithm, which demonstrates the importance of the optimization discussed in this treatise. It also indicates that the specific choice of the D2D-MU matching is more crucial for this sum-rate maximization. Based on the performance results of Figure 5.12 , it is reasonable to set $I_{Th} = 40$ dBm for co-orthogonal deployment, since this choice supports a higher sum-rate for the D2D links than other values of the threshold.

The impact of varying the biasing factor B_p of the PBSs on the D2D sum-rate is then analysed in Figure 5.13. It can be clearly observed that upon increasing the biasing factor, the D2D sum-rate is reduced for all the three spectrum sharing strategies. The reason behind this trend is that upon increasing the biasing factor, the number of MUs associated with PBSs is increased, which in turn implies that the interference imposed by the PBSs is reduced. By conrast, the interference inflicted by the MBS (which has a higher power budget) is increased owing to the equal distribution of power, thereby increasing the overall interference experienced by the D2D links, which in turn results in their lower sum-rate. However, the orthogonal sharing performs best owing to the reduced interference inflicted upon the D2D links, when compared to the other two strategies. Moreover, upon comparing the co-channel and co-orthogonal spectrum sharing, it can be seen from Figure 5.13 that the co-orthogonal regime performs better than the co-channel solution. This trend is due

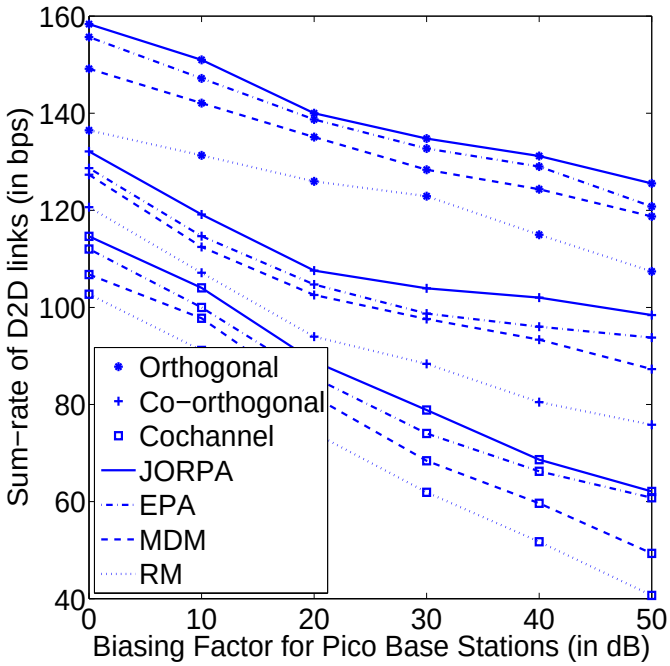

Figure 5.13: Impact of varying the number of D2D links on the D2D sum-rate. All the system parameters are summarized in Table 5.2.

to the availability of RBs suffering from lower interference for reuse by the D2D links due to the resource partitioning into two sub-bands for supporting both orthogonal and co-channel RBs for DL transmission to the MUs in the former case. Again, the heuristic methods were analysed and it was observed that the EPA achieves 96% of the optimal sum-rate, while the other two heuristic algorithms perform worse than the JORPA algorithm and the EPA, which in turn shows that it is necessary to carefully optimize the D2D-MU matching for the sake of sum-rate maximization, as detailed in this treatise. Based on the performance results of Figure 5.13, it is reasonable to set $B_p = 20$ dB, since this supports a better load balancing between the MBS and the PBSs than $B_p = 0$ or 10 dB, while simultaneously supporting a higher sum-rate for the D2D links than higher values of the biasing factor.

Figure 5.14 represents the D2D sum-rate versus the number of PBSs. As the number of PBSs increases, there is a reduction in the traffic on the MBS, which implies that the MUs association with the PBSs increases, hence the transmission power of the PBSs decreases, which in turn reduces the amount of interference experienced by the D2D links from the PBSs. However, the transmit power of the MBS increases owing to the equal power distribution, as discussed in Section 5.3. Therefore, the orthogonal channel deployment performs best, since the D2D links suffer from the interference arriving either from the MBS or PBSs and given the increased number of the PBSs, more MUs are associated with PBSs. Hence, when the D2D links reuse the RBs of MUs associated with PBSs, the interference is further reduced, thereby increasing their sum-rate. However, in case of co-channel deployment the sum-rate decreases, since even though in the presence of more PBSs the MUs tend to become associated with PBSs, which results in a reduction of their transmit power, but at the same time the MBS also shares the spectral resources with PBSs, which results in an increased MBS transmit power owing to its reduced traffic load. Hence,

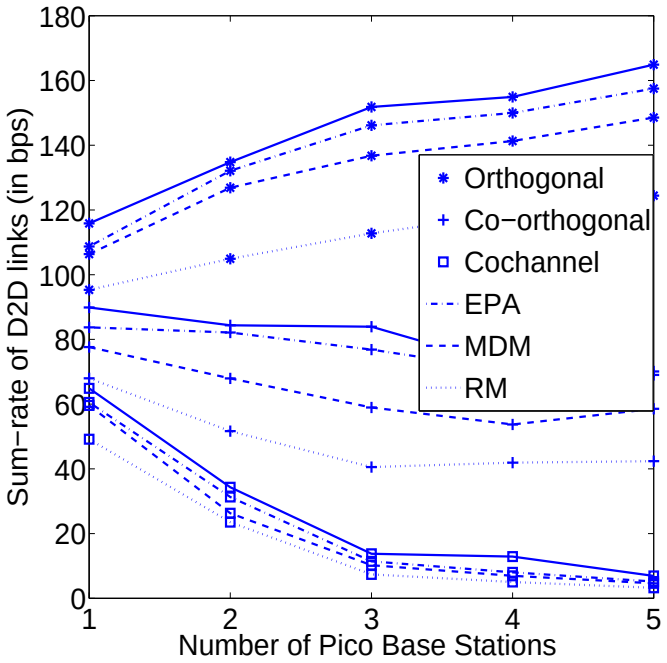

Figure 5.14: Impact of varying the number of Pico Base stations on the D2D sum-rate. All the system parameters are summarized in Table 5.2.

the overall interference experienced by the D2D links is increased due to the co-channel sharing, thereby reducing their sum-rate in the presence of more PBSs. It can also be seen from Figure 5.14 that the co-orthogonal deployment follows similar trends of co-channel deployment owing to the increased interference suffered by the D2D links reusing the RBs in the co-channel sub-band. Nonetheless, it has a better performance than co-channel deployment which is an explicit benefit of partitioning the resources into orthogonal and co-channel sub-bands as well as a benefit of the improved chances of the D2D links becoming matched with MUs supported in orthogonal sub-bands, which reduces the interference. Here again, as expected, the heuristic methods exhibit similar trends, emphasizing the need for optimization, especially that of the D2D-MU matching parameter. Note that for simplicity, the results for the EPA and MDM heuristic algorithms that perform better than the RM heuristic algorithm will only be presented.

The D2D sum-rate recorded is reduced in Figure 5.15 for different values of the throughput requirements of the MUs associated with the MBS, when the throughput threshold of the MUs served by PBSs is fixed. As expected, a diminishing trend is observed upon increasing the throughput threshold of the MUs associated with the MBS, because the power of the MBS transmitted to the MUs should be higher for the sake of increasing the throughput, while a reduced interference should be inflicted upon the MUs, which in turn implies that the interference imposed on the D2D links by the MBS increases, while its transmit power has to be reduced in order to meet the throughput requirements. Moreover, the orthogonal deployment performs better than the other two deployments, since the D2D links are interfered only by a single BS at any particular instant, depending on their D2D-MU matching invoked for resource reuse. On the other hand, the co-orthogonal regime performs better than the co-channel deployment, because in the former case the

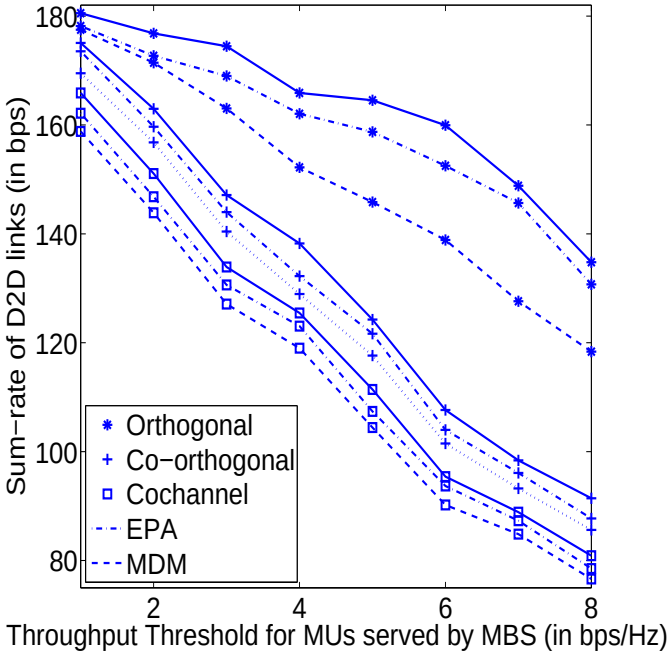

Figure 5.15: Impact of the Quality of Service threshold of MU associated with MBS on the D2D sum-rate. All the system parameters are summarized in Table 5.2.

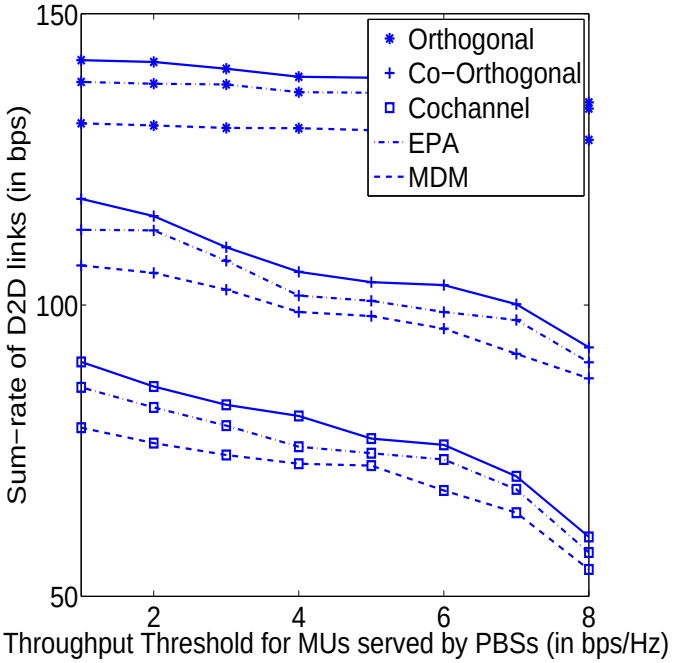

Figure 5.16: Impact of the Quality of Service threshold of the MU associated with PBSs on the D2D sum-rate. All the system parameters are summarized in Table 5.2.

MUs associated with the MBS can either be deployed in an orthogonal or in a co-channel sub-band reuse pattern. Hence, in order to maximize the D2D sum-rate for meeting a higher throughput constraint, depending on their threshold I_{Th}, some D2D links tend to reuse the resources of the MUs supported by orthogonal sub-band, which in turn improves the over-all sum-rate in the former case. Again, similar to the previous results seen in Figure 5.6 - Figure 5.14, the heuristic methods follow their expected trend Figure 5.15

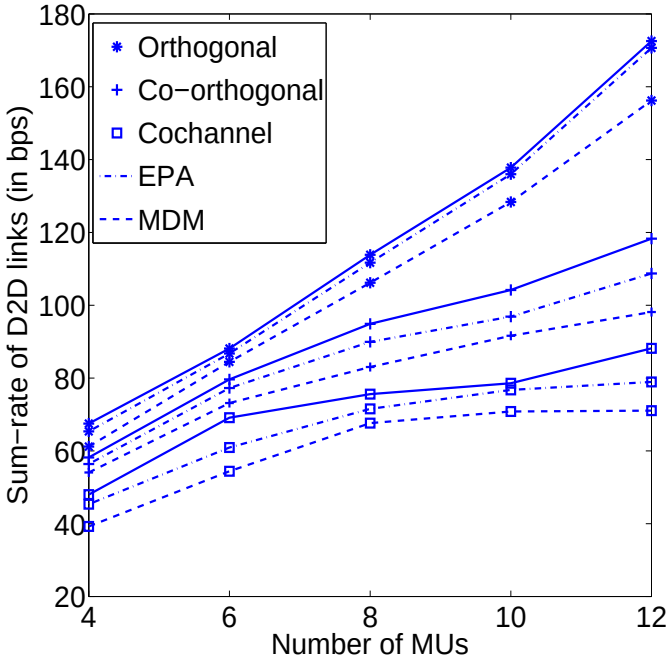

Figure 5.17: Impact of varying the number of MUs on the D2D sum-rate. All the system parameters are summarized in Table 5.2.

The achievable D2D sum-rate is analysed in Figure 5.16 for different values of the throughput target of the MUs associated with the PBS, when that of the MUs associated with the MBS is fixed. Interestingly, it can be observed that upon increasing the throughput requirement of the MUs associated with the PBSs, it is observed that the D2D sum-rate is reduced, albeit at a slower rate. The reason behind this trend is the lower power budget of the PBSs in the system setting. This suggests that for increasing the throughput threshold of the MUs associated with the PBS, the transmit power of the PBS should increase, while the interference experienced at these MUs should be reduced. However, the transmit power of the PBS is limited by its power budget. Hence, the PBS does not increase the interference it imposes on the D2D links beyond a certain limit, which in turn results in a slower rate of decrease in the sum-rate of D2D links, despite increasing the throughput of the MUs associated with the PBS. Moreover, the orthogonal deployment performs better than the other two deployments owing to transmission only by a single BS on each RB, while the co-orthogonal assignment performs better than the co-channel deployment, since it subsumes both the orthogonal and co-channel regimes. Again, the pair of heuristic methods that follow similar trends in Figure 5.16 to those of Figure 5.6 - Figure 5.15, further supporting the fact that using a beneficial D2D-MU matching is important for the maximization of the D2D sum-rate.

Finally, Figure 5.17 characterizes the effect of varying the number of MUs on the D2D sum-rate. As expected, upon increasing the number of MUs, the sum-rate of D2D links is increased for all the three channel sharing scenarios. This trend is observed due to the fact that upon increasing the number of MUs, the number of RBs available for D2D reuse is also increased. Hence the D2D links receive more resources for transmitting their information, thereby enhancing their overall sum-rate. The orthogonal channel deployment performs

best, followed by the co-orthogonal and co-channel deployment owing to the different levels of interference experienced by the D2D links under the different spectrum sharing strategies. Bearing in mind the results Figure 5.6 - Figure 5.16, the heuristic methods are also expected to follow similar trends in Figure 5.17.

Spectrum Sharing	Achieved R_c bps/Hz	Achieved R_p bps/Hz
Co-channel	7.99	3.98
Co-orthogonal	12.16	4.97
orthogonal	8.97	4.16

Table 5.3: Throughput achieved for MUs under different spectrum sharing schemes when JORPA is used for resource allocation on introduction of D2D links. All the system parameters are summarized in Table 5.2.

Table 5.3 shows the throughput achieved for the MUs associated with MBS or PBSs for the different schemes on the introduction of D2D communication, when JORPA is employed for resource allocation. The throughput threshold for MUs associated with MBS is set to $R_c = 8$ bps/Hz, while that with PBSs is set to $R_p = 4$ bpz/Hz. It can be observed in Table 5.3 that for co-channel deployment, throughput achieved for MUs is approximately equivalent to the threshold, while that for the other two deployments surpasses the minimum required throughput threshold. The reason behind this trend is the presence of D2D communication that is reusing the DL resources of MUs imposing additional interference in the existing infrastructure. This implies that for co-channel scenario that already suffers from higher interference is further introduced with interference due to D2D transmission and thus is unable to achieve throughput threshold. Moreover, the proposed co-orthogonal scheme is capable of achieving 50% higher than the required throughput threshold for the MUs associated with the MBS, while only 24% higher than that for the MUs associated with the PBSs. This is due to the higher power budget of the MBS than that of the PBSs as well as due to the interference based switching adopted by the D2D links for reusing the DL resources in either the co-channel or the orthogonal sub-band. Table 5.3 reveals that the presence of D2D communication reduces the throughput experienced by the MUs for co-channel spectrum sharing, while the proposed scheme as well as the orthogonal deployment is still capable of achieving the throughput threshold.

5.6 Summary and Conclusions

Heterogeneous downlink resource reuse solutions were investigated in this chapter relying on a two-tier scenario, where the D2D links reuse the downlink cellular RBs. The D2D links are powered by scavenging energy from the surroundings. The discussions were commenced with the characterisation the network in Section 5.2, where three spectrum sharing strategies were introduced: orthogonal, co-channel and the proposed co-orthogonal spectrum sharing. The specific criteria for D2D link sub-band selection for implementing co-orthogonal spectrum sharing were then presented, where two criteria were introduced -

distance-threshold based as well as interference-threshold based selection. Then the MU-BS association rules were defined based on both the distance as well as on the received signal power. The work has gradually evolved from an unrealistic system specification to a more practical system configuration. An optimization problem was then constructed with the objective of maximizing the D2D sum-rate, without unduly degrading the throughput of the cellular communication.

In order to solve the resultant non-convex problem, it was first transformed to the corresponding convex problem in Section 5.3 by defining the optimal downlink transmit power of each MU for satisfying the throughput constraints. The classic Lagrangian constrained optimization method was then invoked for analytically deriving the resource reuse and power allocation for both the D2D links as well as for the MUs, which was achieved by relaxing the D2D-MU matching variables for the non-causal EH process. An algorithm termed as *joint optimization of RB and power allocation (JORPA)* was then proposed for D2D links, relying on the analytical results of the joint optimization of the three spectrum sharing schemes, whose convergence is established in Figure 5.5. In order to circumvent the potentially excessive complexity of the proposed algorithm, in Section 5.4 three heuristic methods were also conceived, where either the D2D power allocation or the D2D-MU matching was optimized, while the other one of the two parameters was heuristically defined.

The simulation results were divided into two sections, each relying on different criteria for sub-band selection by the D2D links in the co-orthogonal scheme as well as different MU-BS association rule. Specifically, in Section 5.5.1 the results were presented when the D2D links obey the distance-threshold based spectrum switching and the MUs are associated with BSs based on their distance-threshold. On the other hand, in Section 5.5.2 the performance was quantified for a more realistic system relying on MU-BS association based on the signal power received from the BSs, while the D2D links rely on interference-threshold based switching in the co-orthogonal scenario. It was observed from the simulation results that both systems follow similar trends for different parametric settings.

In a nutshell, the simulation results recorded for both system settings reveal that the D2D sum-rate is the highest for the orthogonal spectrum sharing and the lowest for the co-channel arrangement, as determined by the amount of interference experienced by the D2D links. As expected, the presence of D2D communication affects the throughput experienced by MUs due to the increased interference, which is observed most explicitly for co-channel sharing followed by orthogonal sharing, while the proposed co-orthogonal regime is capable of achieving substantially higher throughput for the MUs than the minimum required throughput. Furthermore, the proposed co-orthogonal spectrum sharing scheme strikes a balance between these two richly investigated spectrum sharing scenarios by adopting the best features of these two schemes. This is an explicit benefit of the reduction in interference by the orthogonal sharing, while improving the bandwidth exploitation with the aid of co-channel spectrum sharing. Finally, the analysis of the heuristic methods underlined the importance of optimization in the system. Specifically, optimization of the D2D-MU matching variable is crucial for the maximization of the D2D sum-rate, as revealed by the EPA Algorithm, which achieves 96% (or 98%) of the sum-rate attained by

the JORPA algorithm at a fraction of its complexity, when the interference threshold aided and RSS based system (or distance threshold based system) was considered.

Chapter 6

Conclusions and Future Directions

In this concluding chapter, the findings will be summarized in Section 6.1, while a range of potential future research directions will be discussed in Section 6.2.

6.1 Summary and Conclusion

A huge increase in the spread of mobile devices and mobile multimedia services is being witnessed, which in turn is increasing the demand for data capacity by the users. An undesired consequence is the escalation of energy and bandwidth requirements in wireless communication, which will cause an increase of the global carbon dioxide emissions and impose increased operational costs for operators, respectively. Hence, the energy- and spectral-efficiency are considered to be salient design criteria to be taken into account in the design of future wireless communication networks. In order to improve the energy efficiency of the communication system, different solutions including energy harvesting, power efficient routing protocols, cooperative communication, etc may be exploited. On the other hand, different techniques may be employed for efficient exploitation of the spectrum, including cognitive radio, spectrum sharing, deploying low power base stations, direct D2D communication, etc. Against this background, this thesis aimed to:

- Design energy harvesting aided cooperative communication networks;
- Design resource allocation techniques for direct D2D communication underlaying the downlink of cellular networks employing FFR and SFR for improving the overall spectral efficiency of the system;
- Consider both energy- and spectrum-efficient communication and to design resource allocation techniques for integrated energy harvesting aided D2D and cellular communication, where traditional cellular users and D2D links share their spectral resources without jeopardizing the QoS of the traditional cellular communication.

In the light of these objectives, this thesis was progressed as follows:

- **Chapter 1:** The discourse commenced in Section 1.1 by outlining the motivation for designing resource allocation schemes for energy harvesting as well as D2D communication aided networks both individually and in unison. The historical background of EH aided communication was presented in Section 1.2, while that of D2D communication in cellular networks was discussed in Section 1.3. The historical background of energy harvesting aided D2D communication in cellular networks was described in Section 1.4. The novel contributions of the thesis were highlighted in Section 1.5. Finally, the outline of the thesis was discussed in Section 1.6.

- **Chapter 2:** In this chapter, *energy-efficient* communication was considered, in the light of energy harvesting assisted two-hop networks using a buffer-aided successive relaying protocol. In particular, it focused on the introduction of energy harvesting capabilities at the transmitting nodes arranged in a diamond-topology relay network consisting of a source node and two half-duplex relay nodes with finite battery capacity to store their harvested energy as well as finite data buffer capacity at the relay nodes.

  Explicitly, in Section 2.1, brief review of the family of energy harvesting techniques in the context of different network models was discussed, ranging from simple point-to-point communication to complex cooperative networks. The details of the relay network model was presented, where the transmission of source data to the destination is achieved using a successive relaying protocol in Section 2.2. More specifically, successive relaying protocol is characterised by two phases, in which a FD relay is mimicked by a pair of HD relay nodes, $RN1$ and $RN2$, that are alternating between their transmitter and receiver modes. In this Phase I, SN and $RN2$ are transmitting to the nodes $RN1$ and DN, respectively. Therefore, $RN1$ is in its receiver mode, while $RN2$ is in its transmitter mode for Phase I of the protocol. On the other hand, in Phase II, the relay nodes swap their operational mode. This implies that $RN1$ switches from its receiving mode to its transmitting mode by forwarding the source data to DN, while SN commences its transmission to $RN2$ in Phase II. Therefore, SN is always in its transmitter mode, while DN is always receiving data. The constraints introduced into the system due to its limited energy harvesting capability and limited storage capacity as determined by the size of the energy- and data-buffers at SN, RN1 and RN2 were also detailed. In particular, following constraints were identified in the system:

  - *Energy Causality Constraint:* The total energy harvested by a node until the commencement of its transmission session should exceed the total energy expended by that node during its transmission.
  - *Energy Overflow Constraint:* The energy is lost owing to overflow, when the amount of energy harvested plus the residual energy in the buffer exceeds the storage capacity of the energy buffer at the node.
  - *Data Causality Constraint:* The total amount of data transmitted by a node during the process should not exceed the total data received by that node until that time instant.

– *Data Overflow Constraint:* The amount of data exceeding the storage capacity of data buffer is lost due to overflow.

Then the properties of optimal transmission policy were detailed before delving into the formulation of the optimization problem in Section 2.3. Under the idealized simplifying assumption of known energy arrivals, the related non-convex optimization problem with the objective of maximizing the throughput of the system under the constraints mentioned above was defined. Then, using the *Interior Point Optimization* method, an efficient solution was found for both the proposed optimal and sub-optimal scheme for the sake of maximizing the data delivered to the DN by the deadline.

Finally, the simulation results in Section 2.4 were discussed in four subsections, each justifying different aspects of both the optimal and sub-optimal schemes against the benchmark system [27]:

– In Section 2.4.1, the power allocation schemes were first characterized. Figure 2.3 presented the 'energy feasibility tunnels' for all the EH nodes, where the transmission power lies inside the energy tunnel conforming to the lemmas of Section 2.3 as well as to the constraints of Section 2.2. Since the duration of each of the phases of the successive relaying protocol in an EH epoch is known for the sub-optimal scheme, it was imperative for the sake of maximising the throughput to identify the optimal ratio of the Phase I and II durations. Hence, Figure 2.4 presented the throughput achieved by the sub-optimal scheme upon varying the duration of Phase I and it was indicated that setting this optimal ratio to 50% is best for achieving the maximum throughput.

– Upon finding the optimal ratio to be 50%, in Section 2.4.2, the impact of the buffer size on the throughput of the system was presented. Figure 2.5 portrays a 3-dimensional analysis of both the energy- and data-buffers, which was further divided into the 2-dimensional curves seen in Figure 2.6 and Figure 2.7 for the analysis of each of the buffer capacities. It was observed that the sub-optimal scheme's throughput is about 90% of that of the optimal scheme. Furthermore, the optimal and sub-optimal schemes are capable of achieving upto 92% and 88% of the benchmark scheme's throughput [27] for a sufficiently high energy and data buffer capacity. The impact of sufficient and insufficient energy and/or data buffer capacities on the throughput of the optimal and sub-optimal schemes are quantified in Table 6.1.

– In Section 2.4.3, the impact of asymmetric channel gains was discussed in Figure 2.8 and Figure 2.9. Based on these results it can be inferred that upon increasing the channel gain the throughput of the proposed scheme improves, provided that there is sufficient energy and data buffer capacity. The optimal and sub-optimal schemes consistently achieve 90% and 80% of the benchmark scheme's throughput, respectively. Moreover, the attainable throughput depends on the total collective data (or energy) buffer capacity available in the

Buffer Size	$E_{max} = 5$	$E_{max} = 2$
$B_{max} = 2$	**2.47** 31.35	**18.16** 17.37
$B_{max} = 1$	**17.38** 16.28	**8.60** 7.40

Table 6.1: Comparison of throughput (in bits/sec/Hz) achieved by the optimal (bold) and sub-optimal (normal) scheme for the same sufficient ($E_{max} = 5$ units and $B_{max} = 2$ packets) and insufficient($E_{max} = 2$ units amd $B_{max} = 1$ packet) energy and data buffers at EH nodes. The results were extracted from Figure 2.5 for the parameters of Table 2.1.

network, not only on the smallest data buffer, for different data (or energy) buffer sizes at SN, RN1 and RN2.

- Finally, in Figure 2.10 and Figure 2.11 of Section 2.4.4 the effect of the energy harvesting process was evaluated in terms of the throughput achieved by the schemes as a function of the amount and rate of energy harvested, respectively. The results demonstrated that the throughput of the proposed scheme improves even for insufficient energy buffer capacity with the aid of optimal (or sub-optimal) scheme, consistently achieving 90% (or 80%) of the benchmark scheme's throughput upon increasing the amount of energy.

- **Chapter 3:** In Chapter 2, the benefit of energy harvesting in terms of increasing the energy efficiency of the network were explored. Apart from energy, these wireless nodes need sufficient spectrum for the transmission of their information. Given the growing tele-traffic, the spectrum scarcity is increasing. Hence in Chapter 3 the efficient usage of spectrum is considered by employing D2D communication, which is capable of eliminating the reliance on the MBS. The discussions commenced in Section 3.1, where D2D communication was reviewed with a particular emphasis on resource allocation for D2D communication for managing the interference it imposes on the system. The D2D communication relying on the reuse of RBs allocated to the underlying MUs in the downlink of cellular networks was modelled in Section 3.2. The transmission power of these D2D links was determined by the inverse-power path-loss, where the MBS employed either FFR or SFR for frequency allocation at the MUs. The MUs were classified into CCR and CER users, while the D2D links were categorized into SR and LR links, based on their SIR. Then three frequency allocation schemes were proposed, namely FFA1 and FFA2 when the MBS uses FFR in Section 3.3.1, and SFA when the MBS employs SFR in Section 3.3.2 for the D2D links, which are defined in Figure 3.1:

  - In *FFA*1, the SR D2D links were allocated the CCR frequency (F_0) of the reference macrocell, while the LR D2D links were allocated the CER frequency (F_2 and F_3) of other macrocells.
  - In *FFA*2, both the SR D2D links and LR D2D links were allocated the CER frequency (F_1) of the reference macrocell and the CER frequency (F_2 and F_3)

of other macrocells, respectively.

- In *SFA*, the CER frequency (F_3) and CCR frequency (F_1 and F_2) were allocated to the SR D2D links and LR D2D links, respectively.

Following the definitions of the proposed schemes, in Section 3.3, both the coverage probability as well as the capacity of D2D links were analytically derived, when the MBS employs either UFR, FFR or SFR. The UFR scheme was used as a benchmark scheme for the proposed frequency allocation schemes. Finally, in Section 3.4, the performance results were presented for different parametric setting. It was confirmed that the simulation results tally the analysis. Explicitly, the results section was divided into three parts, each dealing in detail with the performance results of the proposed schemes in FFR and SFR, along with the benefits of power control in D2D links. The frequency allocation schemes significantly outperform the UFR benchmark scheme as revealed by the performance results.

- In the specific scenario, when the MBS employs FFR, in Section 3.4.1 the coverage probability and capacity of the D2D links in Figure 3.5 - Figure 3.8 were presented. It was observed that the FFA2 performs best, followed by FFA1, while the UFR scheme performs worst. These trends confirm the efficiency of the interference management and frequency allocation schemes.
- It was observed that the presence of D2D links degrades the coverage probability of MUs, as shown in Figure 3.9. However, this degradation is higher when UFR is considered than that of FFR.
- In Section 3.4.2, the coverage probability and capacity of D2D links was depicted in Figure 3.10 and Figure 3.11 respectively, when the MBS employs SFR for different power control settings at the MBS. The results reveal that the proposed SFA scheme performs better than the UFR scheme due to the sub-band-based diversity gain achieved by the system, when the D2D links were classified into SR and LR links.
- Finally, the impact of power control was analysed in Section 3.4.3. Relying on the results of Figure 3.12, Figure 3.13 and Table 3.2, it was concluded that the power control factor should be about 0.5 in order to strike an appealing trade-off between the energy consumption and the performance of D2D links.

The performance of the proposed frequency allocation scheme quantified in terms of the coverage probability is summarised in Table 6.2 for different power control factors.

- **Chapter 4:** Having introduced the principles of energy harvesting and D2D communication in Chapter 2 and 3, both techniques were now amalgamated for the sake of efficient energy- and spectrum-management in the network. Therefore, Chapter 4 focused the efforts on designing a downlink resource reuse regime for a cellular network comprised of D2D links and MUs, where the D2D links are capable of harvesting energy from the environment. First of all, the benefits of integrating energy

Power Control Factor	Frequency Allocation Schemes			
ϵ	**FFA**1	**FFA**2	**SFA**	**UFR**
0	0.82	0.76	0.45	0.31
0.5	0.78	0.71	0.34	0.22
1	0.72	0.64	0.23	0.14

Table 6.2: Comparison of coverage probability of the D2D links for achieving target SIR of 10dB under the different frequency allocation schemes when $\beta = 1$ is considered in SFA for fair comparison. These results were extracted from Figure 3.13 for the parameters of Table 3.1.

harvesting and D2D communication were reviewed in Section 4.1. The system model of the energy-harvesting aided D2D links reusing the RBs allocated to MUs in the downlink of cellular networks was then outlined in Section 4.2.1. The following energy harvesting scenarios were considered:

- *Off-line*: An idealistic scenario assuming the non-causal knowledge of the arrival instant and amount of energy, before the commencement of transmission at the energy harvester.
- On-line: A realistic scenario relying on no prior knowledge about the energy harvesting profile.

In Section 4.2.2, the D2D resource allocation problem was formulated as an optimization problem with the objective of maximizing the sum-rate of D2D links, whilst protecting the cellular transmission. Since this is a non-convex mixed integer programming problem, it was first converted into a more tractable convex optimization form. This was achieved by obtaining the optimal MU power, whilst meeting the QoS constraints stipulated. The convexity of this problem was proved before delving into its solution. The optimal resource reuse, power allocation as well as the transmission duration for the D2D links were analytically characterised by invoking the classic Lagrangian method of multipliers for the off-line EH process. Based on the solution of the sum-rate maximization problem, in Section 4.3 a pair of algorithms were proposed for the joint optimization of the D2D-MU matching, of the power allocation and of the transmission duration for both causal and non-causal EH processes at the D2D links as described below:

- *Off-line Joint Optimization Algorithm:* The pseudo algorithm of Algorithm 4.1 formally defines the iterative technique conceived for jointly optimising the power allocation, transmission time and D2D-MU matching under the idealised simplifying assumption of an off-line EH process, where the D2D links are assumed to have perfect non-causal knowledge of the amount of energy and its arrival instants.
- *On-line Joint Optimization Algorithm:* A Dynamic Programming algorithm was invoked, where each stage incorporates a smaller problem solved by using the

Lagrangian method of multipliers developed in Section 4.2.2, when only realistic causal knowledge of the harvested energy is available.

Finally, in Section 4.4, the proposed methods were characterized using the quantitative analysis for different parametric settings. Explicitly, in Figure 4.3 first the reason behind the setting of the optimal distance between each node of a D2D pair to 20 m was provided for further analysis. Then the sum-rate of D2D links was presented as a function of both the number of MUs as well as of the QoS requirement of the MUs in the 3-dimensional diagram of Figure 4.4, which was then partitioned into two separate figures for detailed analysis of the impact of QoS requirements, whilst keeping the number of MUs constant and vice versa in Figure 4.5 and Figure 4.6, respectively. In Figure 4.7, Section 4.4 was concluded with the performance analysis of the sum-rate of D2D links as a function of the number of D2D links. The results revealed that the on-line algorithm advocated is capable of achieving approximately 90% of the sum-rate of the off-line algorithm, which is also summarised inTable 6.3.

Number of MUs	**QoS Target of MUs**	
C	$R_c = 12$	$R_c = 16$
8	**10.02** 9.0	**3.51** 3.11
12	**14.65** 13.78	**4.75** 4.40
15	**17.37** 16.01	**5.74** 5.26

Table 6.3: Comparison of the sum-rate of D2D links (in bps/Hz) achieved by the off-line (bold) and on-line (normal) algorithm for different number of MUs and their QoS threshold. These results were extracted from Figure 4.4 for the parameters of Table 4.1.

- **Chapter 5:** Based on the insights developed in Chapters 2 and 3 as well as on the techniques developed in Chapter 4, the benefits of HetNets and EH aided D2D communication were integrated for the sake of achieving an increased design flexibility in Chapter 5.

  In Section 5.1 the literature was reviewed and the motivation behind this integration was provided. The network was characterized in Section 5.2, where the D2D links harvest energy from the surroundings and reuse the downlink resource of a two-tier HetNet. The three spectrum sharing strategies between the two tiers of the HetNet were introduced:

  - *Orthogonal Sharing:* Each tier is allocated a dedicated set of sub-channels, which are orthogonal to each other.
  - *Co-channel Sharing:* Both the tiers utilise all the available sub-channels for transmission to their associated MUs.

– *Co-orthogonal Sharing:* This proposed strategy is a unification of the above pair of spectrum sharing schemes, where the set of sub-channels is bifurcated into orthogonal and co-channel sharing between two tiers.

For implementing co-orthogonal spectrum sharing, two different criteria were considered for sub-band selection at the D2D links based on a distance threshold as well as on an interference threshold. The MU-BS association rules were also defined based on both the distance as well as on the received signal power. Note that it gradually moved from an idealized system specification to a more practical system configuration. After specifying the details of the network, an optimization problem was constructed for maximizing the D2D sum-rate, without unduly degrading the throughput of cellular communication.

In Section 5.3, the resultant non-convex problem of Eq. (5.4) was first transformed to the corresponding convex problem and then it was solved using the classic Lagrangian method of multipliers for constrained optimization after establishing the convexity of the transformed problem. An algorithm termed as *Joint optimization of RB and power allocation (JORPA)* was then proposed for D2D links in Algorithm 5.1, relying on the analytical results of the joint optimization of the three spectrum sharing schemes considered. The resource reuse and power allocation designed for both the D2D links as well as for the MUs, which was achieved by relaxing the D2D-MU matching variables for the non-causal EH process were derived in *Proposition* 2.

Scheme	**Optimize**	**Heuristic**
EPA	D2D -MU matching	D2D transmit power
RM	D2D transmit power	D2D -MU matching
MDM	D2D transmit power	D2D -MU matching

Table 6.4: Heuristic schemes

In Section 5.4, three low-complexity heuristic methods were also conceived in which either the D2D power allocation or the D2D-MU matching was optimized, while the other one of the two parameters was heuristically defined, as mentioned in Table 6.4. Section 5.5 was split into two sections, each referring to different modelling of the system, starting from an idealized setting and evolving to a more practical model in Sections 5.5.1 and 5.5.2. Specifically, a distance-threshold based spectrum switching regime obeyed by the D2D links, while the MU's are associated with BSs upon satisfying a certain distance-threshold, was considered in detail in Section 5.5.1. It was revealed in Figure 5.6-Figure 5.11 that the orthogonal scheme performs best in terms of achieving maximum D2D sum-rate and the co-channel regime performs worst, while the proposed co-orthogonal strategy strikes a balance between the former schemes. The results for a more realistic system were also quantified in Section 5.5.2, with signal power received from the BSs defining the MU-BS association, while the D2D links rely on the interference-threshold based switching in the co-orthogonal scenario. It was observed from the simulation results of Figure 5.12- Figure 5.17 that

under this system specification, the spectrum sharing schemes follow similar trends for diverse parametric settings.

Specifically, it was observed that the D2D sum-rate is the highest for the orthogonal spectrum sharing and the lowest for the co-channel arrangement for both the system settings due to the increased interference experienced by the D2D links in the latter scheme. The throughput degradation experienced by the MUs in the presence of D2D communication is observed most explicitly for co-channel sharing, followed by orthogonal sharing, while the proposed co-orthogonal regime is capable of achieving a substantially higher throughput for the MUs than the minimum required, as seen in Table 5.3. Finally, the importance of optimizing the system was underlined by the analysis of the heuristic methods. Specifically, the optimization of the D2D-MU matching is crucial for the maximization of the D2D sum-rate, as revealed by the EPA Algorithm of Section 5.4, which achieves 96% (or 98%) of the sum-rate attained by the JORPA algorithm at a fraction of its complexity, when either the interference threshold and RSS based system (or distance threshold based system) is considered.

Based on the analysis in this thesis, the design guidelines for EH and D2D links aided communication systems are summarized as follows:

- The size of energy storage buffer at the devices should be more than the average amount of energy harvested by the node, i.e. $E_{n,max} \geq E_{max}$, as indicated by the results of Figure 2.6.
- For the sake of striking a beneficial trade-off between the energy consumption and the performance of D2D links, the power control factor should be set to 0.5 in order to define the transmit power of D2D links, as depicted by Table 3.2.
- Relying on the results of Figure 4.3, the distance between D2D pair should be around 20m and should not exceed 50m in order to ensure better sum-rate of D2D links.
- In presence of D2D links in heterogeneous network, MBS should be able to support 8bps/Hz throughput to its associated MUs, while PBS can support 4bps/Hz throughput to its associated MU under different spectrum sharing techniques, as indicated by Table 5.3.
- Relying on the analysis in this thesis, it can be deduced that for highly dense networks, the downlink reuse factor that is the number of D2D links reusing each downlink RB of MU's should reduce for ensuring QoS of underlying MUs as well as D2D links.

6.2 Future Directions

In this section, a number of possible future research avenues are briefly discussed.

(a) Chapter 2 considered a buffer aided successive relaying scheme employing energy harvesting. In this successive relaying scheme, a pair of HD relays were employed to

mimic a FD relay. It would be beneficial to introduce a modified successive relaying scheme supporting two-way communication, where the source and destination will be considered as two full-duplex users that can transmit and receive simultaneously. On the other hand, the half duplex relay nodes support two-way relaying. Assuming energy harvesting capabilities at all the nodes along with buffer limitations presents an interesting scenario, which will change the dynamics of the system due to two way communication [113]. Moreover, it will be beneficial to remove the idealized simplifying assumption of non-causal knowledge of energy harvesting events at the transmitters. Incorporating causal knowledge will present a practical model of the network, which might require using a Markov decision process or game-theoretic approach.

(b) Chapter 3 conceived frequency allocation schemes for the D2D links, when the MBS employs static ICIC. It would also be interesting to investigate the performance of these frequency allocation schemes, when multiple antennas are employed at the D2D transmitter and receiver and when the MBS uses ICIC schemes [114]. In this case, the presence of multiple antennas at the receiver of D2D links would help us mitigate the strongest interference at the D2D receiver with the aid of combining techniques. Furthermore, considering dynamic ICIC will provide more flexibility in the system at the expense of increased complexity.

(c) In Chapters 4 and 5, wireless information transfer was considered relying on energy harvesting at the transmitting node, although it can also be integrated with the aid of simultaneous wireless power transfer with the receiver node [40]. In essence, the receiver node may be capable of harvesting energy from the RF signal it has received, utilising it for its own ensuing transmission. Hence, in the context of simultaneous wireless information and power transfer, it will be beneficial to investigate how to efficiently utilize the received wireless power without significantly degrading the information transmission rate by weakening the received signal.

(d) In Chapter 2, energy harvesting was considered for maximizing the throughput of the system by a specific deadline. Since the wireless sensor networks have limited-battery and it is difficult to replenish the batteries if the sensor network is deployed in hard-to-reach places, they limit the lifetime of the network [115]. Incorporating energy harvesting sensors will prolong the network lifetime, where a sensor node can revive itself even after depleting it's battery by the communication process. However, it will be interesting to investigate the efficiency of energy harvesting in order to identify how beneficial it is to consider EH in terms of the network lifetime attained.

(e) Incorporating energy harvesting aided D2D communication into a multicast-aided mobile social network will be interesting, where the content of common interest is disseminated to the users seeking to exploit their social relationships [116]. This allows efficient file sharing among multiple user equipment in the proximity, which can save precious radio resources during content delivery, since there is no need to relay the file to be shared through the BS. However, it is beneficial to design transmission

scheduling by first selecting the most appropriate cluster head, which guarantees reliable transmission as well as the management of interference, when it has energy harvesting capabilities.

Appendix A

Coverage Probability of D2D Links

In this appendix, we detail the derivation of coverage probability of D2D links, which was invoked in Chapter 3. More specifically, in Section A.1, we derive the coverage probability of D2D links when MBS relies on UFR given in Eq. (3.4) of Section 3.3, while in Section A.2 we derive the coverage probability of D2D links when MBS employs FFR while D2D links rely on frequency allocation schemes, FFA1 and FFA2 of Section 3.3.1. Finally in Section A.3, we invoke derivation of coverage probability of D2D links employing SFA when MBS relies on SFR of Section 3.3.2.

A.1 Coverage Probability of D2D Links in UFR

The coverage probability of a D2D link as defined in Section 3.3 is given by

$$\begin{aligned} P[\gamma_U(l,r) > T] &= P\left[\frac{P_d(r)h_d r^{-\alpha}}{I_{cd}+I_d} > T\right] \\ &= P\left[h_d > \frac{T(I_{cd}+I_d)}{P_d(r)r^{-\alpha}}\right]. \end{aligned} \tag{A.1}$$

Since the fading gain of the D2D link is exponentially distributed, i.e., $h_d \sim \exp(1)$, we get,

$$P[\gamma_U(l,r) > T] = E_{h_{cd,i},h_{d,j}}\left[\exp\left(-\frac{T(I_{cd}+I_d)}{P_d(r)r^{-\alpha}}\right)\right]. \tag{A.2}$$

Recall from Eq. (3.2) that $I_{cd} = \sum_{i\in\phi} P_c h_{cd,i} l_i^{-\alpha}, I_d = \sum_{j\in\psi} P_d(r) h_j d_j^{-\alpha}$ as mentioned in Section 3.2. Since we have Rayleigh channels, $h_{cd,i} \sim \exp(1)$ and $h_j \sim \exp(1)$ are considered, hence $I_{cd} + I_d$ is the sum of the weighted exponential variates. By exploiting the fact that the weighted exponential variates $h'_{cd,i} = w h_{cd,i}$ (w is the weight of the exponential random variable $h_{cd,i}$) can be written as exponential variates associated with a weighted scaling parameter, we have, $h'_{cd,i} \sim \exp(w)$. Thus, $I_{cd} + I_d$ is the sum of independent and non-identical exponential variates. Let us now use the moment matching technique for evaluating the equivalent distribution of $I_{cd} + I_d$, namely that of the total interference ex-

perienced by the D2D link. Explicitly the moment matching technique states that the sum of N independent and non-identical Gamma variates $X_i \sim \mathcal{G}(a_i, b_i)$ can be approximated by a single Gamma variate of $Y = \sum_{i=1}^{N} X_i \sim \mathcal{G}(A, B)$, where A and B are defined as

$$A = \frac{(\sum_{i=1}^{N} a_i b_i)^2}{\sum_{i=1}^{N} a_i b_i^2} \text{ and } B = \frac{\sum_{i=1}^{N} a_i b_i^2}{\sum_{i=1}^{N} a_i b_i}. \tag{A.3}$$

Therefore, the distribution of the total interference at the D2D link, obeys $I_{cd}+I_d \sim \mathcal{G}(\theta, \lambda)$, where θ and λ are defined based on Eq. (A.3) and are given by:

$$\theta(l) = \frac{(\sum\limits_{i\in\phi} l_i + \sum\limits_{j\in\psi} d_j)^2}{\sum\limits_{i\in\phi} l_i^2 + \sum\limits_{j\in\psi} d_j^2} \text{ and } \lambda(l) = \frac{\sum\limits_{i\in\phi} l_i^2 + \sum\limits_{j\in\psi} d_j^2}{\sum\limits_{i\in\phi} l_i + \sum\limits_{j\in\psi} d_j}. \tag{A.4}$$

The expression in Eq. (A.2) can then be simplified and written as,

$$P[\gamma_U(l, r) > T] = \left(\frac{P_d(r)}{\lambda(l) T r^{\alpha} + P_d(r)}\right)^{\theta(l)}. \tag{A.5}$$

Using the relationship defined in Eq. (3.1), we can re-write the above expression as:

$$P[\gamma_U(l, r) > T] = \left(\frac{P_d^{max}}{\lambda(l) T r^{\alpha(1-\epsilon)} R_2^{\alpha\epsilon} + P_d^{max}}\right)^{\theta(l)}. \tag{A.6}$$

Therefore, the coverage probability of a typical D2D link can be formulated as:

$$\begin{aligned} CP &= \int_0^{R_c} \int_{R_1}^{R_2} P[\gamma_U(l, r) > T] f_R(r) \mathrm{d}r f_L(l) \mathrm{d}l \\ &= \int_0^{R_c} \int_{R_1}^{R_2} \left(\frac{P_d^{max}}{\lambda(l) T r^{\alpha(1-\epsilon)} R_2^{\alpha\epsilon} + P_d^{max}}\right)^{\theta(l)} \frac{1}{R_2 - R_1} \mathrm{d}r \frac{2l}{R_c^2} \mathrm{d}l \end{aligned} \tag{A.7}$$

where $f_R(r)$ and $f_L(l)$ denote the probability density function of r and l. In this treatise we assume that the distance r between the D2D Tx and Rx pair is uniformly distributed in (R_1, R_2) and these D2D pairs can be located at a distance l from MBS, which is also distributed uniformly in the cell of radius R_c. Therefore, we have $f_R(r) = \frac{1}{R_2 - R_1}$ and $f_L(l) = \frac{2l}{R_c^2}$ in Eq. (A.7). Furthermore, upon solving the inner integral in the above expression given by,

$$CP(l, T) = \int_{R_1}^{R_2} \left(\frac{P_d^{max}}{\lambda(l) T r^{\alpha(1-\epsilon)} R_2^{\alpha\epsilon} + P_d^{max}}\right)^{\theta(l)} \frac{1}{R_2 - R_1} \mathrm{d}r$$

we arrive at Eq. (A.8) given at the top of the next page. Therefore, the coverage probability

$$CP(l,T) = \frac{R_2}{R_2 - R_1} {}_2F_1\left[\frac{1}{\alpha - \alpha\epsilon}, \theta(l), 1 + \frac{1}{\alpha - \alpha\epsilon}, \frac{-\lambda(l) R_2^{\alpha} T}{P_d^{max}}\right] - \frac{R_1}{R_2 - R_1} {}_2F_1\left[\frac{1}{\alpha - \alpha\epsilon}, \theta(l), 1 + \frac{1}{\alpha - \alpha\epsilon}, \frac{-\lambda(l) R_1^{\alpha - \alpha\epsilon} R_2^{\alpha\epsilon} T}{P_d^{max}}\right]. \tag{A.8}$$

of D2D links in the UFR scenario can be written as :

$$CP = \int_0^{R_c} CP(l,T) \frac{2l}{R_c^2} \mathrm{d}l. \tag{A.9}$$

Substituting the value of $CP(l,T)$ from Eq. (A.8) into Eq. (A.9), we will obtain CP as given in Eq. (3.4).

A.2 Coverage Probability of D2D Links in FFR

We would first like to derive the coverage probability of the D2D link corresponding to FFA1 by defining it for both the SR and LR D2D links individually.

The coverage probability of the SR D2D link is given by

$$\begin{aligned} CP_{F,SR}(l,r) &= P[\gamma_U(l,r) > T | \gamma_U(l,r) > S_d] \\ &= \frac{P[\gamma_U(l,r) > \max\{T, S_d\}]}{P[\gamma_U(l,r) > S_d]}. \end{aligned} \tag{A.10}$$

The above conditional probability expression follows from the fact that the SIR of the SR D2D link is higher than S_d. Similarly, the coverage probability of the LR D2D link is given by

$$CP_{F,LR}(l,r) = P[\hat{\gamma}_d^F(l,r) > T | \gamma_U(l,r) < S_d]. \tag{A.11}$$

Note that the LR D2D link reuses the different frequency bands and hence it experiences a new fading power and new interference, which yields a new SIR $\hat{\gamma}_d(l,r)$. Since the fading gains are independent of each other, hence $CP_{F,LR}$ can be simplified as

$$CP_{F,LR}(l,r) = P[\hat{\gamma}_d^F(l,r) > T]. \tag{A.12}$$

Thus the coverage probability of a D2D link at a distance l from the MBS of the reference cell employing FFA1 is given by

$$CP_{FFA1}(l,r) = CP_{F,SR}(l,r) P[\gamma_U(l,r) > S_d] + CP_{F,LR}(l,r) P[\gamma_U(l,r) < S_d] \tag{A.13}$$

Note that $P[\gamma_U(l,r) > S_d]$ denotes the percentage of SR D2D links in the macrocell and thus the first term of Eq. (A.13) gives the coverage probability contribution due to the SR D2D links. Similarly, $P[\gamma_U(l,r) < S_d]$ gives the probability of the D2D links being LR links

and hence the second term in Eq. (A.13) defines the contribution of the LR D2D links to the overall coverage probability of D2D links in the reference macrocell. By substituting Eq. (A.10) and Eq. (A.12) into Eq. (A.13), we can reformulate Eq. (A.13) as :

$$CP_{FFA1}(l,r) = P[\gamma_U(l,r) > \max\{T, S_d\}] + P[\hat{\gamma}_U(l,r) > T]P[\gamma_U(l,r) < S_d]. \tag{A.14}$$

Exploring the process used in Appendix A.1, the coverage probability of a typical D2D link in the network of Figure 3.3 using FFA1 is given by

$$CP_{FFA1} = \int_0^{R_c} CP(l, \max\{T, S_d\}) + \hat{CP}(l,T)(1 - CP(l,S_d))f_L(l)\mathrm{d}l, \tag{A.15}$$

where $CP(l, \max\{T, S_d\})$ and $CP(l, S_d)$ are defined in Eq. (A.8) and similar to $CP(l,T)$, $\hat{CP}(l,T)$ can be derived for a frequency reuse factor of $\frac{1}{3}$.

A.3 Coverage Probability of D2D Links in SFR

The SIR of an SR D2D link that uses F_3 in an SFR scenario can be written as:

$$\begin{aligned} \gamma_S(l,r) &= \frac{P_d(r)h_d r^{-\alpha}}{I_{cd} + I_d}, \\ I_{cd} &= \sum_{i\in\varphi} \beta P_m h_{cd,i} l_i^{-\alpha} + \sum_{i\in\phi\setminus\varphi} P_m h_{cd,i} l_i^{-\alpha}, \\ I_d &= \sum_{j\in\psi} P_d(r) h_j d_j^{-\alpha}, \end{aligned} \tag{A.16}$$

where $\varphi = \{0, 8, 10, 12, 14, 16, 18\}$ denotes the specific cells that interfere the desired signal with the power of βP_m, when using F_3 in their CER. Hence, there is a change in the interference inflicted upon the D2D link in SFR, since the MBS uses power control for cellular communication, which results in a different interference power arriving from each cell. Therefore, corresponding to this definition of SIR, we can define the coverage probability of the SR D2D link in SFA as:

$$\begin{aligned} CP_{S,SR}(l,r) &= P[\gamma_S(l,r) > T | \gamma_S(l,r) > S_d] \\ &= \frac{P[\gamma_S(l,r) > \max\{T, S_d\}]}{P[\gamma_S(l,r) > S_d]}. \end{aligned} \tag{A.17}$$

By contrast, the coverage probability of the LR D2D links in SFA is given by

$$\begin{aligned} CP_{S,LR}(l,r) &\overset{(a)}{=} P[\hat{\gamma}_S(l,r) > T | \gamma_S(l,r) < S_d] \\ &\overset{(b)}{=} P[\hat{\gamma}_S(l,r) > T] \\ &\overset{(c)}{=} P\left[\frac{P_d(r)\hat{h}_d r^{-\alpha}}{I_{cd} + I_d} > T\right], \end{aligned} \tag{A.18}$$

$$\text{where } I_{cd} = \sum_{i\in\varphi'} \beta P_m h_{cd,i} l_i^{-\alpha} + \sum_{i\in\phi\setminus\varphi'} P_m h_{cd,i} l_i^{-\alpha},$$
$$I_d = \sum_{j\in\psi} P_d(r) h_j d_j^{-\alpha}.$$

Here we have $\varphi' = \{2, 4, 6, 7, 11, 15\}$ in (c) of Eq. (A.18), i.e. the set of macrocells that transmit at a power of βP_m, when using the CER frequency of F_1. It is important to note that in case of the LR D2D links, the SFA scheme allocates F_1 and F_2 to these links and since the channels are independent, the fading experienced is also independent, hence the new SIR is denoted by $\hat{\gamma}_S(l, r)$. Referring to Eq. (A.18), $\hat{\gamma}_S(l, r)$ and $\gamma_S(l, r)$ correspond to the SIR of the D2D link, when they are using different frequency bands. Thus, we arrive at (b) of Eq. (A.18) due to the independent fading experienced by the D2D links and hence the corresponding probabilities, i.e. $P[\hat{\gamma}_S(l, r) > T]$ and $P[\gamma_S(l) < S_d]$ are independent probabilities. Therefore, similar to the FFR scenario, the coverage probability of the D2D link in the SFA can be obtained as

$$CP_{SFA} = \int_0^{R_c} \int_{R_1}^{R_2} (P[\gamma_S(l, r) > \max\{T, S_d\}] + P[\hat{\gamma}_S(l, r) > T] P[\gamma_S(l, r) < S_d] f_R(r) \mathrm{d}r f_L(l) \mathrm{d}l. \tag{A.19}$$

Using the process of Appendix A, the coverage probability of a typical D2D link in the network of Figure 3.3 using SFA is given by

$$CP_{SFA} = \int_0^{R_c} CP_S(l, \max\{T, S_d\}) + \hat{CP}_S(l, T)(1 - CP_S(l, S_d)) f_L(l) \mathrm{d}l, \tag{A.20}$$

where similar to $CP(l, T)$ given in Eq. (A.8), $CP_S(l, \max\{T, S_d\})$ and $\hat{CP}_S(l, T)$ can be derived for both the CCR frequency and for the CER frequency.

Appendix B

Lagrangian Method of Multipliers for JORPA

In this appendix, we detail the Lagrangian method of multipliers for the derivation of D2D-MU matching as well as transmission power of D2D links, MBS and PBS, which was invoked in Chapter 5.

In order to derive the results of this proposition, the KKT conditions of Eq. (5.5) were examined. The Lagrangian function for the optimization of the equivalent problem of Eq. (5.5) is defined as follows:

$$\begin{aligned}\mathcal{L} = &- \sum_{i=1}^{K}\sum_{d=1}^{D}\sum_{c=1}^{C} y_{dc,i}\log_2\left(1+\frac{g_{dc}P_{dc,i}}{e_{dc}N_0+f_{dc}P_{dc,i}+I_{dc}}\right)\\
&+\sum_{i=1}^{K}\sum_{c=1}^{C}\eta_{dc,i}\left(\sum_{d=1}^{D} y_{dc,i}-1\right)+\sum_{i=1}^{K}\psi_{dc,i}\left(\sum_{c=1\in C_{co}}\sum_{d=1}^{D}(1-\beta_c)y_{dc,i}-1\right)\\
&+\sum_{i=1}^{K}\sum_{d=1}^{D}\lambda_{d,i}\left(\sum_{c=1}^{C} y_{dc,i}P_{dc,i}-P_D^{max}\right)\\
&+\sum_{i=1}^{K}\sum_{d=1}^{D}\mu_{d,i}\left(\sum_{\kappa=1}^{i}\sum_{c=1}^{C} y_{dc,\kappa}P_{dc,\kappa}\tau_\kappa-\sum_{\kappa=0}^{i-1}E_{d,\kappa}\right)\\
&+\sum_{i=1}^{K}\sum_{p=1}^{P}\omega_i\left(\sum_{d=1}^{D}\sum_{c=1}^{C}(1-x_c)x_{pc}\frac{\alpha_p}{g_{pc}}y_{dc,i}P_{dc,i}g_{dc}^{I}\right.\\
&\qquad\left.-\left(P_p^{max}-\sum_{c=1}^{C}(1-x_c)x_{pc}\frac{\alpha_p}{g_{pc}}\left[(\beta_c x_c+(1-\beta_c))I_M+N_0\right]\right)\right)\\
&+\sum_{i=1}^{K}\gamma_i\left(\sum_{d=1}^{D}\sum_{c=1}^{C}x_c\frac{\alpha_c}{g_c}y_{dc,i}P_{dc,i}g_{dc}^{I}-\left(P_C^{max}-\sum_{c=1}^{C}x_c\frac{\alpha_c}{g_c}\left[(1-\beta_c x_c)I_P)+N_0\right]\right)\right),\end{aligned} \tag{B.1}$$

where $\eta_{dc,i}, \psi_{dc,i}\lambda_{d,i}$, $\mu_{d,i}$, γ_i and ω_i are Lagrangian multipliers associated with the constraints of Eq. (5.5b), Eq. (5.5c), Eq. (5.5d), Eq. (5.5e), Eq. (5.5g) and Eq. (5.5f), respectively. Now, evaluating the differentiation of Lagrangian function with respect to $y_{dc,i}$ and equating them to zero, we get:

$$\begin{aligned}&\frac{\partial\mathcal{L}}{\partial y_{dc,i}}=0\\
&-\log_2\left(1+\frac{g_{dc}P_{dc,i}}{e_{dc}N_0+f_{dc}P_{dc,i}+I_{dc}}\right)+\eta_{dc,i}+(1-\beta_c)\psi_{dc,i}+\\
&\left(\lambda_{d,i}+\mu_{d,i}\tau_i+\omega_i(1-x_c)x_{pc}\frac{\alpha_p}{g_{pc}}g_{dc}^{I}+\gamma_i x_c\frac{\alpha_c}{g_c}g_{dc}^{I}\right)P_{dc,i}=0\end{aligned}$$

$$\eta_{dc,i} + (1-\beta_c)\psi_{dc,i} = \log_2\left(1 + \frac{g_{dc}P_{dc,i}}{e_{dc}N_0 + f_{dc}P_{dc,i} + I_{dc}}\right) - \left(\lambda_{d,i} + \mu_{d,i}\tau_i + \omega_i(1-x_c)x_{pc}\frac{\alpha_p}{g_{pc}}g^I_{dc} + \gamma_i x_c \frac{\alpha_c}{g_c}g^I_{dc}\right)P_{dc,i}.$$

Here we define $H_{dc,i} = \eta_{dc,i} + (1-\beta_c)\psi_{dc,i}$ as given in Eq. (5.16), which is used for obtaining the optimized D2D-CU matching given in Eq. (5.15). Similarly, differentiating $\mathcal{L}$ with respect to $P_{dc,i}$ and equating it to zero, we arrive at:

$$\begin{aligned}
&\tfrac{\partial \mathcal{L}}{\partial P_{dc,i}} = 0 \\
&\tfrac{-y_{dc,i}g_{dc}(I_{dc}+e_{dc}N_0)}{\ln 2(I_{dc}+f_{dc}P_{dc,i}+e_{dc}N_0)(I_{dc}+(f_{dc}+g_{dc})P_{dc,i}+e_{dc}N_0)} + \lambda_{d,i}y_{dc,i} + \\
&\mu_{d,i}y_{dc,i}\tau_i + \omega_i(1-x_c)x_{pc}\frac{\alpha_p}{g_{pc}}y_{dc,i}g^I_{dc} + \gamma_i x_c\frac{\alpha_c}{g_c}y_{dc,i}g^I_{dc} = 0.
\end{aligned}$$

Considering that the d^{th} D2D link reuses the RB of the c^{th} MU, so that $y_{dc,i} = 1$, we simplify the above equation and obtain the following equation:

$$s^{(0)}_{dc}P^2_{dc,i} + s^{(1)}_{dc}P^2_{dc,i} + s^{(2)}_{dc}(\lambda_{dc,i}, \mu_{dc,i}, \gamma_{dc,i}, \omega_{dc,i}) = 0.$$

This equation is quadratic in $P_{dc,i}$, which is solved to obtain $P^*_{dc,i}$ as given in Eq. (5.13), where $s^{(0)}_{dc}, s^{1)}_{dc}$ and $s^{(2)}_{dc}(\lambda_{dc,i}, \mu_{dc,i}, \gamma_{dc,i}, \omega_{dc,i})$ are defined in Lemma 2.

Bibliography

[1] S. Gupta, R. Zhang, and L. Hanzo, "Throughput maximization for a buffer-aided successive relaying network employing energy harvesting," *IEEE Transactions on Vehicular Technology*, vol. 65, no. 8, pp. 6758–6765, Aug 2016.

[2] S. Gupta, S. Kumar, R. Zhang, S. Kalyani, K. Giridhar, and L. Hanzo, "Resource allocation for d2d links in the ffr and sfr aided cellular downlink," *IEEE Transactions on Communications*, vol. 64, no. 10, pp. 4434–4448, Oct 2016.

[3] S. Gupta, R. Zhang, and L. Hanzo, "Energy harvesting aided device-to-device communication underlaying the cellular downlink," *IEEE Access*, vol. PP, no. 99, pp. 1–1, 2016.

[4] S. Gupta and R. Zhang and L. Hanzo, "Energy harvesting aided device-to-device communication in the over-sailing heterogeneous two-tier downlink," *IEEE Access*, vol. PP, no. 99, pp. 1–1, 2017.

[5] M. Agiwal, A. Roy, and N. Saxena, "Next generation 5g wireless networks: A comprehensive survey," *IEEE Communications Surveys Tutorials*, vol. 18, no. 3, pp. 1617–1655, 2016.

[6] C. Han, T. Harrold, S. Armour, I. Krikidis, S. Videv, P. M. Grant, H. Haas, J. S. Thompson, I. Ku, C. X. Wang, T. A. Le, M. R. Nakhai, J. Zhang, and L. Hanzo, "Green radio: radio techniques to enable energy-efficient wireless networks," *IEEE Communications Magazine*, vol. 49, no. 6, pp. 46–54, June 2011.

[7] S. Sudevalayam and P. Kulkarni, "Energy harvesting sensor nodes: Survey and implications," *IEEE Communications Surveys Tutorials*, vol. 13, no. 3, pp. 443–461, 2011.

[8] J. A. Paradiso and T. Starner, "Energy scavenging for mobile and wireless electronics," *IEEE Pervasive Computing*, vol. 4, no. 1, pp. 18–27, Jan 2005.

[9] P. Mach, Z. Becvar, and T. Vanek, "In-band device-to-device communication in ofdma cellular networks: A survey and challenges," *IEEE Communications Surveys Tutorials*, vol. 17, no. 4, pp. 1885–1922, 2015.

[10] N. B. M. Chandra R Murthy, "Energy harvesting wireless communication systems," *National Conference on Communications*, February 2014.

[11] M. Tacca, P. Monti, and A. Fumagalli, "Cooperative and reliable arq protocols for energy harvesting wireless sensor nodes," *IEEE Transactions on Wireless Communications*, vol. 6, no. 7, pp. 2519–2529, July 2007.

[12] L. Varshney, "Transporting information and energy simultaneously," in *IEEE International Symposium on Information Theory, 2008.*, July 2008, pp. 1612–1616.

[13] B. Medepally and N. Mehta, "Voluntary energy harvesting relays and selection in cooperative wireless networks," *IEEE Transactions on Wireless Communications*, vol. 9, no. 11, pp. 3543–3553, November 2010.

[14] P. Grover and A. Sahai, "Shannon meets tesla: Wireless information and power transfer," in *2010 IEEE International Symposium on Information Theory Proceedings (ISIT)*, June 2010, pp. 2363–2367.

[15] O. Ozel, K. Tutuncuoglu, J. Yang, S. Ulukus, and A. Yener, "Transmission with energy harvesting nodes in fading wireless channels: Optimal policies," *IEEE Journal on Selected Areas in Communications*, vol. 29, no. 8, pp. 1732–1743, September 2011.

[16] H. Li and B. Sikdar, "Relay usage scheduling in sensor networks with energy harvesting," in *2010 IEEE International Conference on Communications (ICC)*, May 2010, pp. 1–5.

[17] J. Yang and S. Ulukus, "Optimal packet scheduling in an energy harvesting communication system," *IEEE Transactions on Communications*, vol. 60, no. 1, pp. 220–230, January 2012.

[18] K. Tutuncuoglu and A. Yener, "Optimum transmission policies for battery limited energy harvesting nodes," *IEEE Transactions on Wireless Communications*, vol. 11, no. 3, pp. 1180–1189, March 2012.

[19] O. Ozel and S. Ulukus, "Achieving awgn capacity under stochastic energy harvesting," *IEEE Transactions on Information Theory*, vol. 58, no. 10, pp. 6471–6483, Oct 2012.

[20] J. Yang, O. Ozel, and S. Ulukus, "Broadcasting with an energy harvesting rechargeable transmitter," *IEEE Transactions on Wireless Communications*, vol. 11, no. 2, pp. 571–583, February 2012.

[21] O. Ozel, J. Yang, and S. Ulukus, "Optimal broadcast scheduling for an energy harvesting rechargeable transmitter with a finite capacity battery," *IEEE Transactions on Wireless Communications*, vol. 11, no. 6, pp. 2193–2203, June 2012.

[22] J. Yang and S. Ulukus, "Optimal packet scheduling in a multiple access channel with energy harvesting transmitters," *Journal of Communications and Networks*, vol. 14, no. 2, pp. 140–150, April 2012.

[23] K. Tutuncuoglu and A. Yener, "The energy harvesting multiple access channel with energy storage losses," in *2012 IEEE Information Theory Workshop (ITW)*, Sept 2012, pp. 94–98.

[24] ——, "Sum-rate optimal power policies for energy harvesting transmitters in an interference channel," *Journal of Communications and Networks*, vol. 14, no. 2, pp. 151–161, April 2012.

[25] X. Zhou, R. Zhang, and C. K. Ho, "Wireless information and power transfer: Architecture design and rate-energy tradeoff," *IEEE Transactions on Communications*, vol. 61, no. 11, pp. 4754–4767, November 2013.

[26] O. Orhan and E. Erkip, "Energy harvesting two-hop networks: Optimal policies for the multi-energy arrival case," in *2012 35th IEEE Sarnoff Symposium (SARNOFF)*, May 2012, pp. 1–6.

[27] ——, "Throughput maximization for energy harvesting two-hop networks," in *2013 IEEE International Symposium on Information Theory Proceedings (ISIT)*, July 2013, pp. 1596–1600.

[28] A. Minasian, S. Shahbazpanahi, and R. Adve, "Energy harvesting cooperative communication systems," *IEEE Transactions on Wireless Communications*, vol. PP, no. 99, pp. 1–1, 2014.

[29] I. Ahmed, A. Ikhlef, R. Schober, and R. Mallik, "Joint power allocation and relay selection in energy harvesting af relay systems," *IEEE Wireless Communications Letters*, vol. 2, no. 2, pp. 239–242, April 2013.

[30] A. Nasir, X. Zhou, S. Durrani, and R. Kennedy, "Relaying protocols for wireless energy harvesting and information processing," *IEEE Transactions on Wireless Communications*, vol. 12, no. 7, pp. 3622–3636, July 2013.

[31] B. Gurakan, O. Ozel, J. Yang, and S. Ulukus, "Energy cooperation in energy harvesting communications," *IEEE Transactions on Communications*, vol. 61, no. 12, pp. 4884–4898, December 2013.

[32] C. Huang, R. Zhang, and S. Cui, "Throughput maximization for the gaussian relay channel with energy harvesting constraints," *IEEE Journal on Selected Areas in Communications*, vol. 31, no. 8, pp. 1469–1479, August 2013.

[33] Y. Luo, J. Zhang, and K. Letaief, "Throughput maximization for two-hop energy harvesting communication systems," in *2013 IEEE International Conference on Communications (ICC)*, June 2013, pp. 4180–4184.

[34] K. Tutuncuoglu, B. Varan, and A. Yener, "Optimum transmission policies for energy harvesting two-way relay channels," in *2013 IEEE International Conference on Communications Workshops (ICC)*, June 2013, pp. 586–590.

[35] L. Liu, R. Zhang, and K.-C. Chua, "Wireless information transfer with opportunistic energy harvesting," *IEEE Transactions on Wireless Communications*, vol. 12, no. 1, pp. 288–300, January 2013.

[36] R. Zhang and C. K. Ho, "Mimo broadcasting for simultaneous wireless information and power transfer," *IEEE Transactions on Wireless Communications*, vol. 12, pp. 1989–2001, May 2013.

[37] L. Liu, R. Zhang, and K.-C. Chua, "Wireless information and power transfer: A dynamic power splitting approach," *IEEE Transactions on Communications*, pp. 3990–4001, September 2013.

[38] I. Ahmed, A. Ikhlef, R. Schober, and R. Mallik, "Power allocation for conventional and buffer-aided link adaptive relaying systems with energy harvesting nodes," *IEEE Transactions on Wireless Communications*, vol. 13, no. 3, pp. 1182–1195, March 2014.

[39] R. Zhang, R. G. Maunder, and L. Hanzo, "Wireless information and power transfer: from scientific hypothesis to engineering practice," *IEEE Communications Magazine*, August 2014.

[40] R. Zhang, L. L. Yang, and L. Hanzo, "Energy pattern aided simultaneous wireless information and power transfer," *IEEE Journal on Selected Areas in Communications*, vol. 33, no. 8, pp. 1492–1504, Aug 2015.

[41] J. Garnica, R. Chinga, and J. Lin, "Wireless power transmission: From far field to near field," *Proceedings of the IEEE*, vol. 101, no. 6, pp. 1321–1331, June 2013.

[42] N. Tesla, *The future of wireless art*. Wireless Telegraphy and telephony, 1908.

[43] L. Wei, R. Hu, Y. Qian, and G. Wu, "Enable device-to-device communications underlaying cellular networks: challenges and research aspects," *IEEE Communications Magazine*, vol. 52, no. 6, pp. 90–96, June 2014.

[44] G. Boudreau, J. Panicker, N. Guo, R. Chang, N. Wang, and S. Vrzic, "Interference coordination and cancellation for 4g networks," *IEEE Communications Magazine*, vol. 47, no. 4, pp. 74–81, April 2009.

[45] T. D. Novlan, R. K. Ganti, A. Ghosh, and J. G. Andrews, "Analytical Evaluation of Fractional Frequency Reuse for OFDMA Cellular Networks," *IEEE Transactions on Wireless Communications*, vol. 10, no. 12, pp. 4294–4305, December 2011.

[46] Z. Xu, G. Li, C. Yang, and X. Zhu, "Throughput and Optimal Threshold for FFR Schemes in OFDMA Cellular Networks," *IEEE Transactions on Wireless Communications*, vol. 11, no. 8, pp. 2776–2785, August 2012.

[47] D. Gonzalez, M. Garcia-Lozano, S. Ruiz Boque, and D. S. Lee, "Optimization of Soft Frequency Reuse for Irregular LTE Macrocellular Networks," *IEEE Transactions on Wireless Communications*, vol. 12, no. 5, pp. 2410–2423, May 2013.

[48] J. Zhang, R. Zhang, G. Li, and L. Hanzo, "Distributed Antenna Systems in Fractional-Frequency-Reuse-Aided Cellular Networks," *IEEE Transactions on Vehicular Technology*, vol. 62, no. 3, pp. 1340–1349, March 2013.

[49] S. Kumar, S. Kalyani, and K. Giridhar, "Spectrum Allocation for ICIC Based Picocell," *IEEE Transactions on Vehicular Technology*, vol. PP, no. 99, pp. 1–1, 2014.

[50] F. Jin, R. Zhang, and L. Hanzo, "Fractional Frequency Reuse Aided Twin-Layer Femtocell Networks: Analysis, Design and Optimization," *IEEE Transactions on Communications*, vol. 61, no. 5, pp. 2074–2085, May 2013.

[51] P. Janis, C. Yu, K. Doppler, C. Ribeiro, C. Wijting, K. Hugl, O. Tirkkonen, and V. Koivunen, "Device-to-Device Communication Underlaying Cellular Communications Systems," in *International Journal on Communications, Network and System Sciences*, vol. 2, June 2009, pp. 169–178.

[52] K. Doppler, M. Rinne, C. Wijting, C. Ribeiro, and K. Hugl, "Device-to-device communication as an underlay to LTE-advanced networks," *IEEE Communications Magazine*, vol. 47, no. 12, pp. 42–49, Dec 2009.

[53] K. Doppler, M. P. Rinne, P. Janis, C. Ribeiro, and K. Hugl, "Device-to-device communications; functional prospects for lte-advanced networks," in *2009 IEEE International Conference on Communications Workshops*, June 2009, pp. 1–6.

[54] C. H. Yu, K. Doppler, C. B. Ribeiro, and O. Tirkkonen, "Resource sharing optimization for device-to-device communication underlaying cellular networks," *IEEE Transactions on Wireless Communications*, vol. 10, no. 8, pp. 2752–2763, August 2011.

[55] H. S. Chae, J. Gu, B.-G. Choi, and M. Chung, "Radio resource allocation scheme for device-to-device communication in cellular networks using fractional frequency reuse," in *17th Asia-Pacific Conference on Communications (APCC), 2011*, Oct 2011, pp. 58–62.

[56] G. Fodor, E. Dahlman, G. Mildh, S. Parkvall, N. Reider, G. Miklós, and Z. Turányi, "Design aspects of network assisted device-to-device communications," *IEEE Communications Magazine*, vol. 50, no. 3, pp. 170–177, March 2012.

[57] T. sub Kim, S.-J. Lee, S. Chhorn, C. ho Cho, and S. Ryu, "Resource allocation and power control scheme for interference avoidance in lte-advanced device-to-device communication," in *7th International Conference on Computing and Convergence Technology (ICCCT) 2012*, Dec 2012, pp. 1201–1204.

[58] P. Phunchongharn, E. Hossain, and D. Kim, "Resource allocation for device-to-device communications underlaying LTE-advanced networks," *IEEE Wireless Communications*, vol. 20, no. 4, pp. 91–100, August 2013.

[59] D. Feng, L. Lu, Y. Yuan-Wu, G. Li, G. Feng, and S. Li, "Device-to-Device Communications Underlaying Cellular Networks," *IEEE Transactions on Communications*, vol. 61, no. 8, pp. 3541–3551, August 2013.

[60] X. Lin, J. G. Andrews, and A. Ghosh, "Spectrum sharing for device-to-device communication in cellular networks," *IEEE Transactions on Wireless Communications*, vol. 13, no. 12, pp. 6727–6740, Dec 2014.

[61] D. Zhu, J. Wang, A. Swindlehurst, and C. Zhao, "Downlink Resource Reuse for Device-to-Device Communications Underlaying Cellular Networks," *IEEE Signal Processing Letters*, vol. 21, no. 5, pp. 531–534, May 2014.

[62] W. Oduola, X. Li, L. Qian, and Z. Han, "Power control for device-to-device communications as an underlay to cellular system," in *IEEE International Conference on Communications (ICC), 2014*, June 2014, pp. 5257–5262.

[63] H. Zhu and J. Wang, "Device-to-device communication in cellular networks with fractional frequency reuse," in *IEEE International Conference on Communications (ICC), 2014*, June 2014, pp. 5503–5507.

[64] T. Bansal, K. Sundaresan, S. Rangarajan, and P. Sinha, "R2D2: Embracing device-to-device communication in next generation cellular networks," in *IEEE Proceedings INFOCOM, 2014*, April 2014, pp. 1563–1571.

[65] M. Sheng, Y. Li, X. Wang, J. Li, and Y. Shi, "Energy efficiency and delay tradeoff in device-to-device communications underlaying cellular networks," *IEEE Journal on Selected Areas in Communications*, vol. 34, no. 1, pp. 92–106, Jan 2016.

[66] R. Yin, C. Zhong, G. Yu, Z. Zhang, K. K. Wong, and X. Chen, "Joint spectrum and power allocation for d2d communications underlaying cellular networks," *IEEE Transactions on Vehicular Technology*, vol. 65, no. 4, pp. 2182–2195, April 2016.

[67] A. Sakr and E. Hossain, "Cognitive and energy harvesting-based d2d communication in cellular networks: Stochastic geometry modeling and analysis," *IEEE Transactions on Communications*, vol. 63, no. 5, pp. 1867–1880, May 2015.

[68] H. Yang, J. Lee, and T. Quek, "Heterogeneous cellular network with energy harvesting-based d2d communication," *IEEE Transactions on Wireless Communications*, vol. 15, no. 2, pp. 1406–1419, Feb 2016.

[69] Y. Liu, L. Wang, S. Raza Zaidi, M. Elkashlan, and T. Duong, "Secure d2d communication in large-scale cognitive cellular networks: A wireless power transfer model," *IEEE Transactions on Communications*, vol. 64, no. 1, pp. 329–342, Jan 2016.

[70] L. Jiang, H. Tian, Z. Xing, K. Wang, K. Zhang, S. Maharjan, S. Gjessing, and Y. Zhang, "Social-aware energy harvesting device-to-device communications in 5g networks," *IEEE Wireless Communications*, vol. 23, no. 4, pp. 20–27, August 2016.

[71] Z. Zhou, C. Gao, C. Xu, T. Chen, D. Zhang, and S. Mumtaz, "Energy-efficient stable matching for resource allocation in energy harvesting-based device-to-device communications," *IEEE Access*, vol. PP, no. 99, pp. 1–1, 2017.

[72] K. Han and K. Huang, "Wirelessly powered backscatter communication networks: Modeling, coverage, and capacity," *IEEE Transactions on Wireless Communications*, vol. 16, no. 4, pp. 2548–2561, April 2017.

[73] C. Joo and S. Kang, "Joint scheduling of data transmission and wireless power transfer in multi-channel device-to-device networks," *Journal of Communications and Networks*, vol. 19, no. 2, pp. 180–188, April 2017.

[74] K. Guo, S. Dai, and G. Ascheid, "D2D Underlaying Massive MIMO TWRN With Opportunistic Energy Harvesting," *IEEE Wireless Communications Letters*, vol. PP, no. 99, pp. 1–1, 2017.

[75] Y. Luo, P. Hong, R. Su, and K. Xue, "Resource Allocation for Energy Harvesting-powered D2D Communication underlaying Cellular Networks," *IEEE Transactions on Vehicular Technology*, vol. PP, no. 99, pp. 1–1, 2017.

[76] P. He, L. Zhao, S. Zhou, and Z. Niu, "Recursive waterfilling for wireless links with energy harvesting transmitters," *IEEE Transactions on Vehicular Technology*, vol. 63, no. 3, pp. 1232–1241, March 2014.

[77] C.-C. Kuan, G.-Y. Lin, H.-Y. Wei, and R. Vannithamby, "Reliable multicast and broadcast mechanisms for energy-harvesting devices," *IEEE Transactions on Vehicular Technology*, vol. 63, no. 4, pp. 1813–1826, May 2014.

[78] Z. Fang, T. Song, and T. Li, "Energy harvesting for two-way OFDM communications under hostile jamming," *IEEE Signal Processing Letters*, vol. 22, no. 4, pp. 413–416, April 2015.

[79] I. Ahmed, A. Ikhlef, D. Ng, and R. Schober, "Optimal resource allocation for energy harvesting two-way relay systems with channel uncertainty," in *2013 IEEE Global Conference on Signal and Information Processing (GlobalSIP)*, Dec 2013, pp. 345–348.

[80] N. Roseveare and B. Natarajan, "An alternative perspective on utility maximization in energy-harvesting wireless sensor networks," *IEEE Transactions on Vehicular Technology*, vol. 63, no. 1, pp. 344–356, Jan 2014.

[81] O. Orhan and E. Erkip, "Optimal transmission policies for energy harvesting two-hop networks," in *2012 46th Annual Conference on Information Sciences and Systems (CISS)*, March 2012, pp. 1–6.

[82] A. Wachter and L. T. Biegler, "On the implementation of an interior-point filter line-search algorithm for large-scale nonlinear programming," *Mathematical Programming*, pp. 25–57, 2006.

[83] S. Boyd and L. Vandenberghe, *Convex Optimization*. New York, NY, USA: Cambridge University Press, 2004.

[84] X. Zhu, S. Wen, G. Cao, X. Zhang, and D. Yang, "QoS-based resource allocation scheme for Device-to-Device (D2D) radio underlaying cellular networks," in *19th International Conference on Telecommunications (ICT), 2012*, April 2012, pp. 1–6.

[85] J. Hao, H. Zhang, L. Song, and Z. Han, "Graph-based resource allocation for device-to-device communications aided cellular network," in *IEEE/CIC International Conference on Communications in China (ICCC), 2014*, Oct 2014, pp. 256–260.

[86] S. Sun and Y. Shin, "Resource allocation for D2D communication using Particle Swarm Optimization in LTE networks," in *International Conference on Information and Communication Technology Convergence (ICTC), 2014*, Oct 2014, pp. 371–376.

[87] J. Zhang, R. Zhang, G. Li, and L. Hanzo, "Distributed antenna systems in fractional-frequency-reuse-aided cellular networks," *IEEE Transactions on Vehicular Technology*, vol. 62, no. 3, pp. 1340–1349, March 2013.

[88] W. Wu and Y. Zhang, "Dedicated resource allocation for D2D communications in cellular systems employing FFR," in *Sixth International Conference on Wireless Communications and Signal Processing (WCSP), 2014*, Oct 2014, pp. 1–6.

[89] H. sub Kim, J. hyeon Na, and E. Cho, "Resource allocation policy to avoid interference between cellular and D2D Links/ and D2D links in mobile networks," in *International Conference on Information Networking (ICOIN), 2014*, Feb 2014, pp. 588–591.

[90] P. Bao, G. Yu, and R. Yin, "Novel frequency reusing scheme for interference mitigation in D2D uplink underlaying networks," in *9th International Wireless Communications and Mobile Computing Conference (IWCMC), 2013*, July 2013, pp. 491–496.

[91] M. Zulhasnine, C. Huang, and A. Srinivasan, "Efficient resource allocation for device-to-device communication underlaying LTE network," in *IEEE 6th International Conference on Wireless and Mobile Computing, Networking and Communications (WiMob), 2010*, Oct 2010, pp. 368–375.

[92] T. Novlan, H. Dhillon, and J. Andrews, "Analytical Modeling of Uplink Cellular Networks," *IEEE Transactions on Wireless Communications*, vol. 12, no. 6, pp. 2669–2679, June 2013.

[93] J. Andrews, F. Baccelli, and R. Ganti, "A Tractable Approach to Coverage and Rate in Cellular Networks," *IEEE Transactions on Communications*, vol. 59, no. 11, pp. 3122–3134, November 2011.

[94] D. Feng, L. Lu, Y. Yuan-Wu, G. Y. Li, G. Feng, and S. Li, "Device-to-device communications underlaying cellular networks," *IEEE Transactions on Communications*, vol. 61, no. 8, pp. 3541–3551, August 2013.

[95] X. Lin, J. G. Andrews, A. Ghosh, and R. Ratasuk, "An overview of 3GPP device-to-device proximity services," *IEEE Communications Magazine*, vol. 52, no. 4, pp. 40–48, April 2014.

[96] D. Feng, L. Lu, Y. Yuan-Wu, G. Y. Li, S. Li, and G. Feng, "Device-to-device communications in cellular networks," *IEEE Communications Magazine*, vol. 52, no. 4, pp. 49–55, April 2014.

[97] S. Maghsudi and S. Stańczak, "Hybrid Centralized-Distributed Resource Allocation for Device-to-Device Communication Underlaying Cellular Networks," *IEEE Transactions on Vehicular Technology*, vol. 65, no. 4, pp. 2481–2495, April 2016.

[98] H. H. Nguyen, M. Hasegawa, and W. J. Hwang, "Distributed Resource Allocation for D2D Communications Underlay Cellular Networks," *IEEE Communications Letters*, vol. 20, no. 5, pp. 942–945, May 2016.

[99] Y. Jiang, Q. Liu, F. Zheng, X. Gao, and X. You, "Energy Efficient Joint Resource Allocation and Power Control for D2D Communications," *IEEE Transactions on Vehicular Technology*, vol. PP, no. 99, pp. 1–1, 2015.

[100] K. Tutuncuoglu, B. Varan, and A. Yener, "Throughput maximization for two-way relay channels with energy harvesting nodes: The impact of relaying strategies," *IEEE Transactions on Communications*, vol. 63, no. 6, pp. 2081–2093, June 2015.

[101] Z. Ding, S. M. Perlaza, I. Esnaola, and H. V. Poor, "Power Allocation Strategies in Energy Harvesting Wireless Cooperative Networks," *IEEE Transactions on Wireless Communications*, vol. 13, no. 2, pp. 846–860, February 2014.

[102] F. Malandrino, C. Casetti, and C. F. Chiasserini, "Toward D2D-enhanced heterogeneous networks," *IEEE Communications Magazine*, vol. 52, no. 11, pp. 94–100, Nov 2014.

[103] A. Ghosh, N. Mangalvedhe, R. Ratasuk, B. Mondal, M. Cudak, E. Visotsky, T. A. Thomas, J. G. Andrews, P. Xia, H. S. Jo, H. S. Dhillon, and T. D. Novlan, "Heterogeneous cellular networks: From theory to practice," *IEEE Communications Magazine*, vol. 50, no. 6, pp. 54–64, June 2012.

[104] H. Sun, M. Wildemeersch, M. Sheng, and T. Q. S. Quek, "D2D Enhanced Heterogeneous Cellular Networks With Dynamic TDD," *IEEE Transactions on Wireless Communications*, vol. 14, no. 8, pp. 4204–4218, Aug 2015.

[105] Z. Dai, J. Liu, and C. Wang, "QoS-based device-to-device communication schemes in heterogeneous wireless networks," *IET Communications*, vol. 9, no. 3, pp. 335–341, 2015.

[106] M. Hasan and E. Hossain, "Distributed resource allocation for relay-aided device-to-device communication under channel uncertainties: A stable matching approach," *IEEE Transactions on Communications*, vol. 63, no. 10, pp. 3882–3897, Oct 2015.

[107] F. Malandrino, Z. Limani, C. Casetti, and C. F. Chiasserini, "Interference-Aware Downlink and Uplink Resource Allocation in HetNets With D2D Support," *IEEE Transactions on Wireless Communications*, vol. 14, no. 5, pp. 2729–2741, May 2015.

[108] D. Fooladivanda and C. Rosenberg, "Joint Resource Allocation and User Association for Heterogeneous Wireless Cellular Networks," *IEEE Transactions on Wireless Communications*, vol. 12, no. 1, pp. 248–257, January 2013.

[109] C. J. Zarowski, *An Introduction to Numerical Analysis for Electrical and Computer Engineers*. John Wiley and Sons, Incorporated, 2004.

[110] E. Suli and D. Mayers, *An Introduction to Numerical Analysis*. Cambridge University Press, 2003.

[111] R. Zhang, X. Cheng, L. Yang, and B. Jiao, "Interference Graph-Based Resource Allocation (InGRA) for D2D Communications Underlaying Cellular Networks," *IEEE Transactions on Vehicular Technology*, vol. 64, no. 8, pp. 3844–3850, Aug 2015.

[112] C. Liu and B. Natarajan, "Power-Aware Maximization of Ergodic Capacity in D2D Underlay Networks," *IEEE Transactions on Vehicular Technology*, vol. 66, no. 3, pp. 2727–2739, March 2017.

[113] L. Li, C. Dong, L. Wang, and L. Hanzo, "Spectral-efficient bidirectional decode-and-forward relaying for full-duplex communication," *IEEE Transactions on Vehicular Technology*, vol. 65, no. 9, pp. 7010–7020, Sept 2016.

[114] S. Kumar and S. Kalyani, "Impact of Correlated Interferers on Coverage and Rate of FFR and SFR Schemes," *IEEE Transactions on Vehicular Technology*, vol. PP, no. 99, pp. 1–1, 2015.

[115] H. Yetgin, K. T. K. Cheung, M. El-Hajjar, and L. Hanzo, "Network-lifetime maximization of wireless sensor networks," *IEEE Access*, vol. 3, pp. 2191–2226, 2015.

[116] J. Hu, L. L. Yang, and L. Hanzo, "Delay analysis of social group multicast-aided content dissemination in cellular system," *IEEE Transactions on Communications*, vol. 64, no. 4, pp. 1660–1673, April 2016.

Subject Index

Author Index